CARDIFF UNIVERSTY

Department of Chemistry

Preparation and Characterisation of Vanadium Phosphorus Oxide Catalysts for Butane Oxidation to Maleic Anhydride

Thesis submitted in accordance with the requirements of the University of Cardiff for the degree of

Doctor of Philosophy

By

Raja Lafi AL-Otaibi

January 2010

ProQuest LLC
789 East Eisenhower Parkway
P.O. Box 1346
Ann Arbor, MI 48106-1346

بسم الله الرحمن الرحيم

In The Name Of Allah, The Most Beneficent,

The Most Merciful

Declaration

This work has not previously been accepted in substance for any degree and is not being concurrently submitted in candidature for any degree

Signed ..... (Candidate)

Date.....

Statement 1

This thesis is the result of my own investigation, expect where otherwise stated. Other sources are acknowledged by giving explicit references. A bibliography is attached in the thesis.

Signed ..... (Candidate)

Date.....

Statement 1

I hereby give consent for my thesis, if accepted, to be available for photocopying and for inter-library loan, and for the title and summary to be made available to outside organisation.

Signed ..... (Candidate)

Date.....

For my parents

Acknowledgments

I would like to begin with by thanking Allah the almighty, for his bounties upon us and for his assistance in my studies and without him, nothing is possible.

I am deeply grateful to my supervisor, Professor Graham Hutchings, for his guidance, teachings and constant support. I wish to thankfully acknowledge Dr. Jonathan Bartley for his advice and unlimited support on resolving technical problems and discussing experimental data. I am also very thankful to Dr. Nicholas Dummer for his suggestions and corrections during the writing of this thesis.

Thanks are due to my employer, King Abdulaziz City for Science and Technology (KACST) in Saudi Arabia for financial support. Special thanks to my Friend Salem Bawaked and all my friends in lab 1.88 and 1.96 for their help during my study in Cardiff. Meanwhile I have to thank the Leigh University, USA for getting the TEM images for my study.

To my beloved parents, you know how special you are how much you are loved. Thanks for your prays for me and thanks for being there at the other end of the phone...

Finally, I express my deep thanks to my wife for being here with me during my study period, without you I do not think I could have made it.

Abstract

The selective oxidation of n-butane to maleic anhydride catalysed with vanadium phosphates continues to receive significant research attention due to its importance in academic and industrial sectors. The catalytic performance of vanadium phosphates is highly dependent on the method of preparation of the catalyst precursors $VOHPO_4.0.5H_2O$. The morphology and surface area of the precursor are factors of importance to achieve good catalytic results. This thesis aims the study of new preparative routes to get catalyst precursors $VOHPO_4.0.5H_2O$ with good catalytic performance for the selective oxidation of n-butane to maleic anhydride.

The use of octane as co-solvent shows a significant effect on the morphology of $VOHPO_4.0.5H_2O$ precursor which was prepared via three different routes. The reaction of $VOPO_4.2H_2O$ with octane solvent shows the possibility of the intercalation of the octane solvent between the layers of $VOPO_4.2H_2O$. This can lead to the formation of $VOHPO_4.0.5H_2O$ precursors with a new morphology after the reduction step using 1-butanol. In addition, the use of octane as co-solvent with 1-butanol leads to the formation of $VOHPO_4.0.5H_2O$ with a different XRD pattern and new morphology. Testing these samples shows that the samples with a rosette morphology exhibit the highest conversion and selectivity compared with the new materials prepared.

A study of the factors influencing the preparation of vanadium phosphates during the VPD type alcohol reduction of $VOPO_4{\cdot}2H_2O$. In this thesis, we demonstrate that the use of seed crystals of vanadium phosphate can have a dramatic influence on the morphology and phase identity of the precursor materials. $VOHPO_4{\cdot}0.5H_2O$ was prepared from $VOPO_4{\cdot}2H_2O$ using 1- and 3-octanol, 2-butanol and 2-methyl-1-propanol as both solvent and reducing agent. With 1-octanol the reaction temperature was found to be crucial in obtaining a high yield of the precursor phase, and at temperatures ≥160 °C a solution, containing V^{4+} ions formed in preference to $VOHPO_4{\cdot}0.5H_2O$. However, $VOHPO_4{\cdot}0.5H_2O$ formation can be achieved by the addition of a small amount of V-P-O material as seeds if carrying out the reduction process above this temperature. In contrast, when 3-octanol is used, $VO(H_2PO_4)_2$ is formed solely, but in the presence of a V-P-O seed significant amounts of $VOHPO_4{\cdot}0.5H_2O$ can also be formed.. Studying the reaction time online shows that $VO(H_2PO_4)_2$ could be transformed to $VOHPO_4.0.5H_2O$, which has been attempted previously without success. Finally, testing these samples under reaction conditions shows that they demonstrate high selectivity toward MA and good conversion compared to $VO(H_2PO_4)_2$

Vanadium phosphate catalysts have successfully been prepared in aqueous media using hydrogen. The catalysts precursors obtained were poorly crystalline VOHPO4.0.5H2O and a minor amount of an impurity detected by a reflection in the XRD pattern.

Activating these materials for n-butane oxidation show low selectivity of MA (5%), which could be attributed to the presence of V(V) phases after activation.

Table of contents

CHAPTER 6: Conclusion and future work

CHAPTER 1

INTRODUCTION

1.1 Introduction

The global abundance of short chain alkanes and the huge economic incentive of converting them to more valuable chemicals is a key goal of the petrochemical industry. There has been a great interest in selective oxidation processes to achieve these conversions which is motivated by both the academic and industrial. These processes include ammoxidation, oxidative dehydrogenation and selective oxidation. A well-known catalytic functionalisation of lower alkanes is the selective oxidation of n-butane to maleic anhydride (MA) over vanadium phosphorous oxide catalysts [1].

Originally MA was produced by the partial oxidation of benzene over V_2O_3-MoO_3 catalysts. The conversion of this process was 95%, with selectivity to MA of over 75%, with carbon dioxide and carbon monoxide the main by-products [2]. From the 1970s, butane oxidation over vanadium phosphate catalysts replaced benzene oxidation, as it had the advantages of lower cost, wider feedstock availability, safer operation and environmental benefits.

Vanadium phosphates have been well studied and of significant interest for the last four decades since Bergmann and Frish found them to be effective catalysts for the selective oxidation of n-butane to MA [3].

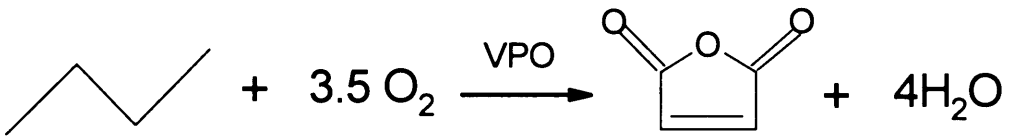

Figure. 1.1. The selective oxidation of n-butane to maleic anhydride.

MA is useful feedstock for unsaturated polyester resins, agricultural chemicals such as herbicides and pesticides. Moreover, it is also used as food additives and has recently been utilized as a raw material for 1,4-butanediol, tetrahydrofuran and γ-butyroloctane. In addition, MA is used as an oil additive, which increases oil life time and improves the engine efficiency of cars.

It is generally accepted that well crystallised $(VO)_2P_2O_7$ (which contains V^{4+} phase) is the active phase for selective catalytic oxidation of n-butane to MA. This phase is obtained by activating the catalyst precursor, vanadyl hydrogen phosphate hemihydrate, $VOHPO_4.0.5H_2O$, under the reaction feedstock of 1.5 % n-butane in air at 400°C [4].

$$VOHPO_4.0.5H_2O \xrightarrow{1.5\%\ \text{n-butane / air}} (VO)_2P_2O_7 + 2H_2O$$

The activated catalysts are formed topotactically from the precursor, so, the final catalyst morphology and surface area are influenced by the precursor morphology, which in turn is influenced by the method of preparation method of the initial precursor [5].

1.2 Reaction Mechanism

The oxidation of n-butane to maleic anhydride involves the abstraction of eight hydrogen atoms and the insertion of three oxygen atoms. This reaction is classified as an extensive 14 electron oxidation when compared with other selective oxidations; which are typically restricted to four electron transfer mechanisms.

To date, many researchers have developed different models for the mechanism of n-butane oxidation on the VPO catalyst [6]. Most of these proposed models are based on some experimental and theoretical findings, although there were no intermediates observed under standard reaction condition. Despite the considerable debate in the literature concerning the active site, the vanadyl pyrophosphate ($(VO)_2P_2O_7$) is generally accepted to be the main active phase in the selective oxidation of butane [5]. Therefore, most of the proposed mechanisms are based on this crystalline phase as the reaction surface.

The mechanism mostly thought to be operative for selective catalytic oxidation over solid oxides is the Mars-Van-Krevelen mechanism, in which the catalyst is alternately reduced by the compound to be oxidised and re-oxidised by gaseous molecular di-oxygen [7].

Taufiq-Yap *et al* [8] reported a study on n-butane, 1-butene and 1,3-butadiene using temperature programmed reaction (TPR) and temperature programmed desorption (TPD). Temperature programmed oxidation experiments proposed that the active oxygen species for selective oxidation of butane was lattice oxygen, and the replenishment of the surface oxygen from the bulk was the rate determining step which can confirm that this catalytic reaction follows Mars-Van-Krevelen mechanism. It is also suggested that the mechanism of the partial oxidation of n-butane on $(VO)_2P_2O_7$ is butane →but-1-ene → but-1,3-diene →dihydrofuran → furan → maleic anhydride.

The active oxygen species was studied by Abon *et al* using isotopic labelling experiments [9]. It was found that lattice oxygen was incorporated into the products and that as the reaction continued this oxygen was replenished by gas phase oxygen.

Centi *et al.* [10] have reported a comparison of the rate constants for depletion of the C_2-C_7 alkane series on a $(VO)_2P_2O_7$ catalyst for the theoretical reaction of simultaneous abstraction of two hydrogen atoms and obtained a linear correlation. Their studies supported a hypothesis that the rate-determining step is the simultaneous removal of two hydrogen atoms from the carbon atoms in the 2- and 3-positions in n-butane. They proposed that the Lewis acid site and the bridging oxygen abstract two hydrogen atoms from the two methylene groups of n-butane via a concerted mechanism.

Although, Centi *et al.* [10] did not give a full mechanism of oxidation of n-butane to maleic anhydride, they pointed out that the Brønsted acid sites may be involved in the intermediate steps following the initial activation of n-butane. The Brønsted acid sites were detected by IR spectroscopy and attributed to the presence of P-OH groups belonging to terminal HPO_4 and $H_2P_2O_7$ species [11]. The P-OH groups may have engaged in different functions such as facilitating the removal of water formed during the partial oxidation, stabilizing the reaction intermediates by forming the surface phosphate esters (P-O-C bonds) and avoiding desorption of these intermediates [12], and also to facilitate the desorption of maleic anhydride preventing its over oxidation [13].

Ziolkowski et al. [14,15] proposed a concerted mechanism of n-butane oxidation to maleic anhydride based on theoretical calculations on the [100] plane of $(VO)_2P_2O_7$ (

Figure 1.2). It is suggested that the reaction occurred in one step after the adsorption of butane on the active site. The adsorbed butane is activated by hydrogen removal to give butadiene before the concerted step to form maleic anhydride. The formation of maleic anhydride creates seven oxygen vacancies on the surface. The re-oxidation of the surface is proposed to be the rate determining step. There is, however, no experimental evidence supporting this mechanism.

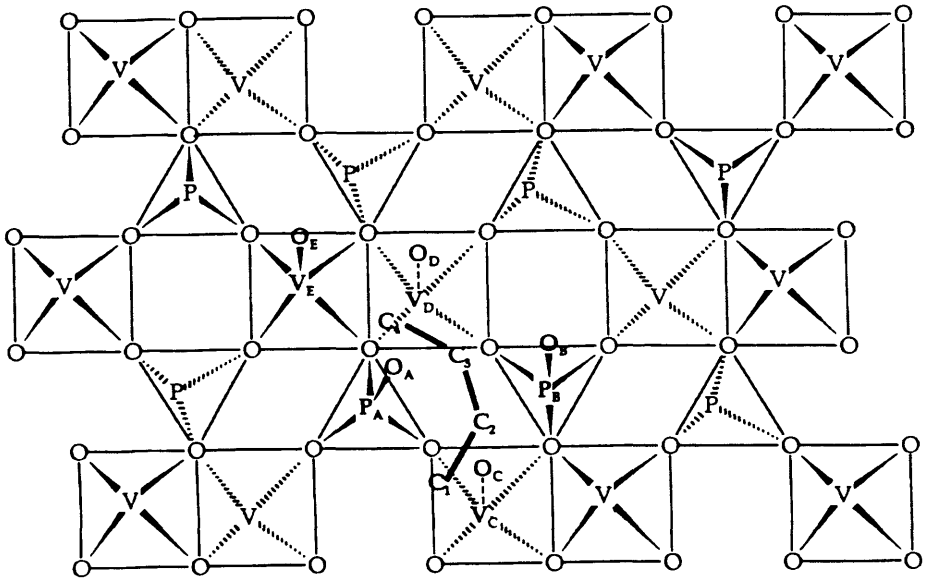

Figure 1.2. The active site for the concerted mechanism proposed by Ziolkowski *et al* [14,15]

The selective oxidation of n-butane to maleic anhydride proceeds via a consecutive alkenyl mechanism has been widely supported by many researchers in literature [16]. Schiøtt and Jørgensen proposed theoretically that once butane has adsorbed onto the vanadium phosphate surface, it is transformed through an adsorbed alkenyl intermediate into maleic anhydride [16, 17]. A summary of the mechanism steps are shown in Figure 1.3.

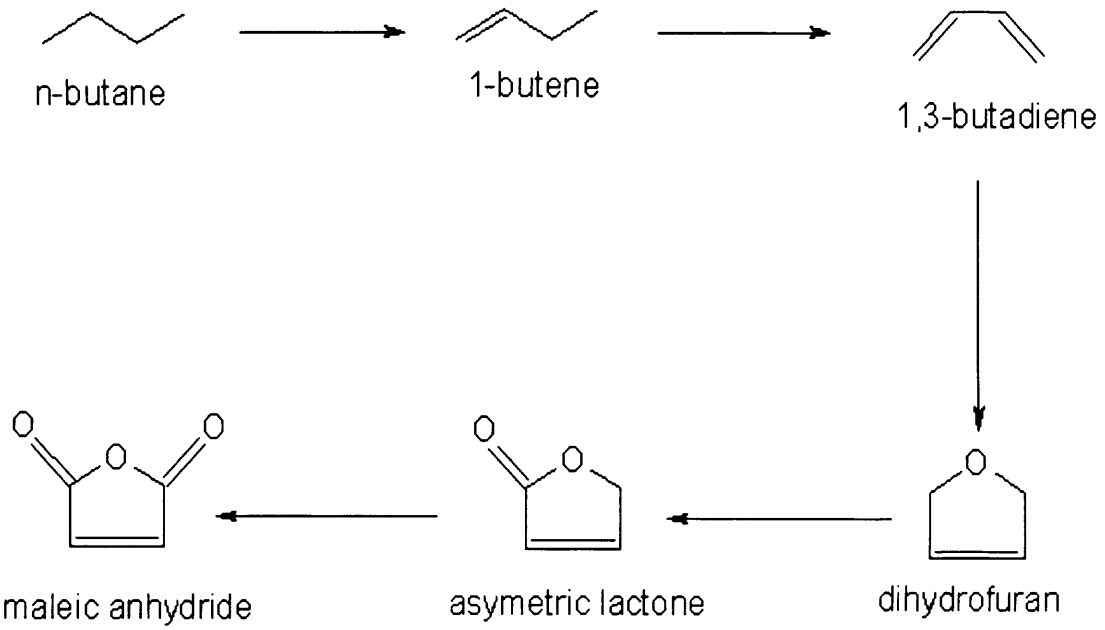

Figure 1.3. Consecutive alkenyl mechanisms as described by Schiøtt *et al.* [16, 17]

From their study, it is proposed that the gaseous oxygen is adsorbed in an η^2-peroxo co-ordination mode. Furan is formed by oxygen insertion into adsorbed 1,3-butadiene. An O-H bond, if formed in C2 and an asymmetric lactone, is subsequently formed by the loss of water. This process is repeated on the C5 to give maleic anhydride. However, the proposed intermediates have been detected under fuel rich gas feed conditions, which is different from the standard reaction conditions.

Zhang-Lin *et al* [18, 19] proposed a consecutive mechanism after investigating the oxidation of butane, 1-butene 1,3-butdiene and furan over $(VO)_2P_2O_7$ and $VOPO_4$ phases. It was suggested from their kinetic study that the results obtained for 1-butene and 1,3-butdiene oxidation can not be applied for the selective oxidation of butane as their oxidation proceeded different pathways. The kinetic data proposed that is not an

intermediate for butane oxidation, but is an intermediate for butadiene oxidation. They suggested a consecutive alkenyl mechanism for the oxidation of the unsaturated reactants and a consecutive alkoxide mechanism for n-butane oxidation. In the alkenyl mechanism, the weakly adsorbed intermediates are in equilibrium with the gas phase, which allows furan to be seen as a product for the oxidation of butene. In the case of butane oxidation, the reaction proceeded via strongly adsorbed alkoxide intermediates which would remain on the surface for the whole oxidation process as shown in figure (1.4).

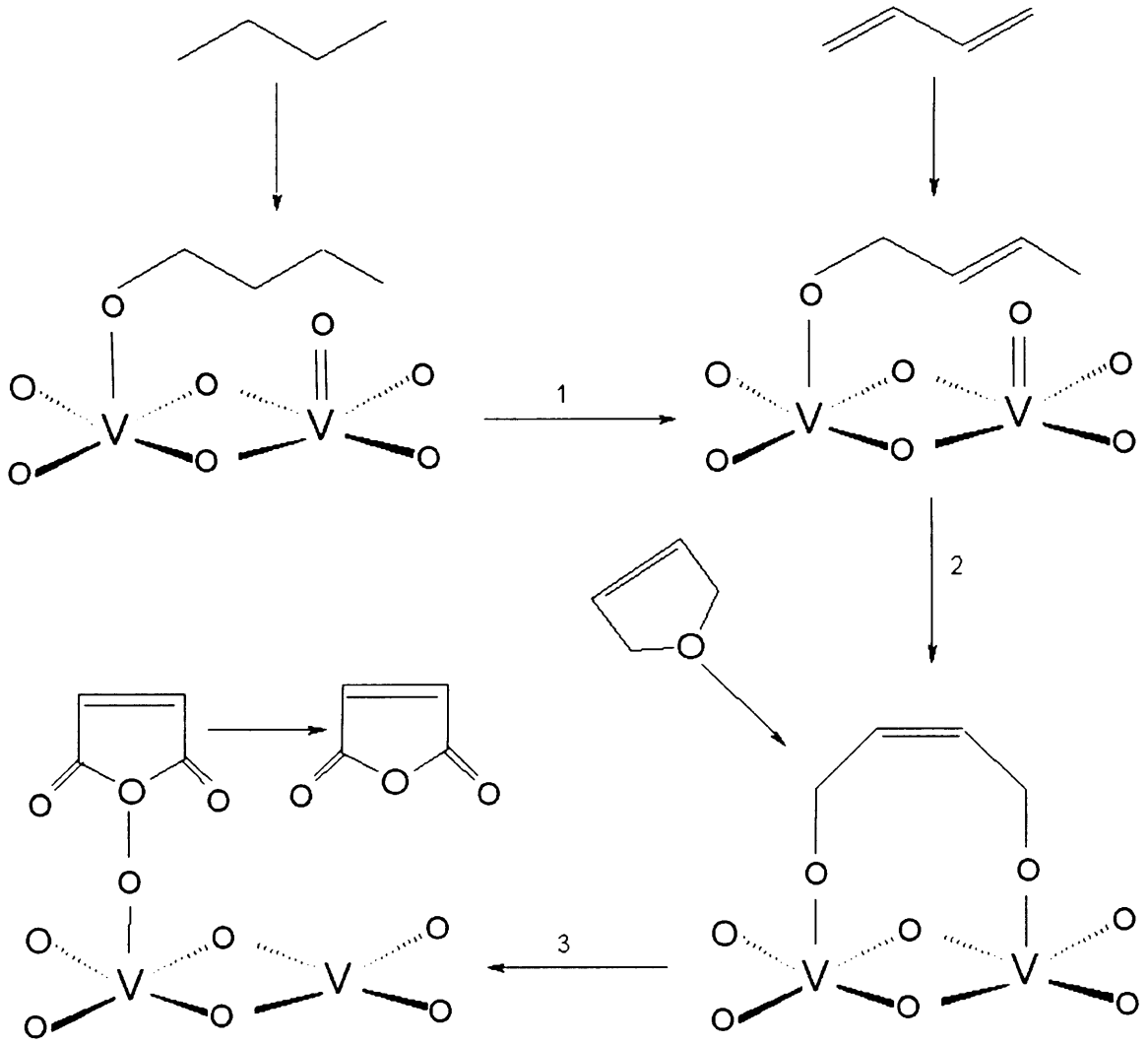

Figure 1.4 Consecutive alkoxide mechanism for butane oxidation proposed by Zhang-Lin et al, [18,19].

Grasselli *et al.* [20] proposed a mechanism of n-butane transformation to 1,3-butadiene at the active sites present on the (200) plane of $(VO)_2P_2O_7$. It is proposed that the dimeric active sites form clusters on the surface, each composed of four vanadyl dimmers, which are isolated from other clusters by terminal pyrophosphate groups. These pyrophosphate groups $[O_3P\text{-}OPO_3H_2]^{2-}$ act as diffusion barriers, preventing over-oxidation of the reactive surface-bound intermediates by the excess oxygen from neighbouring clusters. The $[O_3P\text{-}OPO_3H_2]^{2-}$ groups are also Brønsted acid sites and participate in the overall mechanism of oxidation.

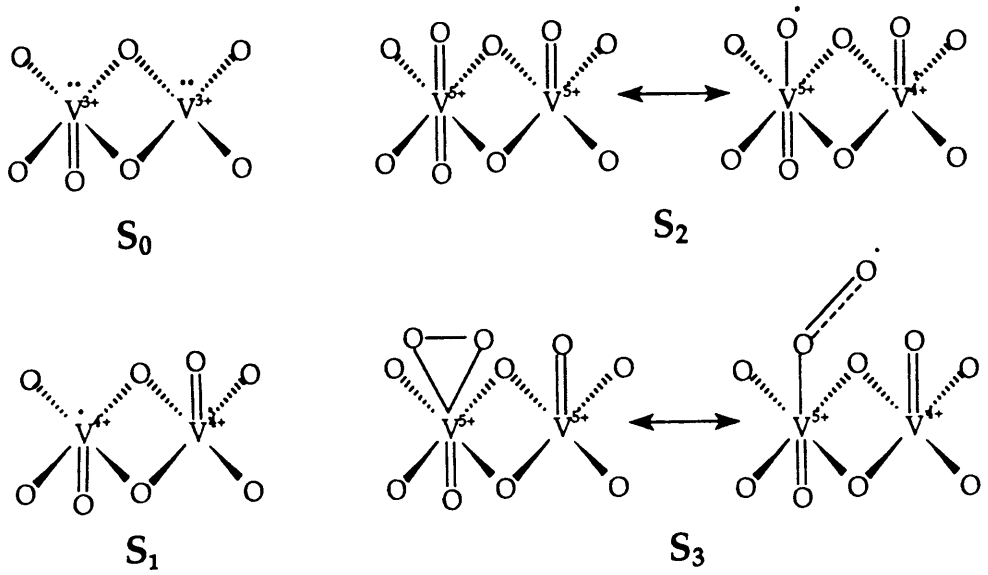

Figure 1.5- Schematic representation of the dynamic states S0-S3 of the possible states of the active site proposed by Grasselli *et al.* [20]

1.3 The active catalyst

The structure of vanadium phosphate catalysts is dependent on a number of factors (i) the gas phase composition of the n-butane/air feed, (ii) the time on stream, and (iii) the activation temperature [21-22]. Although $(VO)_2P_2O_7$ has been recognized as the only crystalline phase present in the best vanadium phosphate catalysts, the V(V) and V(IV)

phosphate phases can be present in both crystalline and disordered state depending on activation procedure and conditions [21]. This complexity of the solid-state chemistry of the vanadium phosphate catalysts has opened a debate whether $(VO)_2P_2O_7$ is indeed the active catalyst, or a combination of phases are responsible for the reaction.

Bordes *et al* [23] proposed that the active sites in n-butane oxidation to maleic anhydride are linked with coherent interfaces between slabs of the (100) planes of a mixture of $VOPO_4$ phases and the (200) planes of $(VO)_2P_2O_7$ along the (001) and (201) planes, respectively. Nevertheless, the best $(VO)_2P_2O_7$ catalysts show a lack of impurity from $VOPO_4$ phases. As a result, the mechanism of Bordes [23] could be suitable to explain the catalytic behaviour of over oxidized or non-equilibrated vanadium phosphate catalysts.

Hutchings *et al.* [24] suggested that the active sites for n-butane oxidation to maleic anhydride comprise a V^{4+}/V^{5+} couple well dispersed on the surface of a range of vanadium phosphate phases. The active phase suggested is well-dispersed micro-crystalline $VOPO_4$ phases detected on the surface of $(VO)_2P_2O_7$ phase.

Centi *et al.* [25] proposed that butane oxidation occurs through a series of redox couples on the vanadium phosphate catalysts and that V^{3+},V^{4+} and V^{5+} must exist for the reaction to occur. The activation of butane requiring a V^{4+}-V^{3+} couple, while the subsequent conversion to maleic anhydride involves V^{5+}-V^{4+} couple.

Volta *et al.* [26] proposed that domains of γ-$VOPO_4$ supported on a $(VO)_2P_2O_7$ matrix are necessary for selective n-butane oxidation, which was confirmed by XRD, ^{31}P MAS

NMR results. Conversely, XRD, Raman and ^{31}P NMR studies demonstrated that the best catalysts did not contain amorphous or microcrystalline V(V) phosphates [27]. Therefore, their mechanism may also explain the performance of only non-equilibrated or over oxidized vanadium phosphate catalysts that could contain $VOPO_4$ phases.

Vanadyl pyrophosphate $(VO)_2P_2O_7$ is generally accepted to be the main active phase for maleic anhydride production. The structure of $(VO)_2P_2O_7$ is made up of pairs of edge sharing VO_6 octahedra with V=O bonds positioned in *trans* position (Figure1.6 (b)). All equatorial positions are linked to PO_4 tetrahedra. The layered are liked to one another forming double columns of distorted VO_6 chains (V=O$\cdots$V=O). Pyrophosphate groups ($P_2O_7^{4-}$) running parallel to the VO_6 chains are formed by PO_4 tetrahedra sharing an oxygen atom with other PO_4 tetrahedra from the adjacent layer as showing Figure1.6 (a).

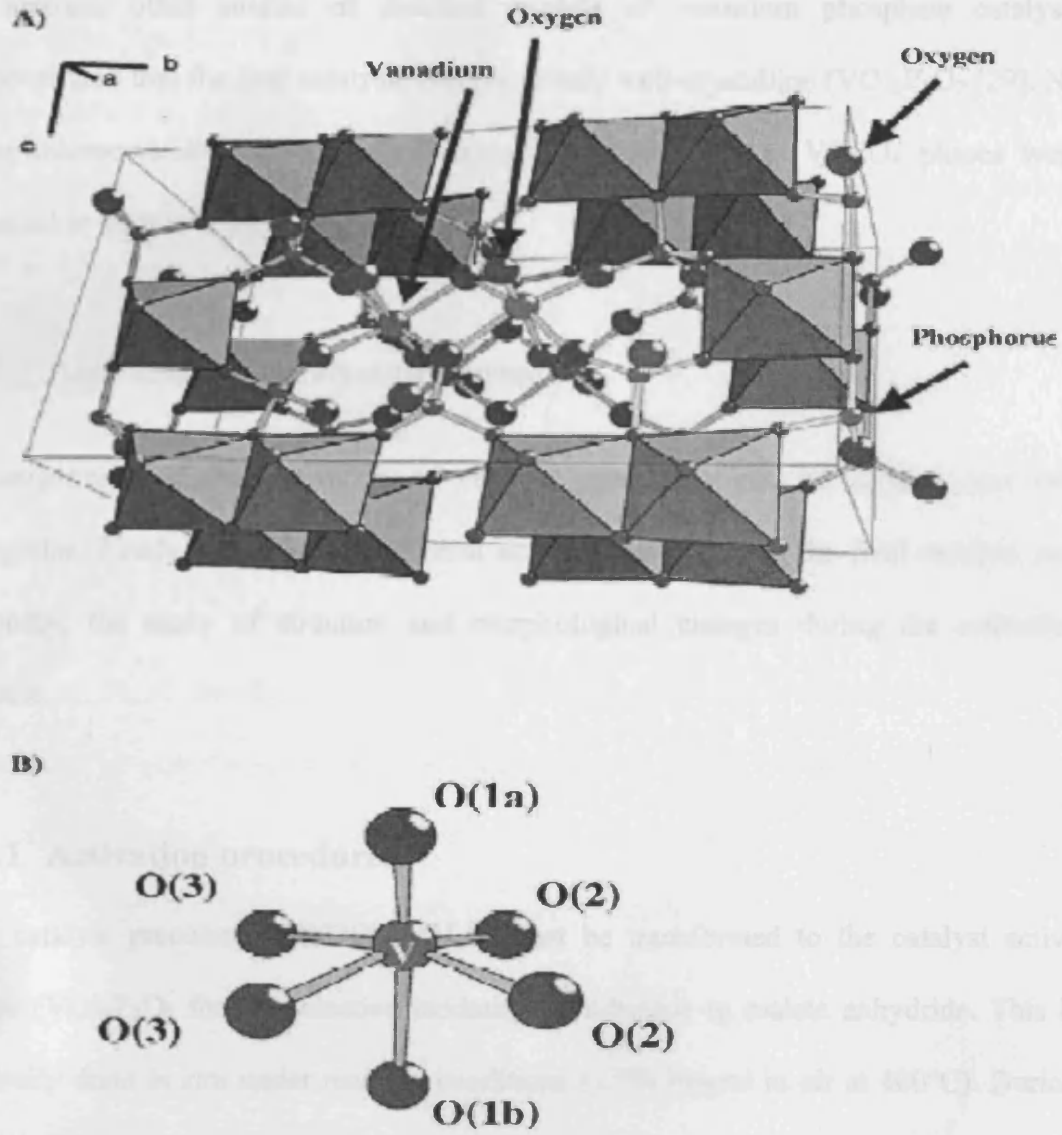

Figure 1.6- Structural model of vanadyl pyrophosphate [28]. (A) View onto the (100) plane. The (b, c) planes are stacked along the *a*-axis. Vanadium, oxygen and phosphorus atoms are represented as balls as indicated. Twinned VO_6 octa-hedra isolated and connected to other octahedra pairs by P_2O_7 double tetrahedra are shown. In the centre of the figure the atomic arrangement of a central vanadium atom surrounded by oxygen atoms inside the highly distorted octahedra is displayed. (B) Detailed view of the V–O octahedra. Three groups of oxygen bound to vanadium can be distinguished: apical oxygen atoms with a short V–O bond O(1a) and a long bond O(1b), planar oxygen atoms O(2) with one V atom and one P atom as nearest neighbours, and planar oxygen atoms O(3) with two V and one P as nearest neighbours.

In contrast, other studies of standard models of vanadium phosphate catalysts demonstrated that the best catalysts contained only well-crystalline $(VO)_2P_2O_7$ [29]. No other microcrystalline or disordered impurity phases such as $VOPO_4$ phases were detected in such catalysts [29].

1.4 Activation of catalyst precursors

Investigation into the activation of catalyst precursors can be divided into two categories. Firstly, the effect of different activation methods on the final catalyst, and secondly, the study of structure and morphological changes during the activation process.

1.4.1 Activation procedures

The catalyst precursor $VOHPO_4.0.5H_2O$ must be transformed to the catalyst active phase $(VO)_2P_2O_7$ for the selective oxidation of n-butane to maleic anhydride. This is typically done *in situ* under reaction conditions (1.7% butane in air at 400°C). During this activation period the catalyst performance increases as the transformation to the active phase $(VO)_2P_2O_7$ occurs. The activation takes approximately 72 hours to achieve stable values of conversion and selectivities. However, a full transformation of the precursor to the active phase $(VO)_2P_2O_7$ requires approximately 1000 hours on-line in order for the catalyst to be considered as totally transformed. Albonetti *et al* [30] reported a comparison between equilibrated and non-equilibrated catalysts. It was found from their studies that equilibrated catalysts that had been on-line for 1000 hours were more crystalline and had higher surface area compared with non-equilibrated catalysts (80-100 hours on-line).

There have been a number of crystalline VPO phases observed during the transformation of the $VOHPO_4.0.5H_2O$ precursor to the active phase $(VO)_2P_2O_7$ [21, 31]. Depending on several factors such as the activation temperature, period, atmosphere, the morphology of the precursor, the P/V ratio in the precursor and the presence defects in the structure.

There are two different activation procedures commonly reported in the literature [6, 32]. Firstly, activation of the catalyst precursor in an inert atmosphere at T 673K, followed by the introduction of the reactant mixture of n-butane in air. $VOHPO_4.0.5H_2O$ transforms to poorly crystalline $(VO)_2P_2O_7$ during the first step, which can be partially oxidized to V(V) orthophosphates (commonly $VOPO_4$ phases) after the introduction of the reactant mixture. Calcination of the catalyst precursor in air at T 673K, after which the reactant mixture is introduced, leads to complete oxidation to V^{5+}.

1.4.2 Structural transformations

Johnson *et al* [33] studied the crystalline structure of precursor and active catalysts and concluded the topotactic nature of this transformation. This means that the $(VO)_2P_2O_7$ catalyst preserves the morphology of the $VOHPO_4.0.5H_2O$ precursor. Insight into how the transformation occurs could assist in the design of pre-treatments and activations of catalyst precursor, which would produce catalysts with enhanced properties.

Kiely *et al* also confirmed that a direct topotactic transformation from catalyst precursor VOHPO4.0.5H2O to $(VO)_2P_2O_7$ occurs at the periphery of the crystallite, whereas

$VOHPO_4.0.5H_2O$ initially transforms epitaxially into δ-$VOPO_4$ in the interior of the crystallite. As the activation time increases the spheres of δ-$VOPO_4$, which are embedded in a disordered matrix, shrink and are further reduced to give the $(VO)_2P_2O_7$ [34].

Hutchings *et al* reported using Raman spectroscopy to study activation and reported that the activation process does not proceed through the simple transformation of crystalline $VOHPO_4.0.5H_2O$ to crystalline $(VO)_2P_2O_7$ only [35]. It was suggested that the bulk of the $VOHPO_4.0.5H_2O$ becomes amorphous on heating in an n-butane air mixture and the crystallization to $(VO)_2P_2O_7$ takes place relatively slowly, which may affect the crystallinity of $(VO)_2P_2O_7$.

Torardi *et al* [36] also investigated the transformation of the $VOHPO_4.0.5H_2O$ precursor into $(VO)_2P_2O_7$ by electron and X-ray diffraction techniques and demonstrated that the transformation was topotactic in the sense that the initial crystal morphology was preserved during the transformation. It was found that single crystals of VOHPO4.0.5H2O were converted to pseudomorphs, which were unchanged in size or shape with respect to the starting crystals of the precursor.

Ryumon *et al* [37] studied the transformation of $VOHPO_4.0.5H_2O$ precursor to $(VO)_2P_2O_7$ using water vapour. For these studies, they used small and large crystallites in the presence and absence of water vapour. It was found that a single-phase of well-crystallized $(VO)_2P_2O_7$ formed within 5 hours under a reaction mixture (0.9% n-butane, 10% O2) containing 40% water vapour using the small crystallites, whereas the transformation took more than 100 hours in reaction mixture without water vapour.

Ryumon *et al* [37] also suggest that under the reaction conditions, water vapour accelerated two processes in the transformation of $VOHPO_4.0.5H_2O$ to $(VO)_2P_2O_7$: the crystallization of the amorphous VPO phase containing V^{4+} and V^{5+} to $(VO)_2P_2O_7$ and δ-$VOPO_4$ and the transformation of δ-$VOPO_4$ to $(VO)_2P_2O_7$. However, water vapour inhibited the topotactic transformation of $VOHPO_4.0.5H_2O$ to $(VO)_2P_2O_7$.

More recently, Imai *et al* reported the transformation of nano-sized $VOHPO_4.0.5H_2O$ crystallites to $(VO)_2P_2O_7$ under reaction mixture [38]. It was found that the crystalline structure of $VOHPO_4.0.5H_2O$ rapidly collapsed to form an oxidized amorphous phase within an hour followed by slow crystallization to $(VO)_2P_2O_7$. This is accompanied by the formation of sharply angular nano-sized crystallites (about 50 nm). Interestingly, no crystalline phases other than $(VO)_2P_2O_7$ were formed during this transformation, which is quite different from the transformation of large and thick $VOHPO_4.0.5H_2O$ crystallites, in which $VOPO_4$ phases have been commonly detected in the resulting catalyst [5].

1.5 The phosphorus to vanadium ratio of the catalyst

Most of the commercial catalysts have been characterised with a slight excess of phosphorus, usually P/V ~1.1 [39]. It has been observed that part of the phosphorus sublimes during standard operation and methods for the replenishment of the catalyst with phosphorus have been reported without considerably interfering with the plant operation [40].

The enhancement of the phosphorus surface concentration has been demonstrated to have a beneficial effect on the performance of VPO catalysts [41]. Some studies [42] claim that a significant excess of surface phosphate (P/V=1.5-3.0) could prevent the bulk oxidation of $(VO)_2P_2O_7$ to the $VOPO_4$ phases, which was characterised by XPS.

Matsuura *et al* [42], suggested that the excess phosphate terminates the side faces of the (200) plane of $(VO)_2P_2O_7$ (i.e. 001, 021, etc.) in the form of the surface $VO(PO_3)_2$ phase, which prevents the oxidation of vanadyl pyrophosphate $(VO)_2P_2O_7$ due to lower oxidizability of $VO(PO_3)_2$. This show the right compromise between reducibility and oxidizability needed in the final catalyst to obtain both high activity and selectivity in *n*-butane oxidation.

However, it is quite clear from a large number of studies that phosphorus in excess of the 1:1 stoichiometric ratio is important for the selective oxidation of n-butane, especially for catalyst prepared in aqueous media. Additionally, phosphorous is added in industrial application to maintain P:V ratios.

1.6 Promoted catalysts

Most of the industrial vanadium phosphates catalysts rarely use a bulk phase. The activity of vanadium phosphates is often enhanced by the addition of low concentrations of metal cations known as promoters, which can act as texture promoters or improve the activity and selectivity of the active catalyst.

The nature, the location and the roles of metal promoters on vanadium phosphate catalysts have been widely reviewed [43,44]. Hutchings [43] has provided an extensive review of most of the promoters addressed in the patent literature. A broad series of promoters have been added to vanadium phosphate catalysts and a beneficial effect has been claimed with Co, Cd, Ni, Bi, Cu, Zn, Zr, Li, Mg, Ti, La, Mo, Nb, B, Fe, Cr, Ce, Pt, W and Ga. These promoters can act in two ways:

- Promoting the formation of the required VPO phases or avoid the formation of spurious phases
- To enable the formation of solid solutions with the active phase and can regulate the catalytic activity.

However, some promoters can act in a different way depending on their interaction with VPO phases and loading preparation methods. A brief introduction to most published papers concerning this point is illustrated.

Sajip *et al* [45] investigated the effect of Co and Fe ions added during the preparation of the catalyst precursor $VOHPO_4.0.5H_2O$ on n-butane oxidation to maleic anhydride. At low levels, both Co and Fe significantly improved the selectivity and intrinsic activity in maleic anhydride formation. They found that the selectivity to maleic anhydride at 25 % n-butane conversion was 63 mol. % for the promoted phases and only 50 mol. % for the unpromoted VPO catalyst at 673 K. It was proposed that Co was insoluble in the $(VO)_2P_2O_7$ phase. It was suggested that the origin of the effect of Co is related to its interaction with the disordered VPO phase. In contrast, Fe ions may be soluble in the $(VO)_2P_2O_7$ lattice and, consequently, it can act as an electronic promoter for this phase,

most likely enabling the re-oxidation of the catalyst or aiding oxygen mobility. It is also possible that Fe is associated with the disordered phase and could act in a similar manner with this material.

Zazhigalov *et al.* modified the redox properties of the VPO catalysts by incorporating metallic Co in the catalyst precursor. It was reported from their study that presence of Co increases the content of phosphorus at the surface, which modifies the surface acidity and in turn improves the selectivity for n-butane oxidation. In addition, Cobalt stabilizes the catalyst performance by forming cobalt phosphate, which reduces phosphorus losses, improves its catalytic properties and prolongs its lifetime [46].

Zazhigalov *et al* also studied a range of alkali and alkaline-earth metal ions as promoters on VPO catalysts [47]. They found that Li, Na, K, Cs, Be, Mg, Ca and Ba cations present at different concentrations, simply donated electrons to the VPO catalysts with P/V ratios of 1.07 and 1.20, leading to increased negative charge on lattice oxygen atoms of the catalyst and improving the butane conversion. The presence of these promoters caused an increase of the surface P/V ratio and corresponding changes of the surface acidity. However, the preparation of a catalyst characterized by high activity in n-butane oxidation and high selectivity to maleic anhydride still needs improvement of the basicity of surface oxygen atoms to facilitate the activation of n-butane and the surface acidity to control the residence times of the reaction intermediates.

Beatriz *et al* [48] studied the promoting effect of some elements (Cr, Mo and W) added to the catalyst precursor $VOHPO_4.0.5H_2O$ using different methods and loads. Cr, Mo or W were either impregnated on catalyst precursor or co-precipitated during the precursor

synthesis. It was found that the addition of the promoters consistently increased the catalytic activity, but in every case there was an optimum load to achieve the best selectivity. They proposed that the reason for this maximum could be attributed to the right balance between the presence of very strong Lewis acid sites and the development of V^{5+} ($VOPO_4$ phases) isolated sites in the matrix of the active phase $(VO)_2P_2O_7$.

Lopez-Nieto *et al* [49] reported the incorporation of Bi in the VPO catalysts. It is found that Bi promoter led to a modification in the surface properties that resulted in improved catalytic performance. They claim that the incorporation of Bi stabilised the active phase $(VO)_2P_2O_7$ structure and led to an increase in the specific surface area, which enhanced the rate of n-butane oxidation.

Taufiq-Yap *et al* [50] studied the addition of Bi and Fe in three different methods: (i) during the refluxing $VOPO_4{\cdot}2H_2O$ with isobutanol, (ii) the simultaneous addition of BiFe oxide powder in the course of the synthesis of precursor $VOHPO_4.0.5H_2O$ and (iii) the mechanochemical treatment of precursor $VOHPO_4.0.5H_2O$ and Bi, Fe oxide in ethanol. It was found that surface area of the modified catalysts had increased except with the simultaneous addition. They concluded that the conversion of *n*-butane decreases with the increase of oxygen species associated with V^{5+}.

More recently, Sartoni *et al* [51] studied gallium promoted on vanadium phosphate catalyst precursor for the mild oxidation of n-butane to maleic anhydride. It was found that Ga promoter "at low concentrations" ($Ga/V \leq 1\%$) improved the crystallinity of the hemihydrates ($VOHPO_40.5H_2O$) precursor phase and increased its surface area comparative to the undoped material. They also found that the presence of Ga

considerably shortens the activation time required to convert the hemihydrates precursor into a well-crystallized vanadyl pyrophosphate $(VO)_2P_2O_7$ phase under reaction condition. In contrast, Ga at high concentrations (Ga/V ≈ 5%), which could be found as a $GaPO_4$ impurity phase, has a detrimental effect on the catalytic performance of the Ga promoted on VPO catalyst.

1.7 Preparation of catalyst precursors $VOHPO_4.0.5H_2O$

The active vanadium phosphate catalysts are commonly obtained by activating the catalyst precursor $VOHPO_4 \cdot 0.5H_2O$ under reaction conditions. This transformation is believed to be topotactic [32]. For this reason, it is of great importance to distinguish between $VOHPO_4 \cdot 0.5H_2O$ precursor prepared via different preparation methods and also to focus on finding new preparative routes for the preparation of the precursor. $VOHPO_4 \cdot 0.5H_2O$ precursor can be prepared via three different preparation methodologies [5].

The VPA method (vanadium phosphate catalyst prepared in aqueous media)

This was used in early patents and involved the use of water as solvent [52]. In this method V_2O_5 is refluxed with hydrochloric acid and in this step V^{5+} is reduced to V^{4+}. H_3PO_4 is then added to the solution (P: V molar ratio ≥ 1.0). This is commonly referred to as the VPA route (Figure 1.8).

$$V_2O_5 + HCl \xrightarrow[(2)\ H_3PO_4]{(1)\ \Delta,\ 2h} VOHPO_4 \cdot 0.5H_2O$$

Figure 1.7- The VPA preparative route.

Other aqueous routes have been used by a number of groups in order to prepare $VOHPO_4 \cdot 0.5H_2O$. Oxalic acid [53], phosphorus acid [54] and $NH_2OH.HCL$ [55] have been reported as reducing agents as an alternative to HCL. However, significant amounts of impurity $VO(H_2PO_4)_2$ are also obtained during the preparation. In addition, this method gives low surface area $VOHPO_4 \cdot 0.5H_2O$ precursors, which lead to lower activity for n-butane oxidation.

The VPO method (vanadium phosphate catalyst prepared in organic media)

In the late 1970s catalyst precursor prepared in organic media became ever more popular. This method is considered to be the standard preparation method and is commonly used in most academic studies [33, 56]. In this method an alcohol is used as a reducing agent and solvent instead of aqueous HCl. V_2O_5 and H_3PO_4 (P: V molar ratio $\geq$ 1.0) are refluxed in an alcohol (alcohol: V molar ratio $\geq$ 50) and a blue $VOHPO_4.0.5H_2O$ precipitate is obtained. A range of alcohols has been used in this preparation but isobutanol is the most common [5]. This is usually referred as the VPO preparative route (Figure 1.8).

$$V_2O_5 + H_3PO_4 + \text{alcohol} \xrightarrow{\Delta,\ 16h} VOHPO_4.0.5H_2O$$

Figure 1.8- The VPO preparative route.

The VPD method (vanadium phosphate catalyst prepared in organic media via $VOPO_4.2H_2O$)

This method was first unveiled by Horowitz *et al* [56] and later described by Johnson *et al* [33]. In this method the preparation involves the reaction of V_2O_5 with H_3PO_4 with water as solvent. This leads to the formation of the V^{5+} phase $VOPO_4.2H_2O$. The $VOPO_4.2H_2O$ is recovered and dried and then refluxed in a second stage with an alcohol as reducing agent to form the $VOHPO_4.0.5H_2O$.

$$V_2O_5 + H_3PO_4 \xrightarrow{H_2O} VOPO_4.2H_2O \xrightarrow{\text{alcohol}} VOHPO_4.0.5H_2O$$

Figure 1.9- The VPD preparative route.

In view of the importance of the morphology of the catalyst precursor, there have been several published studies concerning this topic. Commonly, V_2O_5 is used as a source of vanadium and H_3PO_4 is used as source of phosphorus. Therefore, a reducing agent is required to synthesise the V^{+4} precursor phase. A number of reducing agents and solvents have been used [57]. Early catalyst preparations (VPA method) used water as the solvent, but recently most studies have concentrated on the use of alcohols (VPO and VPD preparative routes) as they result in better catalysts.

Hutchings *et al* reported a comparative study of catalyst precursors prepared via the VPD route with different alcohols [58]. It was found that the catalyst precursors prepared with secondary alcohols had a similar morphology (platelets morphology) and surface area common to VPO catalyst precursors. The catalyst precursors prepared with primary alcohols presented rosette morphology with a high surface area of the catalyst ($40m^2/g$) and were found to be highly active and selective for n-butane oxidation to maleic anhydride compared with the platelets.

1.8 Preparation of other VPO phases

1.8.1 Preparation of $VO(H_2PO_4)_2$

It is generally accepted that the most active and selective catalyst for the oxidation of n-butane to maleic anhydride, is derived from the catalyst precursor $VOHPO_4.0.5H_2O$. However, a number of vanadium phosphate compounds have been reported to be fairly effective catalysts for this reaction. Although a lower activity and selectivity than $(VO)_2P_2O_7$ the $VO(H_2PO_4)_2$ phase, (defined as phase E in this thesis) has been determined to be an impurity formed during the preparation of the catalyst precursor. Ellison *et al.* formed $VO(H_2PO_4)_2$ via a VPD preparation using 3-octanol as the reducing agent [59]. It was reported that phase E has a negligible activity and selectivity under standard reaction conditions [60].

$$VOPO_4.2H_2O + \text{3-octanol} \xrightarrow{\Delta,\ 16h} VO(H_2PO_4)_2$$

Sananés *et al.* [61] have also reported the preparation of $VO(H_2PO_4)_2$ by reacting V_2O_4 with H_3PO_4 using the method previously described by Bordes. [23]

Bartley *et al.* [62] reported the formation of $VO(H_2PO_4)_2$ from the reaction of aldehydes or ketones with V_2O_5 and H_3PO_4 whether aqueous (85%) or crystalline (100%) orthophosphoric acid. It is found that this phase $VO(H_2PO_4)_2$ has been observed with a broad range of aldehydes and ketones (C4–C10). They suggested that these findings supported the fact that the catalyst is derived from a crystalline precursor $VOHPO_40.5H_2O$, formed from the reaction of V_2O_5 and H_3PO_4 with an alcohol. The

alcohol is oxidised to give an aldehyde or ketone as a result of the reaction. The presence of these aldehydes and ketones in the mixture will lead to the formation of $VO(H_2PO_4)_2$ as an impurity. This led to an effect on the final catalyst $VO(PO_3)_2$ and its performance for the selective oxidation of n-butane to maleic anhydride.

1.8.2 Preparation of $VOPO_4$ phases

Some of V^{5+} phases, mainly $VOPO_4$ phases, have been observed in the active catalyst [35-37]. However, the nature of their effect in the active catalyst has been the subject of significant debate in the literature as mentioned in the previous section (1.4.2).

The preparation of $VOPO_4$ phases: α_I- $VOPO_4$, α_{II}- $VOPO_4$, γ-$VOPO_4$, δ-$VOPO_4$ and β-$VOPO_4$ has been reported by Abdelouahab *et al.* [63] *via* calcinations of $VOPO_4.2H_2O$ and $VOHPO_4.0.5H_2O$ in air.

γ-$VOPO_4$, δ-$VOPO_4$ can be prepared by calcination of $VOHPO_4.0.5H_2O$ in air and α_I-$VOPO_4$, α_{II}-$VOPO_4$ can be prepared by calcination of $VOPO_4.2H_2O$ in air. β-$VOPO_4$ can be prepared by the decomposition of $NH_4(VO_2)_2PO_4$ in dry air. A summary of the preparation routes for $VOPO_4$ phases is presented in Figure 1.10. As described by Abdelouahab *et al.* [63]:

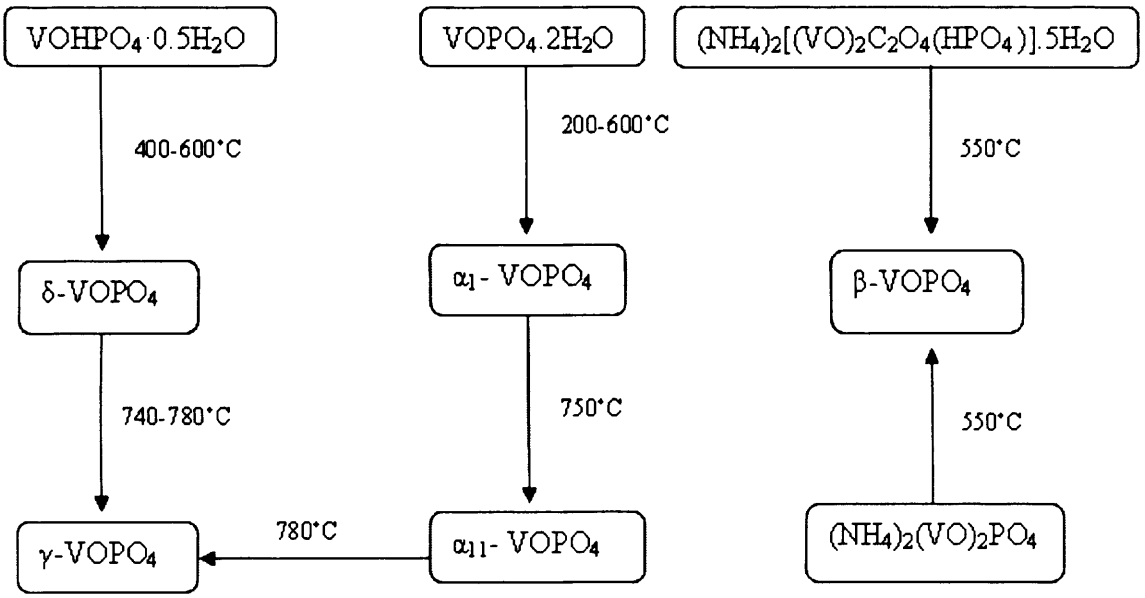

Figure 1.10- Preparation conditions of $VOPO_4$ phases described by Abdelouahab [66].

Bordes *et al.* also reported that some $VOPO_4$ phases could be prepared using oxo dehydration of $VOPO_4.2H_2O$ under a flow of dry air as shown below [23].

$$VOPO_4.2H_2O \xrightarrow{400°C} \alpha_I\text{- } VOPO_4 \xrightarrow{700°C} \alpha_{II}\text{- } VOPO_4 \xrightarrow{750°C} \beta\text{-}VOPO_4$$

1.9 Crystal structures of vanadium phosphate phases $VOPO_4.2H_2O$

The vanadium phosphate dihydrate, $VOPO_4.2H_2O$, has a layered structure in which the VO_6 octahedra and the PO_4 tetrahedra form V-O-P sheets by edge-sharing [64]. These sheets are combined by means of weak hydrogen bonding between the water molecules and the PO_4 groups of the sheet (Figure 1.11). Two water molecules are coordinated to vanadium in trans position to V=O and the remaining two are isolated in the channels

formed by the hydrogen bonding network (Figure 1.12. W1 and W2). The water molecules can be removed from the between the layers to give $VOPO_4$ phases.

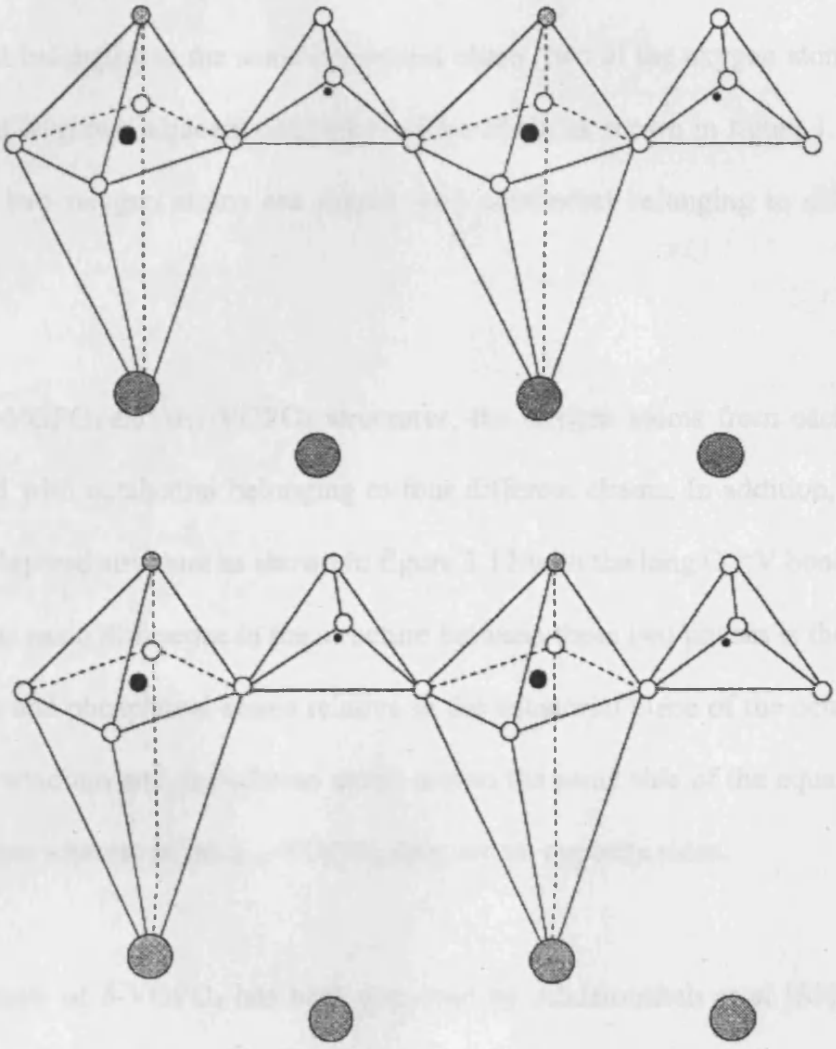

Figure 1.11-The crystal structure of $VOPO_4.2H_2O$.

[●= V, • = P, O= vanadyl oxygen, ●=O, ●= H_2O free or co-ordinated to vanadium]

The V^{5+} structures are consisted of VO_6 octahedra sharing each equatorial oxygen with different PO_4 tetrahedra. α_I-, α_{II} and β-$VOPO_4$ are made up of PO_4 tetrahedra and distorted VO_6 octahedra. In the β-$VOPO_4$ structure each PO_4 tetrahedron links two octahedral belonging to the same octahedral chain (two of the oxygen atoms of the PO_4 are shared with two adjacent octahedral of the chain as shown in figure 1.12. Whereas, the other two oxygen atoms are shared with octahedral belonging to different chains [56].

In the α_I-$VOPO_4$ and α_{II}-$VOPO_4$ structures, the oxygen atoms from each tetrahedron are shared with octahedral belonging to four different chains. In addition, these phases display a layered structure as shown in figure 1.12 with the long O·····V bonds linking the layers. The main difference in the structure between these two phases is the positions of vanadium and phosphorus atoms relative to the equatorial plane of the octahedra. In α_I-$VOPO_4$ vanadium and phosphorus atoms are on the same side of the equatorial oxygen atoms plane whereas in the α_{II}-$VOPO_4$, they are on opposite sides.

The structure of δ-$VOPO_4$ has been proposed by Abdelouahab *et al* [63] as shown in figure in Figure 1.12. The VO_6 octahedra are linked by oxygens of PO_4 tetrahedron as in α_I-$VOPO_4$ and α_{II}-$VOPO_4$ structures, but the V=O bonds of the linked octahedral sharing a floor are trans orientated towards each other.

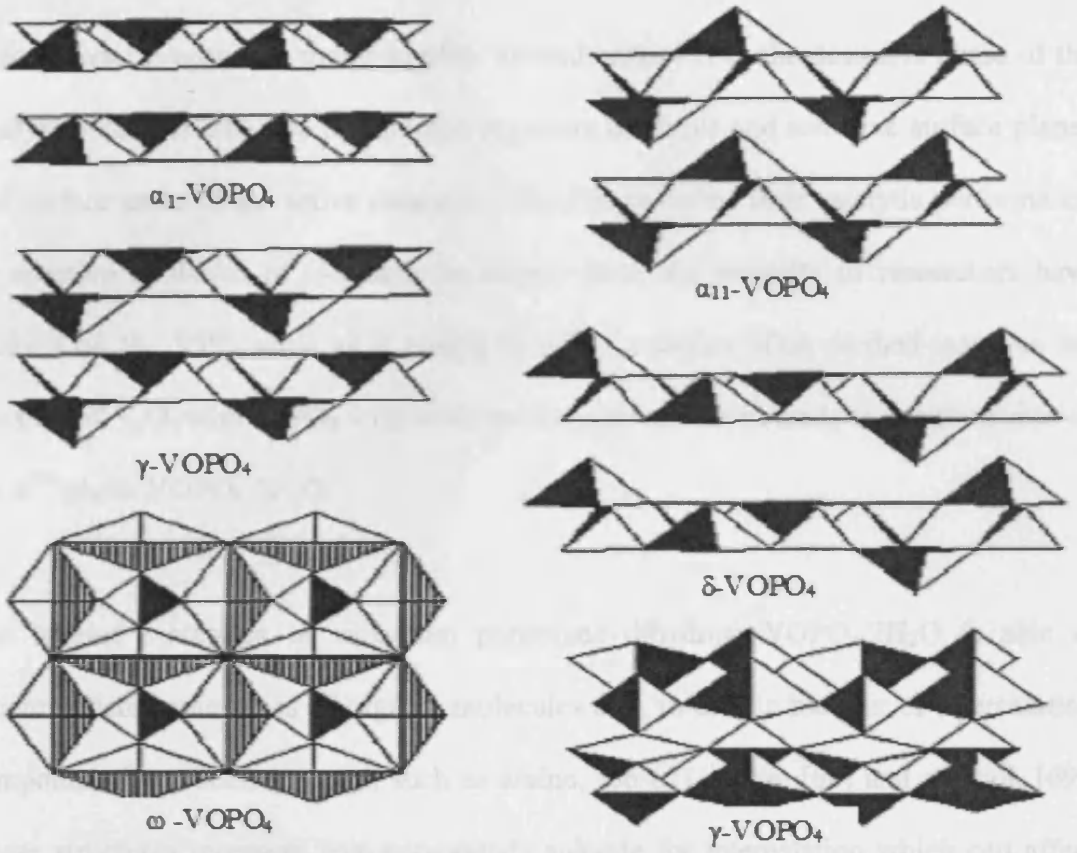

Figure 1.12- Schematic view of the different forms of $VOPO_4$. Square pyramids are VO_5, key: disordered ''double pyramids'' for the o-form) and tetrahedra are PO_4 [65].

The structures of γ-$VOPO_4$ is also proposed to be similar to that of δ-$VOPO_4$ with the difference of the V=O bonds in γ-$VOPO_4$ point in the same direction. Both δ-$VOPO_4$ and γ-$VOPO_4$ structures are proposed to have layered structure with different orientation of the V=O bonds (Figure 1.12 δ-$VOPO_4$ and γ-$VOPO_4$).

1.10 New preparative routes

Conventional preparation methods offer limited control over the desirable phase of the catalyst precursor and also preferential exposure of active and selective surface planes and surface areas of the active catalysts. All of these define their catalytic performance in selective oxidation of n-butane. In recent years, the majority of researchers have focused on the VPD route as it results in better catalysts. This method involves the reaction of V_2O_5 with H_3PO_4 with water as the solvent, which leads to the formation of the V^{5+} phase $VOPO_4.2H_2O$.

The layered structures of vanadium phosphate dihydrate $VOPO_4.2H_2O$ is able to accommodate some types of organic molecules and, to date, a number of intercalation compounds have been reported, such as amine, [66-67] amide, [68] and alcohol, [69]. These structures represent host compounds suitable for intercalation which can affect physical and chemical properties of the structures and can thus provide us with the possibility to obtain catalyst precursors with high surface area with improved activities for n-butane oxidation.

Iwamoto *et al.* [70] synthesised mesostructured vanadium phosphate compounds using alkyl-trimethyl ammonium surfactants. However, the mesostructure in the precursor phases was lost after activation for n-butane oxidation.

Doi and Miyake [71] have reported the synthesis of hexagonal mesostructured vanadium phosphate compounds from $VOHPO_4.0.5H_2O$ by surfactant intercalation and subsequent hydrothermal treatment. Nevertheless, these materials demonstrated very

low thermal stability under the reaction condition and low phosphorus content that are detrimental for their potential applications in n-butane oxidation.

Mount *et al.* have investigated the use of an autoclave reactor to produce $VOHPO_4.0.5H_2O$ from reacting V_2O_5 and H_3PO_4 in the presence of H_3PO_3 [72]. The catalysts obtained reported about 15% better yield of maleic anhydride than VPA catalyst. However, these results are lower than catalysts prepared in an organic route which are, therefore, still preferred.

Antonio *et al.* reported the synthesis of $VOHPO_4{\cdot}0.5H_2O$ using V_2O_4 and either H_3PO_4 or $H_4P_2O_7$ as a starting material with water as solvent. The surface area of the precursor was significantly enhanced when water was added as a solvent. From their study it was found that the catalytic performance data is comparable to other non-promoted vanadium phosphate catalysts [73].

More recently, Okuhara *et al.* reported the intercalation and exfoliation of $VOPO_4.2H_2O$ in primary and secondary alcohols [74]. This was achieved with stepwise heating at a low temperature and the subsequent reduction of the exfoliated $VOPO_4.2H_2O$. It was found that the $VOHPO_4.0.5H_2O$ precursor was obtained with a different morphology. In addition, the $(VO)_2P_2O_7$ obtained from the precursor was found to be highly active and selective for the selective oxidation of n-butane.

1.11 The aims of this study

It has been addressed that the catalytic activity of the active vanadium phosphate catalysts is dependent on the synthesis of the catalyst precursor. In addition, it has been mentioned earlier that the transformation of the catalyst precursor $VOHPO_4.0.5H_2O$ to the active phase $(VO)_2P_2O_7$ is repeatedly believed to be topotactic, which implies that the morphology of the final catalyst is controlled by the morphology of the precursor.

The preparation of the catalyst precursor $VOHPO_4.0.5H_2O$ is controlled by a number of factors such as vanadium phosphate sources, reducing agents, solvents, temperature and reaction time. Co-solvents can play important roles in the preparation of vanadium phosphate catalysts and only a few studies have focused on this work, mainly mixed alcohols have been used.

The first aim of the study, demonstrated in this thesis, is the study of precursor preparation method with an alkane as a co-solvent using $VOPO_4.2H_2O$ as starting material.

To the best of my knowledge, there has not been any report investigating the use of V-P-O seeds in the preparation of the catalyst precursor and their effects. Therefore, the second aim of the study is to investigate the effects of using V-P-O seeds in primary (1-octanol, iso-butanol) and secondary (2-butanol, 3-octanol) alcohols. The use of vanadium phosphate seeds will be discussed with a view to better understanding the formation of the catalyst precursor. A novel transformation of $VO(H_2PO_4)_2$ to catalyst precursor $VOHPO_4.0.5H_2O$ via seeding the reaction mixture will be investigated and discussed.

CHAPTER 1

Attempts to prepare new vanadium phosphate materials by the reduction of $VOPO_4.2H_2O$ using hydrogen in aqueous media and strong reducing agents (N_2H_4 and $NaBH_4$). A direct reduction of $VOPO_4.2H_2O$ at different temperatures will also be investigated.

1.12 References:

[1] Y. H. Taufiq-Yap, C. S. Saw, R. Irmawati Catal. Lett. 105 (2005)103.

[2] A. Cruz-Lo´pez, N. Guilhaume, S. Miachon, J. Dalmon. /Catal. Today 107 (2005) 949.

[3] R. L. Bergmann and N. W. Frisch, US Patent 3293268, (1966).

[4] J.K. Bartley, J. Lopez-Sanchez, G. Hutchings. Catal. Today 81 (2003) 197.

[5] G.J. Hutchings, J. Mater. Chem 14 (2004) 3385.

[6] Cavani, F. Trifiro`, Catalysis, 1994, 11, 246.

[7] P. Mars, D.W. van Krevelen, Chem. Eng. Sci. Spec. Suppl. 3 (1954), 41

[8] Y. H. Taufiq-Yap, B. H. Sakakini, K. C. Waugh, Catal. Lett. 46 (1997) 273-277.

[9] M Abon, K. E. Béré and P. Delichére, Catal. Today, (1997), 33, 15-23

[10] G. Centi, F. Trifiro` , J.R. Ebner, V.M. Franchetti, Chem. Rev.1988, 88, 55

[11] J.R. Ebner, M.R. Thompson, Catal. Today 1993, 16, 51.

[12] G. Centi, F. Trifiro` , G. Busca, J.R. Ebner, J. Gleaves, Faraday Disc. Chem. Soc. 1989,87, 215.

[13] V.A. Zazhigalov, J. Haber, J. Stoch, A.I. Pyatnitskaya, G.A. Komashko, V.M. Belousov, Appl. Catal. A 1993, 96, 135.

[14] J. Ziolkowski, E. Bordes, and P. Courtine. J. Mol., Catal., (1993), 84, 307-326

[15] J. Ziolkowski, E. Bordes. and P. Courtine. J. Catal., (1990), 122, 126-150

[16] B. Schiøtt, K. A. Jørgensen, Catal. Today,(1993), 16-79

[17] B. Schiøtt, K. A. Jørgensen, and R. Hoffmann, J. Phys. Chem., (1991), 95, 2297-2307

[18] Y. Zhang-lin, M. Forissier , R. P. Sneeden, J. C. Vedrine, J. C. Volta, J. Catal. 1994, 145, 256-266.

[19] Y. Zhang-lin, M. Forissier, J. C. Vedrine, J. C. Volta, J. Catal. 1994, 145, 267-275.

[20] P.A. Agaskar, L. DeCaul, R.K. Grasselli, Catal. Lett.1994, 23, 339.

[21] G. Centi, F.Trifiro` , J.R. Ebner, V.M. Franchetti, Chem. Rev.1988, 88, 55.

[22] G. Centi, Catal. Today 1993, 16, 1.

[23] E. Bordes, Catal. Today 1987, 1, 499.

[24] G.J. Hutchings, C.J. Kiely, M.T. Sananes-Schulz, A. Burrows, J.C. Volta, Catal. Today 1998, 40(2-3), 273.

[25] G. Centi, G. Fornasari, F. Trifiro, J. Catal. (1984), 89, 44-51.

[26] N. Harrouch-Batis, H. Batis, A. Ghorbel, J.C. Vedrine, J.C. Volta, J. Catal.1991, 128, 248.

[27] V.V. Guliants, J.B. Benziger, S. Sundaresan, I.E. Wachs, J.M. Jehng, J.E. Roberts, Catal. Today 1996, 28, 275.

[28] M. Hävecker, A. Knop-Gericke, R. W. Mayer, M. Fait, H. Bluhm, R. Schlögl, *J. Electron Spectrosc. Relat. Phenom.* 125 (2002) 79 –87

[29] G. Centi, F. Cavani, F. Trifiro, Selective Oxidation by Heterogeneous Catalysis. Fundamental and Applied Catalysis, Kluwer Academic/Plenum Publishers: New York, 2001.

[30] S. Albonetti, F. Cavani, F. Trifiro, P.Venturoli, G. Calestani, M. Granados, J. L. G. Lopez; Fierro, J. Catal.1996, 160, 1, 52.

[31] P. Ruiz, B. Delmon, Catal. Today 1987, 1, 2.

[32] L. M. Cornaglia, C. Caspani, E. A. Lombardo, Appl. Catal.1991, 74, 15.

[33] J. W. Johnson, D. C. Johnson, A. J. Jaceobson and J. F. Bordy, J. Am Chem. Soc., (1984), 106, 8123-8128.

[34] C. J. Kiely, A. Burrows, G. J. Hutchings, K. E. Bere, J. C. Volta, A. Tuel, M. Abon, Faraday Discuss. 105 (1996) 103

[35] G. J. Hutchings, A. Desmartin-Chamel, O. Oliver, J. C. Volta, Nature 348 (1994) 41.

[36] C.C. Torardi, Z.G. Li, H.S. Horowitz, W. Liang, M.-H. Whangbo, J. Solid State Chem.1995, 119, 2, 349.

[37] N. Ryumon, H. Imai, Y. Kamiya, T. Okuhara, Appl. Catal. 297 (2006) 73–80.

[38] H. Imai, Y. Kamiya, T. Okuhara H. Imai, Appl. Catal. 255 (2008) 213–219.

[39] M. O'Connor, F. Dason, B. K. Hodnett, Appl. Catal. 1990, 64, 161.

[40] B. K. Hodnett, Catal. Rev. Sci. Eng., (1983), 27, 373-425

[41] B. K. Hodnett, □Heterogeneous Catalytic Oxidation", John Wiley & Sons LTD, 2000, ISBN 0471489948

[42] I. Matsuura, M. Yamazaki, In New Developments in Selective Oxidation, G. Centi, F. Trifiro` , Eds.; Elsevier: Amsterdam, 1990, 563.

[43] G. J. Hutchings, Appl. Catal. 1991, 72, 1-32

[44] G. J. Hutchings,R. Higgins, J. Catal. 1996, 162,2, 153.

[45] S. Sajip, J.K. Bartley, A. Burrows, M.T. Sananes-Schulz, A. Tuel, J.C. Volta, C.J. Kiely, G.J. Hutchings, New J. Chem. 2001, 25,1, 125.

[46] V. A. Zazhigalov, J. Haber, J. Stoch, A. I. Pyatnitzkaya, G. A. Komashko, V. M. Belousov, Appl. Catal. 1993, 96, 135.

[47] V.A. Zazhigalov, J. Haber, J. Stoch, I.V. Bacherikova, G.A. Komashko, A.I. Pyatnitskaya, Appl. Catal. 1996, 134, 2, 225.

[48] B. T. Pierini, E. A. Lombardo, Catal. Today 107–108 (2005) 323–329

[49] B. Solsona, V. A. Zazhigalov, J. M. Lopez Nieto, I. V. Bacherikova, E. A. Diyuk, Appl. Catal. A, 2003, 249, 81.

[50] C.K. Goh, Y.H. Taufiq-Yap, G.J. Hutchings, N. Dummer, J. Bartley,Catal. Today 131 (2008) 408–412

[51] L. Sartoni, A. Delimitis, J. K. Bartley, A. Burrows, H. Roussel, J. Herrmann, J. Volta, C. J. Kielyc and G. J. Hutchings, J. Mater. Chem., 2006, 16, 4348–4360

[52] G. Centi, Catal. Today, 1994, 16.

[53] G. Poli, I. Resta, O. Ruggeri and F. Triifro, Appl. Catal., (1981), 1, 395-404

[54] G. J. Hutchings and R. Higgins, Appl. Catal., A, 1997, 154, 103.

[55] T. Shimoda, T. Okuhara and M. Misono, Bull. Chem. Soc. Jpn., (1985), 58, 2163-2171

[56] H. S. Horowitz, C. M. Blackstone, A. W. Sleight and G. Teufer, Appl. Catal., 1988, 38, 211.

[57] J. A. Lopez-Sanchez, L. Griesel, J K. Bartley, R P. K. Wells, A. Liskowski, D. Su, b R. Schlogl, J. Volta, and G. J. Hutchings. Phys. Chem., 5 (2003) 3525.

[58] G. J. Hutchings, M. T. Sananes, S. Sajip, C. J. Kiely, A. Burrows, I. J. Ellison, J. C. Volta, Catal. Today 1997, 33, 161.

[59] M. T. Sananes, I. J. Ellison, S. Sajip, A. Burrows, C. J. Kiely, J. C. Volta and G. J. Hutchings, J. Chem. Soc., Faraday Trans., 1996, 92, 1, 137.

[60] M. O, Connor, F. Dason and B. K. Hodnett, Appl. Catal., (1990), 64, 161-171.

[61] M. T. Sananes, G. J. Hutchings and J. C. Volta, J. Chem. Soc., Chem. Commun., (1994), 243-244

[62] J. K. Bartley, R. P. K. Wells and G .J. Hutchings, J. Catal. 195 (2000) 423

[63] F. Ben Abdelouahab, J.C. Volta, R. Olier, J. Catal. 148 (1994) 334.

[64] H. R Tietze, J. Aust. Chem. 1981, 34, 2035.

[65] N. Dupre, G. Wallez, J. Gaubicher and M. Quarton. / Journal of Solid State Chemistry 177 (2004) 2896–2902.

[66] K. Beneke, G. Lagaly, Inorg. Chem. 1983, 22, 1503

[67] T. Yatabe, M. Nakano,; G. Matsubayashi, J. Mater. Chem. 1998, 8, 699.

[68] M. M. Lara, L. M.;Real, A. J. Lopez, S. B. Gamez, A. R.Garcia, Mater. Res. Bull. 1986, 21, 13.

[69] L. Benes, V. Zima, K. E. Melanova, J. Inorg. Chem. 2001, 1883.

[70] T. Abe, A. Taguchi, M. Iwamoto, Chem. Mater.1995, 7, 1429.

[71] T. Doi, T. Miyake, Chem. Commun.1996, 1635.

[72] Ramon A. Mount and Harold Raffelson, assigned to Monsanto Company U.S.A patent 4,337,174 (1982).

[73] J. K. Bartley, J. A. Lopez-Sanchez, G. J. Hutchings, Catal. Today, 81 (2003) 197–203.

[74] N. Yamamoto, N. Hiyoshi, and T. Okuhara, Chem. Mater. 2002, 14, 3882-3888.

EXPERMINTAL DETAILS

2.1 Catalyst Preparation

2.1.1 Standard V-P-O catalysts

2.1.1.1 Preparation of $VOPO_4.2H_2O$

Vanadium phosphate dihydrate was carried out following the procedure described by Sananes *et al.* [1].

V_2O_5 (10g, Aldrich) and H_3PO_4 (60 ml, 85%, Aldrich) were refluxed in distilled water (120 ml) under reflux conditions for 24 hours. The yellow solid was recovered by vacuum filtration, washed with cold water (100 ml) and acetone (100 ml) and dried in air at 110°C for 24 hours.

2.1.1.2 Preparation of $VOHPO_4.0.5H_2O$ via $VOPO_4.2H_2O$ using high-pressure autoclave. (A route as defined in chapter 3)

The $VOPO_4.2H_2O$ (1 g) (V: alcohol = 1:50) was reacted with 1-butanol (23 ml) in an autoclave at 150°C (0 bars) for 24 hours. The resultant solid was recovered by vacuum filtration, and then washed with acetone (100 ml) and dried in air at 110°C for 24 hours.

2.1.1.2 Preparation of $VOHPO_4.0.5H_2O$ using co solvent method (D route as defined in chapter 3)

The $VOPO_4.2H_2O$ (1 g) was reacted with 1-butanol (23 ml) with octane (23 ml) in an autoclave at 150°C (0 bars) for 24 hours. The resultant solid was recovered by vacuum filtration, and then washed with acetone (100 ml) and dried in air at 110°C for 24 hours.

2.1.1.3 Preparation of $VOHPO_4.0.5H_2O$ using co solvent (C route as defined in chapter 3)

The $VOPO_4.2H_2O$ (1 g) (V: octane = 1:50) was reacted with octane (23 ml) in an autoclave at 150°C (0 bars) in the first step and then the materials reduced with 1-butanol in second step for 24 hours. The resultant solid was recovered by vacuum filtration, and then washed with acetone (100 ml) and dried in air at 110°C for 24 hours.

2.1.2 Preparation of $VOHPO_4.0.5H_2O$ by Seeding effect

2.1.2.1 Preparation of $VOHPO_4.0.5H_2O$ using 1-octanol

The $VOPO_4.2H_2O$ (2g) was refluxed in 1-octanol (100ml) for 24 hours at (different temperatures). The resultant solid was recovered by vacuum filtration, and then washed with acetone (100 ml) and dried in air at 110°C for 24 hours.

2.1.2.2 Preparation of $VOHPO_4.0.5H_2O$ using alcohols by seeding with vanadium phosphate phases

The $VOPO_4.2H_2O$ (2g) was refluxed with $VOHPO_4 \cdot 0.5H_2O$ (rosette and platelet morphologies) or $VO(H_2PO_4)_2$ seeds (0.01, 0.05, 0.1g) in alcohol(1-octanol, isobutanol and 2-butanol) (100ml) for 24 hours at (185 °C) The resultant solid was recovered by vacuum filtration, and then washed with acetone (100 ml) and dried in air at 110°C for 24 hours.

2.1.2.3 Preparation of $VO(H_2PO_4)_2$ using 3-octanol

The $VOPO_4.2H_2O$ (2g) was refluxed in 3-octanol (100ml) for 24 hours at (different temperatures). The resultant solid was recovered by vacuum filtration, and then washed with acetone (100 ml) and dried in air at 110°C for 24 hours.

2.1.2.4 Preparation of $VOHPO_4.0.5H_2O$ using 3-octanol by seeding with $VOHPO_4.0.5H_2O$ (rosette and platelets).

The $VOPO_4.2H_2O$ (2g) was refluxed with $VOHPO_4 \cdot 0.5H_2O$ (rosette and platelets morphology) seed (0.01, 0.05, 0.1g) in 3-octanol (100ml) for 24h at (172 °C) The resultant solid was recovered by vacuum filtration, and then washed with acetone (100 ml) and dried in air at 110°C.

2.1.3 Preparation of $VOHPO_4.0.5H_2O$ by new route using hydrogen as reducing agent in water

The $VOPO_4.2H_2O$ (1g) was reacted in (30ml) water under hydrogen pressure in autoclave at 150 °C for 24 hours. The resultant solid was recovered by vacuum filtration, and then washed with acetone (100 ml) and dried in air at 110°C for 24 hours.

2.1.4 Direct reduction of $VOPO_4.2H_2O$ to $(VO)_2P_2O_7$

This experiment was carried out on the dihydrate $VOPO_4 \cdot 2H_2O$ material on attempt to reduce the V(V) phase ($VOPO_4 \cdot 2H_2O$) to vanadyl pyrophosphate vanadium (IV) phase.

Dihydrate $VOPO_4 \cdot 2H_2O$ (1g) was heated to different temperatures (250, 350, and 450°C) with 5% hydrogen flow in argon (50 cm^3 $min.^{-1}$) for 24 hours.

2.1.5 The reaction of $VOPO_4.2H_2O$ with strong reducing agents

2.1.5.1 The reaction of $VOPO_4.2H_2O$ with Hydrazine (N_2H_4)

The VOPO4.2H2O (1g) was refluxed with (10 ml hydrazine 51%) (1:30 mole ratio) in water (30ml) at different time (30 minutes, 2, 6 and 24 hours). The resultant solid was

recovered by vacuum filtration, and then washed with acetone (100 ml) and dried in air at 110°C for 24 hours.

2.1.5.2 The reaction of $VOPO_4.2H_2O$ with $NaBH_4$

The $VOPO_4.2H_2O$ (1g) was refluxed with (2g NaBH4) in 30ml ethanol (1: 12 mole ratio) at different time (30 minutes, 2, 6 and 24 hours). The resultant solid was recovered by vacuum filtration, and then washed with water (100 ml) and acetone (100 ml) and dried in air at 110°C for 24 hours.

2.2 Catalyst testing

A number of selected catalyst precursors were tested for the selective oxidation of n-butane to maleic anhydride. The reaction took place in a continuous flow microreactor placed inside a cylindrical furnace as shown in Figure 2.1. Mass flow controllers feed the reactant gases to the microreactor and the products are analysed by on-line gas chromatography before collection in a glass tube. These were carried out in the instrument schematically shown below in Figure 2. 1.

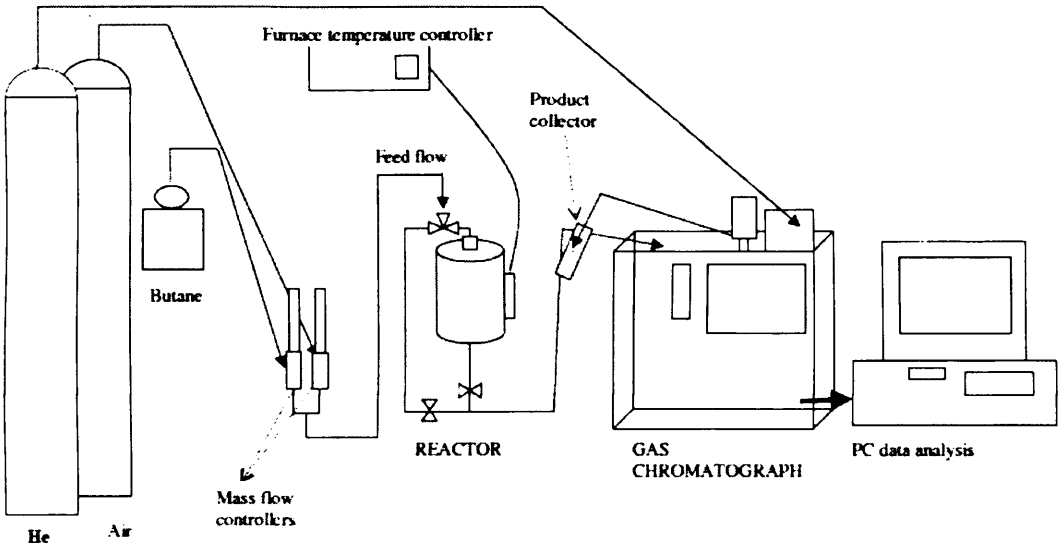

Figure 2. 1. Schematic diagram of the reactor system used for catalysts testing of n-butane to maleic anhydride.

2.2.1 Microreactor

The feed gases, butane (BOC, 99.95%) and air (BOC) were passed into the system through Brooks 5850TR mass flow controllers (butane 0-3 ml min^{-1}, air 0-100 ml min^{-1}) set by a multi-channel control box (Brose 5878). The gas flow rate was controlled using mass flow controllers (Brooks Mass Flow 5850 Series) and flow rate was measured by a digital flow meter.

All the lines are made from (1/4") stainless steel. The reactor exit lines are heated with heating tape to avoid the condensation of the reaction products. The reactor tube consisted of 3/8" stainless steel with the catalyst held in the centre of the tube by holding it on quartz wool. Typically, the catalyst occupied a volume of approx. (0.3 ml). The reactor is heated by a furnace (LPC Elements) controlled by a Eurotherm controller. The exit gas flowed through the heated lines to the on-line gas chromatograph.

2.2.2 Experimental procedure

Catalyst powder was pressed (5 tons) and sieved (250 μm – 1mm) in order to obtain pellets, 0.2 g. (approx. 0.3ml) of precursor was placed in the centre of the reactor tube for evaluation. All catalysts precursors were activated in situ under the following reaction conditions. Precursors were activated for a minimum period of time of 72 hours or until stable conversion and selectivities were observed. The activation conditions were normally:

- Feed flow rate of (10 ml/min) with 1.7% of butane in air
- A gas hourly space velocity (GHSV) of 2000 h^{-1} which can be defined as a GHSV = (volumes of feed as gas at STP/hr) / (volume of the reactor or its content of catalyst)
- Testing reaction temperature of 400°C with a temperature ramp of 3°C/min.

2.2.3 Product analysis

The product analysis was carried out by using a Varian 3400 gas chromatograph. The instrument is programmed to automatically make an injection at intervals of 34 minutes approximately, so that a detailed profile of the composition of the exhaust gases can be obtained as a function of time.

The GC used helium as the carrier gas, and two columns were used to separate the components of the gas mixture. CO_2, n-butane and maleic anhydride were eluted from a Porapak Q (PQ, 2m x 2mm i.d.) while O2, N2, and CO were eluted in a Molecular sieve

13X (MS13X, 2m x 2mm i.d.). A thermal conductivity detector (TCD) was used for the detection and quantification of the products and un-reacted gases.

In the 3400 GC chromatograph varian, the sample loop (250 μL) is constantly filled with the reactor effluent mixture. When an injection takes place, the carrier gas (helium) injects the gases contained in the sample loop into the Porapak Q which is connected in series to the molecular sieve column (both kept at 80°C). After 0.9 minutes the molecular sieve column is parked, at this time, the lighter gases (O_2, N_2 and CO) have been eluted from the Porapak Q to a molecular sieve and are retained on the latter column. CO_2 and H_2O are now eluted from the Porapak Q and detected for analysis. The molecular sieve is re-connected and O_2, N_2 and CO are now eluted to the detector. When CO is finally eluted, the molecular sieve is bypassed again and the temperature of the oven is heated to 220°C with a ramp of 50°C/min. This allows a quick elution of the un-reacted butane and finally the elution of maleic anhydride from the Porapak Q. The retention times are shown in Table 2. 1.

Table 2. 1. The retention times of the main products

Entry	Eluted product	Retention Time (min)
1	carbon dioxide	0.90
2	oxygen	4.40
3	nitrogen	5.50
4	carbon monoxide	10.15
5	*n*- butane	13.6
6	maleic anhydride	26

A TCD detects the difference between the heat capacities of a reference gas flow (carrier gas, He) and the sample gas flow (reactor products plus carrier gas). Differences in the heat capacities of different compounds mean that the results need to be corrected with a response factor (RF). The peaks are integrated and the numeric value of each integrated peak is divided by the relative response factor of the compound. The result is the true response values. The response factors of the products were obtained from Dietz et al. [2]. Normalising the true response values gives the volume percentage of each compound. The carbon mass balances were approximately 94 to 106 for all catalytic testing results presented.

All the products formed were identified according to the chromatogram retention time observed (Table 2. 1). For each tested sample, conversion, selectivity and carbon mass balances were calculated and plotted as function of time on line (T.O.L). The conversion of butane at a specific time was obtained by dividing the difference between the response value of the butane peak when no reaction takes place and its value at that specific time by the response value of the butane peak when no reaction takes place. To obtain the response value of butane in the feed flow (blank run), the reactor was cooled to 200°C after each catalytic test and measurements taken for several runs. The selectivity was defined as the amount of product formed divided by the total amount of products formed and corrected for molar ratios.

An example calculation for specific activity and intrinsic activity for each catalyst presented in thesis is illustrated as follow:

Sample A (Table 3.6)	
Surface area (m^2/g)	32
n-butane Conversion (%)	50
MA Selectivity (%)	61
Gas mixture	1.7
Flow rate (ml/min)	10
Butane volume (ml/min)	0.17

To calculate the maleic anhydride volume = butane volume × MA Selectivity (%) × n-butane Conversion (%)

= 0.17 × (61/100) × (50/100) = 0.05185 ml /min MA

From the gas flow

Number of moles MA = (0.05185 ml/min × 1 atom) / ((82.06 $cm^3.atom.K^{-1}.mole^{-1}$) × 673 K) = 9.4×10^{-7} mole MA /min

= $9.4\times10^{-7}\times60 = 5.63\times10^{-5}$ mole MA/h

Therefore, the specific activity = 5.63×10^{-5} mole MA/h / 0.2 g of catalyst = 2.8×10^{-4} mole MA/g/h

And intrinsic activity can be expressed as follow

= (2.8×10^{-4} mole MA/g/h) / ($32m^2/g$) = 8.8×10^{-6} mole $MA/m^2/h$.

2.3 Experimental techniques

A variety of experimental and characterisation techniques have been used in the characterisation of heterogeneous catalysis to determine their physical and chemical properties. It this study, a number of these techniques has been used to characterise the prepared catalyst precursors.

2.3.1 X-ray powder diffraction (XRD)

X-ray diffraction (XRD) is well-known as a powerful technique for the characterisation of crystalline materials. It is extensively used as a characterisation technique for heterogeneous catalysis and VPO materials in particular. XRD allows the identification of crystalline samples, but cannot detect phases with crystallite size lower than 20Å. When the X-rays strike the powdered sample, parts of them are reflected off the crystal plane with the angle of reflection equal to the angle of incidence. When Bragg's law (equation 2.1) is satisfied, the reflected beams interfere constructively and a diffracted beam is produced (Figure 2.2).

Equation 2. 1. $n\lambda = 2d \sin\theta$

Where n is an integer, λ is the X-ray wavelength, d is the spacing between the crystal planes and θ is the Bragg diffraction angel.

If the angle of incidence does not satisfy Bragg's law, a destructive interference is occurring and therefore it will not be detected.

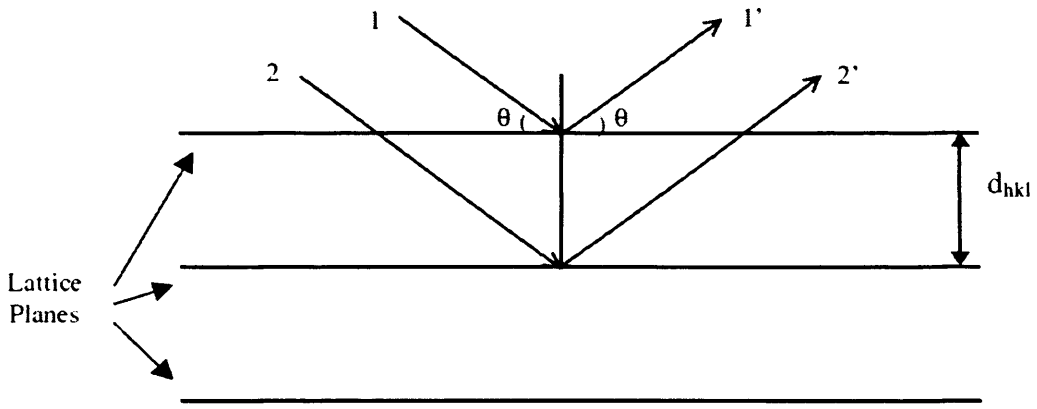

Figure2.2.- Bragg's angle and incident beam.

The X-ray diffraction experiment requires an X-ray source, a sample, and a detector to pick up the diffracted X-rays. In this study, a Panatytical X-ray diffacrtomete generating CuKα radiation was used for the XRD analysis of the samples. Samples were ground into powder using mortar and pestle (in order to insure that sufficient grain of the various compounds contribute to the reflection of the beam) and placed in a sample holder. The X-ray generator was set at 40 mA current and 40 kv tension. Each sample was scanned from $2\theta = 5$ to 80.

Diffraction data was collected for a certain time. Most of the precursors described in this thesis displayed very well resolved diffraction patterns in a few minutes, and a 30 minutes accumulation time was established. All the reflections obtained were compared with the reference VPO phases reported in the literature [3, 4] and a typical example of XRD pattern for the $VOPO_4.2H_2O$ prepared via standard route is shown in figure 2.3.

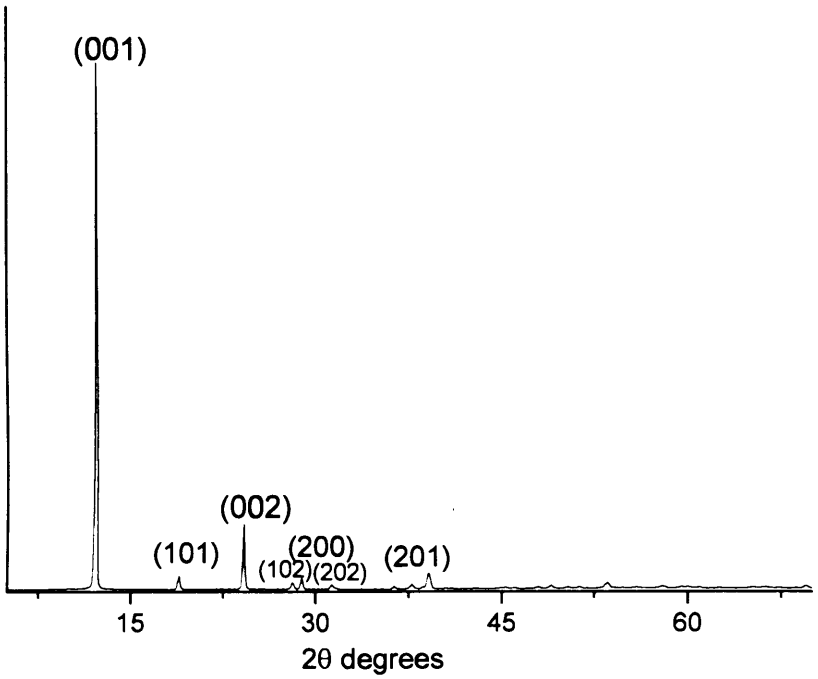

Figure 2.3 – A typical powder diffraction pattern of $VOPO_4.2H_2O$ prepared via standard roure.

Table 2.2 - The XRD reflexions of $VOPO_4.2H_2O$ prepared [d-calc=calculated d-spacing, d-obs= observed d-spacing, I/I_0 = relative intensity]

$VOPO_4.2H_2O$ [4]		$VOPO_4.2H_2O$ (prepared)	
HKL	d-calc	d-obs	I/I_0
001	7.40	7.27	100
101	4.75	4.69	5
002	3.70	3.67	13
102	3.18	3.17	3
200	3.10	3.09	5
201	2.86	2.85	3
202	2.378	2.38	2

One of the limitations of XRD is the lack of sensitivity. Some materials contain small amount of other phases as minor phase that cannot be detected by XRD. Therefore,

XRD is used with other characterisation techniques (Raman spectroscopy and Electron microscopy) to achieve a clear picture of catalyst structure and nature.

2.3.2 Laser Raman spectroscopy (LRS)

Laser Raman spectroscopy (LRS) has become one of the most useful characterisation techniques in particular for investigating vanadium phosphate catalysts [5]. Extensive work has been done for the characterisation of VPO materials with this technique. A numbers of VPO phases involved in the preparation of catalyst precursors can be distinguished and identified by using this technique.

The Raman effect occurs when a molecule is subjected to an electromagnetic field of radiation of frequency ν. Through the irradiation, the incident light excites molecules in the sample, which therefore scatter the light. Scattering can either be elastic or inelastic. The elastic manner is known as Rayleigh scattering while the inelastic is known as Raman scattering. In Rayleigh scattering, the emitted photon has a wavelength similar to the incident photon. As a result of the inelastic collision between the incident photon and the molecule, the vibration energy of the molecule is changed by an amount ΔE_m.

Equation 2.2. $\mathbf{h\nu_i - h\nu_s = \Delta E_m}$

Where $h\nu_i$ is the energy of the incident photon and $h\nu_s$ is the energy of the scattered photon.

The energy of the scattered photon ($h\nu_s$), must be different from the energy of the incident photon ($h\nu_i$) by the amount equivalent to ΔE_m

If the molecule gains energy, ΔE_m is become positive, giving rise to Stoke Radiation. If the molecule loses energy, ΔE_m is become negative, giving rise to anti-Stoke Radiation.

As shown in figure 2.4 the vibrational energy levels of the molecule. The energy increase or decrease from the excitation depending on the vibrational energy spacing in the ground electronic state of the molecule and therefore the wavenumber of the stokes and anti-stokes lines are a straight measure of the vibrational energies of the molecule. Typically, anti-stokes lines are particularly less intense compared with stoke lines.

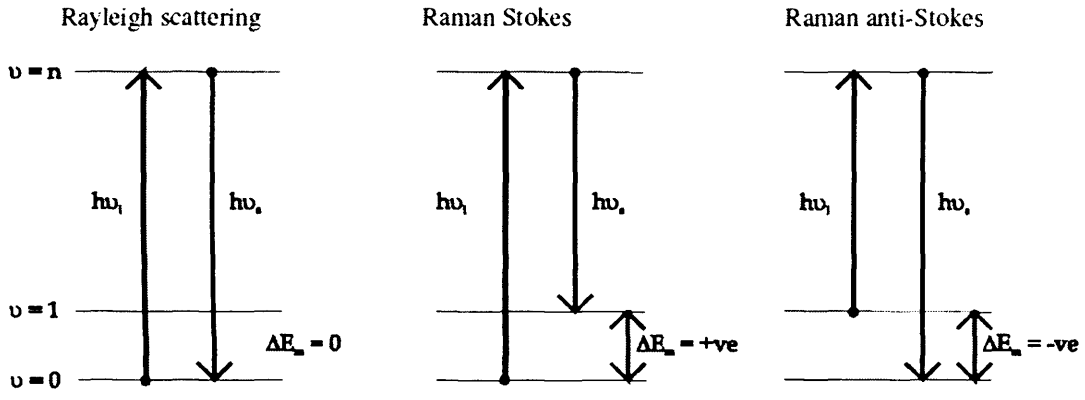

Figure 2.4- Raman and Rayleigh scattering.

This process is called elastic scattering or Rayleigh effect (Figure 2.4). In a minornumber of cases, the excited molecule fall to a different energy level than their initial one. In that case inelastic collision between the molecule and the incident photon has occurred. This is the Raman effect and photons will be re-emitted with different frequency than they had when adsorbed. If the exited molecule falls into a lower level of energy from their initial one, the emitted photons will have higher frequency than the incident photons and Raman anti-Stokes scattering is produced. In contrast, the exited

electrons might fall into a higher energy level, the molecule gains energy, and photons will be emitted with lower frequency. Raman Stokes scattering takes place.

The Raman spectra of all samples were obtained using a Renishaw system 1000 Raman microscope (Figure 2.5). An argon ion laser (514.532 nm) was used as an excitation source. All the samples were used in a fine powder and were placed on a microscope slide. An optical system directs the laser light onto the sample and collects and analyses the returning light. The optical signals produced by the sample are detected by a charge couple device (CCD) camera and the laser was focused onto the sample by means of an Olympus BH2-UMA microscope.

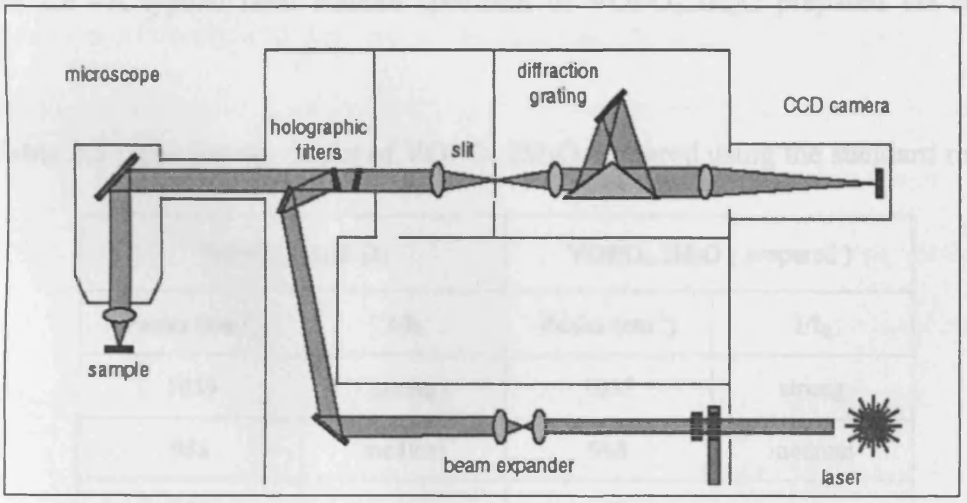

Figure 2. 5- Schematic diagram of. Laser Raman spectroscopy (LRS)

The spectra obtained in this study were compared with the reference VPO phases reported in the literature [3, 5] and a typical example of Raman spectrum for the $VOPO_4.2H_2O$ prepared via standard route is shown in figure 2.6.

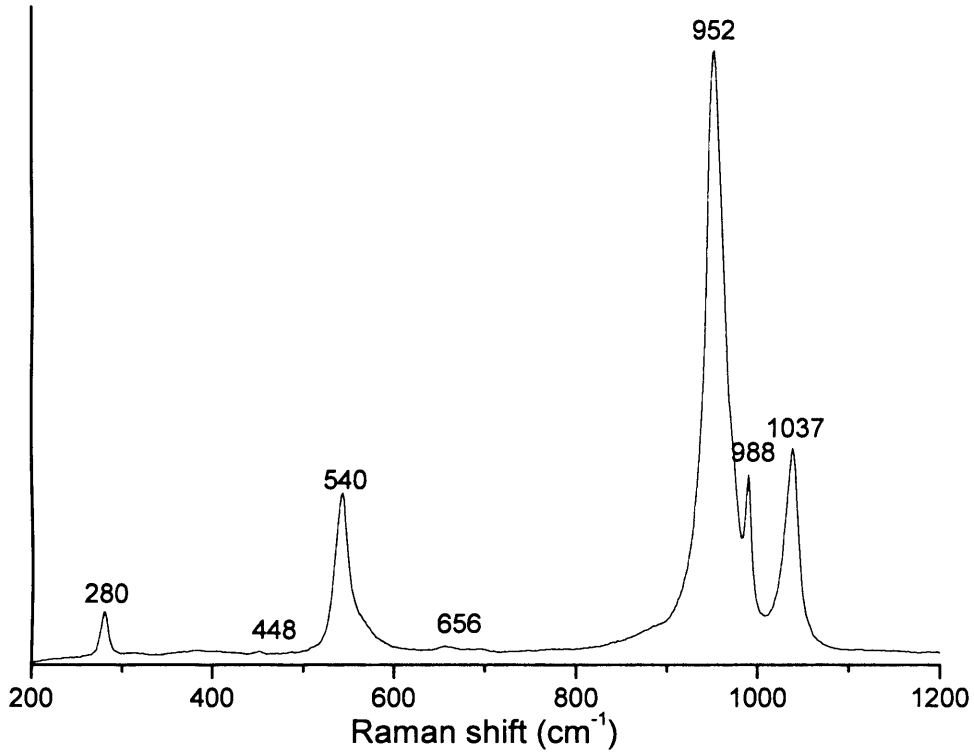

Figure 2.6 –A typical laser Raman spectrum of $VOPO_4.2H_2O$ prepared via standard route.

Table 2.3 - The Raman peaks of $VOPO_4.2H_2O$ prepared using the standard route

$VOPO_4.2H_2O$ [3]		**$VOPO_4.2H_2O$ (prepared)**	
Peaks (cm^{-1})	**I/I_0**	**Peaks (cm^{-1})**	**I/I_0**
1039	strong	1037	strong
988	medium	988	medium
952	very strong	952	very strong
658	weak	656	weak
542	strong	540	medium
451	weak	448	very weak
281	medium	280	medium

2.3.3 Electron microscopy (SEM and TEM)

Scanning Electron microscopy (SEM) can present a clear image of the material particles and determine their morphologies before and after catalysis. In addition, using the SEM can provide an image of the catalyst precursor particles, and also to estimate the amount of each individual phase present and its morphology.

The SEM uses a focused beam of high-energy electrons rather light to give an image with a high magnification. This technique has a great depth of field, which can allow a large amount of sample to be focus at the same time. Areas ranging from approximately 1 cm to 5 microns in width can also be imaged in a scanning mode using SEM technique. In the SEM electromagnets are used to bend an electron beam which is scanned over the sample to produce an image shown on a screen. This electron beam is produced by passing current in tungsten loop which works as cathode. A voltage is applied to the loop causing it to heat up and the anode which is a positive forms powerful attractive force for the electrons causing them to accelerate through the column of the microscopy. The beam in the column is condensed by a condenser lens and focused as a very fine spot on the sample by the objective lens. As the beam hits the sample, a backscattering take place. The backscattering electrons are been detected as a function of the position of the primary beam using a appropriate detector. The received signals are converted to voltage signal which is sent to viewing screen to create the image of the sample.

SEM images shown in this study were obtained using CARL ZEISS EVO 40 instrument, at chemistry department. A typical example of the SEM micrograph of $VOPO_4.2H_2O$ is shown in Figure 2.7.

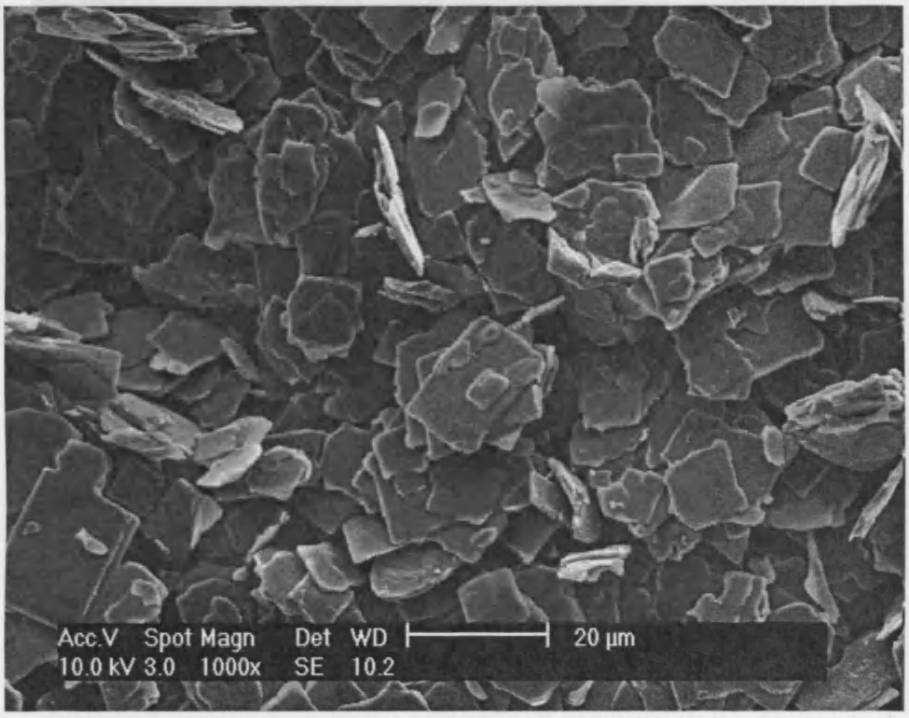

Figure 2.7 – The SEM micrographs of $VOPO_4.2H_2O$

TEM images were obtained by Professor Kiely and his group in the material science department at the Lehigh University, USA. The samples were prepared by grinding the catalyst powder in high purity ethanol using an agate pestle and mortar. Then a drop of the suspension to evaporate was placed on a holey carbon film supported on a 300 mesh copper TEM grid. TEM analyses were carried out in a 200kV JEOL 2000FX electron microscope equipped with a thermionic LaB6 source. Typical examples of the TEM micrographs of $VOPO_4.2H_2O$ are shown in figure 2.8.

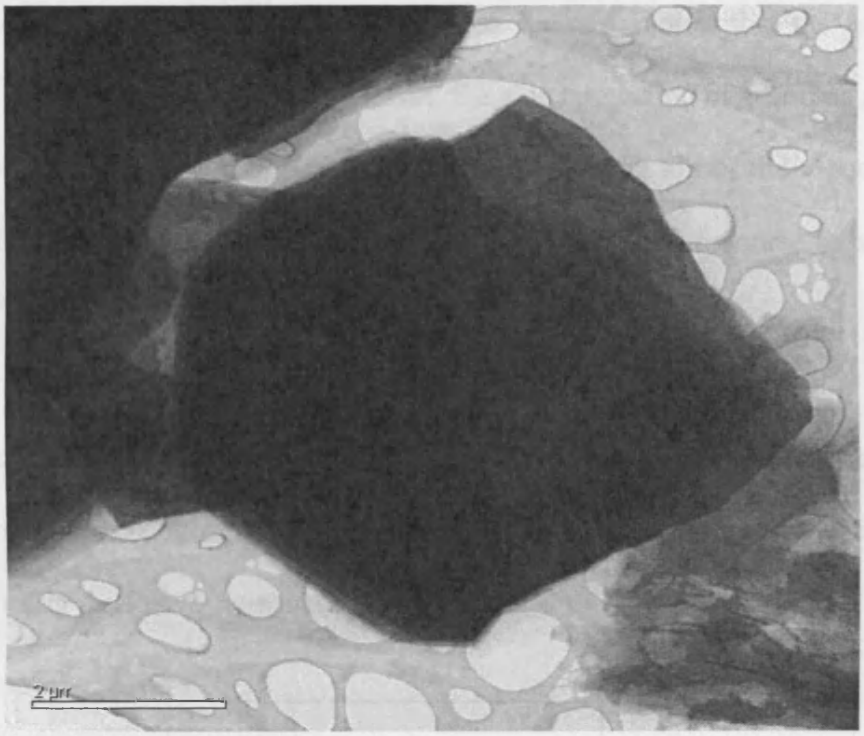

Figure 2.8 – The TEM micrographs of $VOPO_4.2H_2O$

2.3.4 Surface area measurements (BET)

One of the most common techniques of measuring the surface area, and commonly used in most catalysts studies, is that developed by Brunaure, Emmett, and Teller in the late 1930's [7]. The Surface areas were calculated using the Brunauer-Emmett-Teller (BET) isotherm equation which gives a straight line [6]:

$$\frac{P}{V\,(P_o - P)} = \frac{1}{V_m\,C} + \frac{C - 1}{V_m\,C}\,\frac{P}{P_o}$$

Where V is the volume of gas adsorbed at pressure P, V_m is the volume of gas required to form an adsorbed monolayer, P_o is the saturation vapour pressure of the gas at the measurement temperature and C is a constant, related to the heat of adsorption and

condensation of gas. This equation is based on the assumption that the heat of the adsorption of the first monolayer is constant, the side interaction of adsorbed molecules is negligible, multilayer of adsorption can take place on the top of the monolayer and the heat of adsorption for all layers apart from the first layer is assumed to be equal to the heat of condensation of the adsorbed gas.

V_m is calculated from the isotherm, and the surface area is determined by assuming each molecule of adsorbed nitrogen occupied x = 0.162 nm^2 (x is the area covered by a N_2 molecule) using the following equation:

$$\mathbf{SA(m^2/g) = (V_m/22414)N_a x}$$

Where N_a is Avogadro's number (6.023 X 10^{23}),

A Micromiretics 2000 ASAP instrument controlled by a PC computer was used, with all adsorption carried out at liquid nitrogen temperature (77.35 K at one atmosphere pressure). After degassing the samples were degassed for one hour at 120°C prior to the analysis.

2.4 References

[1] M. T. Sananes, I. J. Ellison, S. Sajip, A. Burrow, C. J. Kiely, J. C. Volta and G. J. Hutchings, J. Chem. Soc., Faraday Trans., 1996, 92, 137.

[2] W. A. Deitz, Journal of Gas Chromatography, (February 1967), 70-74

[3] V. V Guliants,. J. B. Benziger, S.Sundaresan, I. E. Wachs, J. M. Jehng, [3] J.E.Roberts, Catal. Today, 28(1996)275-295.

[4] E. Bordes, Catal. Today (1987), 1, 499

[5] F. Ben Abdelouahab, R. Olier, N. Guilhaume, F. Lefebvre and J. C. Volta, J. Catal., (1992), 134, 151-167

[6] S. Brunauer, P. H. Emmett and E. Teller, *J. Am. Chem. Soc.*, 1938, 60, 309.

[7] S. H. Nieman, Principle of instrumental Analysis. 1997.

CHAPTER 3

THE INFULANCE OF ALKANE CO-SOLVENT ON V-P-O PRECORSUR SYTHESIS

3.1 Introduction

Vanadium phosphate catalysts for the selective oxidation of n-butane to maleic anhydride represent one of the most well-studied heterogeneous catalysts [1]. $(VO)_2P_2O_7$ is usually prepared by the topotactic transformation of $VOHPO_4.0.5H_2O$ under the reaction feedstock of 1.5% n-butane in air at 400°C , in which the morphology of the catalyst precursor $VOHPO_4.0.5H_2O$ is preserved.

In view of the importance of the morphology of the catalyst precursor, several studies have been published concerning this topic. Commonly, V_2O_5 is used as a source of vanadium and H_3PO_4 is used as source of phosphorus. Therefore, a reducing agent is required to synthesise the V^{+4} precursor phase. A number of reducing agents and solvents have been used [7]. Early catalyst preparations (VPA method) used water as the solvent, but recently, most studies have concentrated on the use of alcohols (VPO and VPD methods), as they result in better catalysts. The VPD method was first unveiled by Horowitz *et al.* [8] and later described by Johnson *et al.* [9] This method involves the reaction of V_2O_5 with H_3PO_4 with water as the solvent. This leads to the formation of the V^{5+} phase $VOPO_4.2H_2O$. The $VOPO_4.2H_2O$ is recovered and dried and then refluxed in a second stage with an alcohol as the reducing agent to form $VOHPO_4.0.5H_2O$.

Kamiya *et al.* [10] reported that intercalation and exfoliation of $VOPO_4 \cdot 2H_2O$ crystallites proceeded with a stepwise heating below refluxing temperature in 2-butanol and the subsequent reduction of the exfoliated $VOPO_4 \cdot 2H_2O$ brought about $VOHPO_4 \cdot 0.5H_2O$ crystallites of thin sheet. In addition, they found that the active phase $(VO)_2P_2O_7$ obtained from the precursor was highly active and selective for the selective oxidation of n-butane.

In this chapter, the use of autoclave reactors for the preparation of vanadium phosphate catalysts by the reduction of $VOPO_4.2H_2O$ with 1-butanol is described and discussed with the aim of producing catalysts with a new morphology for the selective oxidation of n-butane to maleic anhydride. To this purpose the addition of an alkane as co-solvent for the reduction step of $VOPO_4.2H_2O$ (dihydrate – here after Dih) is studied using a high-pressure autoclave method.

3.2 Experimental

3.2.1 Preparation of catalyst Precursors

A detailed description of the new preparation procedure is described in the experimental chapter (Sections 2.1.1.2, 2.1.1.3 and 2.1.1.4). Three different routes of preparation have been designed using octane as co-solvent and other solvents also investigated.

3.2.2 Characterisation

The newly prepared materials and activated catalyst were characterised with X-ray powder diffraction (XRD), laser Raman spectroscopy (LRS), scanning electron

microscopy (SEM), transmission electron microscopy (TEM) and nitrogen adsorption (BET surface area measurements).

3.2.3 Catalyst Testing

The catalyst test from which the data are presented here were carried out under the following reaction conditions: a gas mixture of 1.7% butane to air, a gas hourly space velocity of $2000h^{-1}$, 0.2g of catalyst (approx. 0.3ml), and 400°C (ramp rate 3°C min^{-1}). Measurements were taken for 72h or until stable conversion and selectivities were observed.

3.3 Results and Discussions

It this chapter, the results are divided in two sections. The first section is mainly a characterisation of the starting materials of vanadium phosphate dihydrate $VOPO_4.2H_2O$ which will be the starting materials of all reactions carried out in this thesis. The second section is a characterisation of the new hemihydrate $VOHPO_4.0.5H_2O$ precursor prepared via three different routes using co-solvents as illustrated in the experimental diagram (figure 3.5)

3.3.1 Characterisation of $VOPO_4.2H_2O$

The x-ray diffraction patterns of $VOPO_4.2H_2O$ prepared using the standard route, as reported in the literature [24], are shown in figure 3.1. This shows all the peaks can be indexed to $VOPO_4.2H_2O$ with the dominant reflection at 12.1° (d-spacing = 7.27Å) indexed to the (001) plane. The d-spacing and relative intensities of the XRD peaks of $VOPO_4.2H_2O$ are shown in Table 3.1.

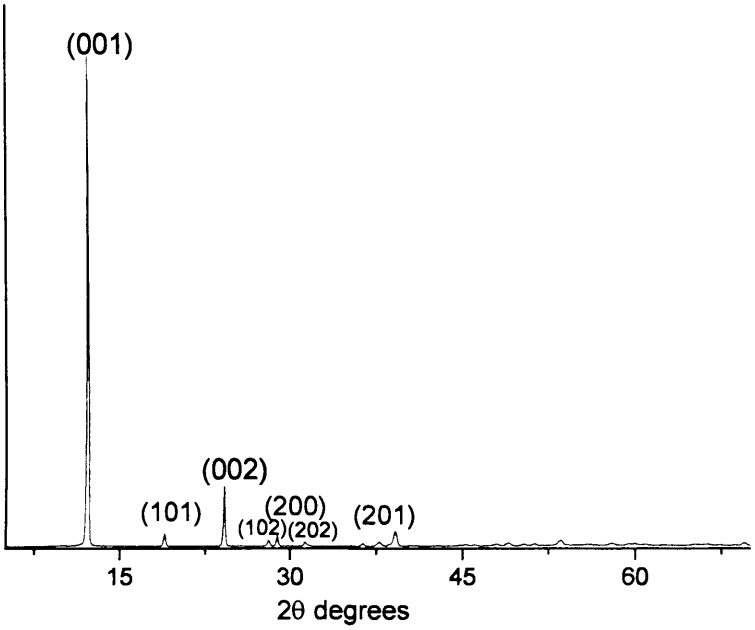

Figure 3.1 - Powder diffraction pattern of $VOPO_4.2H_2O$ prepared using the standard route.

Table 3.1 - The XRD reflexions of $VOPO_4.2H_2O$ prepared [d-calc=calculated d-spacing, d-obs= observed d-spacing, I/I_0 = relative intensity]

$VOPO_4.2H_2O$ [24]		$VOPO_4.2H_2O$	
HKL	d-calc	d-obs	I/I_0
001	7.40	7.27	100
101	4.75	4.69	5
002	3.70	3.67	13
102	3.18	3.17	3
200	3.10	3.09	5
201	2.86	2.85	3
202	2.378	2.38	2

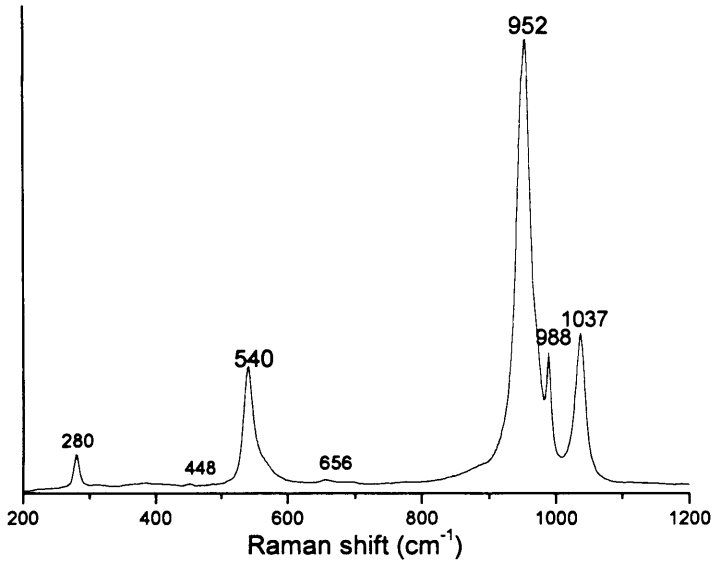

Figure 3.2 - Laser Raman spectrum of $VOPO_4.2H_2O$ prepared using the standard route.

The Raman spectrum of the $VOPO_4.2H_2O$ prepared via the standard route is shown in Figure 3.2. The Raman spectrum is in agreement with reported spectra of $VOPO_4.2H_2O$ [3]. The main bands at 1037cm^{-1} and 988 cm^{-1} are due to the V-O-P and V-O stretching modes, respectively. The band at 952 cm^{-1} is due to the symmetric stretch of P-O in PO_4^{-3} tetrahedra.

Table 3.2 - The Raman peaks of $VOPO_4.2H_2O$ prepared using the standard route

$VOPO_4.2H_2O$ [3]		**$VOPO_4.2H_2O$ (dih)**	
Peaks (cm^{-1})	**I/I_0**	**Peaks (cm^{-1})**	**I/I_0**
1039	strong	1037	strong
988	medium	988	medium
952	very strong	952	very strong
658	weak	656	weak
542	strong	540	medium
451	weak	448	very weak
281	medium	280	medium

The SEM micrographs (Figure 3.3) of the $VOPO_4.2H_2O$ illustrate that the samples have random thick square platelet morphology. The image shows angular platelets with a size range from 3 to 20 μm. The TEM micrographs of the VOPO4.2H2O sample show that the plates have an angular shape. The selected area of the isolated platelet shows typical diffraction patterns of [001] corresponding to $VOPO_4 \cdot 2H_2O$ (Figure 3.4 a and b).

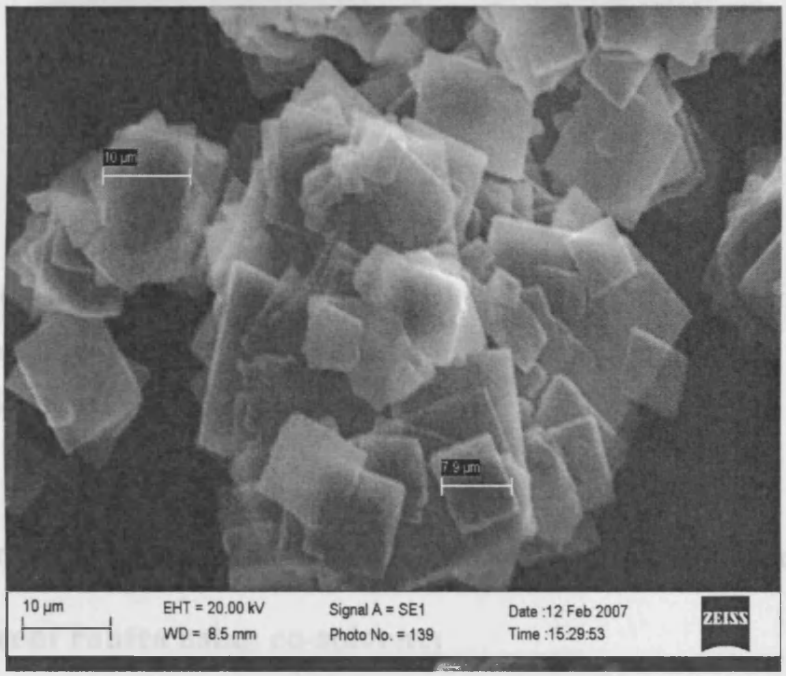

Figure 3.3 - SEM micrographs $VOPO_4.2H_2O$ prepared using the standard route.

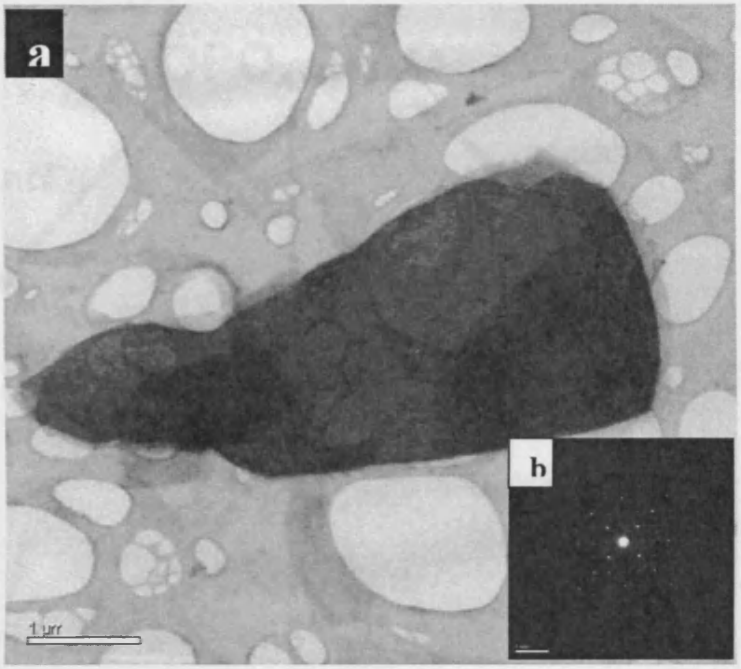

Figure 3.4- (a) The TEM micrograph of $VOPO_4 \cdot 2H_2O$, (b) SADP* corresponds to polycrystalline [001] $VOPO_4 \cdot 2H_2O$ prepared using the standard route.

*: SADP: selected area diffraction pattern

3.3.2 Characterisation of $VOHPO_4.0.5H_2O$ precursor prepared via three different routes using co-solvents

The new hemihydrate $VOHPO_4.0.5H_2O$ precursor prepared via three different routes using co-solvents as illustrated in Figure 3.5. It should be noted that the materials prepared in this chapter were labelled according to figure 3.5 below and chosen for catalyst testing as they were shown to be a good example of each preparation route.

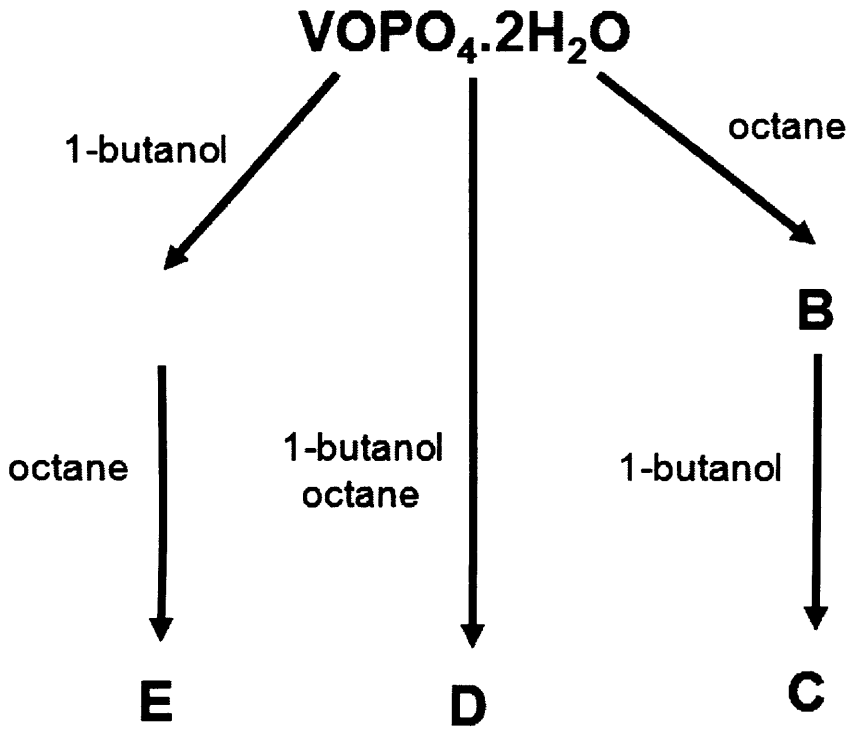

Figure 3.5 - Experimental diagram for preparation of catalyst precursors VOHPO4.0.5H2O.

3.3.2.1 The Reaction of $VOPO_4.2H_2O$ with 1-butanol followed by the reaction with octane solvent (route A)

The first route named route A which represent the standard VPD preparation method using 1-butanol solvent and followed by the reaction of octane. The XRD and Raman of the material prepared after reaction with 1-butanol and after treating with octane solvent are shown in Figure 3.6.and Figure 3.7 respectively. Both samples gave a characteristic pattern of VOHPO4.0.5H2O for which the [220] reflection was virtually the only feature of the diffraction pattern. The Raman spectrum for the VOHPO4.0.5H_20 that were prepared using 1-butanol is shown in figure 3.7 A. The main band observed at 986 cm^{-1} is assigned to the P-O stretch of $VOHPO_4.0.5H_2O$, which is in agreement with the

literature [3]. There was no effect on the VOHPO4.0.5H2O precursor after reaction with octane at 150 °C as shown from the XRD pattern and Raman (Figure 3.6 B and 3.7 B).

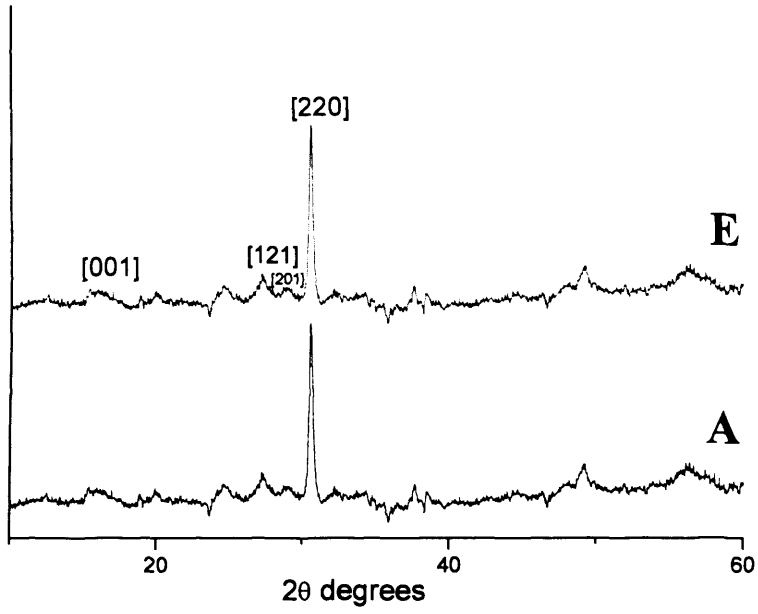

Figure 3.6 - Powder diffraction pattern of prepared V-P-O materials via standard VPD method using 1-butanol (A) and after the subsequent reaction of (A) with octane (E).

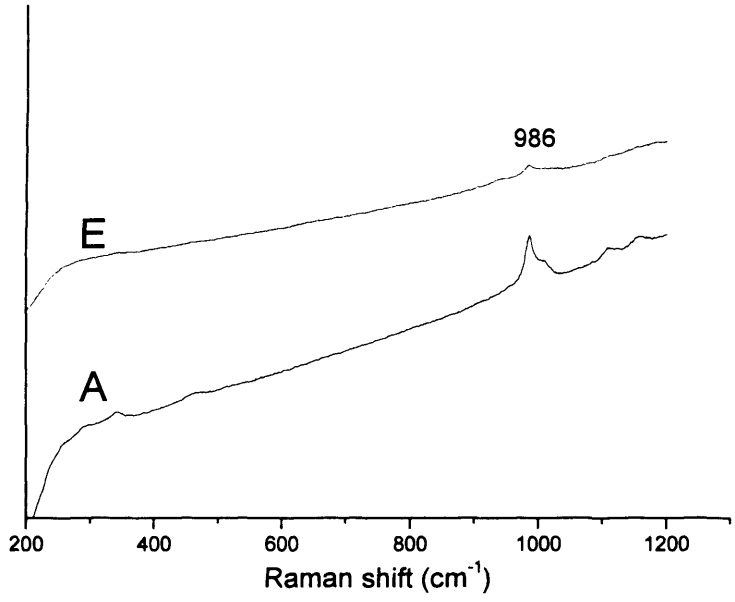

Figure 3.7 - Laser Raman spectrum of prepared V-P-O materials via standard VPD method using 1-butanol (A) and after the subsequent reaction of (A) with octane (E).

The SEM micrographs of the $VOHPO_4.0.5H_2O$ precursors (Figure 3.8 A) display the rosette structure. In addition, when sample A was treated with octane at 150 °C, it gave a similar pattern, as shown in Figure 3.8 E. The TEM micrographs of the $VOHPO_4.0.5H_2O$ precursors prepared via standard routes (sample A and E are shown in Figures 3.9 respectively. Samples A and E show an isolated irregular platelet probably from the rosette-like structure.

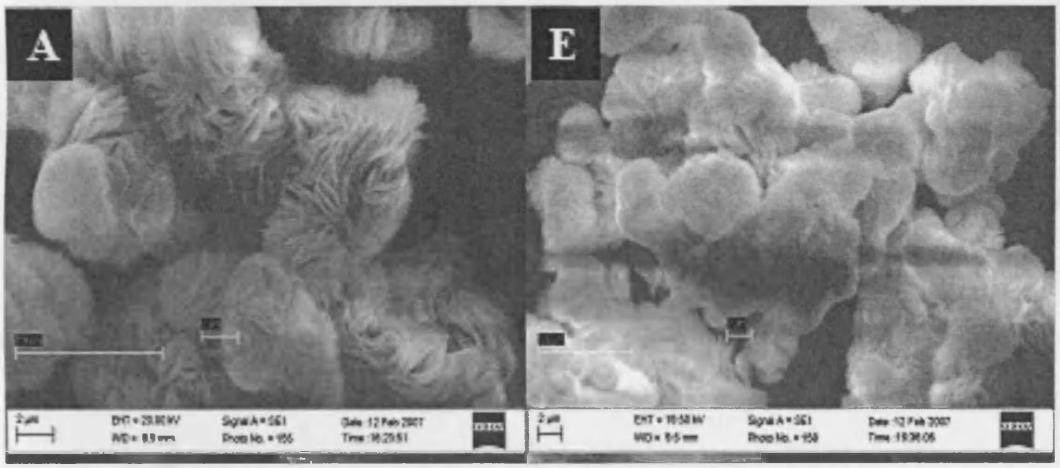

Figure 3.8 –The SEM micrographs of prepared V-P-O materials via standard VPD method using 1-butanol (A) and after the subsequent reaction of (A) with octane (E).

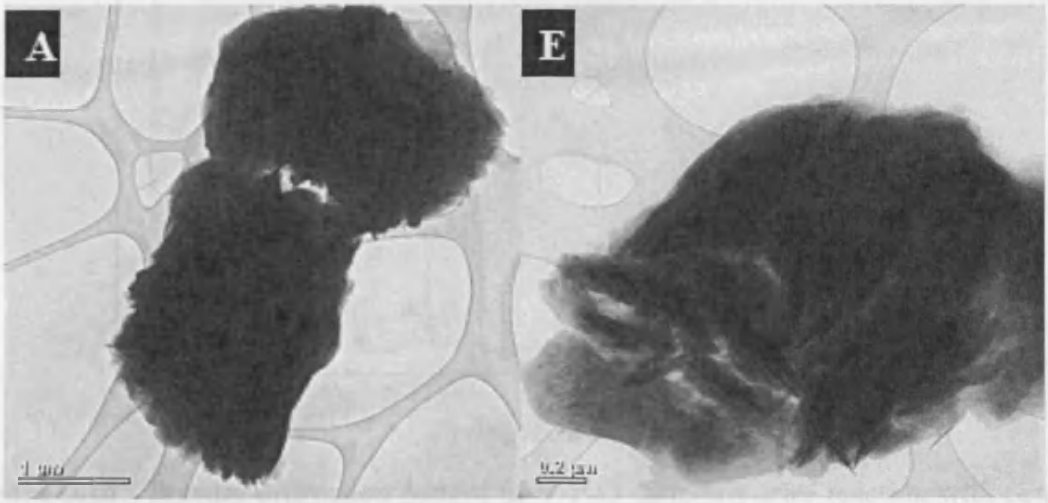

Figure 3.9 - The TEM micrographs of prepared V-P-O materials via standard VPD method using 1-butanol (A) and after the subsequent reaction of (A) with octane (E).

3.3.2.2 The Reaction of $VOPO_4.2H_2O$ with octane solvent followed by the reaction with 1-butanol (C route)

In this route the dihydrate was reacted with octane in the first step and then the resulting materials was reacted with 1-butanol in a separated step in autoclave at 150°C. The XRD and Raman of the new material prepared after reaction with octane are shown in Figure 3.10.and Figure 3.11 respectively. The XRD pattern is similar to $VOPO_4.2H_2O$ with most peaks indexed to the dihydrate with some loss of crystallinity. However, the main peaks are broadening, which can be attributed to the intercalation of VOPO4.2H2O in octane. In addition, a small peak was observed at 2θ (15.8), which can be assigned to $VOHPO_4.0.5H_2O$ being formed due to alcohol impurities associated with octane solvent. All the main peaks are listed in Table 3.3 and it seems that there is a shift in the d-spacing compared to the starting materials $VOPO_4.2H_2O$

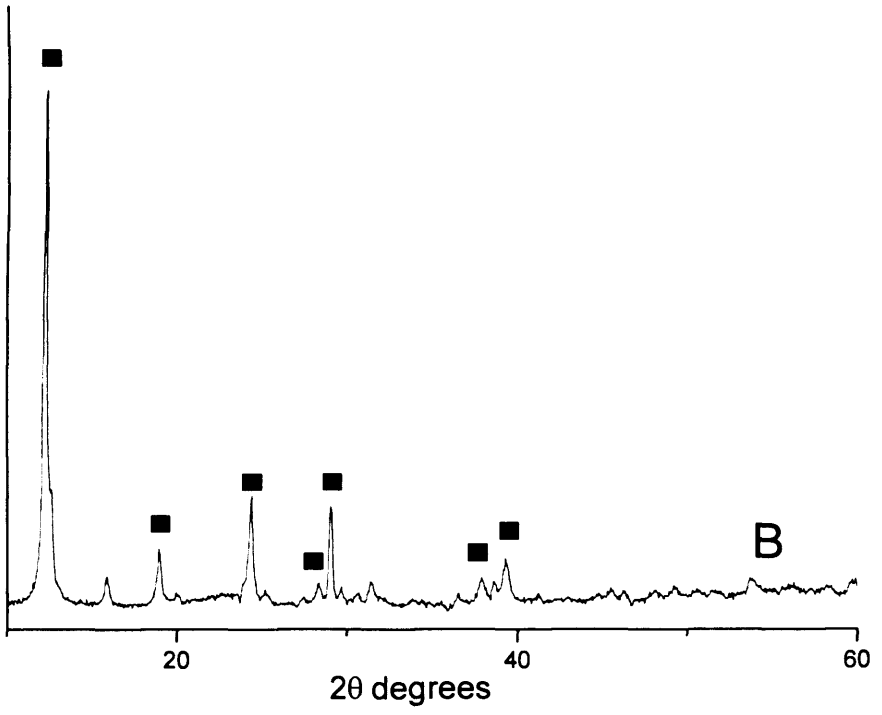

Figure 3.10 - Powder diffraction pattern of V-P-O materials after reaction with octane at 150°C. Key: ■ $VOPO_4.2H_2O$

Table 3.3 - The XRD reflexions of the material (B) prepared after reaction with octane at 150°C [d-calc=calculated d-spacing, d-obs= observed d-spacing, I/I_0 = relative intensity]

$VOPO_4.2H_2O$		Sample B	
d-obs	I/I_0	D-obs	I/I_0
7.27	100	7.22	100
4.69	5	4.67	15
3.67	13	3.66	25
3.17	3	3.14	9
3.09	5	3.07	23
2.85	3	2.84	9
2.38	2	2.37	10

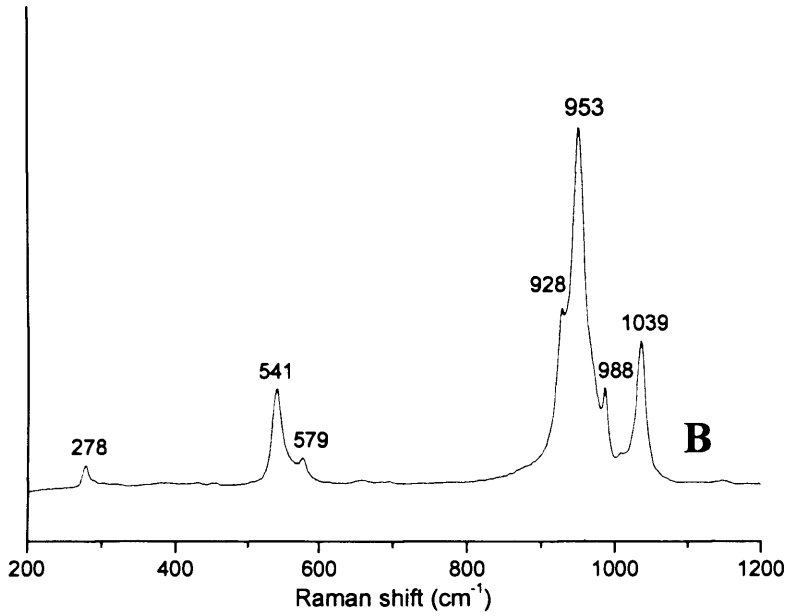

Figure 3.11 - Laser Raman spectrum of V-P-O materials after reaction with octane at 150°C.

In addition, laser Raman spectroscopy (Figure 3.11 B) shows that the B sample seems to partially dehydrate to form α_1–$VOPO_4$, which can be assigned to the presence of Raman bands at (1143 Weak, 1035 Sharp, 963 shoulder, 943 shoulder, 926 shoulder, 661 Weak, 576 Medium, 539 Medium, 457 Weak, 429 Weak 302 Medium and 291

Medium,) cm^{-1}. Although the main bands at (1035 S, 988 M, 952 vS, 658 W, 542 S, 451 W and 281 M), which also remain in Figure 3.11 B, are assigned to $VOPO_4.2H_2O$, the morphology seems unchanged after reaction with octane, as is shown in Figure 3.12 B. The TEM micrographs of the materials (B) after reaction with octane show that the plates have a wall-like structure and the platelet consists of many small angular platelets as shown in Figure 3.13.

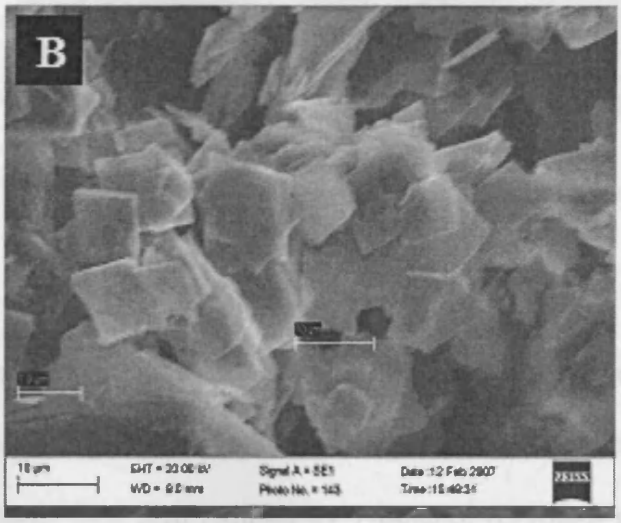

Figure 3.12 - SEM micrographs of V-P-O materials after reaction with octane at 150°C.

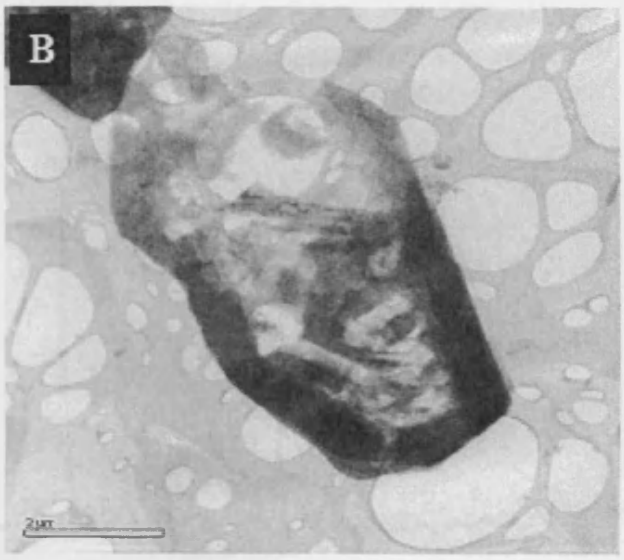

Figure 3.13- The TEM micrograph of V-P-O materials after reaction with octane at 150°C.

The XRD and Raman of the new material that obtain after reaction with 1-butanol via (route C) are shown in Figures 3.14.and 3.15 respectively. In contrast, the sample that was treated with octane first then reduced by 1-butanol (C route) gave a characteristic pattern of $VOHPO_4.0.5H_2O$ with a different ratio of [001]/ [220] intensity, as the [001] plane is the main feature. The Raman spectrum is in agreement with XRD pattern where the main band observed at 986 cm^{-1} is assigned to the P-O stretch of $VOHPO_4.0.5H_2O$.

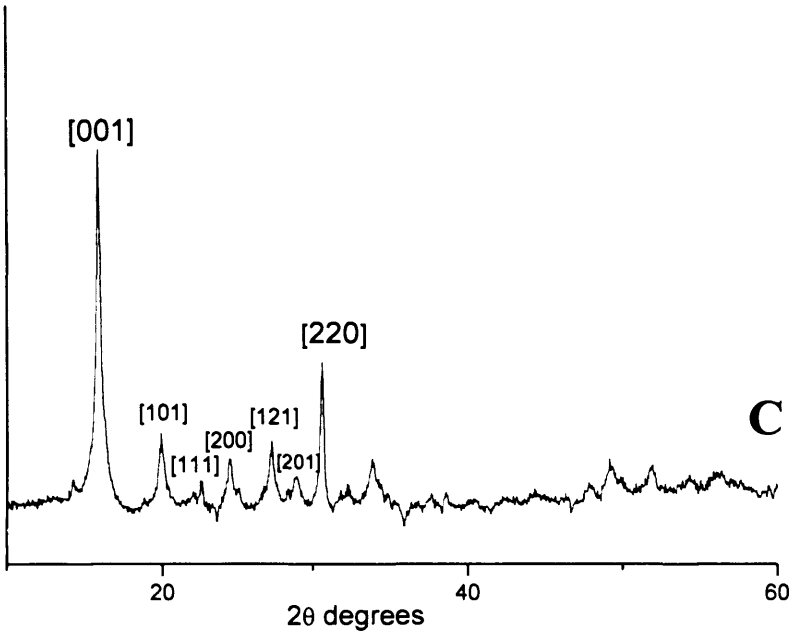

Figure 3.14 - Powder diffraction pattern of $VOHPO_4.0.5H_2O$ precursors prepared via reaction of dihydrate with octane followed by reaction with 1-butanol at 150°C (C route)

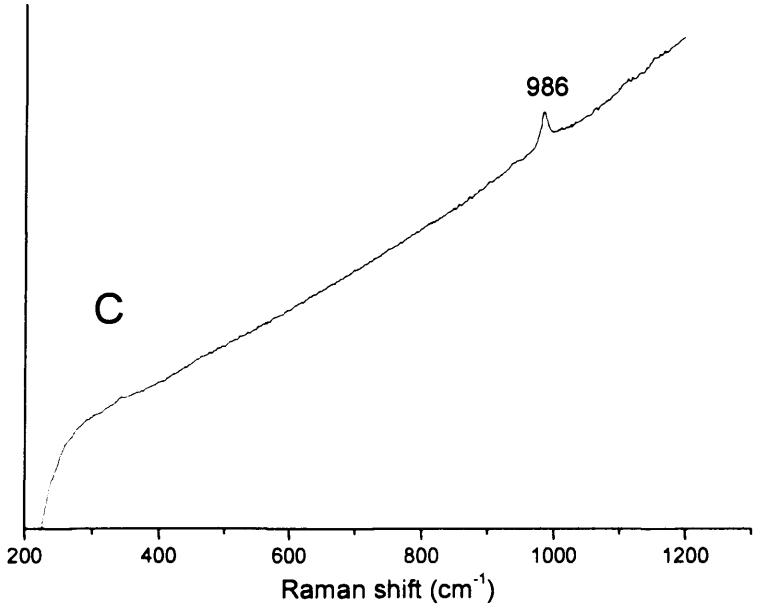

Figure 3.15 - Laser Raman spectrum of $VOHPO_4.0.5H_2O$ precursors prepared via reaction of dihydrate with octane followed by reaction with 1-butanol at 150°C (C route)

The SEM micrographs of the materials derived from the reaction of $VOPO_4.2H_2O$ with octane and then reduced by 1-butanol demonstrated a new morphology, as shown in Figure 3.16 C, which shows a cloud-shaped morphology with random thin platelets. This morphology is different from the material derived from the standard method using 1-butanol as shown in Figure 3.8 A. The TEM micrographs of the material derived from the reaction of $VOPO_4.2H_2O$ with octane and then reduced by 1-butanol, is shown in Figure 3.17 C. This material show random rhombus platelets with thickness between 20 and 100 nm.

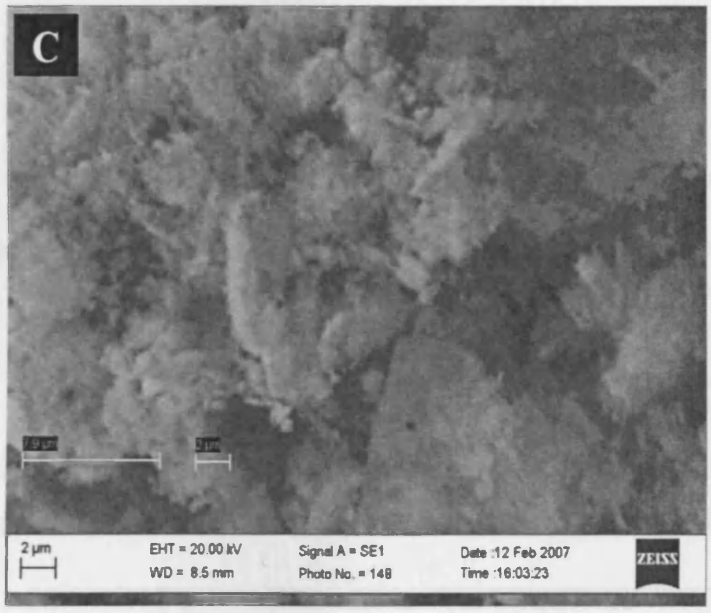

Figure 3.16 - SEM micrographs of $VOHPO_4.0.5H_2O$ precursors prepared via reaction of dihydrate with octane followed by reaction with 1-butanol at 150°C (C route)

Figure 3.17- The TEM micrograph of the $VOHPO_4.0.5H_2O$ precursors prepared via reaction of dihydrate with octane followed by reaction with 1-butanol at 150°C (C route)

It was decided to extend the investigations of C route to see the effect of other solvents prior to the reduction step to give $VOHPO_4.0.5H_2O$. Cyclooctane and toluene have been chosen instead of octane as summaries in table 3.4.

Table 3.4 – Experimental details of material prepared via reaction of $VOPO_4.2H_2O$ with cyclooctane and toluene solvents and then reduced with 1-butanol (C route)

Entry	Solvent	Sample name
1	Cyclooctane	B_{co}
2	Toluene	B_{tu}
3	1-butanol	C_{co}
4	1-butanol	C_{tu}

Reaction condition: 1g $VOPO_4.2H_2O$ 150 **°C**

The XRD and Raman of the new materials prepared after reaction with cyclooctane and toluene are shown in Figures 3.13.and 3.14 respectively. The XRD pattern shows some of the main peaks of $VOPO_4.2H_2O$ remain with a loss of crystallinity. Although these peaks are broadening, this can be attributed to the intercalation of $VOPO_4.2H_2O$ with cyclooctane and toluene. In addition, there are some reflections at $2\theta = 21.91°$, 29.10° with d-spacing (4.04 and 3.06 respectively). These reflections can be assigned to the α_1-VOPO phase. The Raman spectra show bands at (1036, 988, 942 cm^{-1}), which can be assigned to $VOPO_4.2H_2O$. In contrast, there are bands at (927 cm^{-1}) and (572cm^{-1}), which could be due to the presence of α1-VOPO phase. This suggests that $VOPO_4.2H_2O$ seems to be partially dehydrated to give the α1-VOPO phase.

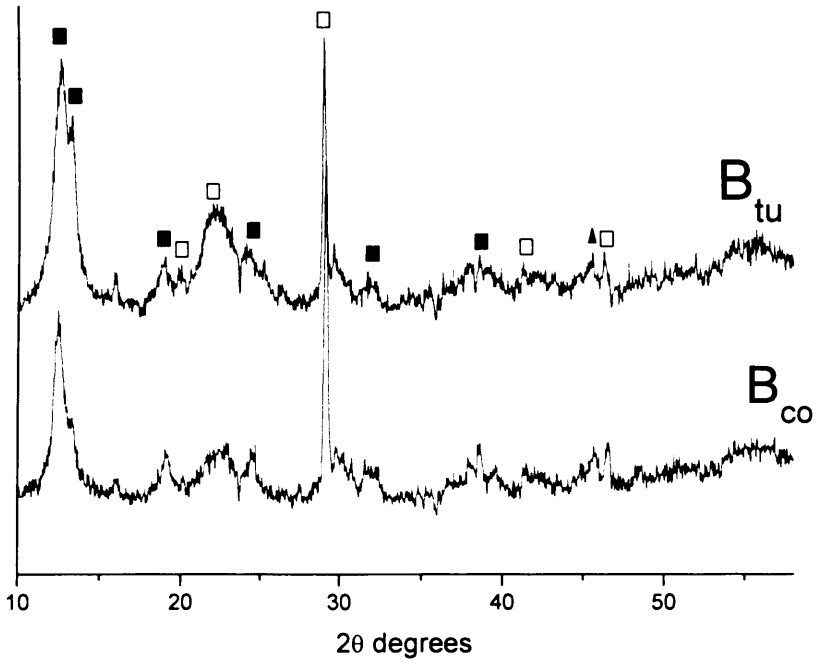

Figure 3.18- Powder diffraction pattern of (B_{co}) after reaction of $VOPO_4.2H_2O$ with cycloctane and (B_{tu}) after reaction with toluene at 150°C. Key: ■ $VOPO_4.2H_2O$, □ α_1-$VOPO_4$.

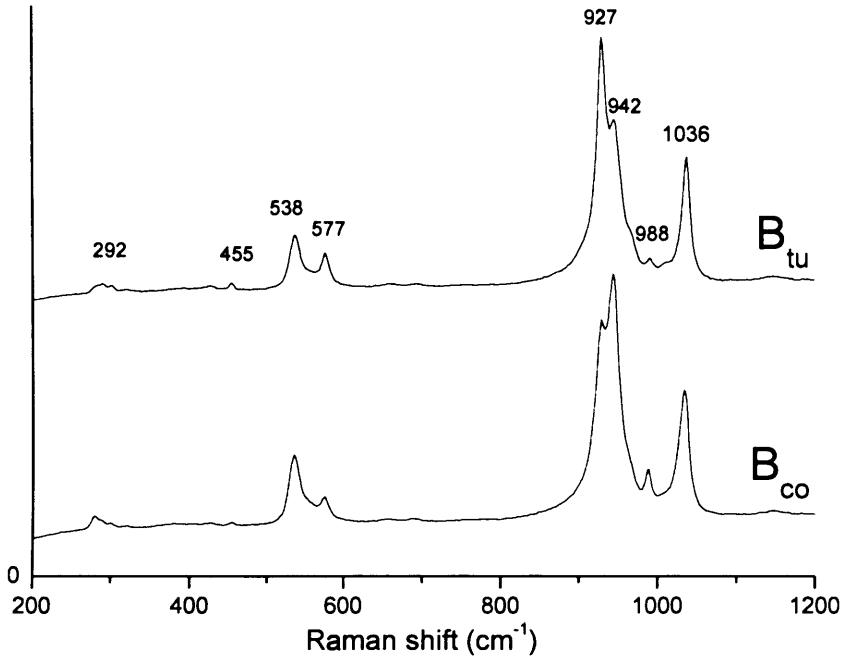

Figure 3.19- Laser Raman spectrum of (B_{co}) after reaction of $VOPO_4.2H_2O$ with cycloctane and (B_{tu}) after reaction with toluene at 150°C.

The XRD patterns of a material prepared via reaction of $VOPO_4.2H_2O$ with cyclooctane and toluene and then reduced in 1-butanol are shown in Figure 3.15 C_{co} and C_{tu} respectively). These patterns indicate that the two samples consist of crystalline vanadyl hemihydrates ($VOHPO_4.0.5H_2O$) with different ratios of [001]/ [220] intensity as the [001] plane is the main feature.

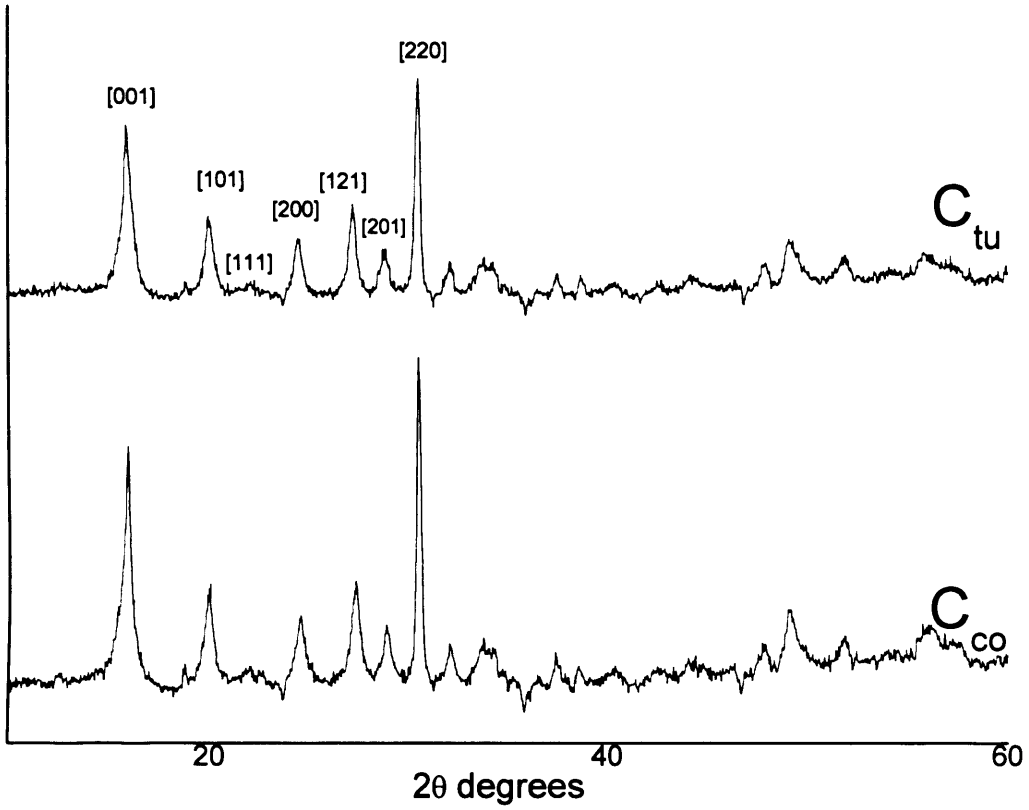

Figure 3.20 - Powder diffraction pattern of $VOHPO_4.0.5H_2O$ prepared using (C route)with cycloctane (C_{co}) and toluene (C_{tu}) at 150°C.

The SEM micrographs of the $VOHPO_4.0.5H_2O$ precursors prepared using (route C) (C_{co}) and (C_{tu}) show that the precursor consists of random thin platelets and has a new cloud-shaped morphology (Figure 3.15 C_{co} and C_{tu}). Most particles have a diameter lying between 1 and 4 μm and display random shapes. In addition, their morphology seems to be comparatively similar to the material prepared using octane solvent (Figure 3.13 C) although they have a different ratio of [001]/ [220] intensity of their XRD pattern compared with octane (Figure 3.10 C).

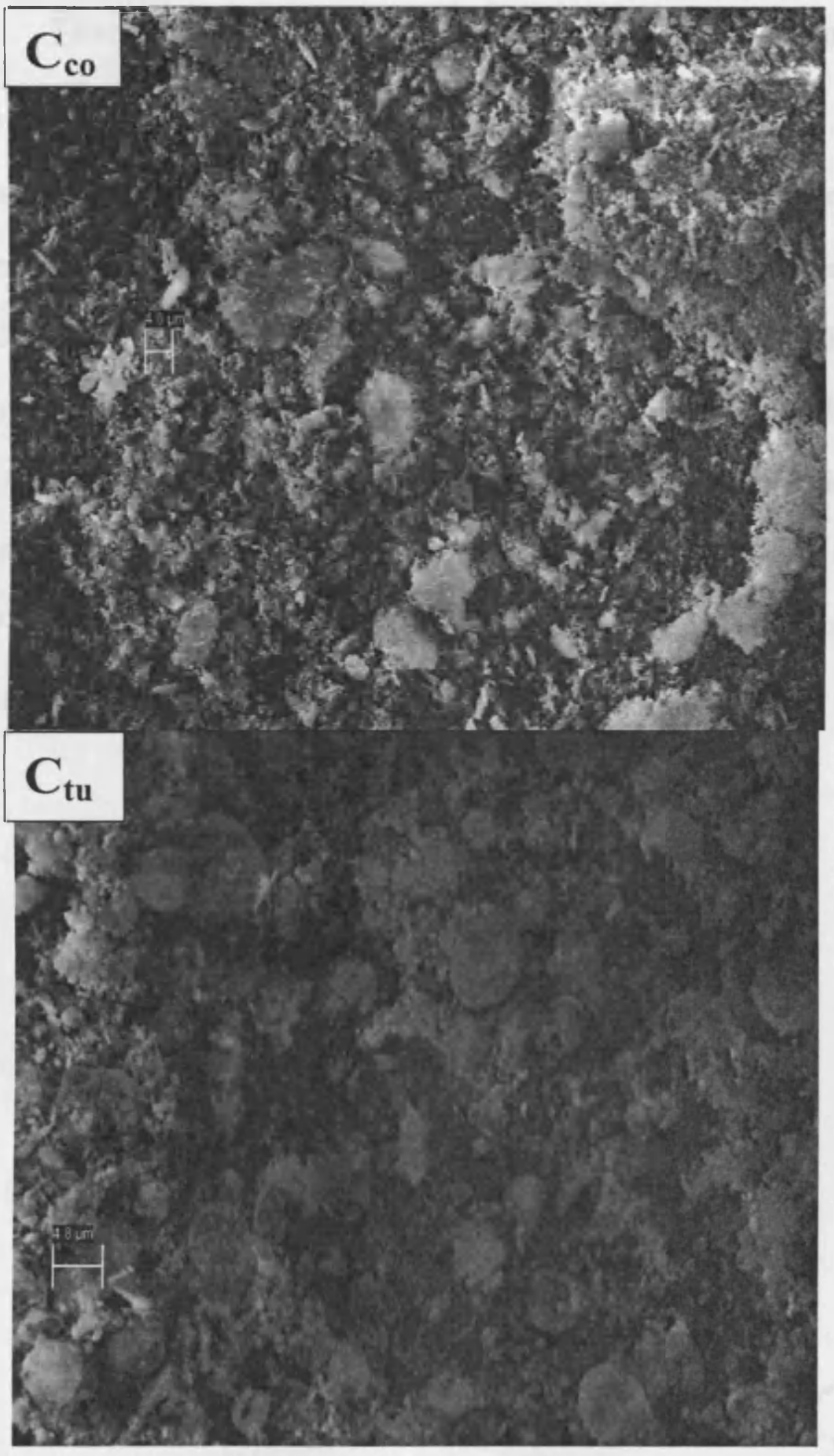

Figure 3.21 - SEM micrographs of $VOHPO_4.0.5H_2O$ prepared using C route with cycloctane (C_{co}) and toluene (C_{tu}) at 150°C.

3.3.2.3 The Reaction of $VOPO_4.2H_2O$ with 1-butanol and octane (D route)

In this route, the $VOPO_4.2H_2O$ was reacted with 1-butanol and octane solvent together (D route) in one step in autoclave at 150°C. The XRD and Raman of the new material prepared after reaction with mixed solvent are shown in Figure 3.22.and Figure 3.23 respectively. Sample D of $VOHPO_4.0.5H_2O$, which was prepared using 1-butanol and octane together, exhibited a different XRD pattern with a comparable ratio of [001]/ [220] intensity. The Raman spectrum of the material prepared using D route is shown in Figure 3.23 and is in agreement with XRD pattern where the main band observed at 986 cm^{-1} is assigned to the P-O stretch of $VOHPO_4.0.5H_2O$.

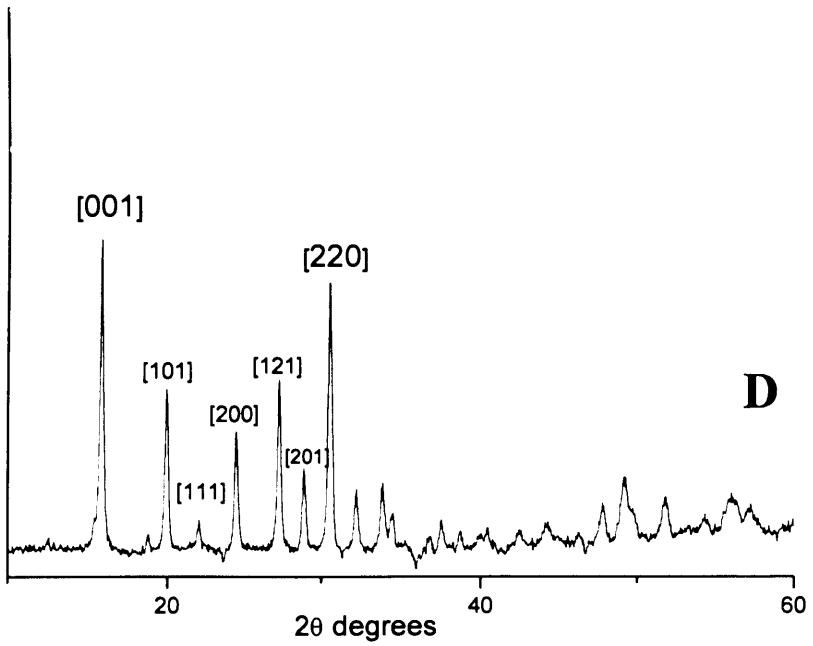

Figure 3.22 - Powder diffraction pattern of $VOHPO_4.0.5H_2O$ prepared using D route via reaction of dihydrate with 1-butanol and octane together at 150°C.

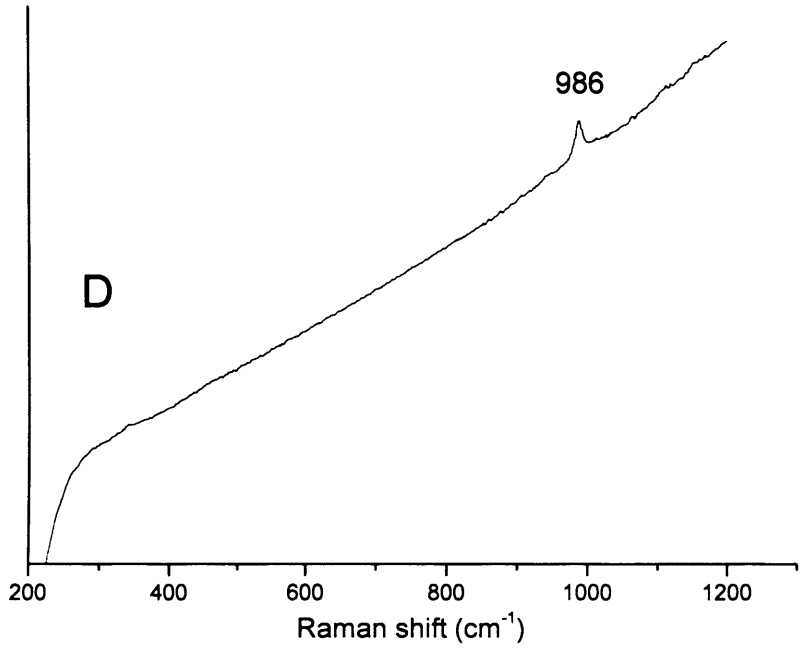

Figure 3.23 - Laser Raman spectrum of $VOHPO_4.0.5H_2O$ prepared using D route via reaction of dihydrate with 1-butanol and octane together at 150°C.

The SEM micrographs of the $VOHPO_4.0.5H_2O$ precursors prepared using D route is shown in Figure 3.24 which shows that the morphology tended to form very thin platelets with random shapes, which was also in agreement with the XRD pattern of the $VOHPO_4.0.5H_2O$ precursors.(Figure 3.22). The TEM micrographs of the $VOHPO_4.0.5H_2O$ precursors prepared D route is shown in Figure 3.24. This material which shows a plane view of major rhombus platelets multi-layer structure.

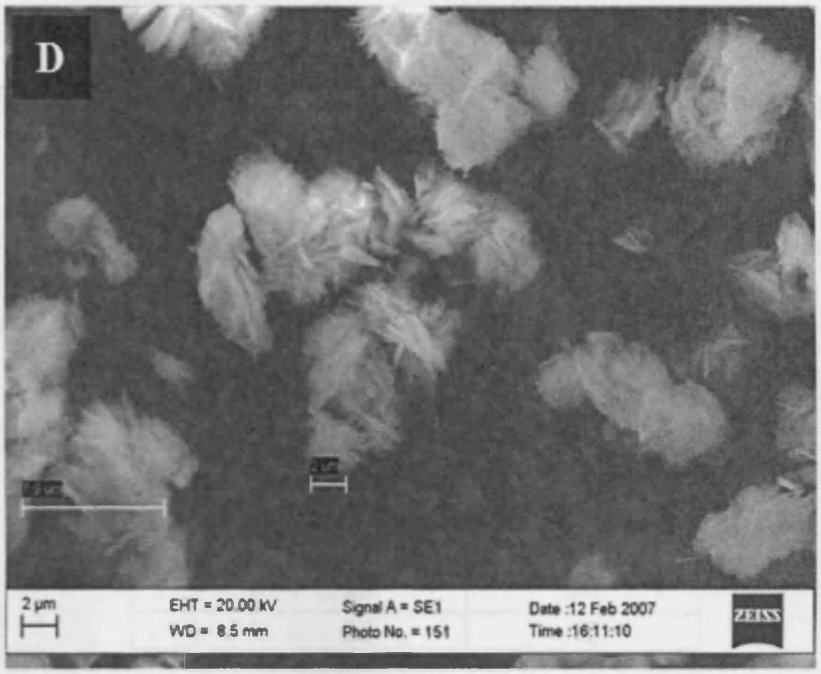

Figure 3.24- The SEM micrograph of the $VOHPO_4.0.5H_2O$ precursors prepared using D route at 150 °C.

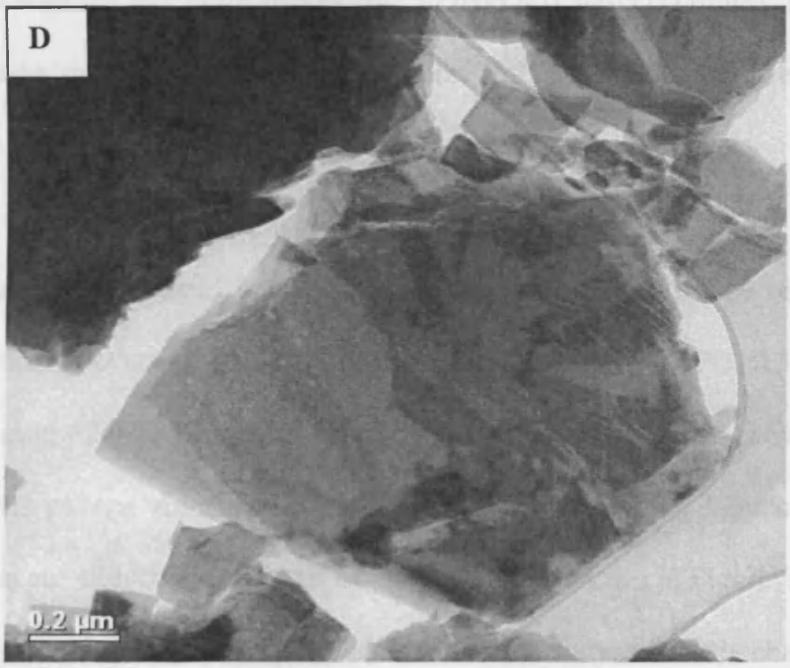

Figure 3.25- The TEM micrograph of the $VOHPO_4.0.5H_2O$ precursors prepared using D route at 150 °C.

For this purpose, it has been decided to extend the investigation of octane addition with 1-butanol (D route) by varying the amount of octane and increasing the temperatures

Table 3.5- Experimental details of the materials derived from the reduction of $VOPO_4.2H_2O$ with 1-butanol using different amount of octane.

Entry	1-butanol (ml)	Octane (ml)
1	25	10
2	25	20
3	25	30
4	25	40

Reaction condition: 1g $VOPO_4.2H_2O$ 150 **°C**

In this set of experiments, 1-butanol and octane solvent were used to investigate the solvent effect with the reduction step to give $VOHPO_4.0.5H_2O$ (D route). The XRD and SEM of the new material prepared after reaction with 1-butanol and different amounts of octane are shown in Figures 3.21.and 3.22 respectively.

The XRD pattern of material prepared using 1-butanol (25ml) as the reducing agent with the addition of octane (10 and 20ml), shows a pattern of $VOHPO_4.0.5H_2O$ with the [220] (d- spacing =2.9A) with small intensity for [001] reflection as shown in Figures 3.26. The XRD pattern observed for the materials prepared using 1-butanol (25ml) as the reducing agent with the addition of octane (30ml), as shown in Figure 3.26, have the [220] reflection with [001] reflection with relative intensity, which is characteristic of the platelet morphology. This indicates the [001]/ [220] intensities ratio increased when the amount of octane solvent was increased to a certain level. Furthermore, X-ray broadening decreases with increases in the amount of octane solvent, which can indicate

that large crystallites were obtained, as shown in Figure 3.26 which concurs with observations from the SEM micrographs (Figure 3.27).

A typical $VO(H_2PO_4)_2$ phase was formed, as shown in Figure 3.26, for the materials prepared using 1-butanol (25ml) as the reducing agent with the addition of octane solvent (40ml); this shows the influence of the octane solvent to switch the formation from $VOHPO_4.0.5H_2O$ to $VO(H_2PO_4)_2$.

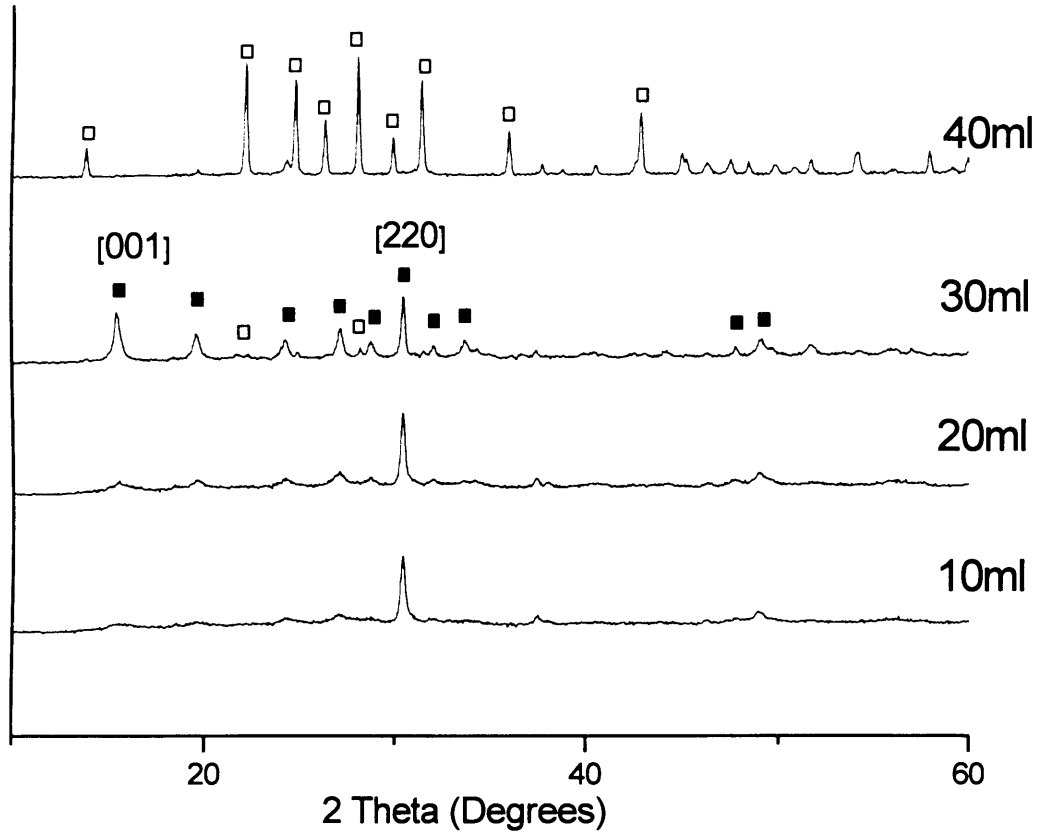

Figure 3.26- Powder X-ray diffraction pattern of the materials derived from the reduction of $VOPO_4.2H_2O$ with 1-butanol using different amount of octane solvent. Key: ■ $VOHPO_4.0.5H_2O$ □ $VO(H_2PO_4)_2$.

The SEM micrographs of the materials derived from the reduction of $VOPO_4.2H_2O$ with 1-butanol using 10, 20, 30 and 40ml of octane are shown in Figure 3.27. The materials prepared using 10, and 20ml of octane solvent the addition of octane solvent

show a rosette morphology that is related to $VOHPO_4.0.5H_2O$. This rosette morphology is looks similar to the material prepared using 1-butanol under the same reaction condition. In contrast, the material prepared with 1-butanol using 30ml of octane has a platelet morphology of random size that corresponds to $VOHPO_4.0.5H_2O$.

The SEM micrographs of the materials derived from the reduction of $VOPO_4.2H_2O$ with 1-butanol using 40ml of octane exhibit a different morphology that shows a mixture of irregular square blocks and isolated platelets as fragments. This was due to the fact that a new phase was formed, $VO(H_2PO_4)_2$, which has a typical block-shape morphology.

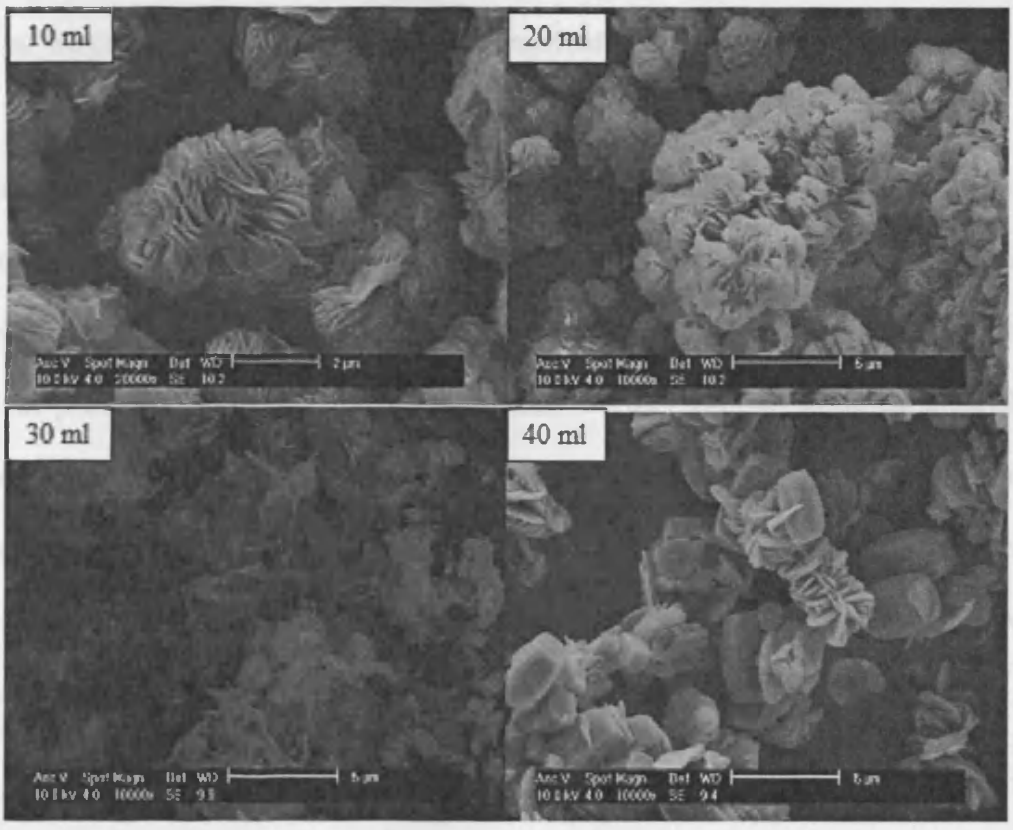

Figure 3.27- SEM micrographs of the materials derived from the reduction of $VOPO_4.2H_2O$ with 1-butanol using different amount of octane solvent.

It is clear that adding octane to the reaction of $VOPO_4.2H_2O$ with 1-butanol at 150°C can change the morphology of $VOHPO_4.0.5H_2O$ from a rosette morphology to platelets and then switch the reaction to form a new phase $VO(H_2PO_4)_2$ with the addition of octane (40 ml). A similar reaction was carried out at the higher temperature of 200 °C, and it was found that the formation of the $VO(H_2PO_4)_2$ phase occurs with the addition of less co-solvent (30ml octane).

3.3.3 Summary

Vanadium phosphate dihydrate $VOPO_4.2H_2O$ material has been characterised and recognized by matching the prepared materials with well-known vanadium phosphate dihydrate $VOPO_4.2H_2O$ from the literature [24]. $VOPO_4.2H_2O$ described here will be used as starting materials for all preparation methods investigated in this thesis.

In this chapter, three different routes have been investigated using octane and other solvents for the preparation of catalyst precursor $VOHPO_4.0.5H_2O$ as stated in the experimental diagram in Figure 3.5. Each route demonstrated a new morphology of the catalyst precursor $VOHPO_4.0.5H_2O$ depending on the reaction order of alcohol (1-butanol) and the co-solvent (octane) and also the addition of octane together with 1-butanol. The XRD patterns and SEM micrographs of the four samples of $VOHPO_4.0.5H_2O$ precursors which represent an example of these routes are shown in Figure 3.28 and 3.29 respectively.

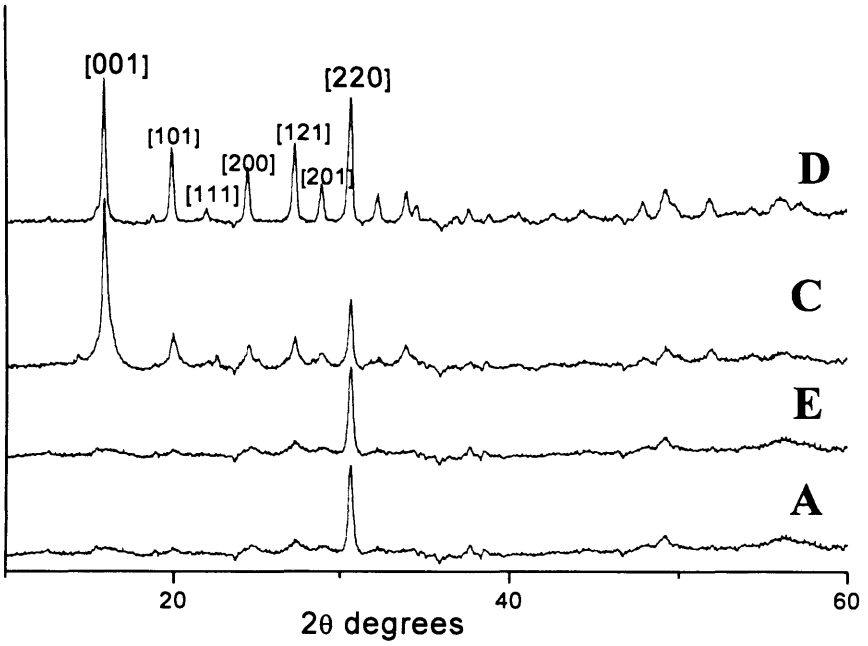

Figure 3.28 - XRD pattern of $VOHPO_4.0.5H_2O$ precursors prepared via (A) reaction with 1-butanol (E), after reaction with octane (C), route (reaction of dihydrate with octane followed by reaction with 1-butanol, (D) via D route (reaction of dihydrate with1-butanol with octane together.

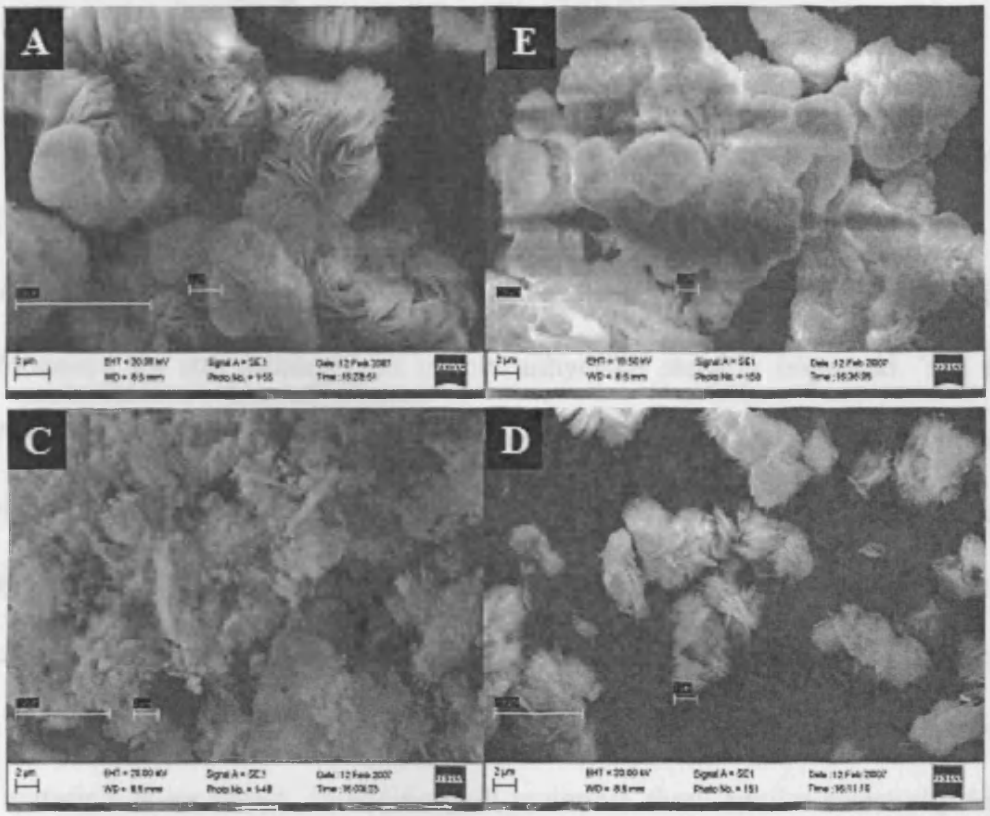

Figure 3.29 - The SEM micrographs of $VOHPO_4.0.5H_2O$ precursors prepared via (A) reaction with 1-butanol (E), after reaction with octane (C) via C route (reaction of dihydrate with octane followed by reaction with 1-butanol, (D) via D route (reaction of dihydrate with1-butanol with octane together.

These samples have been selected as an example of each reaction route and tested for the oxidation of butane to maleic anhydride to evaluate their activity as catalyst precursors.

3.3.4 Catalytic testing and characterisation:

3.3.4.1 Catalyst testing

As described in the experimental chapter, the four catalyst precursors were activated in situ using flowing n-butane (1.7%) in air at 400°C (ramp rate 3°C min^{-1}) for 72 h until stable conversion and selectivities were observed. During this time the catalyst performance for the formation of maleic anhydride steadily improved. The catalyst performance data, when steady state had been obtained, are shown in Table 3.6 together with the surface areas of the precursor and the catalysts. The material prepared from A route (Figure.3.1) gives the highest conversion under these condition. However, the C route gave the lowest conversion (29 %) after the activation period of 72 h which can be attributed to the new morphology of this material. On activation the surface area of most the materials is increased. In addition, all materials show similar selectivity for M A except sample D which gave lower selectivity (55 %). Although, sample D and E gave intrinsic activity of 9.9 mol MA formed/m^2/h which shows a higher activity compared to the standard route (sample A).

Table 3.6, Catalyst performance of vanadium phosphate for the oxidation of n-butane. [a]

Catalyst	Surface area m^2/g [b]		n-Butane Conversion (%)	Malic anhydride Selectivity (%)	Specific Activity ($x10^{-4}$)[c]	Intrinsic Activity ($x10^{-6}$)[d]
	precursor	catalyst				
A	27	32	50	61	2.8	8.8
E	18	27	50	58	2.4	9.9
C	22	20	29	59	1.6	7.9
D	17	24	47	55	2.1	9.9

a Reaction conditions: 400 .C, 1.7 % *n*-butane in air, GHSV = 2000 h^{-1}.

b All samples were degassed for an hour at 120°C before analysis and were labelled according to the experimental diagram (figure 3.1)

c Specific activity: mol maleic anhydride formed/g catalyst/h.

d Intrinsic Activity : mol maleic anhydride formed/m^2/h.

3.3.4.2 Catalyst characterisation

The catalyst samples after testing were characterized by powder XRD and laser Raman spectroscopy. The results are presented in Figures 3.30 and 3.31 respectively. The XRD patterns of the four activated catalysts are very similar and the main reflections can all be assigned to poorly crystalline $(VO)_2P_2O_7$. The only remarkable difference is the ratios of the [200] and [024] intensity; this decreases in the order C > D > E ≥ A. The Raman spectra are also very similar and bands at 925(vs), 1130 and 1180 cm^{-1}(w) can all be assigned to $(VO)_2P_2O_7$ [3]. The interesting point is that there is no other phase such as α_1-$VOPO_4$ formed after the activation of all materials.

.

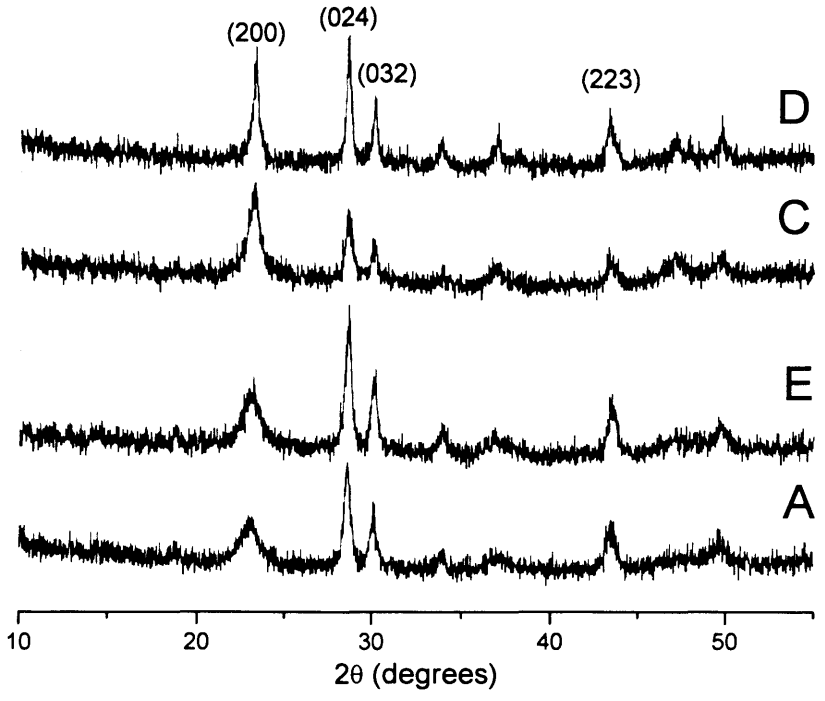

Figure 3.30- XRD patterns for the activated catalysts. . (A), (E), (C) and (D).

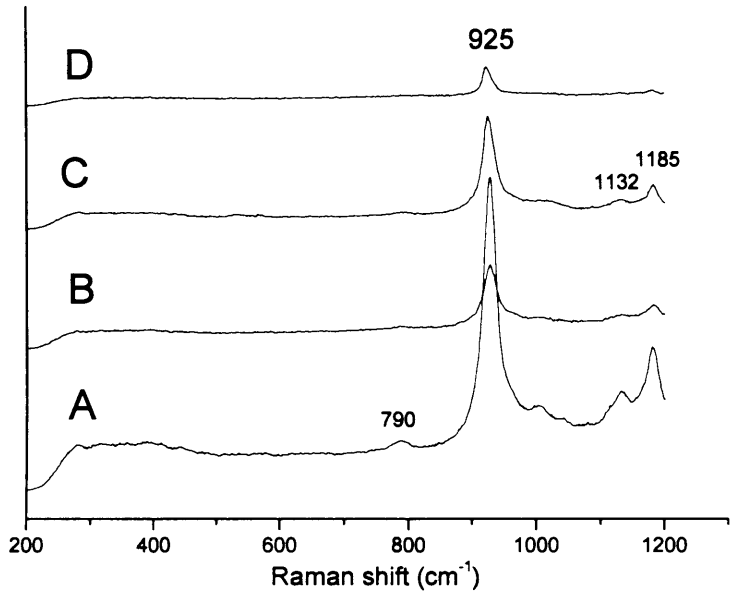

Figure 3.31- Laser Raman spectra for the activated catalysts. (A), (E), (C) and (D).

The SEM micrographs of A, E, C and D ex-reactor samples are shown in Figures 3.32, 3.33, and 3.34 respectively. Samples A and E are shown to consist of irregular bulks with minor morphology showing rosette-like structures. It seems that rosettes collapse and merge. In contrast, SEM micrographs of C and D samples show irregular platelets and particles when compared with the corresponding precursors (Figure.3.29). This is consistent with the significant enhancement in surface area that is observed (Table 3.6).

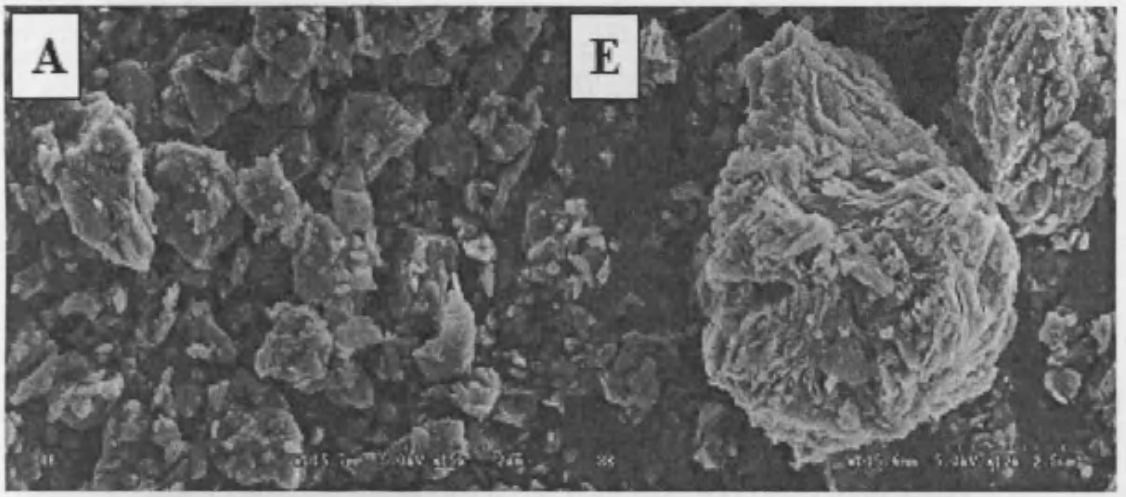

Figure 3.32 - SEM micrographs of final catalyst prepared (A) via standard VPD using 1-butanol (B) after reaction of A sample with octane.

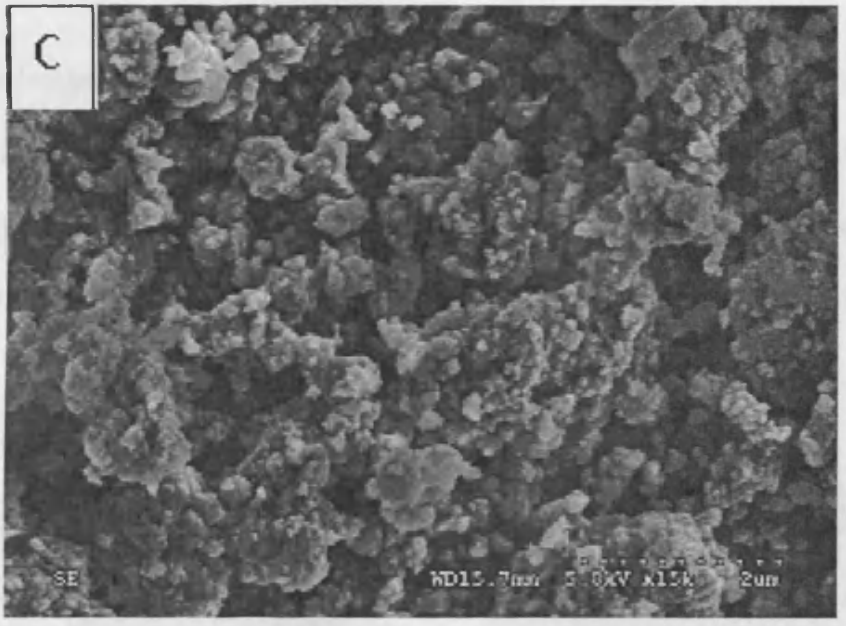

Figure 3.33 - SEM micrographs of final catalyst prepared using prepared using C route at 150 °C.

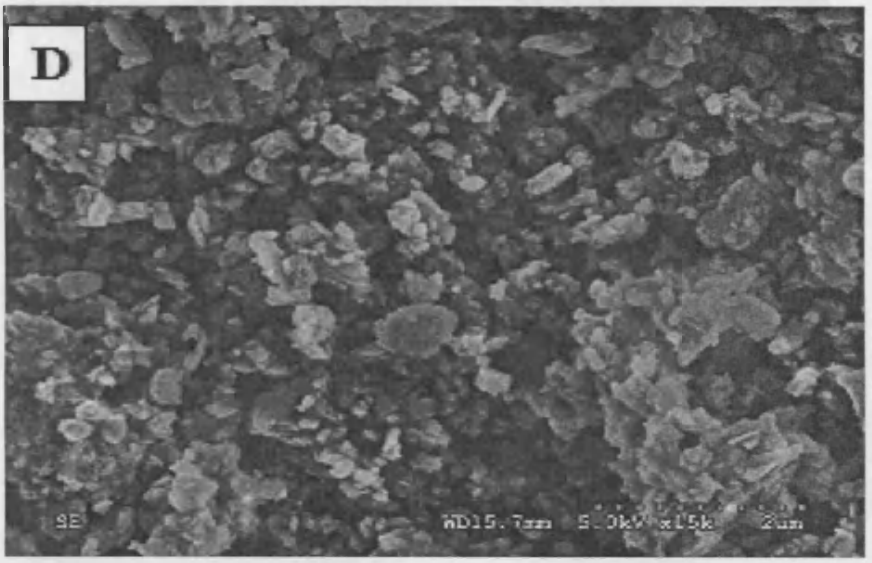

Figure 3.34 - SEM micrographs of final catalyst prepared using prepared using D route at 150 °C.

The TEM micrographs of A, E, C and D after activation for n-butane oxidation at 400°C are shown in Figures 3.35, 3.36, and 3.37 respectively. They are all shown to consist of small irregularly shaped platelets with cracks and voids in the platelets due to dehydration. They all show a thickness ranging from approximately 50 to 200 nm.

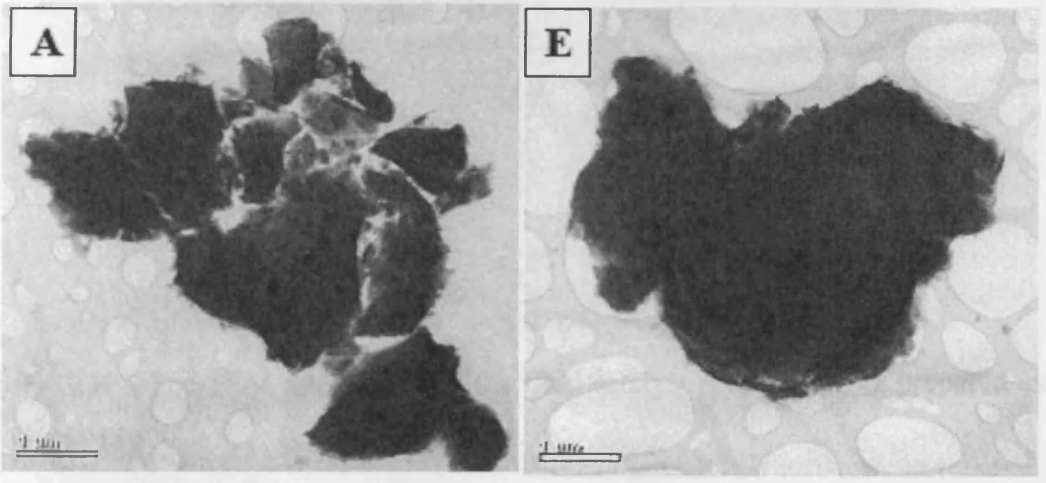

Figure 3.35 - The TEM micrograph of final catalyst prepared (A) via standard VPD using 1-butanol (E) after reaction of A sample with octane.

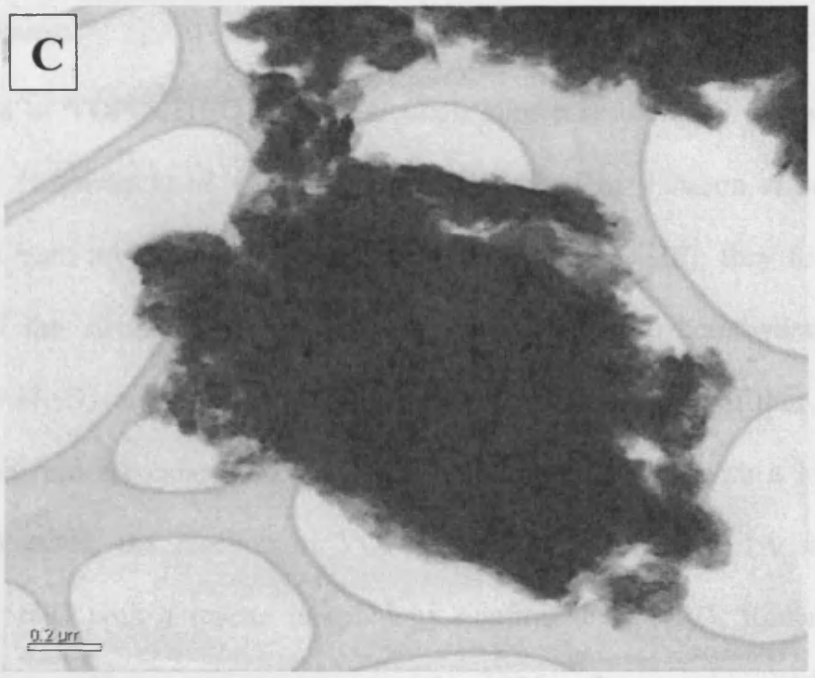

Figure 3.36 - The TEM micrograph of the final catalyst prepared using prepared using C route at 150 °C.

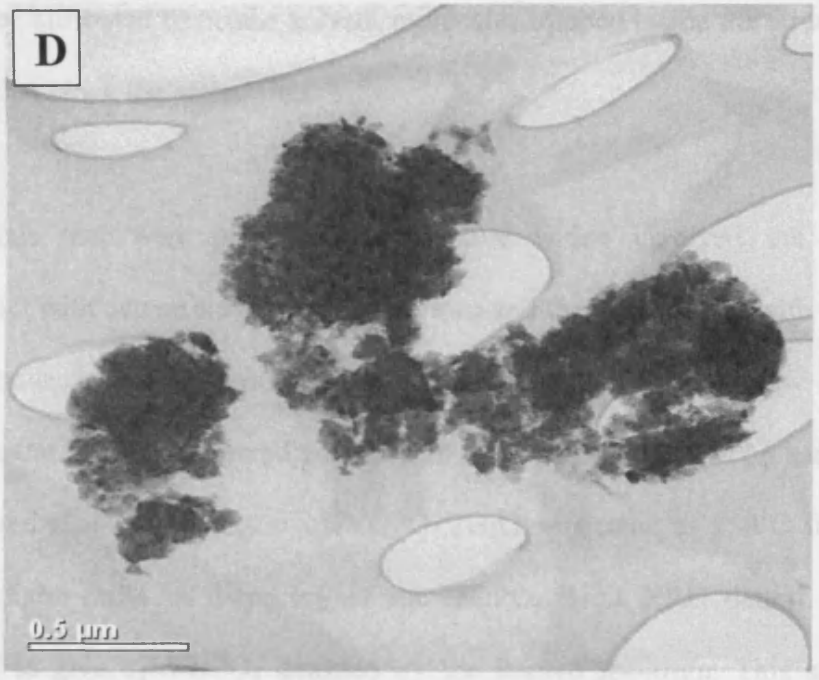

Figure 3.37 - The TEM micrograph of the final catalyst prepared using prepared using D route at 150 °C.

3.4 Discussion

The reaction of $VOPO_4.2H_2O$ with an alcohol, known as the VPD method, was first revealed by Horowitz *et al.* [17] and further described by Johnson *et al.* [16]. This method has been investigated in detail by Hutchings *et al.* [18]; they found that the structure of the alcohol determines the morphology of the hemihydrate precursor ($VOHPO_4.0.5H_2O$), and primary alcohols produce rosette clusters of thin hemihydrate platelets, whereas secondary alcohols produce thicker platelets with a lower surface area. As expected, the reaction of $VOPO_4.2H_2O$ with 1-butanol (A sample) gave $VOHPO_4.0.5H_2O$ with a rosette morphology confirmed by XRD, Raman and SEM characterizations. This precursor seems to be stable after reaction with octane (E sample). The only effect is that the surface area decreases from 27 m^2/g to 18 m^2/g, which can be attributed to octane solvent molecules trapped inside the structures of the precursors that block the active sites.

The materials that were prepared via C route which involved the reaction of $VOPO_4.2H_2O$ with octane solvent in the first step and then reducing it with 1-butanol in a subsequent separate step, showed different XRD patterns and a new morphology compared to the material prepared via standard route using 1-butanol (A sample). It has been observed that the treatment of $VOPO_4.2H_2O$ in octane at 150°C for 24 hours results in slight shifts in d-spacing of the $VOPO_4.2H_2O$ XRD pattern and partial dehydration to give α_I–$VOPO_4$ detected by the Raman spectrum. This suggests that $VOPO_4.2H_2O$ could be intercalated with octane. Moreover, changing the octane solvent for others, such as cyclooctane and toluene, results in greater dehydration of $VOPO_4.2H_2O$ to give $VOPO_4$ phases with some intercalated $VOPO_4.2H_2O$. This suggests the capability of partial intercalation of $VOPO_4.2H_2O$ with these solvents

under the reaction conditions. Reacting these materials with 1-butanol in the second step (C route) produced catalyst precursors $VOHPO_4.0.5H_2O$ with a different ratio of [001]/ [220] intensity of their XRD patterns. These materials shows a new morphology compared to the materials that prepared using 1-butanol only which indicate the effect of octane solvent on $VOPO_4.2H_2O$ prior to the reduction step.

Recently, Yamamoto *et al.* [15] reported the intercalation of alcohol into layers of $VOPO_4.2H_2O$, exfoliation using alcohol into delaminated sheets, and following reduction by reflux in alcohol into thin-layered $VOHPO_4.0.5H_2O$. It was found from their studies that the processes of intercalation, exfoliation and reduction in alcohol are important for the catalyst precursor and, consequently, for the final catalyst. As mentioned previously that $VOPO_4.2H_2O$ has a capability to accommodate some types of organic molecules due to its layered structure. This means that the octane solvent could be intercalated into the layers of $VOPO_4.2H_2O$ which therefore gave $VOHPO_4.0.5H_2O$ precursor with a new morphology.

The second route that was investigated was the reaction of $VOPO_4.2H_2O$ with octane solvent and 1-butanol as the reducing agent together (D route). It was clear that, with addition of octane, the morphology of the catalyst precursor $VOHPO_4.0.5H_2O$ changed from a rosette morphology to random platelets with the addition of 30ml of octane. In contrast, a new phase $VO(H_2PO_4)_2$ was formed when 40ml of octane was added to the reaction mixture. This indicates that the octane solvent can play an important role of controlling the morphology of the catalyst precursors. However, this reaction was carried out in a high pressure autoclave reactor with 70ml maximum volume, so a similar study was conducted to investigate the reaction at the higher temperature of

200°C, and it was found that the formation of the new phase $VO(H_2PO_4)_2$ occurred with less amount of octane (30ml). This shows also that the temperature has a great influence on the preparation of the catalyst precursors.

Moreover, it is has been reported in the literature [19] that $VO(H_2PO_4)_2$ can be prepared from $VOPO_4.2H_2O$ when the V/P ratio is changed from 1:1 to 1>2 whereas $VOHPO_4.0.5H_2O$ has 1:1 V/P ratio. This indicates that $VOPO_4.2H_2O$ dissociates in the alcohol and then V^{5+} species are reduced to V^{4+} by the alcohol.

Another investigation, recently reported by Umacaran [20], demonstrates that the use of a long chain alkane as a co-solvent using the reflux method can control the morphology of $VOHPO_4.0.5H_2O$. It was found that, the addition of a high amount (50-100ml) of alkane reduces the concentration of alcohol in the reaction mixture. The low concentration results in a decreased reaction rate of the reduction step (1-butanol and $VOPO_4.2H_2O$) and consequently affects the V^{4+}: P ratio, which determines the formation of the phase formed.

It was also found from this study that adding octane with 1-butanol for the reduction of $VOPO_4.2H_2O$ in a high pressure autoclave can control the morphology of the catalyst precursors $VOHPO_4.0.5H_2O$ (D route). Furthermore, adding 40ml of octane switched the formation from $VOHPO_4.0.5H_2O$ to $VO(H_2PO_4)$, which shows the influence of the co-solvent. It can be said that the use of octane as co-solvent can control the reaction by changing the alcohol (1-butanol): alkane (octane) volume ratio, which therefore, can alter the concentration of alcohol. In addition, the present of the co-solvent with alcohol

can also affect the reduction step of the $VOPO_4.2H_2O$ to give the catalyst precursors $VOHPO_4.0.5H_2O$.

Three different morphologies of $VOHPO_4.0.5H_2O$ precursor have been successfully prepared using octane solvent. Evaluations of these precursors for *n*-butane oxidation to maleic anhydride demonstrate that all of the catalyst precursors have transformed topotactically to give poorly crystalline $(VO)_2P_2O_7$. However, the only significant difference is the ratio of the [200] and [024] intensity, which is believed to be essential for the catalyst activity. Torardi et al. [21] reported that the poorly crystalline $(VO)_2P_2O_7$ depends on the presence of structural defects in the $VOHPO_4{\cdot}0.5H_2O$ structure. The $VOHPO_4{\cdot}0.5H_2O$ precursors usually exhibit crystallographic disorder associated with its retained alcohol (used in the preparation), which translates into a similar disorder in the active phase $(VO)_2P_2O_7$ after activation at 400°C and is likely to be responsible for the appearance of an amorphous intermediate.

In contrast, Hutchings *et al.* [22] reported that the transformation does not only proceed through the simple transformation of crystalline $VOHPO_4.0.5H_2O$ to crystalline $(VO)_2P_2O_7$, rather the majority of the $VOHPO_4.0.5H_2O$ becomes amorphous on heating in an n-butane/air mixture and the crystallization to $(VO)_2P_2O_7$takes place relatively slowly, which may affect the crystallinity of $(VO)_2P_2O_7$.

After the activation, the surface areas of most of the materials increase as the $VOHPO_4.0.5H_2O$ precursor is heated; the trapped alcohol molecules are released, which creates structural defects, microcracks and increases the surface area which may also suggest the effect of the retained alcohol solvent on the final catalyst

3.5 Conclusion

Three different morphologies of $VOHPO_4.0.5H_2O$ precursor have been successfully prepared via three different routes with the use of octane solvent. From these results, we can say that octane solvent can plays an important role in $VOHPO_4 \cdot 0.5H_2O$ preparation. The reaction of $VOPO_4.2H_2O$ with octane solvent shows the possibility of the intercalation of the octane solvent between the layers of $VOPO_4.2H_2O$. This can lead to the formation of $VOHPO_4.0.5H_2O$ precursors with a new morphology after the reduction step using 1-butanol. In addition, adding the solvent together with the reducing agent leads to the formation of $VOHPO_4.0.5H_2O$ with a different XRD pattern and new morphology.

Finally, testing these samples shows that the new materials prepared with octane (sample D) gave a higher activity compared to material prepared via the standard route (sample A).

3.6 References

[1] G. J. Hutchings, Appl. Catal., 1991, 72, 1.

[2] L. Griesel, J. K. Bartley, R. P.K. Wells and G. J. Hutchings, Journal of Mol. Catal. A: Chemical 220 (2004) 113–119

[3] V. V Guliants,. J. B. Benziger, S.Sundaresan, I. E. Wachs, J. M. Jehng, J.E.Roberts, Catal. Today, 28(1996)275-295.

[4] F.J. Cabello Sanchez, J.A. Lopez Sanchez, R.P.K. Wells, C. Rhodes, A. Isfahani, G.J. Hutchings, Catal. Lett. 77 (2001) 189.

[5] J.K. Bartley, J. Lopez-Sanchez, G. Hutchings. Catal. Today 81 (2003) 197.

[6] G. Hatchings. J. Mater. Chem., 14(2004) 3385.

[7] G. Centi, Catal. Today, 1994, 16.

[8] H. S. Horowitz, C. M. Blackstone, A. W. Sleight and G. Teufer, Appl. Catal. 38 (1988) 211.

[9] J. W. Johnson, D. C. Johnston, A. J. Jacobson and J. F. Brody,J. Am. Chem. Soc. 106 (1984) 8123.

[10] N. Hiyoshi, N. Yamamoto, T. Okuhara, Chem. Lett. (2001) 484.

[11] C.C. Torardi, Z.G. Li, H.S. Horowitz, W. Liang, M.-H. Whangbo, J. Solid State Chem.1995, 119, 2, 349.

[12] G.J. Hutchings, A. Desmartin-Chamel, O. Oliver, J.C. Volta, Nature 348 (1994)

[13] I. J. Ellison, G. J. Hutchings, M. T. Sananes, J. C.Volta, J.Chem. Soc., Chem. Commun. 1994, 1093.

[14] Umacaran. Sithamparappillai, Ph.D thesis, Cardiff University, 2008.

[15] N. Yamamoto, N. Hiyoshi, and T. Okuhara, Chem. Mater. 2002, 14, 3882-3888.

[16] J. W. Johnson, D. C. Johnston, A. J. Jacobson and J. F. Brody, J. Am. Chem. Soc., 1984, 106, 8123.

[17] H. S. Horowitz, C. M. Blackstone, A. W. Sleight and G. Teufer, Appl. Catal., 1988, 38, 211.

[18] M. T. Sananes, I. J. Ellison, S. Sajip, A. Burrow, C. J. Kiely, J. C. Volta and G. J. Hutchings, J. Chem. Soc., Faraday Trans., 1996, 92, 137

[19] E. Bordes, Catal. Today, 1987, 1, 499.

CHAPTER 4

Vanadium phosphate oxide seeds and their influence on the formation of V-P-O catalyst precursors

4.1 Introduction

Vanadium phosphate catalysts have been extensively studied for the selective oxidation of n-butane to maleic anhydride (MA). Vanadyl pyrophosphate, $(VO)_2P_2O_7$, is believed to be the main active phase for the butane oxidation. This phase is usually derived from the precursor $VOHPO_4.0.5H_2O$ via topotactic transformation [1–3].

There are many reports that describe the preparation methods of $VOHPO_4.0.5H_2O$ [4, 6] including the use of $VOPO_4.2H_2O$ as a starting material. Johnson *et al.* [5] reported that $VOHPO_4.0.5H_2O$ can be prepared via the direct reduction of $VOPO_4.2H_2O$ using alcohols. Hutchings *et al.* [6] reported that the morphology of the resulting $VOHPO_4.0.5H_2O$ was controlled by the nature of the alcohol used in the reduction of $VOPO_4.2H_2O$. It has been found that catalysts derived from the reduction of $VOPO_4.2H_2O$ with 1-alcohols tend to give high activity catalysts by virtue of the high surface area material (typically 40 m^2/ g) produced by this preparation method.

In contrast to using 1-octanol, Ellison *et al.* reported that refluxing $VOPO_4{\cdot}2H_2O$ with 3-octanol produces $VO(H_2PO_4)_2$ phase [7]. $VO(H_2PO_4)_2$, (defined as phase E in this thesis) has been classified as an impurity formed during the preparation of the catalyst precursor [8]. This phase displays distinctive cuboidal particles about 10μm in size and with a low surface area of ca. 2 m^2/g. It was reported that $VO(H_2PO_4)_2$ has a negligible activity and selectivity under standard reaction conditions [9].

Presented here are our investigations of the factors influencing the preparation of vanadium phosphates during the VPD type alcohol reduction of $VOPO_4 \cdot 2H_2O$ and the effect of reaction temperatures on the preparation using long chain alcohols (1-octanol 3-octanol). In particular, the use of seed crystals of vanadium phosphate can have a dramatic influence on the morphology and phase identity of the precursor materials.

4.2 Experimental

4.2.1 Precursors preparation

A detailed description of the preparation methods is given in the experimental chapter (sections 2.1.2.1, 2.1.2.2, 2.1.2.3 and 2.1.2.4).

4.2.2 Characterisation

All the new prepared materials and activated catalysts were characterised using a combination of X-ray powder diffraction, laser Raman spectroscopy, scanning electron microscopy (SEM), transmission electron microscopy (TEM) and BET surface area measurements.

4.2.3 Catalyst Testing

All the catalyst tests from which the data are presented here were carried out under the following reaction conditions: a gas mixture of 1.7% butane to air, a gas hourly space velocity of $2000h^{-1}$, 0.2g of catalyst (approx. 0.3ml), and 400°C (ramp rate 3°C min^{-1}). Measurements were taken for 72h or until stable conversion and selectivities were observed.

4.3 Results

The characterisation and catalytic performance of the materials obtained before and after activation for the selective oxidation of n-butane to maleic anhydride are presented in five sections (see Table 4.1). In the final discussion section, the results obtained from different alcohols are summarised and correlated. In Table 4.1, a summary of samples selected as vanadium phosphate seeds is detailed. The reaction conditions and the new materials prepared with different seeds using different alcohols are included.

Table 4.1. A summary of samples selected as vanadium phosphate seeds and their reaction conditions and the new materials prepared with different seeds using different alcohols

Entry	Sample name	Seed	Solvent	Temperature (°C)	Yield (g)
Vanadium phosphate Seeds	Rosette seed (a)	—	1-octanol	120	2
	Platelet seed (b)	—	2-butanol	98*	1.6
	$VO(H_2PO_4)_2$ seed (c)	—	3-octanol	175*	1.15
1-octanol	1CR	Rosette seed	1-octanol	185*	1.62
	1CP	Platelet seed	1-octanol	185*	1.7
	1CE	$VO(H_2PO_4)_2$ seed	1-octanol	185*	1
iso-Butanol	IBR	Rosette seed	iso-Butanol	105*	1.67
	IBP	Platelet seed	iso-Butanol	105*	1.61
2-Butanol	2BR	Rosette seed	2-Butanol	98*	1.47
	2BP	Platelet seed	2-Butanol	98*	1.41
3-octanol	3CR	Rosette seed	3-octanol	175*	1.6
	3CP	Platelet seed	3-octanol	175*	1.67

* = reflux temperature

4.3.1 Seed preparation via standard methods

Vanadium phosphate seeds were prepared via the VPD methodology, i.e., reduction of a dihydrate ($VOPO_4 \cdot 2H_2O$) with an alcohol temperature of the solvent. The alcohols used were 1-octanol, 2-butanol and 3-octanol. They each yielded vanadium phosphate material; hemi-hydrate ($VOHPO_4 \cdot 0.5H_2O$) with rosette (Table 4.2 entry 1, Figure 4.1a) and platelet (Table 4.2 entry 2, Figure 4.1b) morphologies and $VO(H_2PO_4)_2$ (Table 4.2 entry 3, Figure 4.1c). These standard vanadium phosphate materials were used in small quantities as seeds in subsequent experiments, which are discussed later.

Table 4.2-Standard preparation information

Entry	**Sample name**	**Preparation method** (all with 2 g $VOPO_4 \cdot 2H_2O$)	**BET** (m^2/g)	**T** (°C)	**Yield** (g)
1	Rosette seed **(a)**	1-octanol (100ml)	30	120	2
2	Platelet seed **(b)**	2-butanol (50ml)	9	98*	1.60
3	$VO(H_2PO_4)_2$ seed **(c)**	3-octanol (100ml)	2	174*	1.15

* = Reflux temperature

The XRD patterns and SEM micrographs of V-P-O material prepared using the VPD routes are shown in Figure 4.1. The 1-octanol gave VOHPO4.0.5H_20 crystals for which the [220] reflection was virtually the only feature of the diffraction pattern (Figure 4.1a) with a rosette morphology. Whereas 2-butanol gave VOHPO4.0.5H_20 for which the [001] reflection was the dominant feature of the diffraction pattern with discrete rhomboidal platelets morphology (Figure 4.1b), the use of 3-octanol as a reducing agent led to the exclusive formation of $VO(H_2PO_4)_2$ with an octagonal blocky morphology, as shown in Figure 4.1c.

The TEM micrographs of these materials are shown in Figure 4.2, with the rosette-type precursor showing a rosette-like morphology (Figure 4.2 a). The discrete rhomboidal platelets (Figure 4.2 b) prepared using 2-butanol of $VOHPO_4 \cdot 0.5H_2O$ also showed tombstone platelets ranging from 0.5 μm to 3 μm in length and with a thickness of 200 nm. The $VO(H_2PO_4)_2$ seed material formed using 3-octanol showed octagonal platelets with {110} and {010} facets (Figure 4.2 c).

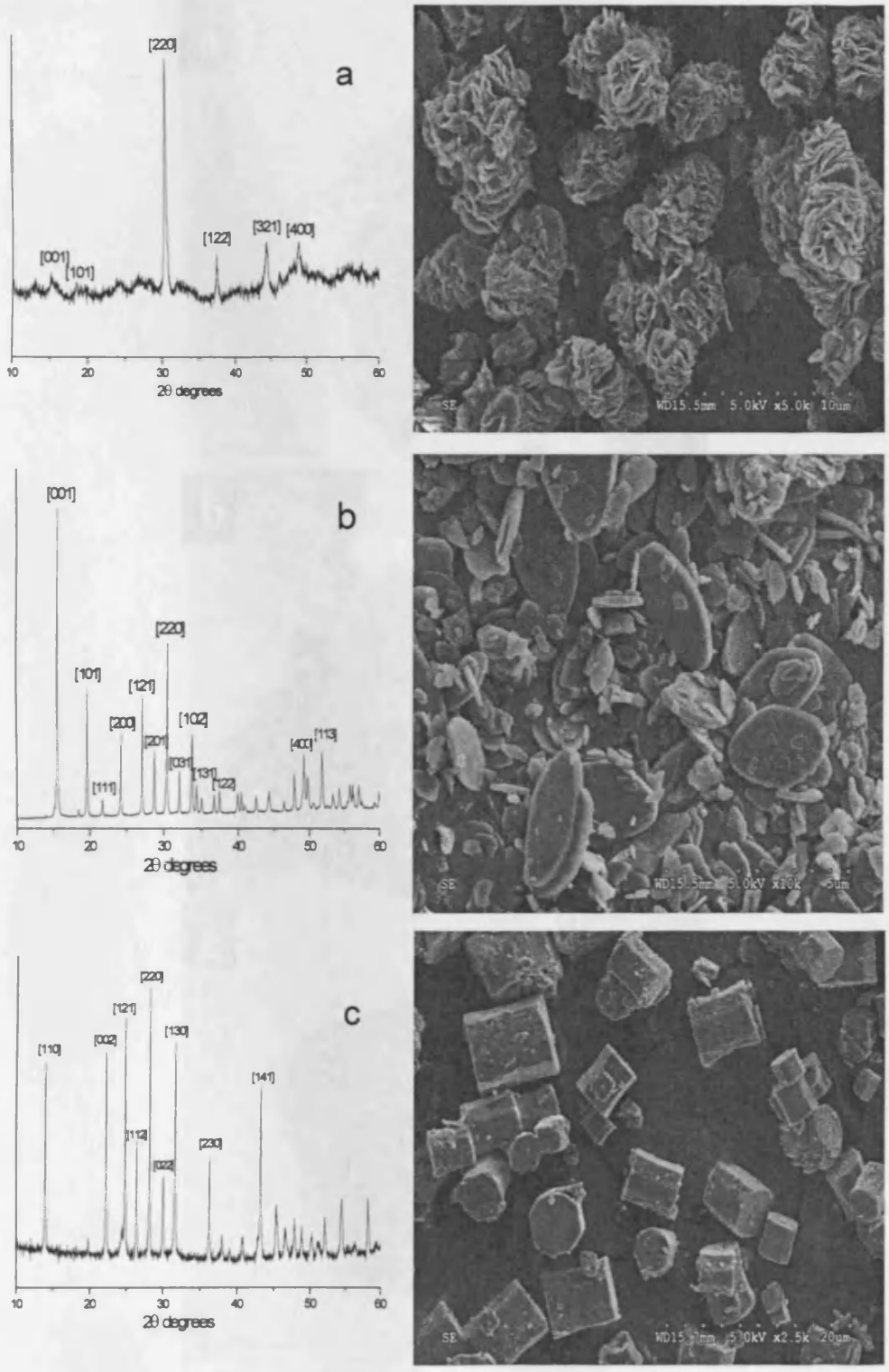

Figure 4.1-Powder XRD patterns and SEM micrographs of V-P-O material recovered from standard VPD reaction with; (a) 1-octanol ($VOHPO_4 \cdot 0.5H_2O$ rosette), (b) 2-butanol ($VOHPO_4 \cdot 0.5H_2O$ platelet) and (c) 3-octanol $\{VO(H_2PO_4)_2\}$.

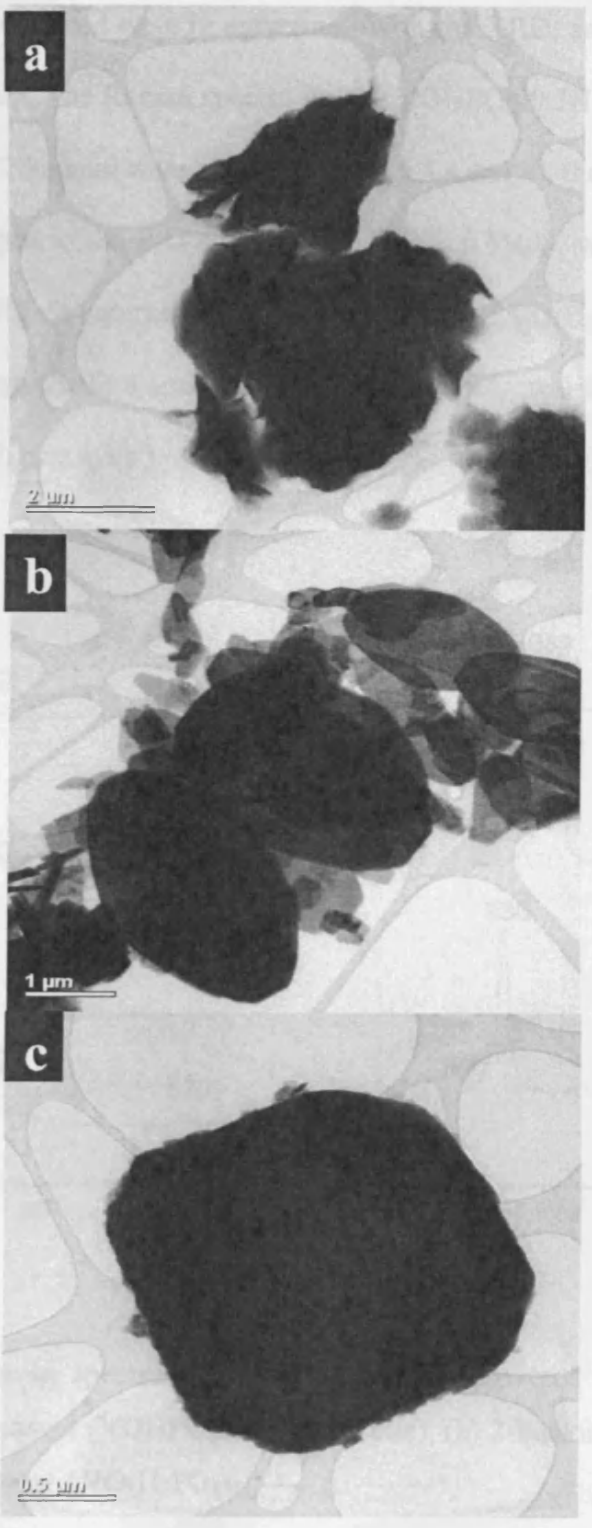

Figure 4.2- The TEM micrograph of V-P-O material recovered from standard VPD reaction with; (a) 1-octanol ($VOHPO_4 \cdot 0.5H_2O$ rosette), (b) 2-butanol ($VOHPO_4 \cdot 0.5H_2O$ platelet) and (c) 3-octanol $\{VO(H_2PO_4)_2\}$.

The Raman spectra obtained were in agreement with the XRD, as shown in Figure 4.3 a, b and c respectively. The Raman spectra for the VOHPO4.0.5H_20 that were prepared using 1-octanol and 2-butanol were similar (Figure 4.3 a and b); the main band observed at 986 cm^{-1} is assigned to the P-O stretch of $VOHPO_4.0.5H_2O$, which is in agreement with the literature [10]. In contrast, the Raman spectrum of $VO(H_2PO_4)_2$ showed a very strong peak at 936 cm^{-1} with a small shoulder at 900 cm^{-1}, which is the characteristic band of this phase (Figure 4.3 c).

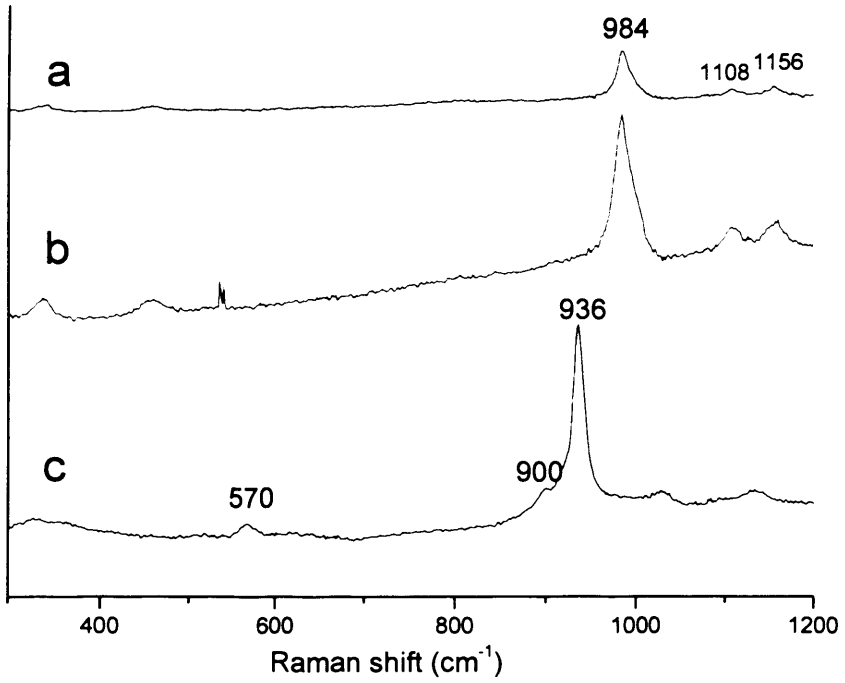

Figure 4.3-Laser Raman spectrum of V-P-O material recovered from standard VPD reaction with; (a) 1-octanol ($VOHPO_4 \cdot 0.5H_2O$ rosette), (b) 2-butanol ($VOHPO_4 \cdot 0.5H_2O$ platelet) and (c) 3-octanol $\{VO(H_2PO_4)_2\}$.

4.3.2 Temperature effect and addition of V-P-O seeds with 1-octanol

It was observed that heating vanadium phosphate dihydrate $VOPO_4 \cdot 2H_2O$ in 1-octanol led to the formation of $VOHPO_4 \cdot 0.5H_2O$ in a high yield (Table 4.3, entry 1-4) as expected. However, when the reaction was carried out at a temperature of > 160°C, the recovered mass of the expected $VOHPO_4 \cdot 0.5H_2O$ decreased (Table 4.3 entry 5-7) despite the boiling point of 1-octanol being 185°C. Usually such reactions are conducted under the reflux conditions of the alcohol used.

Table 4.3- Recovered mass of material formed from the reaction of dihydrate and 1-octanol at different temperatures [a]

Entry	T (°C)	Recovered mass (g)
1	118	1.8
2	125	1.9
3	144	2.07
4	155	2.02
5	167	0.27
6	179	0.05
7	185	0.06

[a] Conditions: $VOPO_4 \cdot 2H_2O$ (2 g), 1-octanol (100 ml), 24 hours

The powder XRD patterns shown in Figure 4.4a-d demonstrate that the recovered material was $VOHPO_4 \cdot 0.5H_2O$ with a typical rosette morphology at a temperature of < 160°C. Interestingly, when this same reaction was carried out at a temperature of > 160°C (Table 4.3, entry 5-7), it gave a blue/black solution containing only minor amounts of $VOHPO_4 \cdot 0.5H_2O$ phase. The powder XRD pattern of the minor amounts of the material that were recovered indicates that it was largely amorphous, with a very small reflection at [220] of $VOHPO_4 \cdot 0.5H_2O$ phase (Figure 4.4 at167-185°C). A UV/VIS analysis of this solution showed that the solute phase contained V^{4+} ions, which

means that the high temperature could inhibit the formation of $VOHPO_4 \cdot 0.5H_2O$ structure when this alcohol is used.

The Raman spectra obtained were in agreement with the XRD pattern, as shown in Figure 4.5. For the Raman spectra for the VOHPO4.0.5H20 that were prepared using 1-octanol at different temperatures, the main band was observed at 984 cm^{-1} , which is assigned to the P-O stretch of $VOHPO_4.0.5H_2O$; this is in agreement with the literature [10]. However, this band tended to disappear at higher temperatures (179 and 185°C), which may also indicate that the recovered material was largely amorphous.

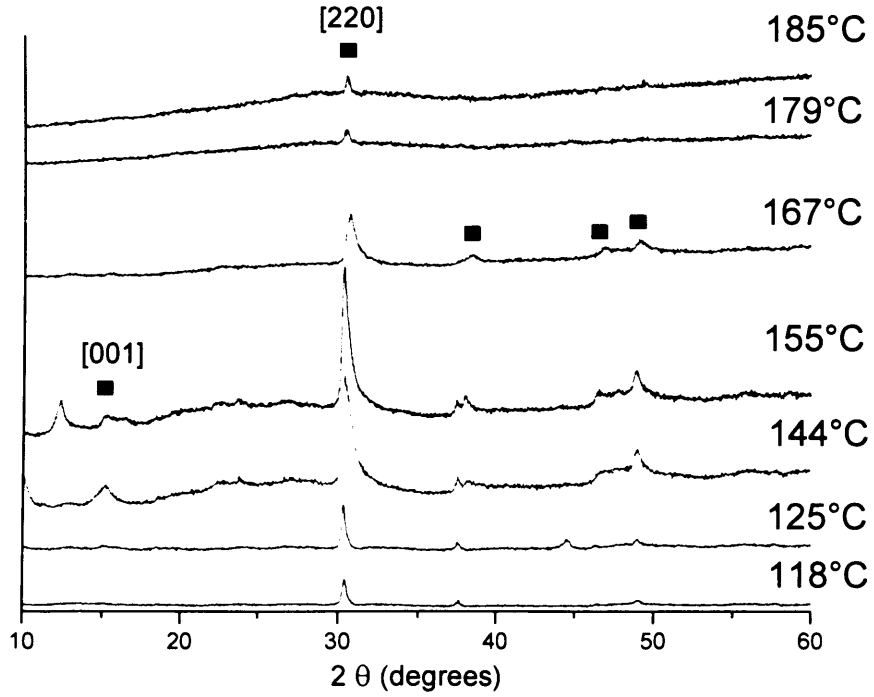

Figure 4.4-Powder diffraction pattern of materials prepared at different temperatures using 1-octanol.

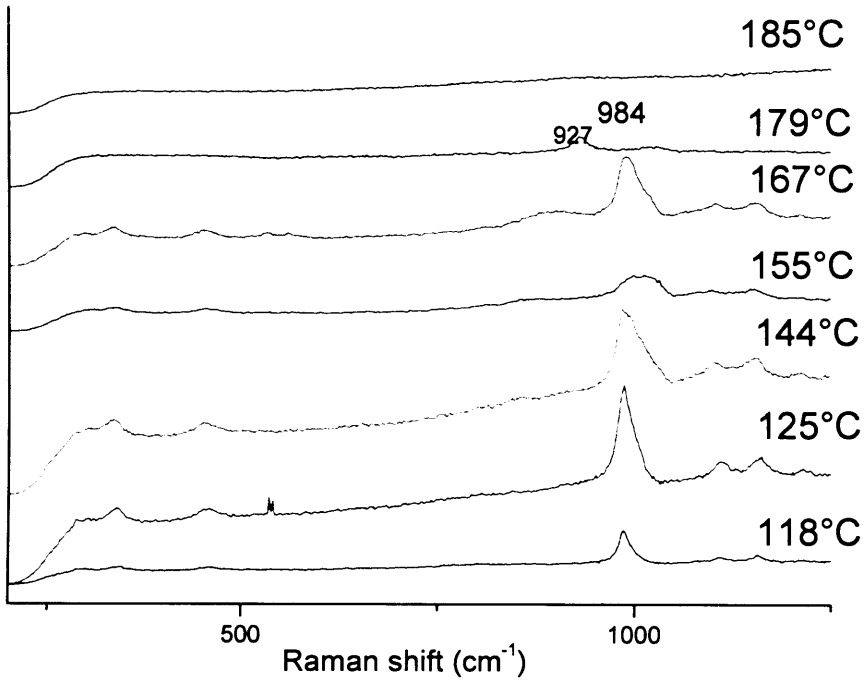

Figure 4.5- Laser Raman spectrum of materials prepared at different temperatures using 1-octanol.

4.3.2.1 V-P-O seeds with 1-octanol

In this section, an investigation of the addition of V-P-O seeds was studied for the preparation of catalyst precursors $VOHPO_4 \cdot 0.5H_2O$ using 1-octanol as a solvent. A summary of the materials prepared with different V-P-O seeds is presented in Table 4.4. Interestingly, the addition of a small amount of $VOHPO_4 \cdot 0.5H_2O$ (0.05 g) as a seed to the reaction mixture before increasing the reflux temperature to 185°C resulted in a high yield of $VOHPO_4 \cdot 0.5H_2O$ even at reflux temperatures (Figure 4.6). Even the small amount of $VOHPO_4 \cdot 0.5H_2O$ seed (0.01g added to the reaction mixture served to produce a crystal to act as a nucleation site. This infers that seeding can increase the rate of $VOHPO_4 \cdot 0.5H_2O$ formation.

Table 4.4. BET surface area and yield of material recovered from reactions with different V-P-O seeds using 1-octanol solvent.

Entry	Sample name	V-P-O seed	BET (m^2/g)	T (°C)	Yield (g)
1	1CR	$VOHPO_4 \cdot 0.5H_2O$ (rosette)	38	185	1.62
2	1CP	$VOHPO_4 \cdot 0.5H_2O$ (platelet)	30	185	1.7
3	1CE	$VO(H_2PO_4)_2$ (E)	10	185	1

Conditions: 1-octanol (100ml), V-P-O seed (0.05 g)

The XRD patterns of the $VOHPO_4 \cdot 0.5H_2O$ prepared with V-P-O seeds are presented in Figure 4.6 (1CR, 1CP and 1CE) respectively. When rosette seeds were used, the $VOHPO_4 \cdot 0.5H_2O$ recovered had XRD patterns that were comparable to the XRD pattern of a standard VPD reaction in 1-octanol (Figure 4.1a), which produced $VOHPO_4 \cdot 0.5H_2O$ where the (220) reflection was dominant with a clear appearance of other reflections (Figure 4.6 1CR).

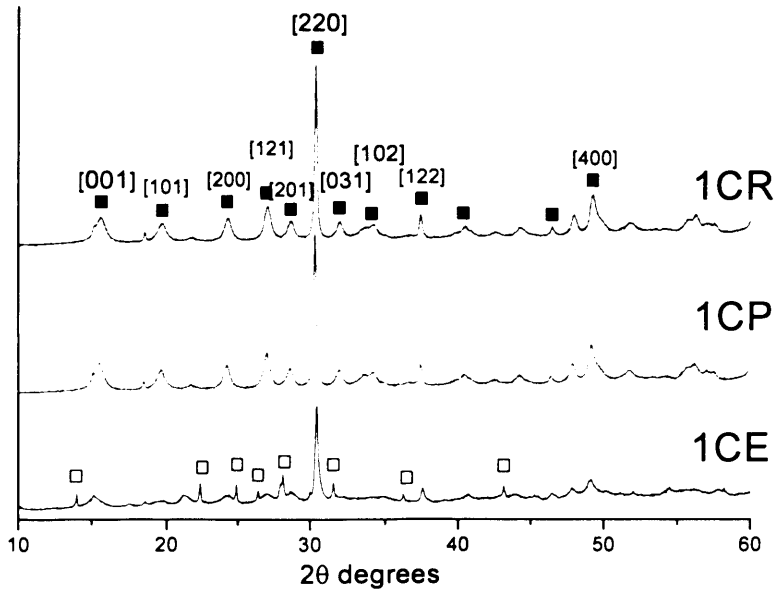

Figure 4.6-Powder XRD patterns of V-P-O material recovered from seeding reactions; (1CR) with a rosette $VOHPO_4 \cdot 0.5H_2O$ seed, (1CP) with a platelet $VOHPO_4 \cdot 0.5H_2O$ seed and (1CE) with $VO(H_2PO_4)_2$ seed. Key: (■) = $VOHPO_4 \cdot 0.5H_2O$ and (□) = $VO(H_2PO_4)_2$

This was also confirmed by SEM and TEM analysis for the 1CR sample (Figure 4.8 1CR and Figure 4.8 1CR respectively), which consisted of rosettes that were radically more open-spaced compared with its starting seed morphology (see Figure 4.1A). Morphological differences are apparent from the XRD pattern (Figure 4.6 1CP) and SEM micrographs (Figure 4.7 1CP) of the sample 1CP with the use of a platelet $VOHPO_4 \cdot 0.5H_2O$ seed. This yielded an aggregated $VOHPO_4 \cdot 0.5H_2O$ product consisting of a mixture of closely spaced rosettes and platelets. However, the XRD patterns of the material prepared with a platelet $VOHPO_4 \cdot 0.5H_2O$ looked quite similar to those prepared with rosettes, as shown in Figure 4.6 1CR and 1CP.

Interestingly, the $VOHPO_4 \cdot 0.5H_2O$ resulting from the addition of a $VO(H_2PO_4)_2$ seed (Figure 4.6 1CE) had a dominant reflection at (220) with the other reflections indexed as (110), (002), (121) and (112) corresponding to the $VO(H_2PO_4)_2$ phase. In addition, the SEM micrograph of this precursor (Figure 4.7 1CE), showed more close-spaced $VOHPO_4 \cdot 0.5H_2O$ rosettes and cubic crystallites corresponding to $VO(H_2PO_4)_2$ phase. This minor phase was confirmed by TEM micrograph to be $VO(H_2PO_4)_2$ as shown in Figure 4.8 1CE. However, the $VO(H_2PO_4)_2$ crystallites appeared to have a more cuboidal morphology (arrowed in Figures 4.7 1CE and 4.8, 1CE) after the reaction as compared to the octagonal-shaped starting $VO(H_2PO_4)_2$ seeds.

This work was extended by the use of different amounts of the V-P-O seed with 1-octanol, which showed that even a small amount of the seed (0.01g) can alter the reaction and give a high yield of recovered $VOHPO_4 \cdot 0.5H_2O$.

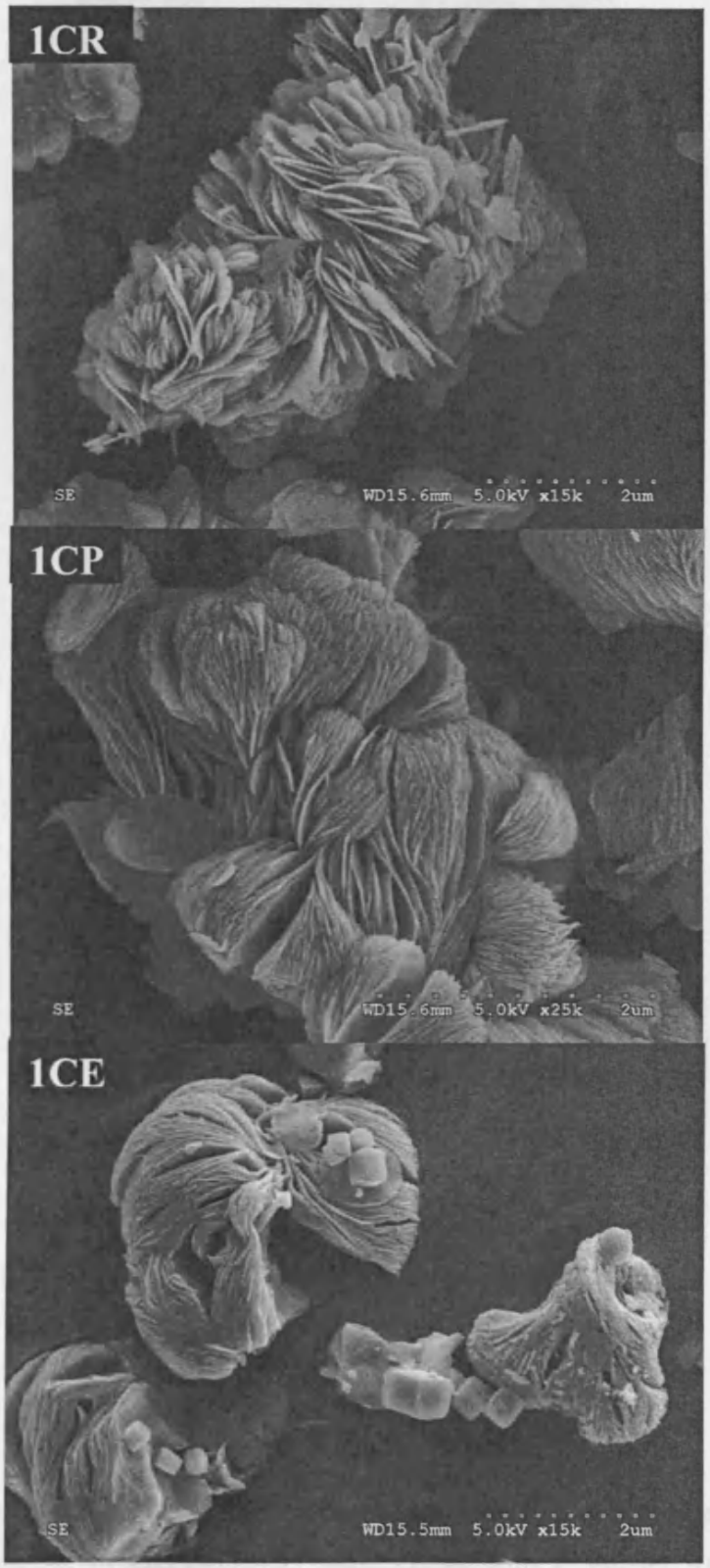

Figure 4.7-SEM micrographs of materials recovered from seeding reactions; (1CR) with a rosette $VOHPO_4 \cdot 0.5H_2O$ seed, (1CP) with a platelet $VOHPO_4 \cdot 0.5H_2O$ seed and (1CE) with $VO(H_2PO_4)_2$ seed using 1-octanol.

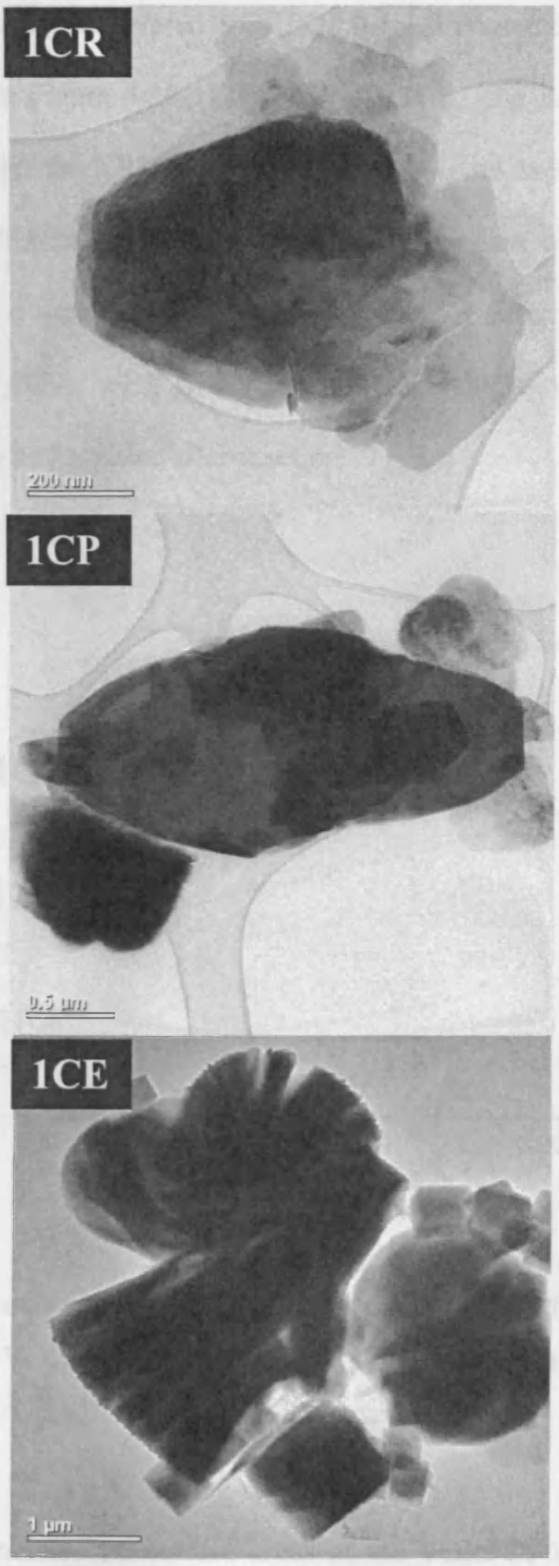

Figure 4.8- The TEM micrograph of V-P-O material recovered from seeding reactions; (1CR) with a rosette $VOHPO_4 \cdot 0.5H_2O$ seed, (1CP) with a platelet $VOHPO_4 \cdot 0.5H_2O$ seed and (1CE) with $VO(H_2PO_4)_2$ seed using 1-octanol.

The Raman spectra of the recovered VOHPO4.0.5H_20 prepared with different V-P-O seeds are presented in Figure 4.10 1CR, 1CP and 1CE. The Raman spectra obtained were in agreement with the XRD. The main band observed at 980 cm^{-1} is assigned to the P-O stretch of $VOHPO_4.0.5H_2O$, which is in agreement with the literature [10]. However, there was a small band at 931 cm^{-1} for the recovered VOHPO4.0.5H_20 prepared with $VO(H_2PO_4)_2$ seed, which is the characteristic band of this phase and confirms the presence of the phase after reaction.

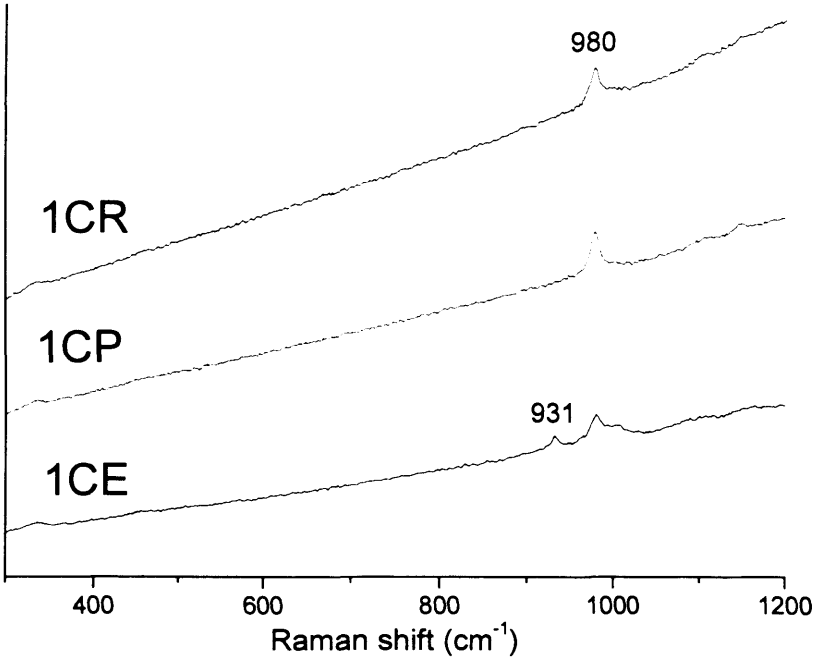

Figure 4.9-Laser Raman spectrum of V-P-O material recovered from seeding reactions; (1CR) with a rosette $VOHPO_4 \cdot 0.5H_2O$ seed, (1CP) with a platelet $VOHPO_4 \cdot 0.5H_2O$ seed and (1CE) with $VO(H_2PO_4)_2$ seed using 1-octanol.

The use of seeds influences the surface areas of the $VOHPO_4 \cdot 0.5H_2O$ phases that are formed as presented (Table 4.4). Without seeding, a typical preparation with 1-octanol leads to a surface area of 33 m^2/g. With rosette seeds, the area increased to 38 m^2/g, but

the use of platelet seeds and $VO(H_2PO_4)_2$ seeds led to a decrease in surface area. These observations are consistent with the microscopy described previously.

(1) Appendix 4.1- The XRD patterns of new materials prepared using different amounts of rosette seed (0.01, 0.05 and 0.1g)

(2) Appendix 4.2- The XRD patterns of new materials prepared using different amounts of $VO(H_2PO_4)_2$ seed (0.01, 0.05 and 0.1g)

4.3.2.2 Inorganic materials and phosphate compounds seeds with 1-Octanol

Various inorganic materials were added to the reaction in place of V-P-O seeds to determine whether the nature of the material was important and to examine their effect as a seed. Silica, activated carbon, silicon carbide, boron nitride, boron phosphate, vanadium pentoxide, titania and alumina were used as the seed for the reaction of $VOPO_4 \cdot 2H_2O$ with 1-octanol. However, the recovered amounts of materials were ca. 5% excluding the original mass of "seed", which indicates that these compounds had no effect on the reaction.

A summary of these materials with the XRD patterns of the recovered mass are shown in Appendix 4.3

4.3.3 Influence of different alcohols on morphology

The use of the V-P-O seeds in the VPD type preparation using other alcohols, i.e., 2-methy-1-propanol, 2-butanol and 3-octanol, was also studied. These particular solvents were selected based on the morphology of the resulting V-P-O material during a standard VPD preparation.

4.3.3.1 2-methy-1-propanol

In this section, an investigation of different $VOHPO_4 \cdot 0.5H_2O$ seeds (platelet and rosette) was studied for the preparation of catalyst precursors $VOHPO_4 \cdot 0.5H_2O$ using 2-methy-1-propanol as a solvent. A summary of the materials prepared with different $VOHPO_4 \cdot 0.5H_2O$ seeds (platelet and rosette) is presented in Table 4.5.

Table 4.5. BET surface area and yield of material recovered from reactions with platelet and rosette $VOHPO_4 \cdot 0.5H_2O$ seeds using 2-methy-1-propanol solvent.

Entry	Sample name	V-P-O seed	BET (m^2/g)	T (°C)	Yield (g)
1	IBR	$VOHPO_4 \cdot 0.5H_2O$ (rosette)	17	Reflux	1.67
2	IBP	$VOHPO_4 \cdot 0.5H_2O$ (platelet)	14	Reflux	1.61

Conditions: 2-methy-1-propanol (50ml) + V-P-O seed (0.05 g)

The XRD patterns of the recovered $VOHPO_4 \cdot 0.5H_2O$ prepared with rosette and platelet seeds are shown in Figure 4.10 IBR and IBP respectively. Both materials have similar patterns with (220) reflection as the dominant reflection with a clear appearance of other reflections of $VOHPO_4 \cdot 0.5H_2O$. However, the intensities of the reflections and the (001) / (220) ratio are higher for the materials prepared with platelet seeds than with rosette

seeds indicating that the type of seed could affect the final morphology of the precursor $VOHPO_4 \cdot 0.5H_2O$.

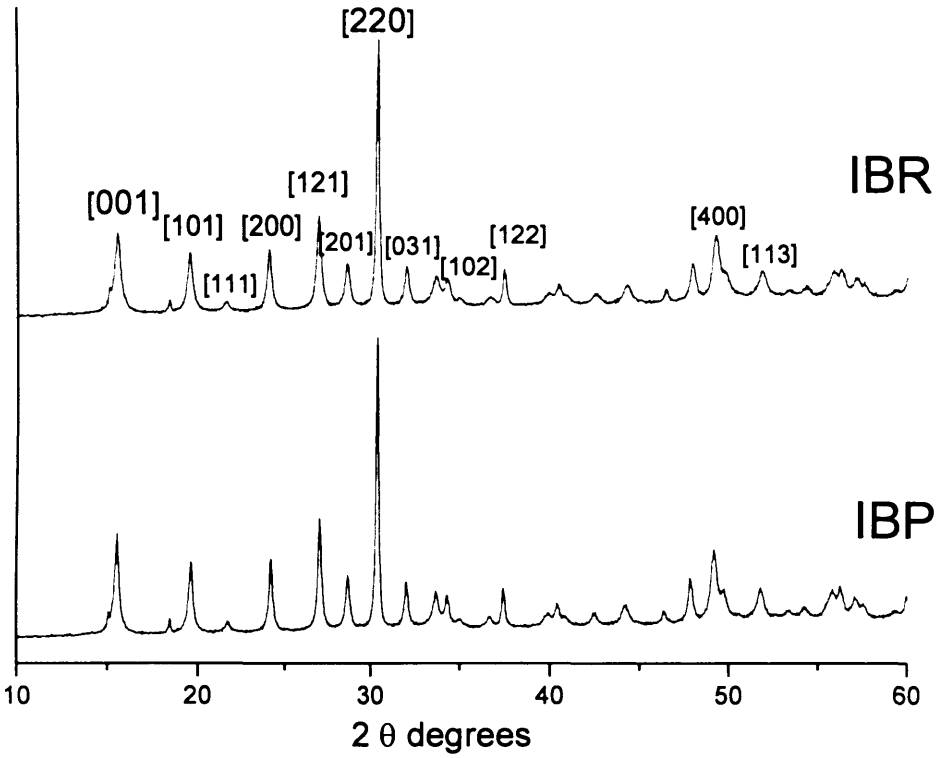

Figure 4.10-Powder XRD patterns of V-P-O material recovered from seeding reactions; (IBR) with a rosette $VOHPO_4 \cdot 0.5H_2O$ seed, (IBP) with a platelet $VOHPO_4 \cdot 0.5H_2O$ seed using 2-methy-1-propanol.

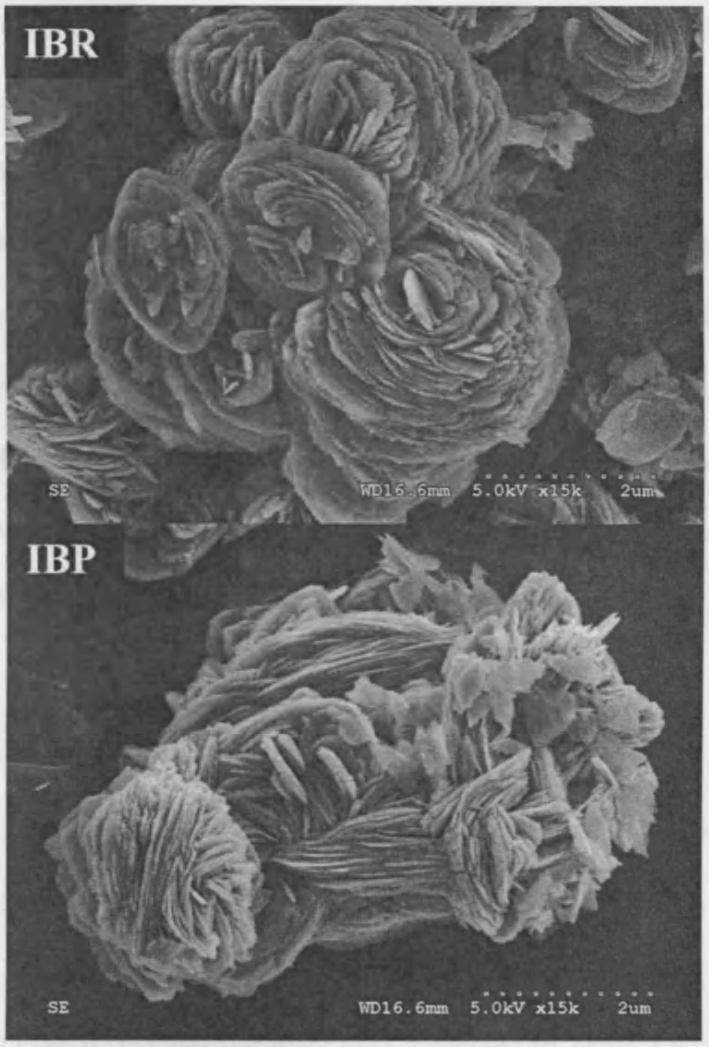

Figure 4.11-SEM micrographs of materials recovered from seeding reactions; (IBR) with a rosette $VOHPO_4 \cdot 0.5H_2O$ seed, (IBP) with a platelet $VOHPO_4 \cdot 0.5H_2O$ seed, using 2-methy-1-propanol.

The SEM micrographs of the recovered $VOHPO_4 \cdot 0.5H_2O$ prepared with rosette and platelet seeds are shown in Figure 4.11 IBR and IBP respectively. Regardless of which $VOHPO_4 \cdot 0.5H_2O$ seed (platelet or rosette) was used, both the resulting materials consisted of similar $VOHPO_4 \cdot 0.5H_2O$ platelets agglomerated in a characteristic rosette-like morphology. However, these materials s showed differences in their morphology compared with the materials prepared using 1-octanol solvent, which showed more close-spaced rosettes.

The BET surface area of the resulting $VOHPO_4 \cdot 0.5H_2O$ precursor differed from the original seeds prepared via the standard preparation methods. In particular, the material formed with platelet seeds (IBP) showed an increase in BET surface area to 14 m^2/g as compared to the 9 m^2/g exhibited by the platelet seed materials. In contrast, the product of the rosette seeding experiment (IBR) showed a decrease of BET surface area to 17 m^2/g from the 33 m^2/g presented by the original rosette seed. XRD analyses (Figure.4.10 IBR and IBP) of these products are in good agreement with the SEM and BET results showing decreased intensity (220) reflections and increased intensity (001) reflections as compared to the rosette seed (Figure 4.1 (a)).

4.3.3.2 2-butanol

In this section, an investigation of different $VOHPO_4 \cdot 0.5H_2O$ seeds (platelet and rosette) was studied for the preparation of catalyst precursors $VOHPO_4 \cdot 0.5H_2O$ using 2-butanol as a solvent. A summary of the materials prepared with different $VOHPO_4 \cdot 0.5H_2O$ seeds (platelet and rosette) is presented in Table 4.6.

Table 4.6. BET surface area and yield of material recovered from reactions with platelets and rosettes $VOHPO_4 \cdot 0.5H_2O$ seeds using 2-butanol solvent.

Entry	Sample name	V-P-O seed	BET (m^2/g)	T (°C)	Yield (g)
1	2BR	$VOHPO_4 \cdot 0.5H_2O$ (rosette)	13	Reflux	1.41
2	2BP	$VOHPO_4 \cdot 0.5H_2O$ (platelet)	8	Reflux	1.47

Conditions: 2-butanol (50ml) + V-P-O seed (0.05 g)

The XRD patters of the recovered $VOHPO_4 \cdot 0.5H_2O$ prepared with rosette and platelet seeds are shown in Figure 4.13 2BR and 2BP respectively. The materials in Figure 4.12 2BR and 2BP demonstrate a switch in the relative intensity of the (001) and (220)

reflections where the (220) reflection noticeably became the dominant peak as compared to the original seed, where the (001) reflection was the dominant peak, as shown in Figure 4.1(b). This indicates the gradual progression towards a rosette-type structure particularly when rosette seed was used, as shown in Figure 4.12 2BR. The BET surface areas for these recovered $VOHPO_4 \cdot 0.5H_2O$ precursors are 13 and 8 m^2/g for the rosette and platelet seeded reactions respectively.

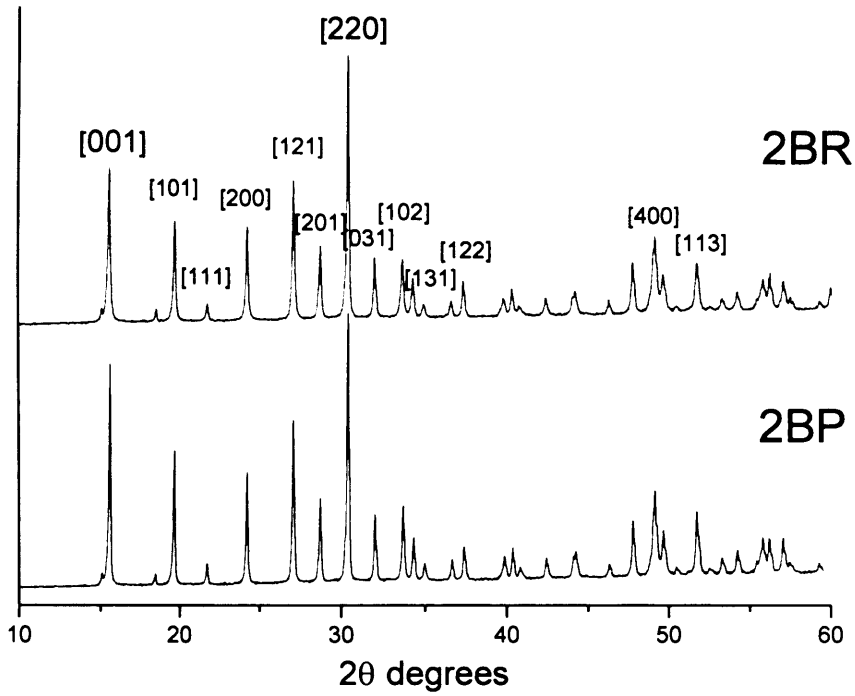

Figure 4.12-Powder XRD patterns of V-P-O material recovered from seeding reactions; (2BR) with a rosette $VOHPO_4 \cdot 0.5H_2O$ seed, (2BP) with a platelet $VOHPO_4 \cdot 0.5H_2O$ seed using 2-butanol.

The SEM micrographs of the recovered $VOHPO_4 \cdot 0.5H_2O$ precursors prepared with rosette and platelet seeds are shown in Figure 4.13 2BR and 2BP respectively. Both of the resulting $VOHPO_4 \cdot 0.5H_2O$ precursors consisted of platelets with a rhomboidal appearance and an average thickness between 200~300 nm with a length of (1~5 μm). In addition, the recovered $VOHPO_4 \cdot 0.5H_2O$ precursors prepared with rosettes

demonstrated rhomboidal platelets and rosette-like aggregation (30~40 vol %), as shown in Figure 4.13 (a, b), which may suggest that the nature of the seed can affect the formation of the $VOHPO_4 \cdot 0.5H_2O$ precursor.

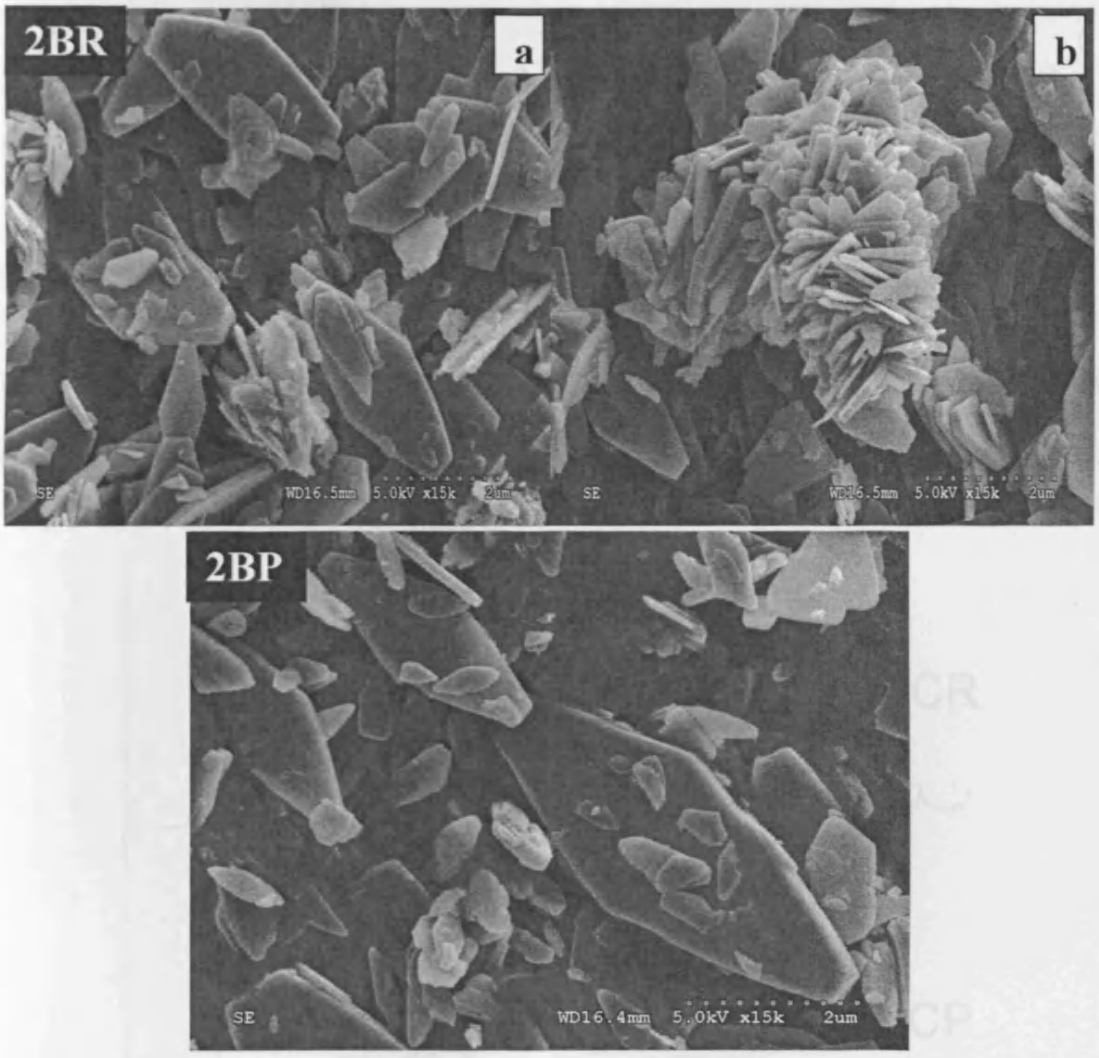

Figure 4.13-SEM micrographs of materials recovered from seeding reactions; (2BR (a and b) with a rosette $VOHPO_4 \cdot 0.5H_2O$ seed, (2BP) with a platelet $VOHPO_4 \cdot 0.5H_2O$ seed using 2-butanol.

4.3.3.3 3-octanol

In this section, an investigation of different $VOHPO_4 \cdot 0.5H_2O$ (platelets and rosettes) was studied for the preparation of catalyst precursors $VOHPO_4 \cdot 0.5H_2O$ using 3-octanol

as a solvent. A summary of the materials prepared with different $VOHPO_4 \cdot 0.5H_2O$ seeds (platelet and rosette) is presented in Table 4.7.

Table 4.7. BET surface area and yield of material recovered from reactions with platelets and rosettes $VOHPO_4 \cdot 0.5H_2O$ seeds using 3-octanol solvent.

Entry	Sample name	V-P-O seed	BET (m^2/g)	T (°C)	Yield (g)
1	3CR	$VOHPO_4 \cdot 0.5H_2O$ (rosette)	3	Reflux	1.60
2	3CP	$VOHPO_4 \cdot 0.5H_2O$ (platelet)	4	Reflux	1.67

Conditions: 3-octanol (100ml), V-P-O seed (0.05 g)

The reaction of the dihydrate ($VOPO_4 \cdot 2H_2O$) using 3-octanol at the reflux temperature usually leads to the formation of the $VO(H_2PO_4)_2$ phase as reported in most studies[11].

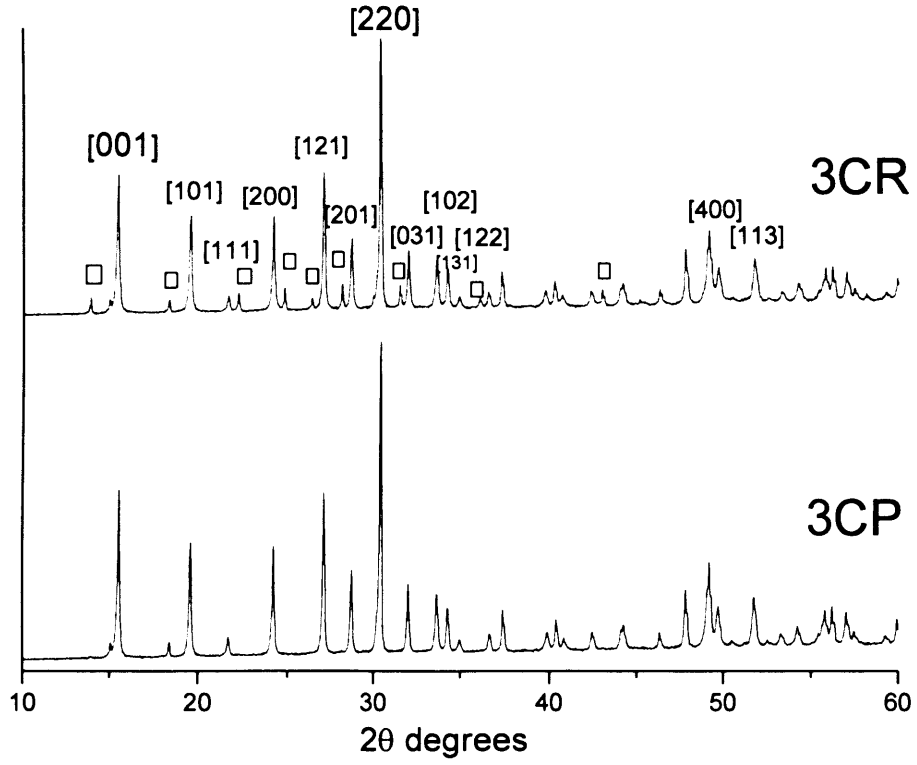

Figure 4.14-Powder XRD patterns of V-P-O material recovered from seeding reactions; (3CR) with a rosette $VOHPO_4 \cdot 0.5H_2O$ seed, (3CP) with a platelet $VOHPO_4 \cdot 0.5H_2O$ seed using 3-octanol. Key: (□) = $VO(H_2PO_4$

The powder XRD pattern and SEM micrograph of this material are shown in Figure 4.1(c). However, the use of a rosette $VOHPO_4 \cdot 0.5H_2O$ seed in this reaction resulted in mixed phase material, as shown by the XRD pattern and Raman spectrum (Figure 4.14 3CR and 4.15, 3CR respectively). The mixed phase material shows the expected phase $VO(H_2PO_4)_2$ as a minor phase and $VOHPO_4 \cdot 0.5H_2O$ phase is the main component, as determined by the XRD intensities ratio of the two phases and the presence of the Raman peak at 935 cm^{-1} of $VO(H_2PO_4)_2$. Interestingly, the use of a platelet seed with the reaction showed only $VOHPO_4 \cdot 0.5H_2O$ phase as presented in the XRD pattern and Raman spectrum (Figure 4.14 3CP and 4.15 3CP respectively). However, the dominant plane in the XRD pattern is now the (220) reflection for both materials, instead of the (001) reflection compared to the standard platelet morphology (Figure 4.1 c).

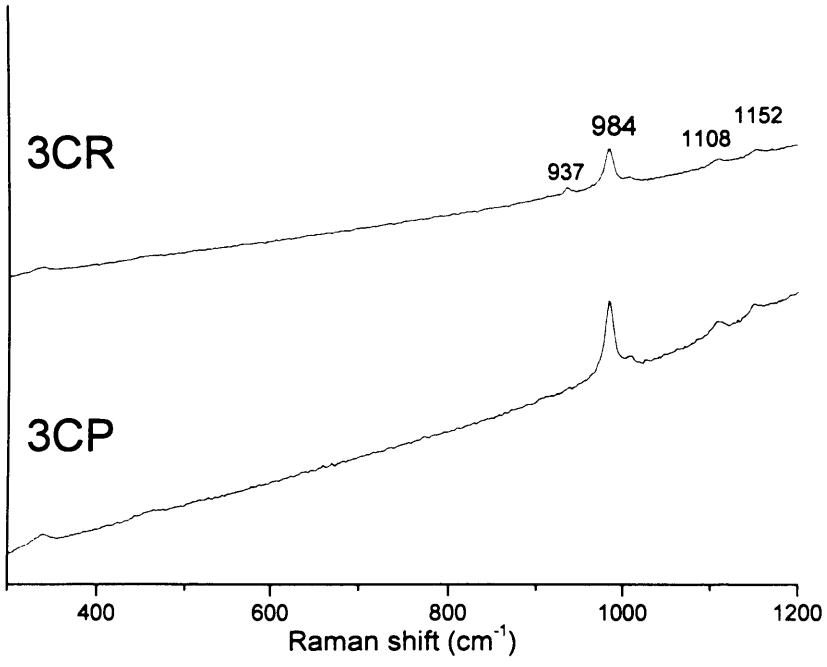

Figure 4.15-Laser Raman spectrum of V-P-O material recovered from seeding reactions; (3CR) with a rosette $VOHPO_4 \cdot 0.5H_2O$ seed, (3CP) with a platelet $VOHPO_4 \cdot 0.5H_2O$ seed using 3-octanol.

The SEM micrographs of the recovered $VOHPO_4 \cdot 0.5H_2O$ prepared with rosette and platelet seeds are shown in Figure 4.16 3CR and 3CP respectively. Both samples showed aggregation of irregular angular platelets. In addition, the sample that was prepared with a rosette seed also showed an aggregation of many platelets retaining a rosette-like structure, similar to the materials prepared using 2-butanol with rosettes (see Figure 4.14 (b).

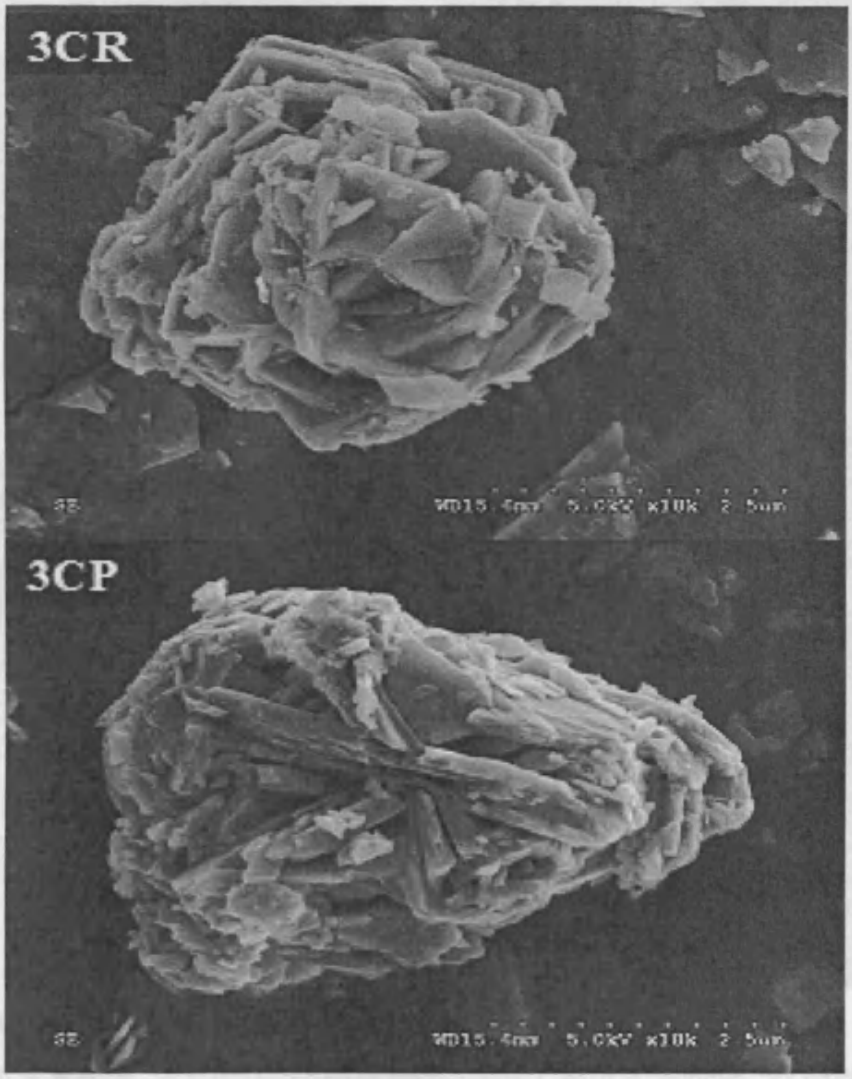

Figure 4.16-SEM micrographs of materials recovered from seeding reactions; (3CR) with a rosette $VOHPO_4 \cdot 0.5H_2O$ seed, (3CP) with a platelet $VOHPO_4 \cdot 0.5H_2O$ seed using 3-octanol.

The TEM micrographs of the recovered $VOHPO_4 \cdot 0.5H_2O$ prepared with rosette and platelet seeds are shown in Figure 4.17 3CR and 3CP respectively. Both materials showed typical angular platelets $VOHPO_4 \cdot 0.5H_2O$. Selected area diffraction patterns (Figure 4.17 3CR (b) and 3CP (b)) obtained at normal incidence to the isolated platelets gave a characteristic pattern corresponding to [001] $VOHPO_4 \cdot 0.5H_2O$.

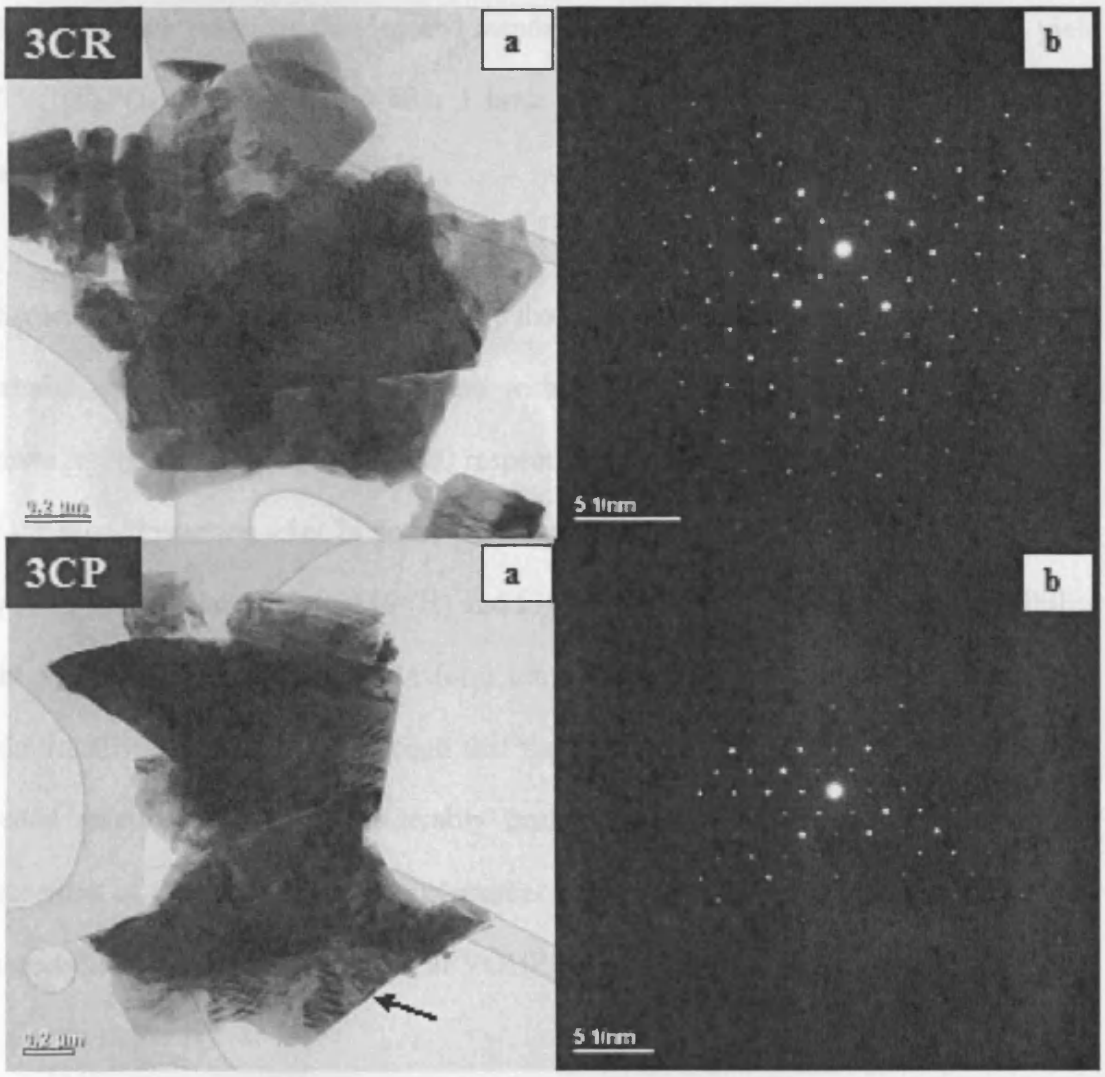

Figure 4.17-(a) TEM micrographs of materials recovered from seeding reactions; (3CR) with a rosette $VOHPO_4 \cdot 0.5H_2O$ seed, (3CP) with a platelet $VOHPO_4 \cdot 0.5H_2O$ seed using 3-octanol (b) SADP* of the arrowed platelet corresponding to [001] $VOHPO_4 \cdot 0.5H_2O$

*: SADP: selected area diffraction pattern

4.3.3.4 Synthesis time online

Comparison studies were carried out online for 24 hours where a platelet $VOHPO_4 \cdot 0.5H_2O$ seed (0.05) was added and compared to the standard reaction using 3-octanol, as illustrated in Figure 4.18. It was observed that the recovered materials with the seeded reaction had a higher reaction rate compared to the standard reaction. Moreover, both reactions (seeded and standard) reached the expected theoretical yield of $VO(H_2PO_4)_2$ phase (~ 0.6g) after 1 hour and remained constant for up to 8 hours time-on-line.

Characterisations by XRD and Raman of the seeded materials show that the recovered material comprised $VO(H_2PO_4)_2$ phase with $VOHPO_4 \cdot 0.5H_2O$ as a minor phase, as shown in Figure 4.19 and Figure 4.20 respectively. Interestingly, the recovered material of the seeded reaction after 24 hours was mainly $VOHPO_4 \cdot 0.5H_2O$ phase, as confirmed by XRD and Raman (Figure 4.19 (H) and Figure 4.20 (H)). This leads to the possibility that $VO(H_2PO_4)_2$ phase could transform into the catalyst precursor $VOHPO_4 \cdot 0.5H_2O$. Additionally, it should be mentioned that the mass of the recovered material from the seeded reaction increased considerably from 8 hours to 24 hours. Furthermore, the intensities of the main peaks for the present phases changed with time-on-line and the characteristic peaks corresponding to $VOHPO_4 \cdot 0.5H_2O$ phase increased systematically, as shown in Table 4.8.

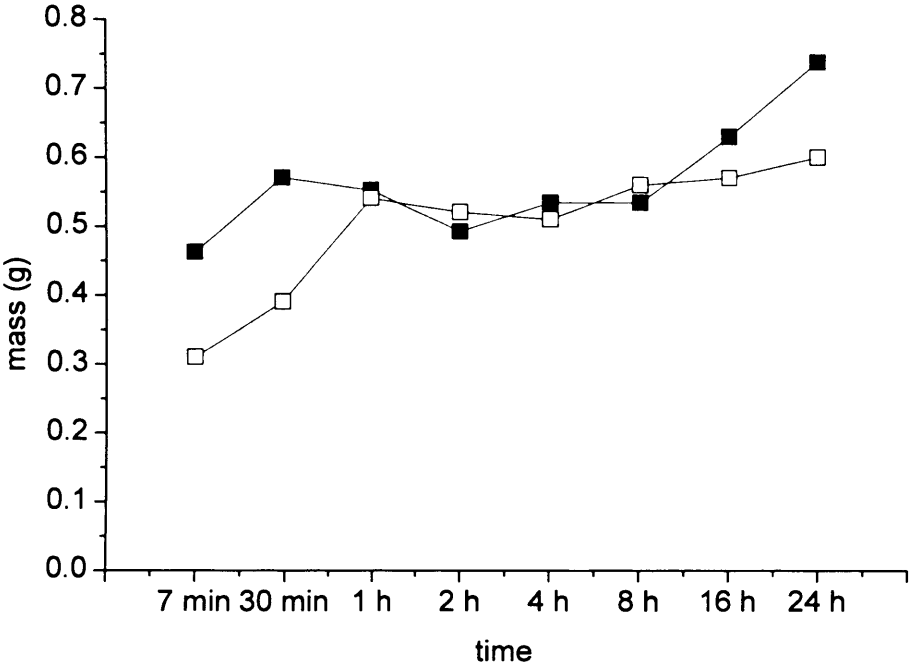

Figure 4.18-The recovered mass of V-P-O material with time of reaction; key: □ the standard reaction ($VOPO_4 \cdot 2H_2O$ + 3-octanol): ■ the addition of platelet seeds (0.05 g).

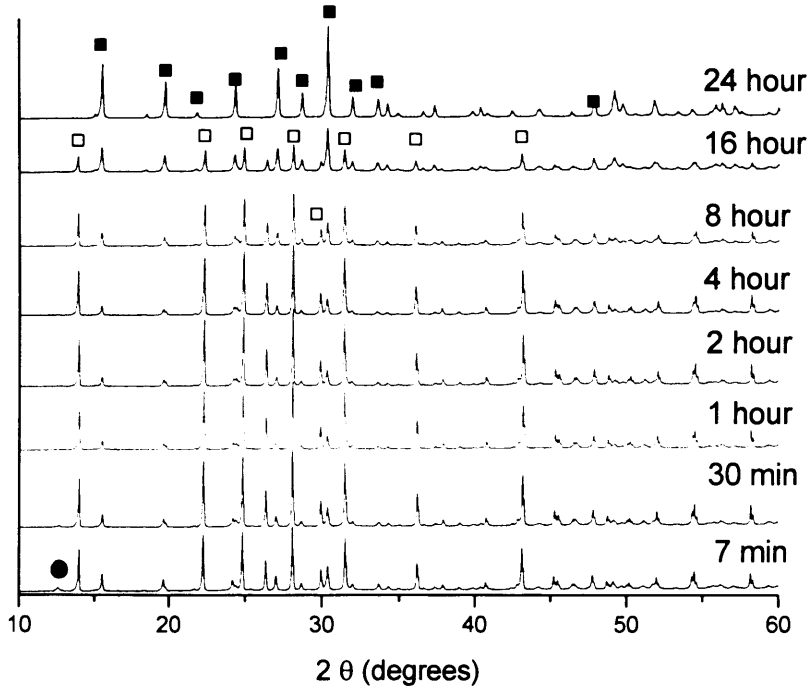

Figure 4.19-Powder XRD pattern of recovered V-P-O material as a function of time of reaction of $VOPO_4 \cdot 2H_2O$ + 3-octanol with addition of platelet seeds (0.05 g). Keys: ■; $VOHPO_4 \cdot 0.5H_2O$, □; $VO(H_2PO_4)_2$ and ●; $VOPO_4 \cdot 2H_2O$.

Table 4.8- XRD assignations of the most intensive peaks for the recovered V-P-O materials as a function of time of reaction of $VOPO_4 \cdot 2H_2O$ + 3-octanol with addition of platelet seeds (0.05 g)

7 min			**30 min**		
Entry	d-spacing [Å]	Rel. Int. [%]	Entry	d-spacing [Å]	Rel. Int. [%]
3	5.71	29	3	5.71	19
5	4.52	23	5	4.51	18
6	3.99	88	6	3.99	88
7	3.58	88	7	3.58	89
9	3.28	18	9	3.29	17
10	3.17	100	10	3.17	100
11	2.95	22	11	2.96	12
12	2.83	85	12	2.83	87
1 hour			**2 hour**		
Entry	d-spacing [Å]	Rel. Int. [%]	Entry	d-spacing [Å]	Rel. Int. [%]
2	5.70	15	2	5.71	14
3	4.50	14	3	4.51	13
6	3.58	90	4	3.99	91
7	3.37	46	6	3.58	88
8	3.29	13	8	3.29	14
9	3.17	100	9	3.17	100
10	2.96	14	10	2.96	12
11	2.83	87	11	2.83	86
4 hour			**8 hour**		
Entry	d-spacing [Å]	Rel. Int. [%]	Entry	d-spacing [Å]	Rel. Int. [%]
2	5.71	16	2	5.71	29
4	4.51	12	4	4.52	22
5	3.99	87	5	3.99	86
7	3.59	86	7	3.59	87
9	3.28	12	9	3.28	24
10	3.17	100	10	3.17	100
11	2.96	10	11	2.95	27
12	2.83	89	12	2.83	88
16 hour			**24 hour**		
Entry	d-spacing [Å]	Rel. Int. [%]	Entry	d-spacing [Å]	Rel. Int. [%]
2	5.71	83	1	5.71	54
4	4.53	45	3	4.52	38
5	3.99	53	6	3.29	53
7	3.58	56	8	2.94	100
8	3.29	67			
9	3.17	65			
10	2.94	100			
12	2.83	58			

Keys: $VOHPO_4 \cdot 0.5H_2O$ (red colour) and $VO(H_2PO_4)_2$ (black colour)

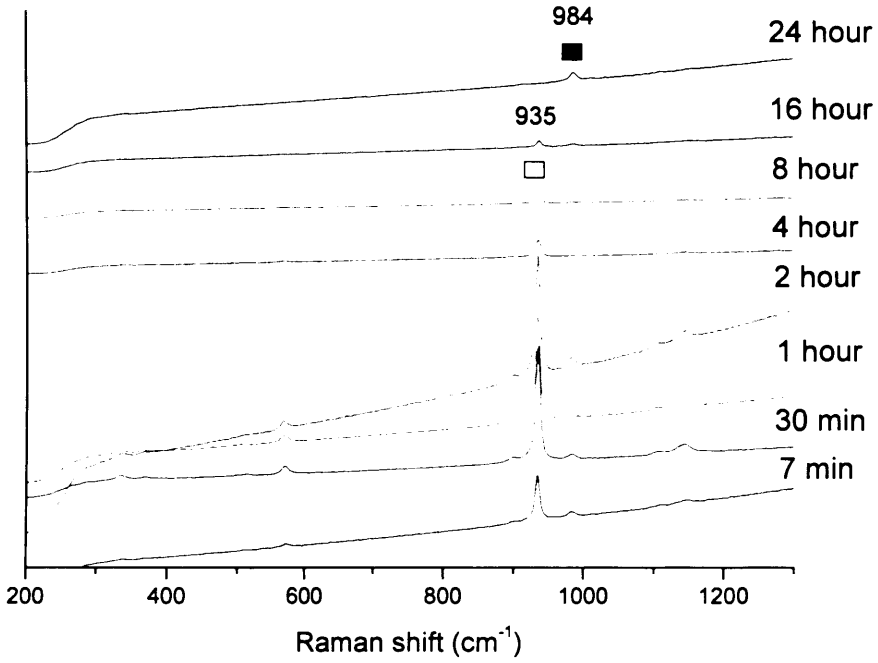

Figure 4.20-Powder XRD pattern of recovered V-P-O material as a function of time of reaction of $VOPO_4 \cdot 2H_2O$ + 3-octanol with addition of platelet seeds (0.05 g). Keys: ■; $VOHPO_4 \cdot 0.5H_2O$, and □; $VO(H_2PO_4)_2$

(4) Appendix 4.4- The XRD patterns of new materials prepared using 3-octanol with different amounts of rosette seed (0.01, 0.05 and 0.1g)

(5) Appendix 4.5- The XRD patterns of new materials prepared using 3-octanol with different amounts of platelet seed (0.01, 0.05 and 0.1g)

4.3.4 Catalytic testing

Table.4.9 Catalytic performance of the catalyst derived from using the recovered V-P-O material seeded with platelet (P) and rosette (R) $VOHPO_4 \cdot 0.5H_2O$ prepared with 2-methyl-1-propanol (IBP and IBR) and with 2-butanol (2BP and 2BR) for n-butane oxidation [a].

Catalyst	Surface area (m^2/g) (b)		Butane conversion (%)	MA selectivity (%)	Specific Activity ($x10^{-4}$)[c]	Intrinsic Activity ($x10^{-5}$)[d]
	precursor	catalyst				
IBP	14	20	57	64	3.4	1.7
IBR	17	25	61	65	3.7	1.5
2BP	8	12	43	59	2.3	2.0
2BR	13	19	44	52	2.1	1.1

a Reaction conditions: 400 .C, 1.7 % *n*-butane in air, GHSV = 2000 h.1.
b All samples were degassed for an hour at 120°C before analysis
c Specific activity: mol maleic anhydride formed/g catalyst/h.
d Intrinsic Activity : mol maleic anhydride formed/m^2/h.

The BET surface areas for the recovered V-P-O material with 2-methyl-1-propanol (IBP and IBR) are 14 and 17 m^2/g for the platelet and rosette seeded reactions respectively. Evaluation of these materials gave specific activities of 3.4 and 3.7 x 10^{-4} mol_{MA}/g catalyst/h respectively (Table 4.9).

The BET surface areas for the recovered V-P-O material with 2-butanol (2BP and 2BR) are 8 and 13 m^2/g for the platelet and rosette seeded reactions respectively. Evaluation of these materials gave specific activities of 2.3 and 2.1 x 10^{-4} mol_{MA}/g catalyst/h respectively (Table 4.9).

Table 4.10. Evaluation of butane oxidation using the recovered V-P-O material seeded with platelet (3CP) and rosette (3CR) $VOHPO_4 \cdot 0.5H_2O$ and standard VPD reaction with 3-octanol $\{VO(H_2PO_4)_2\}$ in 3-octanol

Catalyst	Surface area (m^2/g)		Butane conversion (%)	MA selectivity (%)	Specific Activity ($x10^{-4}$)[c]	Intrinsic Activity ($x10^{-5}$)[d]
	precursor	catalyst				
3CP	4	8	45	65	2.7	3.4
3CR	3	11	30	55	1.5	1.4
$VO(H_2PO_4)_2$	2	4	3	0	0	0

a Reaction conditions: 400 .C, 1.7 % *n*-butane in air, GHSV = 2000 h.1.
b All samples were degassed for an hour at 120°C before analysis
c Specific activity: mol maleic anhydride formed/g catalyst/h.
d Intrinsic Activity : mol maleic anhydride formed/m^2/h.

The BET surface areas for the recovered V-P-O material with 3-octanol (3CP and 3CR) are 4 and 3 m^2/g for the platelet and rosette seeded reactions which is comparable to $VO(H_2PO_4)_2$ which has a surface area of 2 m^2/g. Butane oxidation experiments conducted using these materials, (Table 5, A and B) indicate that despite the low surface area of these precursors, they still perform reasonably well. In particular, the sample recovered from a platelet seeded reaction, having an intrinsic activity of 3.4 x 10^{-5} $mol_{MA}/m^2 \cdot h$ is significantly higher than that of a standard VPD rosette material (*ca.* 1.9 x 10^{-5} $mol_{MA}/m^2 \cdot h$). The presence of minor quantities of the $VO(H_2PO_4)_2$ phase in the rosette seeded sample concurs with the lower measured intrinsic activity (1.4 x 10^{-5} $mol_{MA}/m^2 \cdot h$) as compared to the former material. The enhanced intrinsic activity of this mixed phase material is of interest since the presence of $VO(H_2PO_4)_2$ typically leads to lower activity.

4.4 Discussion

4.4.1 1-octanol

The XRD patterns of VOHPO4.0.5H_20 precursors prepared using the primary alcohols (1-octanol in this study) are identical (Figure 4.1) with the [220] reflection; this was virtually the only feature of the diffraction pattern, which is characteristic of VOHPO4.0.5H_20 with a rosette morphology. The SEM micrographs (Figure 4.1a) of these precursors showed a rosette-like morphology, which is in agreement with previous studies using primary alcohols.

It was observed that heating vanadium phosphate dihydrate $VOPO_4 \cdot 2H_2O$ in 1-octanol led to the formation of $VOHPO_4 \cdot 0.5H_2O$ in a high yield (as illustrated in Table 4.3). However, when the reaction was carried out at a temperature of > 160°C, the recovered mass of the expected $VOHPO_4 \cdot 0.5H_2O$ decreased giving a small amount, which indicates the effect of temperature on the formation of $VOHPO_4 \cdot 0.5H_2O$ despite the boiling point of 1-octanol being 185°C. Usually, such reactions are conducted under reflux conditions although a small amount of $VOHPO_4 \cdot 0.5H_2O$ formed under the reflux condition of 1-octanol, which was confirmed by the XRD patterns and Raman spectra (Figure 4.3 and Figure 4.4).

Moreover, the UV/VIS analysis of the recovered blue/black solution showed that the solute phase contained V^{4+} ions, which also contained minor amounts of the $VOHPO_4 \cdot 0.5H_2O$ phase. This means that refluxing $VOPO_4 \cdot 2H_2O$ with 1-octanol can give $VOHPO_4 \cdot 0.5H_2O$ with a low yield (< 10%) compared with when the reaction is carried out at a low temperature (< 160°C), which usually gives a (>90%) yield of $VOHPO_4 \cdot 0.5H_2O$.

Interestingly, the addition of a small amount of $VOHPO_4 \cdot 0.5H_2O$ (0.05 g) as a seed to the reaction mixture before increasing the reflux temperature to 185°C resulted in a high yield of $VOHPO_4 \cdot 0.5H_2O$ even at reflux temperatures (Figure 4.6). This seed served to produce a crystal that could be acted upon as a nucleation site, therefore, lowering the energy of $VOHPO_4 \cdot 0.5H_2O$ formation.

For this reason, a comparison study was conducted where the yield of hemi-hydrate product was monitored as a function of time-on-line for reactions using 1-octanol with and without a '$VOHPO_4 \cdot 0.5H_2O$ seed'. This is presented in Figure 4.21, which shows that the $VOHPO_4 \cdot 0.5H_2O$ material recovered an almost complete yield after 24h refluxing at 185°C with the seed. The presence of the $VOHPO_4 \cdot 0.5H_2O$ seed (having a rosette morphology) resulted in rapid $VOHPO_4 \cdot 0.5H_2O$ formation. This method, as a result, overcomes the formation of the blue/black V^{4+} solute, which was observed at reflux condition. It was also observed that the $VOHPO_4 \cdot 0.5H_2O$ material recovered an almost complete yield after 24h refluxing at 185°C with the seed. This indicates that the nucleation process occurs at *ca.* 8 minutes from the beginning of heating the reaction from room temperature.

This finding is highly important for two reasons. Firstly, this is the first report of the use of a seed to direct the formation of V-P-O materials. Secondly, the use of the seed can lead to dramatic morphological changes in the resulting material compared to the material prepared without the seed as illustrated in this report.

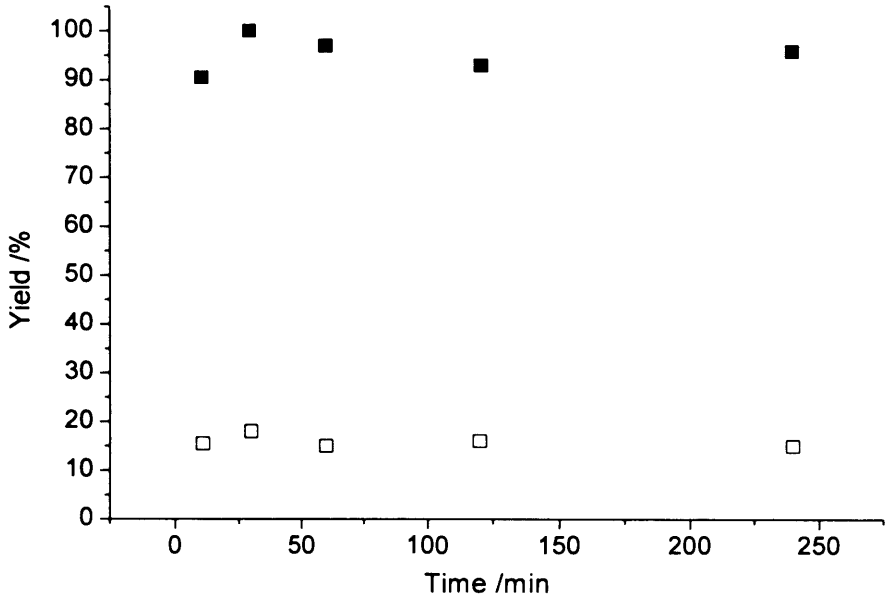

Figure. 4.21-Yield of V-P-O material from a reaction at reflux temp (185°C) of 1-octanol; (closed squares) with rosette seed (0.05 g) and (open squares) standard preparation.

To test the hypothesis that the addition of a minor amount of hemihydrate $VOHPO_4.0.5H_2O$ material to the reaction mixture serves to create nucleation or seeding sites, a small amount of the $VOHPO_4.0.5H_2O$ rosette material (shown in Figures 4.1 a) was refluxed on its own for 2 h at 185°C in 1-octanol. Not all the $VOHPO_4.0.5H_2O$ dissolved in this time and the residual material was recovered and dried. It can be seen from the SEM and TEM micrographs presented in Figures 4.22 a and b respectively, that some of the petals of the rosette which were originally about 2μm in lateral size have fragmented to produce much smaller platelets that are only about 0.1-0.2μm in dimension. Electron diffraction confirmed these entities to be poorly crystalline $VOHPO_4.0.5H_2O$, and it thought that these smaller platelet fragments serve as the 'seed' crystallites and act a template for subsequent $VOHPO_4.0.5H_2O$ growth.

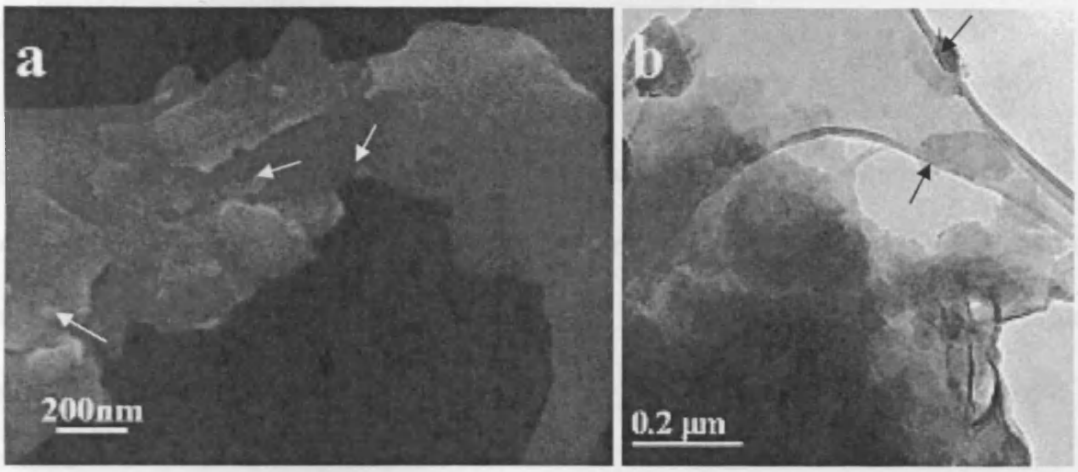

Figure 4.22- a) High resolution SEM and b) BF TEM micrographs of a disintegrated "petal" from a recovered rosette-type seed precursor that was refluxed in 1-octanol for 2h at 185°C. Some residual [001] $VOHPO_4 \cdot 0.5H_2O$ fragments (arrowed) remain which can act as seeding templates.

Furthermore, the addition of small amounts of different morphology V-P-O seeding material led to dramatic morphological changes in the resulting materials with the reaction of 1-octanol. When a rosette-type seed was used, the $VOHPO_4 \cdot 0.5H_2O$ recovered consisted of rosettes, which were radically more open-spaced than the starting seed morphology whereas an aggregated $VOHPO_4 \cdot 0.5H_2O$ product consisting of a mixture of closely spaced rosettes and platelets formed with the use of a platelet $VOHPO_4 \cdot 0.5H_2O$ seed (Figure 4.7 1CR and 1CP).

Interestingly, the use of $VO(H_2PO_4)_2$ as a seed gave $VOHPO_4 \cdot 0.5H_2O$ with more close-spaced rosettes and cubic crystallites corresponding to the $VO(H_2PO_4)_2$ phase, which shows that this phase can act as a nucleation site to form $VOHPO_4 \cdot 0.5H_2O$ at reflux conditions with a unique morphology (Figure 4.7 1CE). However, the recovered $VOHPO_4 \cdot 0.5H_2O$ yield was less compared with $VOHPO_4 \cdot 0.5H_2O$ seeds' reaction and

the surface area was also small, which indicates the influence of the original seed on the final recovered $VOHPO_4 \cdot 0.5H_2O$ materials.

The seeding study was extended using various inorganic materials, which were added to the reaction in place of V-P-O seeds with 1-octanol solvent. However, the recovered amounts of materials were *ca.* 5% excluding the original mass of "seed", which indicates that these compounds had no effect on the reaction of $VOPO_4 \cdot 2H_2O$ with 1-octanol.

4.4.2 2-methy-1-propanol

The use of the $VOHPO_4 \cdot 0.5H_2O$ seeds (platelet and rosette) with the reaction of $VOPO_4 \cdot 2H_2O$ with iso-butanol showed a significant effect on the recovered $VOHPO_4 \cdot 0.5H_2O$ precursors. Irrespective of whether a $VOHPO_4 \cdot 0.5H_2O$ platelet or rosette seed was used, the resulting materials both consisted of similar $VOHPO_4 \cdot 0.5H_2O$ plates agglomerated in a characteristic rosette-like morphology (Figure 4.11 IBR and IBP. However, these materials showed a significant difference in the morphology compared with the materials prepared using 1-octanol solvent, which showed more close-spaced rosettes (Figure 4.7 1CR).

4.4.3 2-Butanol

As previously reported, the use of 2-butanol with $VOPO_4 \cdot 2H_2O$ in a standard un-seeded VPD preparation resulted in $VOHPO_4 \cdot 0.5H_2O$ for which the [001] reflection was the dominant feature of the diffraction pattern with discrete rhomboidal platelet morphology (Figure 4.1b).

In contrast, the recovered $VOHPO_4 \cdot 0.5H_2O$ prepared with rosette and platelet seeds using 2-butanol with $VOPO_4 \cdot 2H_2O$ demonstrated a switch in the relative intensity of the (001) and (220) reflections where the (220) reflection became noticeably the dominant peak, as shown from their XRD patterns (Figure 4.13 2BR and 2BP). This indicates the gradual progression towards a rosette-type structure, particularly when rosette seed was used, as shown in Figure 4.12 2BR. In addition, both materials prepared using different seeds showed highly crystalline rhomboidal platelet morphology.

4.4.4 3-octanol

A number of groups have studied $VO(H_2PO_4)_2$ as a catalyst precursor for the oxidation of butane to maleic anhydride [12-13]. Mount and Raffelson [14] reported a preparation of $VO(H_2PO_4)_2$ via heating V_2O_5 and H_3PO_4 in autoclave at 150 °C. They found this material decomposed at 360°C to give $VO(PO_3)$ phase.

As mentioned previously, refluxing $VOPO_4 \cdot 2H_2O$ with 3-octanol produced $VO(H_2PO_4)_2$ phase, which also gave $VO(PO_3)$ after activation for n-butane oxidation [7]. This is in agreement with previous studies that have shown $VO(PO_3)$ is not as catalytically active as $(VO)_2P_2O_7$, which is typically obtained after activating $VOHPO_4.0.5H_2O$ precursor for n-butane oxidation.

Interestingly, the use of a platelet seed with the reaction of dihydrate ($VOPO_4 \cdot 2H_2O$) using 3-octanol at the reflux temperature showed only $VOHPO_4 \cdot 0.5H_2O$ phase as shown in the XRD pattern (Figure 4.14, 3CP). However, the use of rosette $VOHPO_4 \cdot 0.5H_2O$ seed in this reaction results in the mixed phases where $VO(H_2PO_4)_2$ phase as a minor

phase and $VOHPO_4 \cdot 0.5H_2O$ phase is the main phase. This suggests that the presence of a $VOHPO_4 \cdot 0.5H_2O$ seed within the reaction mixture can act as a nucleation site and can direct the reaction to the formation of $VOHPO_4 \cdot 0.5H_2O$ phase.

Studying this reaction online with a platelet $VOHPO_4 \cdot 0.5H_2O$ seed and compared to standard reaction of $VOPO_4 \cdot 2H_2O$ with 3-octanol which suggests that $VO(H_2PO_4)_2$ phase could transforms into the catalyst precursor $VOHPO_4 \cdot 0.5H_2O$. This shows a novelty of this transformation compared with the initial findings that the $VOHPO_4 \cdot 0.5H_2O$ seed can act as a nucleation sites and can direct the reaction to the formation of $VOHPO_4 \cdot 0.5H_2O$.

For this reason, a new experiment has been designed to support this hypothesis. Where $VOPO_4.2H_2O$ (1 g) was refluxed in 3-octanol (50 ml) for 2 hour and then a small amount of the formed material was taken (for analysis). After that a platelet $VOHPO_4 \cdot 0.5H_2O$ seed was added (0.05g) to the reaction mixture and reflux further for 24 hours.

Table 4.11. Reaction condition of illustrating the transformation of standard $VO(H_2PO_4)_2$ material to $VOHPO_4 \cdot 0.5H_2O$

Sample name	Preparation method	Run time (h)	T °C
A	1g dih + 50ml 3-octanol	**2 h**	172
B	sample A + **0.05** platelet seed and reflux for 24h	**24** h	172

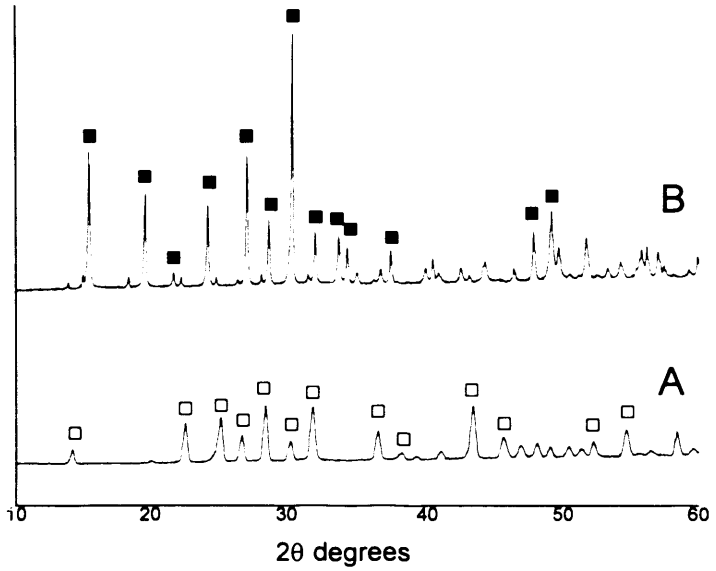

Figure 4.23-Powder XRD pattern illustrating the transformation of standard $VO(H_2PO_4)_2$ material to $VOHPO_4 \cdot 0.5H_2O$ Keys:■;$VOHPO_4 \cdot 0.5H_2O$, □; $VO(H_2PO_4)_2$

It clear that the reaction of $VOPO_4.2H_2O$ with 3-octanol under reflux conditions gave exclusively $VO(H_2PO_4)_2$ phase, as shown from the XRD pattern, which is considered an expected product from this reaction (Figure 4.23 A). Interestingly, the addition of a platelet $VOHPO_4 \cdot 0.5H_2O$ seed 2 hours after the initial reaction demonstrated a strong support of the transformation of $VO(H_2PO_4)_2$ to $VOHPO_4 \cdot 0.5H_2O$ with the presence of a minor amount of $VO(H_2PO_4)_2$ phase, as shown in Figure 4.23 B. This was also supported by the comparison study of this reaction ($VOPO_4.2H_2O$ with 3-octanol) with a platelet $VOHPO_4 \cdot 0.5H_2O$ seed and without it, which demonstrated that both reactions reached the maximum theoretical yield of $VO(H_2PO_4)_2$ within 2 hours and remained constant for about 8 hours. This means that $VO(H_2PO_4)_2$ formed at the beginning of the reaction and then transformed to $VOHPO_4 \cdot 0.5H_2O$ with the presence of a $VOHPO_4 \cdot 0.5H_2O$ seed.

4.5 Conclusion

The use of small amounts of vanadium phosphate materials as seeds during the reaction of $VOPO_4.2H_2O$ with alcohols has been shown to be effective not only in altering the morphology of the product, but also in inducing certain phase transformations. The use of a seed in these cases shows that the rate of material formation can be increased. In the case of reactions in 1-octanol, this overcomes a barrier to hemihydrate formation that prevents the hemihydrate material crystallising and aggregating at reflux temperatures. This has proved beneficial in the formation of catalyst precursors for the partial oxidation of butane to MA.

This study also demonstrates that seeding $VOHPO_4.0.5H_2O$ seeds (rosette or platelet) with $VOPO_4.2H_2O$ using 3-octanol can control the reaction and form $VOHPO_4.0.5H_2O$ with a distinctive morphology. Studying the reaction time online shows that $VO(H_2PO_4)_2$ could be transformed to $VOHPO_4.0.5H_2O$, which has been attempted previously without success. This is the first report of such a transformation occurring in the liquid phase. Finally, testing these samples under reaction conditions shows that they demonstrate high selectivity toward MA and good conversion compared to $VO(H_2PO_4)_2$

4.6 References

[1] G. Centi, F. Trifiro` , J.R. Ebner, V.M. Franchetti, Chem. Rev. 88 (1998) 55.

[2] R. J. Ebner, R. M. Thompson, Catal. Today, 18, 51 (1994)

[3] G.J. Hutchings, J. Mater. Chem. 14 (2004) 3385.

[4] Johnson, J. W.; Johnson, D. C.; Jacobson, A. J.; Brody, J. F. J. Am. Chem. Soc. 1984, 106, 8123.

[5] Bordes, E.; Courtine, P.; Johnson, J. W. J. Solid State Chem. 1984, 55, 270.

[6] Hutchings, G. J.; Sananes, M. T.; Sajip, S.; Kiely, C. J.; Burrows, A.; Ellison, I. J.; Volta, J. C. Catal. Today 1997, 33, 161.

[7] Ellison, I. J.; Hutchings, G. J.; Sananes, M. T.; Volta, J. C. J. Chem. Soc., Chem. Commun. 1994, 1093.

[8] M. T. Sananes, I. J. Ellison, S. Sajip, A. Burrows, C. J. Kiely, J. C. Volta and G. J. Hutchings, J. Chem. Soc., Faraday Trans., 1996, 92, 1, 137.

[9] M. O, Connor, F. Dason and B. K. Hodnett, Appl. Catal., (1990), 64, 161-171.

[10] V. V Guliants,. J. B. Benziger, S.Sundaresan, I. E. Wachs, J. M. Jehng, J.E.Roberts, Catal. Today, 28(1996)275-295.

[11] J. K. Bartley, C. Rhodes, C. J. Kiely, A. F. Carley, G. J. Hutchings, *Phys. Chem. Chem. Phys.* 2000, *21,* 4999-5006.

[12] J. K. Bartley, R. P. K. Wells, and G. J. Hutchings, J. Catal. (2000) 195, 423–427.

[13] M. T. Sananes, G. J Hutchings and J. C. Volta, J. Chem. Soc., (1995) 243.

[14] R. A. Mount, H. Raffelson and W. D. Robinson, Monsanto Co. U.S. Pat. 4116868, 1978.

[15] R. Higgins and G. J. Hutchings, U.S. Pat., 4222945, 1980.

CHAPTER 5

The reaction of $VOPO_4.2H_2O$ with different hydrogen sources

5.1 Introduction

Vanadium phosphate catalysts have been widely studied for the selective oxidation of n-butane to maleic anhydride (MA). Vanadyl pyrophosphate, $(VO)_2P_2O_7$, is the main active component and is usually derived from the precursor $VOHPO_4.0.5H_2O$ via topotactic transformation[1–3]. However, there remains some uncertainty about the role and the nature of phases present in the active catalysts. Some researchers favour a single compound, $(VO)_2P_2O_7$, as the only active phase [2]. Others claim the presence of V^{5+} phases are important to enhance catalyst performance [4].

The standard catalyst precursor used in the preparation of the active catalyst is the vanadium (IV) hydrogen phosphate hemihydrate, $VOHPO_4.0.5H_2O$ which is commonly obtained from the reaction between V_2O_5 and H_3PO_4 in the presence of a reducing agent. In view of this and as discussed in chapter one, vanadium pentoxide is commonly used as the vanadium source and phosphoric acid is used as a source of phosphorus. Consequently, a reducing agent is usually required in order to synthesise the $VOHPO_4.0.5H_2O$ precursor. A number of reducing agents have been reported in the literature [5-6]. Most studies have focused on the use of alcohols as reducing agent and solvent, which has produced a better catalyst precursor with high surface area. However, there are a few studies focus on the use of new reducing agents. This suggests that employing new reducing agents can produce a catalyst precursor with new morphology and high surface area.

CHAPTER 5

In this chapter, several attempts have been investigated to reduce $VOPO_4.2H_2O$ with different hydrogen sources which include:

- Reduction of $VOPO_4.2H_2O$ with hydrogen in aqueous media using autoclave reactors.
- Reduction of $VOPO_4.2H_2O$ using hydrogen gas at different temperatures
- The use of strong reducing agents (N_2H_4 and $NaBH_4$) is also investigated and compared to the reduction of $VOPO_4.2H_2O$.

5.2 Experimental

Different experiments were carried out on the dihydrate materials in order to tentatively reduce the V(V) phase $VOPO_4.2H_2O$ to catalyst precursor $VOHPO_4.0.5H_2O$ (IV) or directly to vanadyl pyrophosphate (IV). Different reducing agents were used in the liquid phase and at the gas-solid interface; in particular hydrogen and strong reducing agent (N_2H_4 and $NaBH_4$). (For further details, see Chapter 2).

All the prepared materials were characterised using a combination of X-ray powder diffraction, laser Raman spectroscopy and BET surface area measurements.

5.3 Results

The characterisation and catalytic properties of the new materials before and after activation for the selective oxidation of n-butane to maleic anhydride are presented in three sections. In the final discussion section the results obtained for the three new preparative routes are summarised and correlated.

5.3.1 The reaction of $VOPO_4.2H_2O$ with hydrogen as reducing agent in water

5.3.1.1 Characterisation of new materials prepared using hydrogen as reducing agent

A series of new materials were prepared via a novel route described in (section 2.1.3) via varying the hydrogen pressure in an autoclave (20, 25 and 30 bar).

XRD shows that the new materials obtained after 24 hours reaction with 20bar hydrogen pressure appears to be poorly crystalline $VOHPO_4.0.5H_2O$ (Figure5.1) by the reduced intensity of the reflections. Except for reflections at $2\theta=13°$ (d-spacing = 6.7Å) and $2\theta=25.6°$ (d-spacing = 3.4 Å) which can be assigned to unreacted $VOPO_4.2H_2O$, all major reflections match those attributed to the $VOHPO_4.0.5H_2O$ reported by Bordes *et al* [9] as shown in table 5.1. In one of his studies of his patent, Roffelson *et al.* report a reflection not assigned to the $VOHPO_4.0.5H_2O$ at the same *d*-spacing (*d*-spacing = 6.7Å) in the XRD of the precursor obtained after refluxing V_2O_5 and $H_3PO_4$with H_3PO_3 in water [7]. The Raman spectra obtained were in agreement with the XRD, as shown in Figure 5.2. The main band observed at 984 cm^{-1} is assigned to the P-O stretch of $VOHPO_4.0.5H_2O$, which is in agreement with the spectra reported in the literature [10] for the $VOHPO_4.0.5H_2O$ as shown in table 5.2. The band appeared at 951 cm^{-1}which is assigned to unreacte$VOPO_4.2H_2O$ present after reaction for 24 hours. However, broad bands were appearing at 521cm^{-1} and 695 cm^{-1}which can correspond to the appearance of V_2O_5 during the reaction (Figure 5.2).

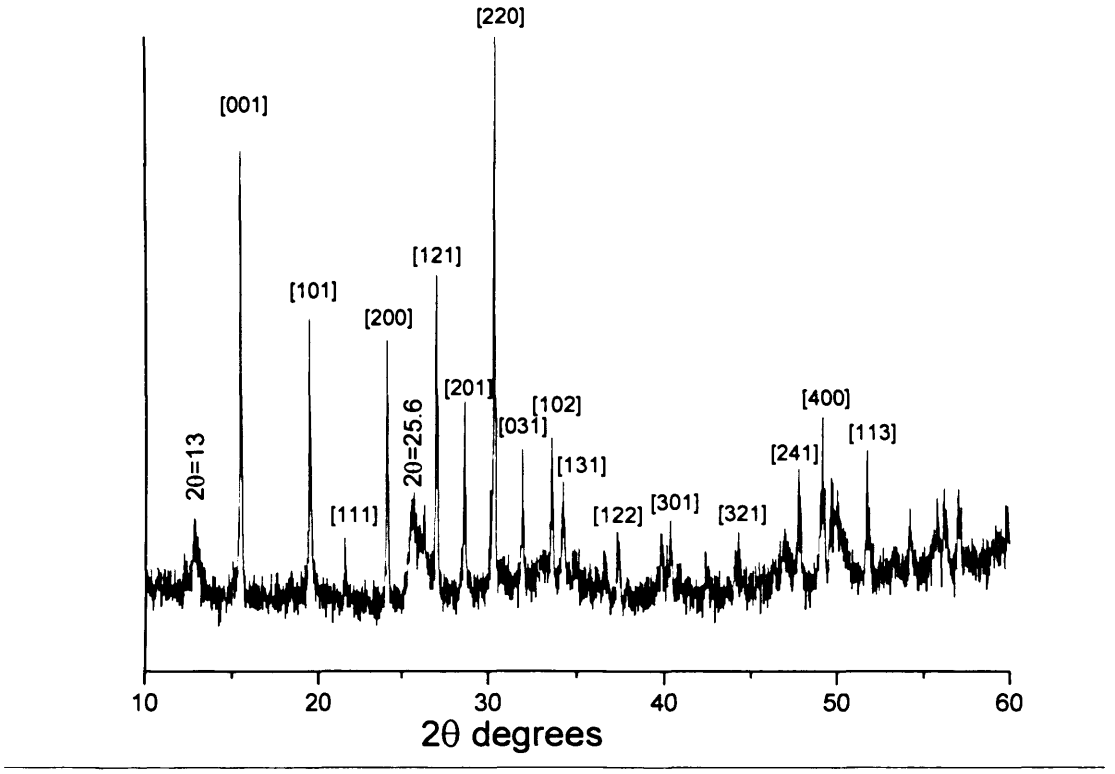

Figure. 5.1- Powder diffraction pattern of new materials (VH2) prepared using hydrogen (25bars) at 150°C.

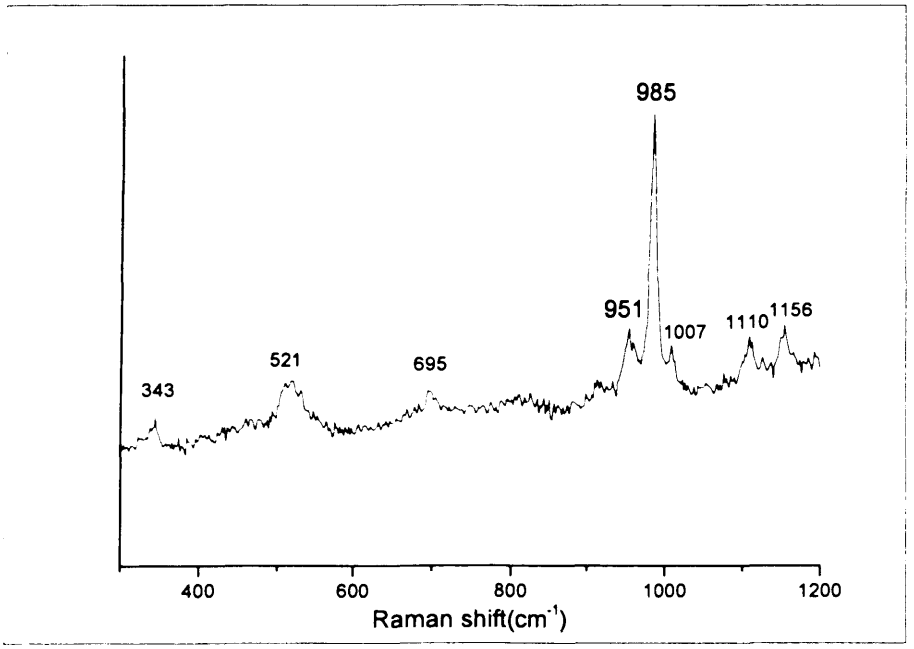

Figure. 5.2- Laser Raman spectrum of new material (VH2) prepared using hydrogen (25bars) at 150°C.

Table 5.1 XRD assignations of the new material (VH2) prepared using (25bar) hydrogen, and following assignations by Bordes [9]

VH2			$VOHPO_4.0.5H_2O$		
refl.	d_{obs}	I/I_0	d_{obs}	I/I_0	**plane**
1	6.77	7			
2	5.7	80	5.72	100	001
3	4.81	10	4.82	2	020
4	4.52	43	4.53	40	101
5	4.09	15	4.09	5	111
6	3.67	42	3.68	23	200
7	3.41	15			
8	3.29	50	3.30	32	121
9	3.11	25	3.11	18	201
10	2.93	100	2.94	35	220
11	2.79	21	2.79	10	031
12	2.65	23	2.63	27	102
13	2.61	15	2.61	7	131
14	2.56	15	2.56	5	112
15	2.45	14	2.45	6	022
16	2.41	10	2.40	4	040
17	2.26	12	2.26	6	301
18	2.22	11	2.23	4	231
19	2.12	9	2.13	5	032
20	2.04	12	2.05	4	321
21	1.91	19	1.90	7	241
22	1.85	24	1.85	9	400
23	1.83	18	1.83	8	103

Table 5.2 The Raman peaks of the new material (VH2) prepared using (25bars) hydrogen, compared to those reported in literature for $VOHPO_4.0.5H_2O$ [10]

VH2		**$VOHPO_4.0.5H_2O$**	
Peaks (cm^{-1})	I/I_0	Peaks (cm^{-1})	I/I_0
1156	medium	1154	medium
1110	medium	1109	medium
1007	weak	1007	weak
985	very strong	981	very strong
951	medium	-	
695	weak	-	
521	medium	509	very weak
344	medium	339	medium

The new material was also characterised using scanning electron microscopy (Figure 5.3). The sample comprised random platelets with broad range of crystallite size.

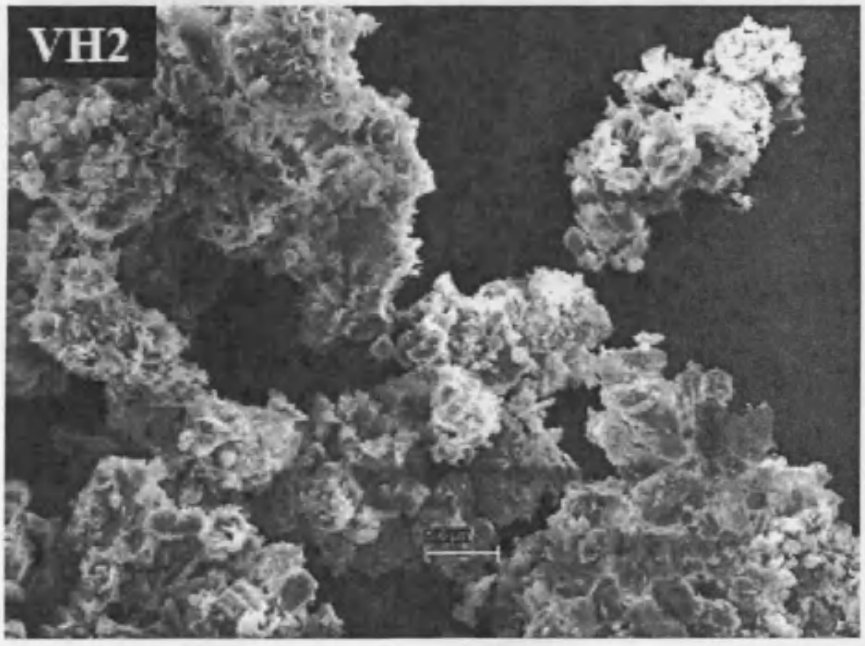

Figure. 5.3- SEM micrographs of new materials (VH2) prepared using hydrogen (25 bars) at 150°C.

A series of new materials was prepared described (section2.1.3) with varying hydrogen pressure in the autoclave (20, 25 and 30 bar). The XRD and Raman spectroscopy of the new materials are shown in Figures 5.4.and 5.5 respectively. The XRD patterns appear to be poorly crystalline $VOHPO_4.0.5H_2O$ phase with reflections at $2\theta=13^\circ$ (d-spacing = 6.7Å), which can be assigned to un-reacted $VOPO_4.2H_2O$ and $2\theta=25.6^\circ$ (d-spacing = 3.4Å), which could be assigned to the presence of $VOPO_4$ phases.

Table 5.3– Experimental details of materials prepared via reduction of $VOPO_4.2H_2O$ under various hydrogen pressure in autoclave in (30ml) water.

Entry	Sample name	solvent	H_2 pressure (bar)	T °C	Weight (g)
a	VH1	water	20	150	0.55
b	VH2	water	25	150	0.52
c	VH3	water	30	150	0.54

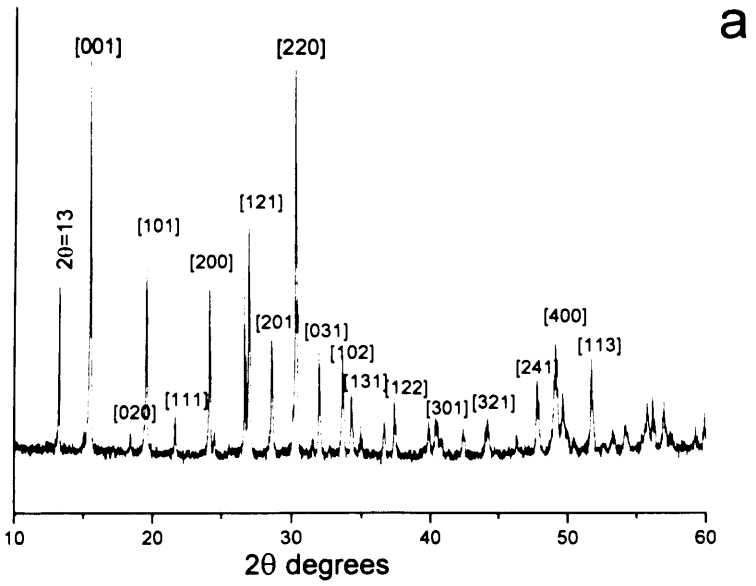

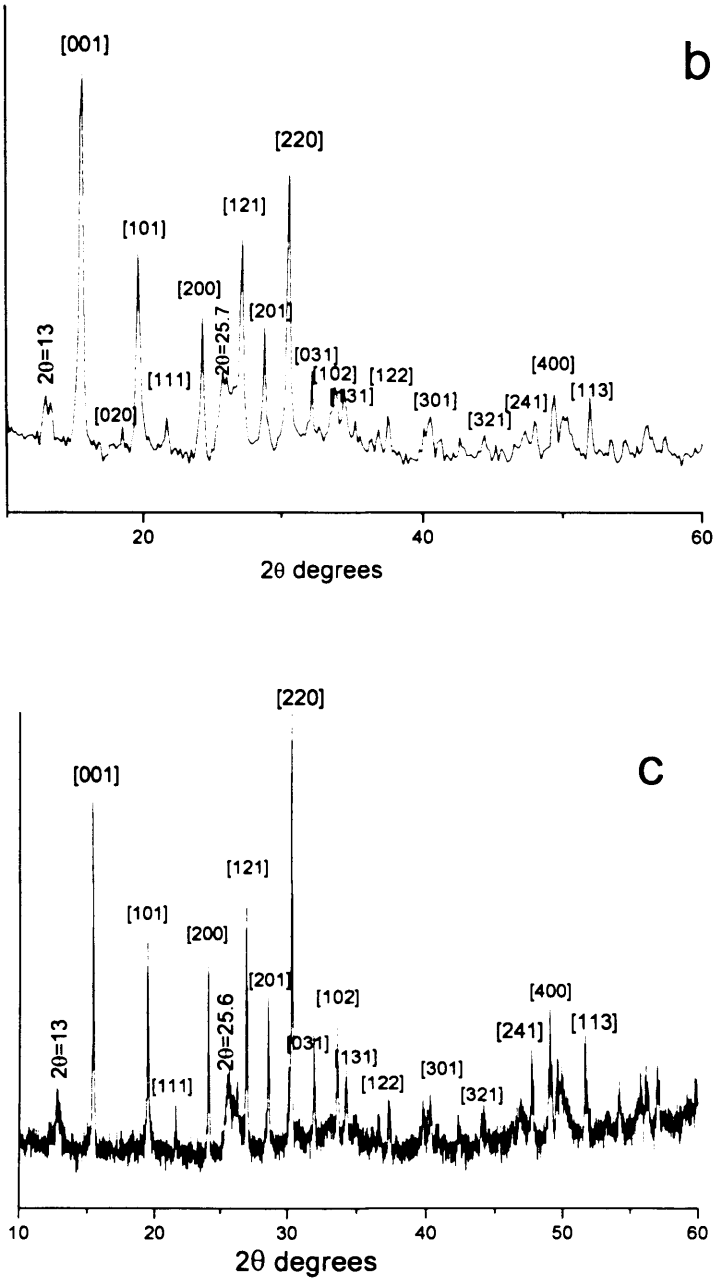

Figure. 5.4-Powder diffraction pattern of materials prepared using hydrogen at 150°C under various pressures (a) 20bar, (b) 25bar, (c) 30bar.

The Raman spectra show the main band at 984 cm^{-1}, which is a characteristic feature for $VOHPO_4.0.5H_2O$. In contrast, there are bands at (697 cm^{-1}) and (521cm^{-1}), which could be due to the appearance of V_2O_5 during the reaction as shown in Figure 5.5c.

Antonio *et al.* reported that a similar bands at 697 cm^{-1} and 521cm^{-1} which appeared after 5 hours during the reaction of V_2O_5 with H_3PO_4 and $H_4P_2O_7$ as a starting material with water as solvent. These bands disappeared after 24hours of the reaction [8].

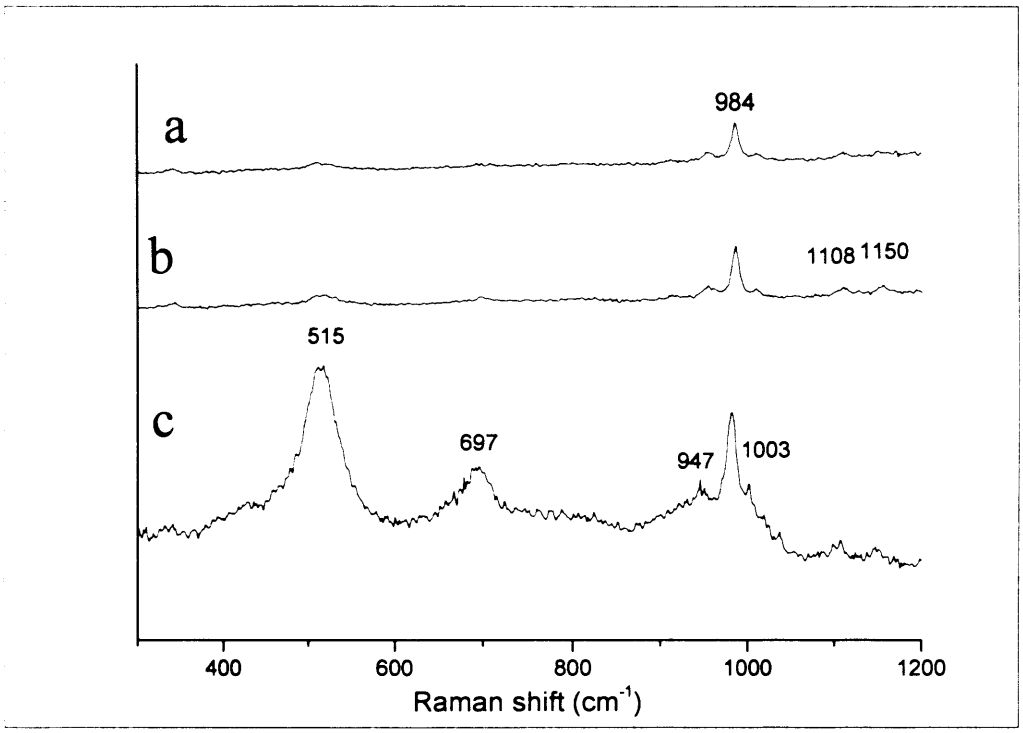

Figure. 5.5- Laser Raman spectrum of materials prepared using hydrogen at 150°C under various pressure (a) 20bar (b) 25bar, (c) 30bar.

5.3.1.2 Catalytic testing

The new catalyst precursor prepared using hydrogen (VH2) was tested for the oxidation of butane to maleic anhydride as presented in table 5.4. This sample showed only 5.3% selectivity for MA and 44% conversion. The surface area decreased from 12 to 7 m^2/g after activation.

Table 5.4 Catalyst performance of vanadium phosphate for the oxidation of n-butane.

Catalyst	Surface area m^2/g		n-butane Conversion (%)	Selectivity (%)			Specific Activity $(x10^{-5})^c$	Intrinsic Activity $(x10^{-6})^d$
	precursor	catalyst		MA	CO	CO_2		
VH2	12	7	44	5.3	81	14	2.0	2.9

a Reaction conditions: 400 .C, 1.7 % *n*-butane in air, GHSV = 2000 h.1.
b All samples were degassed for an hour at 120°C before analysis
c Specific activity: mol maleic anhydride formed/g catalyst/h.
d Intrinsic Activity : mol maleic anhydride formed/m^2/h.

5.3.1.3 Characterisation of activated samples

The catalyst sample after testing was characterised by powder XRD and laser Raman spectroscopy and is presented in Figures 5.6 and 5.7 respectively. The XRD patterns of the activated catalyst comprised of a mixture of $(VO)_2P_2O_7$, α_1-$VOPO_4$, γ-$VOPO_4$ and β-$VOPO_4$. The Raman spectra of the sample after activation, confirms the information obtained from XRD. The spectrum of the catalyst shows how reaction conditions have transformed the precursors to a mixture of V^{4+} and V^{5+} phases.

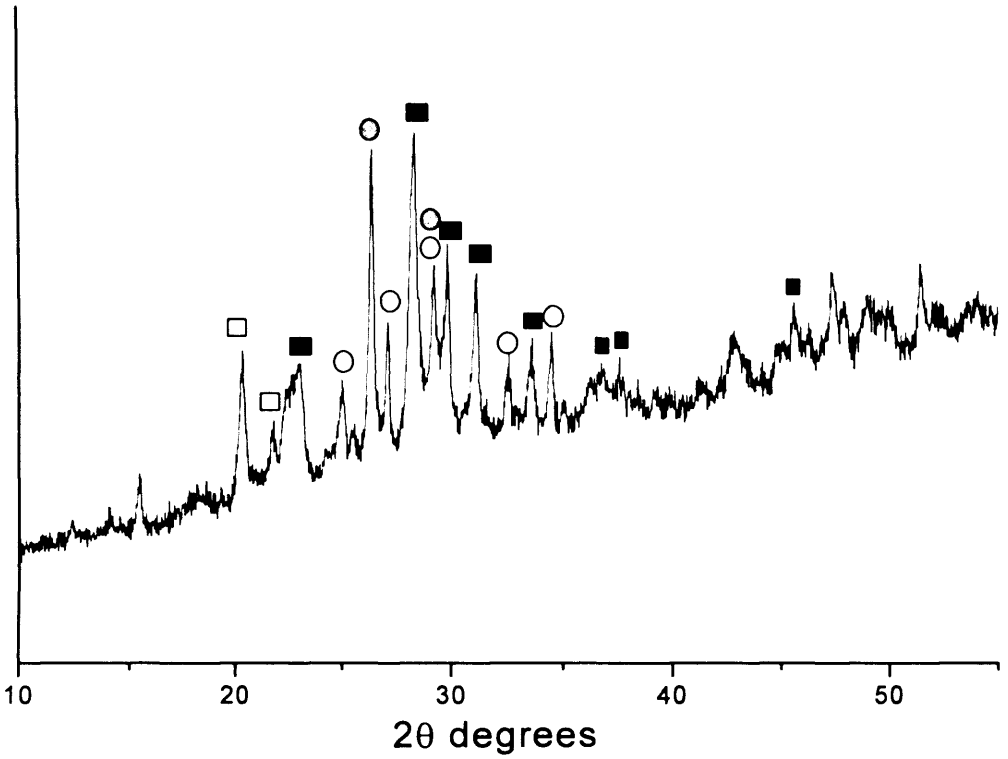

Figure. 5.6- XRD patterns for the activated catalysts prepared using hydrogen at 150°C. Key: ■ (VO)$_2P_2O_7$, □ α1-$VOPO_4$, ○ γ-$VOPO_4$, . β-$VOPO_4$

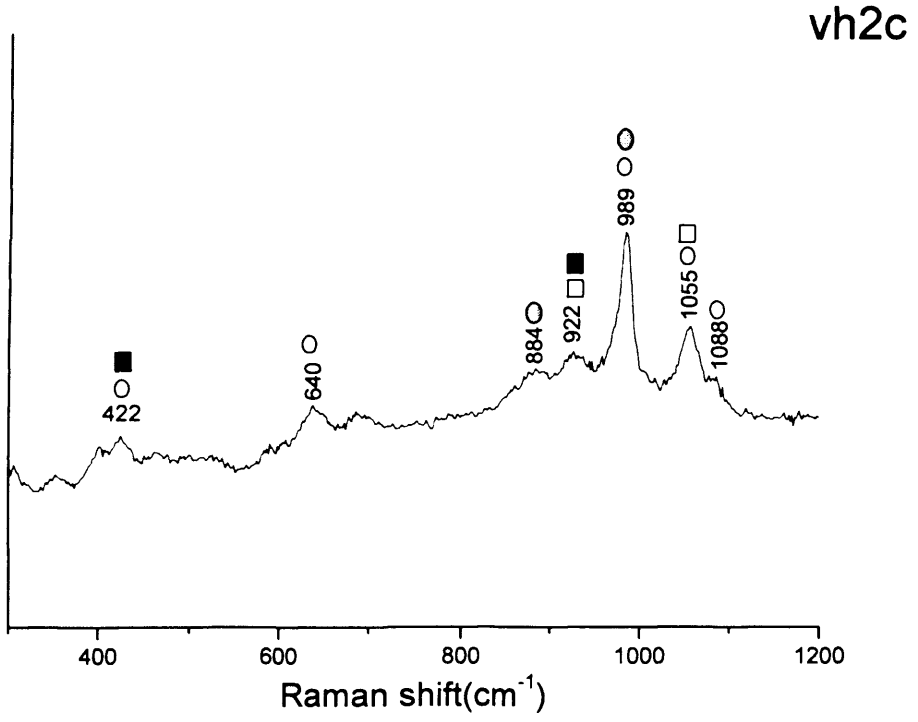

Figure. 5.7- Laser Raman spectra for the activated catalysts prepared using hydrogen at 150°C. Key: ■ (VO)$_2P_2O_7$, □ α1-$VOPO_4$, ○ γ-$VOPO_4$. O β-$VOPO_4$

5.3.2.1 Characterisation of the new material prepared using direct reduction

As has been shown in the previous section (5.3.1), a new material of catalyst precursor $VOHPO_4.0.5H_2O$ has been successfully prepared using hydrogen in liquid phase (aqueous media). At the present time, there have been few studies concerning the direct reduction of $VOPO_4{\cdot}2H_2O$ to the active phase $(VO)_2P_2O_7$ in solid state using hydrogen and the effect of water on the reaction. A set of experiments were carried out on the dihydrate materials for the purpose of tentatively reducing the V(V) phase $VOPO_4.2H_2O$ directly to vanadyl pyrophosphate $(VO)_2P_2O_7$ (IV) at different temperatures as described in table 5.5 below

Table 5.5 Summary for the materials prepared via direct route and the reaction conditions

Entry	Sample name	T °C	Hydrogen flow through water vapour
1	DH_{450}	450	Yes
2	D_{450}	450	No
3	D_{350}	350	No
4	DH_{250}	250	Yes
5	D_{250}	250	No

Condition 5%H_2/Ar (50ml/min) for 24h

XRD patterns of the materials obtained at 450°C from the reduction of $VOPO_4.2H_2O$ are shown in Figure 5.8 a, and b respectively. Both samples show typical patterns of

very crystalline $(VO)_2P_2O_7$ with the [200] and [042] reflections as the main feature of the diffraction pattern. However, the sample that has been prepared with hydrogen flow through a water vapour (DH_{450}) shows others peaks, which can be assigned to $VOPO_4.2H_2O$ and α-$VOPO_4$ indicating that the presence of water with hydrogen flow can affect the dehydration of $VOPO_4.2H_2O$.

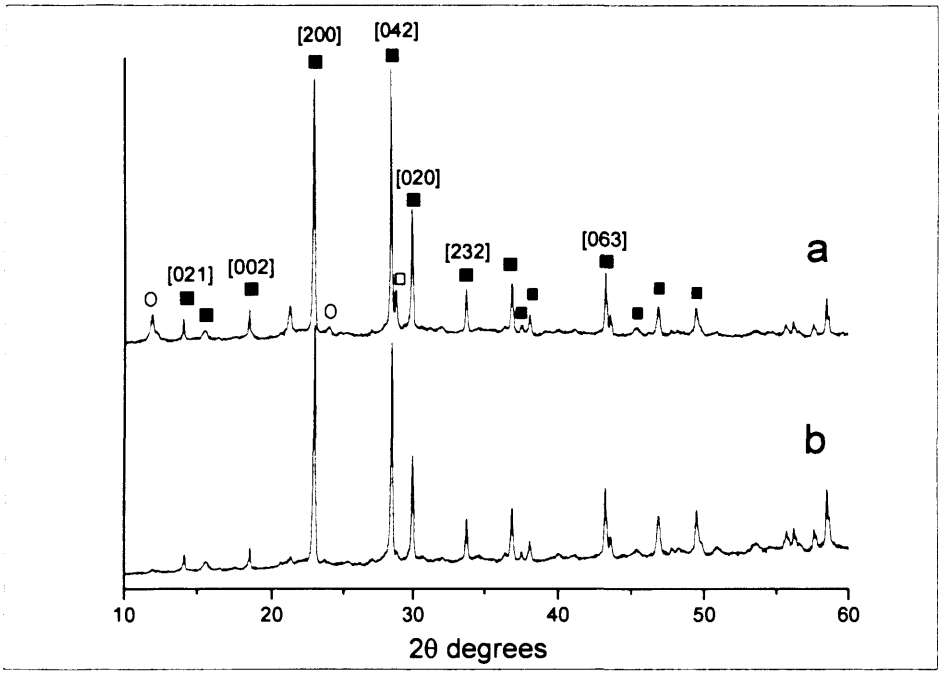

Figure. 5.8- Powder diffraction patterns of materials prepared using direct reduction, (a) (Dh_{450}) through a water vapour and (b) (D_{450}) Key: ■ $(VO)_2P_2O_7$, ○ $VOPO_4{\cdot}2H_2O$, and □ α-$VOPO_4$.

The Raman spectra obtained is in agreement with the XRD (Figure 5.9, a and b). Both samples have a band at 921cm^{-1} as the main band, which is characteristic of $(VO)_2P_2O_7$ phase. Sample DH_{450} (Figure 5.8 a) shows an additional band at 949cm^{-1} indicating also the presence of un-reacted $VOPO_4{\cdot}2H_2O$.

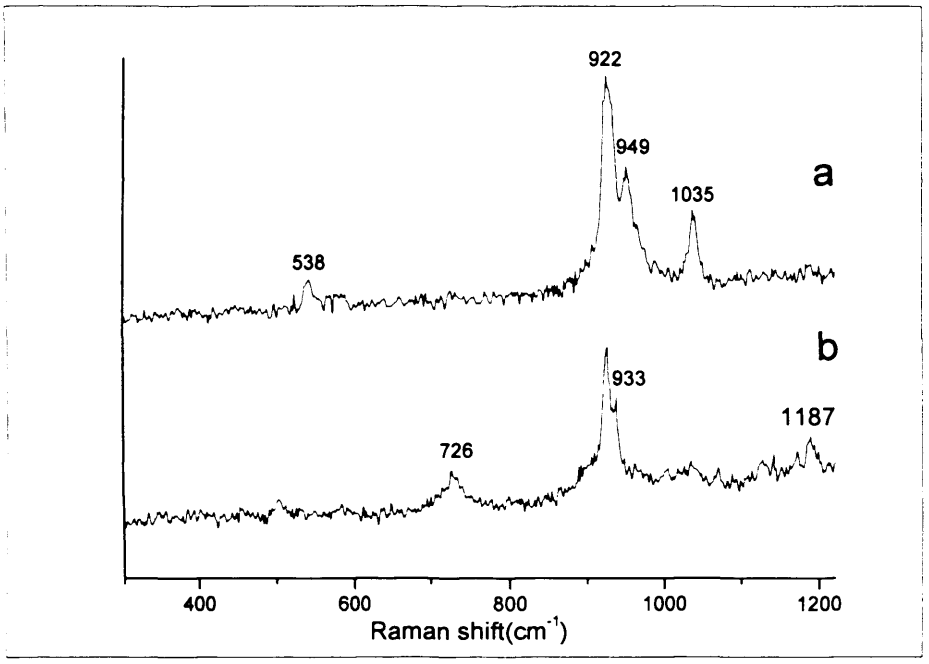

Figure. 5.9- Laser Raman spectrum of the materials prepared using direct reduction a (DH_{450}) through a water bubble and b (D_{450}).

Table 5.6- The Raman peaks of the materials prepared using direct reduction a (DH_{450}) through a water vapour and b (D_{450}).

$(VO)_2P_2O_7$ [10]		a:DH_{450}		b:D_{450}	
Peaks (cm-1)	**I/I0**	**Peaks (cm-1)**	**I/I0**	**Peaks (cm-1)**	**I/I0**
1191	weak	1187	Very weak	1189	weak
1135	weak	1035	Strong	1035	weak
930	Strong sh	949	Strong sh	933	Strong sh
920	Very strong	922	Very strong	922	Very strong
797	Very weak	-		727	weak
457	Very weak	540	weak	458	Very weak

XRD patterns and the Raman spectra of the materials obtained at 250°C through a water vapour at 250°C and 350°C are shown in Figures 5.10 and 5.11 respectively. These XRD patterns show that there are similarities between the three samples. The patterns have one main peak (2θ=21.24°) with d-spacing = 4.18Å, which is not present in any of the published vanadium phosphate phases. However, there are some other reflections present that can be assigned to α_I-$VOPO_4$ indicating the dehydration of $VOPO_4 \cdot 2H_2O$ at these temperatures.

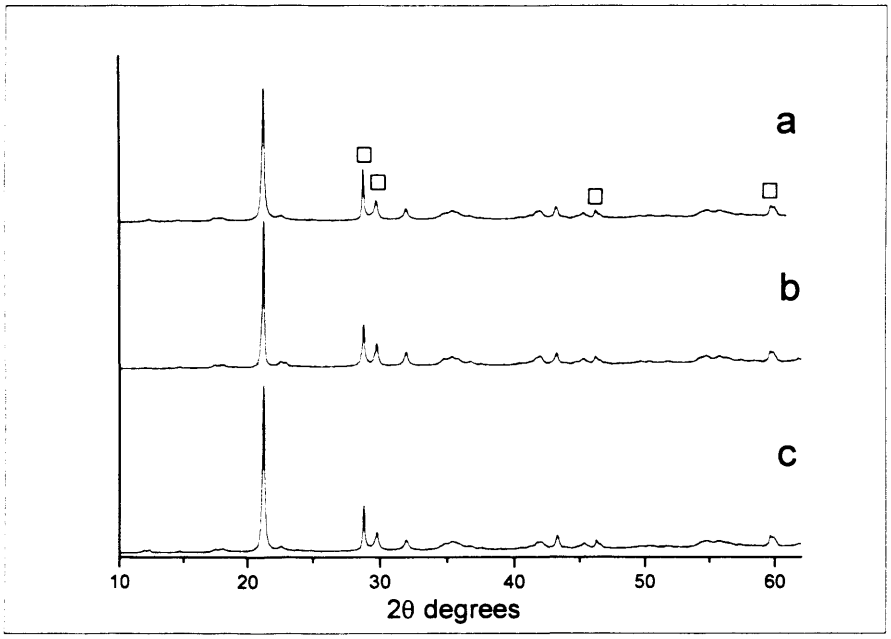

Figure. 5.10- Powder diffraction patterns of materials prepared using direct reduction at different temperatures (a) 250°C, (b) 250°C through a water vapour, (c) 350°C. Key: □ α_I-$VOPO_4$.

The Raman spectra of the samples are very similar (Figure 5.11) and show a strong correlation with the published spectrum for α_I-$VOPO_4$ indicating the dehydration of $VOPO_4 \cdot 2H_2O$ under the reaction conditions. Table 5.7 lists the main peaks present after the reaction.

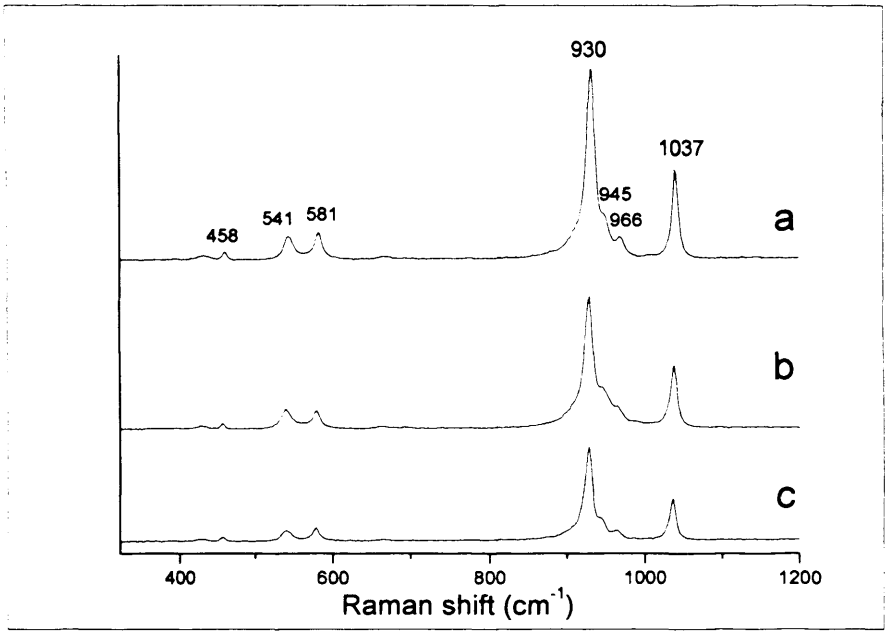

Figure. 5.11- Laser Raman spectrum of materials prepared using direct reduction, at different temperatures (a) 250°C, (b) 250°C through a water vapour, (c) 350°C.

Table 5.7- The Raman peaks of the materials prepared using direct reduction at different temperatures.

α_1-$VOPO_4$ [10]		a:D_{250}		b:DH_{250}		c:D_{350}	
Peaks (cm-1)	**I/I_0**	**Peaks (cm-1)**	**I/I_0**	**Peaks (cm-1)**	**I/I_0**	**Peaks (cm-1)**	**I/I_0**
1143	weak	1144	weak	1144	weak	1144	weak
1035	strong	1037	strong	1037	strong	1037	strong
963	medium	966	medium	966	medium	966	medium
943	medium	945	shoulder	945	shoulder	945	shoulder
926	Very strong	930	Very strong	930	Very strong	930	Very strong
661	weak	662	weak	662	weak	662	weak
576	medium	580	medium	580	medium	580	medium
539	medium	541	medium	541	medium	541	medium
457	weak	458	weak	458	weak	458	weak

5.3.2.2 Characterisation of activated samples

The $(VO)_2P_2O_7$ phase and α1-$VOPO_4$ known to stable phase at the reaction temperature for the oxidation of n-butane to maleic anhydride (400°C). There were no changes observed on their XRD and Raman patterns after activation for 24 hours and their XRD patterns are shown in appendix (6).

(6) Appendix 5.1- The XRD patterns of activated samples prepared using direct route at 450 °C and 250 °C respectively.

5.3.3 Characterisation of materials prepared using (N_2H_4 and $NaBH_4$) as reducing agent

Previous studies have focused on the use of alcohols as reducing agent and solvent. However, there have not been any published studies focusing on the use of strong reducing agents for the reduction of $VOPO_4.2H_2O$.

Hydrazine is commonly used for the reduction of metal cations to metal nano-particles in solutions [11, 13]. Sodium borohydride ($NaBH_4$) is classified as a strong reducing agent and widely used in the manufacture of pharmaceuticals and other organic and inorganic compounds as reducing agent [12, 14].

In this section, the use of strong reducing agents such as hydrazine and sodium borohydride is investigated for reduction of $VOPO_4.2H_2O$ to catalyst precursors and compared to the methods in the previous sections of this chapter.

5.3.3.1 Characterisation of materials prepared using hydrazine N_2H_4

A series of new materials were prepared via a reduction of $VOPO_4.2H_2O$ with hydrazine as described in section 2.1.4 and at different reaction time (30 minutes, 2 hours, 6 hours and 24hours). The materials were characterised using X-ray diffraction, laser Raman spectroscopy and BET surface area measurements.

Table 5.9 –Experimental details of materials prepared via reduction of $VOPO_4.2H_2O$ with hydrazine solution 51% in water.

Entry	Sample name	Reaction time (hours)	T °C
1	VPH_{30min}	0.5	reflux
2	VPH_{2h}	2	reflux
3	VPH_{6h}	6	reflux
4	VPH_{24h}	24	reflux

XRD shows that after 30 minutes of reaction, the $VOPO_4.2H_2O$ partially starts to dehydrate to give $VOPO_4{\cdot}H_2O$ as shown in Figure 5.12. As the reaction time increased (2h, 6h and 24h) the materials tended to give a different phase with main reflections at $2\theta=13.88^\circ$ (d-spacing = 6.22Å) and $2\theta=28^\circ$ (d-spacing = 3.16Å), which cannot be assigned to any known vanadium phosphate phases. Moreover, the peaks tended to broaden as the reaction time increase which may indicate the intercalation of $VOPO_4{\cdot}H_2O$ with the hydrazine.

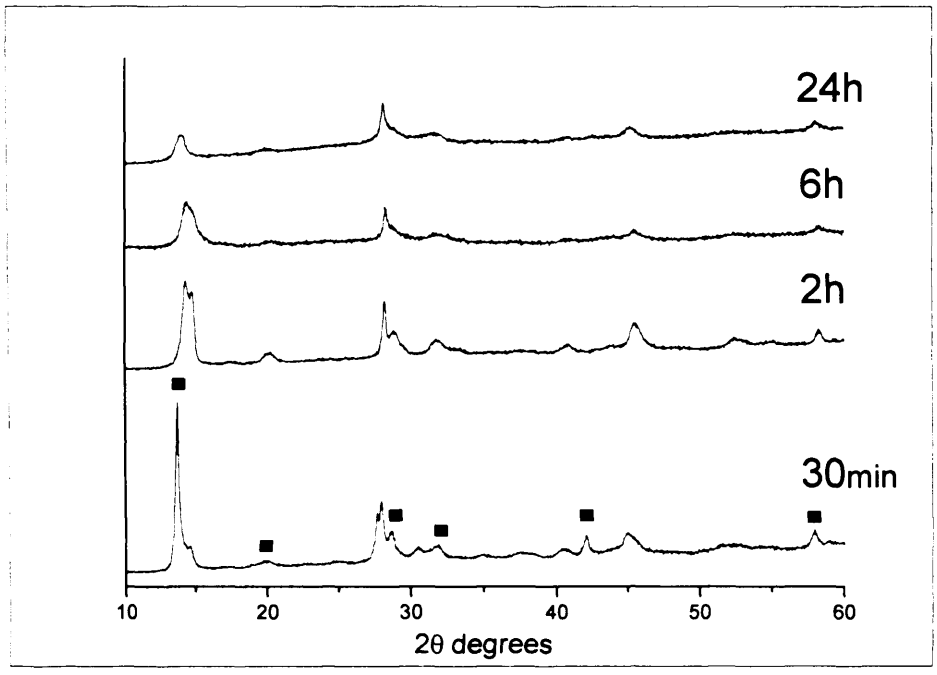

Figure. 5.12- Powder diffraction patterns of materials prepared over time using hydrazine, Key: ■ $VOPO_4 \cdot H_2O$

Table 5.10- XRD possible assignations of the new materials prepared via reduction of $VOPO_4.2H_2O$ with hydrazine at different times.

VPH_{30min}			**VPH_{2h}**		
No.	**d_{obs}**	**Possible assignations**	**No.**	**d_{obs}**	**Possible assignations**
1	6.46	VOPO4·H2O	1	6.2	
2	6.05		2	6.03	
3	4.42	VOPO4·H2O	3	4.41	
4	3.19		4	3.17	
5	3.11	VOPO4·H2O	5	3.1	
6	2.92		6	2.81	
7	2.8	VOPO4·H2O	7	2.21	
8	2.23		8	2.00	
9	2.14	VOPO4·H2O			
10	1.59	VOPO4·H2O			
VPH_{6h}			**VPH_{24h}**		
No.	**d_{obs}**	**Possible assignations**	**No.**	**d_{obs}**	**Possible assignations**
1	6.18		1	6.22	
2	4.39		2	4.35	
3	3.16		3	3.17	
4	2.8		4	2.78	
5	1.99		5	1.97	

The Raman spectra of the samples are presented in Figure 5.13 and shows that a strong band at 978 cm^{-1} appeared after 30 minutes of the reaction. This band corresponds to asymmetric P-O stretch in the PO_4 tetrahedra. After 2 hours of the reaction, the band shifted to 960 cm^{-1} and then disappeared after 24 hours with the appearance of another band at 896 cm^{-1}, indicating the transformation of $VOPO_4.2H_2O$ to a new phase. It is well known that the Raman bands in vanadium phosphate are related to the different V-O and P-O bonds present in the structures [15]. The Raman bands between 850cm^{-1} 1200 cm^{-1} are related to the stretching modes of V-O and P-O bonds [15]. Furthermore, most of the VPO phases show the strongest bands in the region between 900 and 1000 cm^{-1}, making it difficult to recognize the phase or phases present. In the case of the material that was prepared for 24 hours, only a small broad band is visible at 896 cm^{-1} which is difficult to assign to any published VPO phases. However, the disappearance of the bands as the reaction time increased may also support the possibility of the intercalation of hydrazine with $VOPO_4.H_2O$.

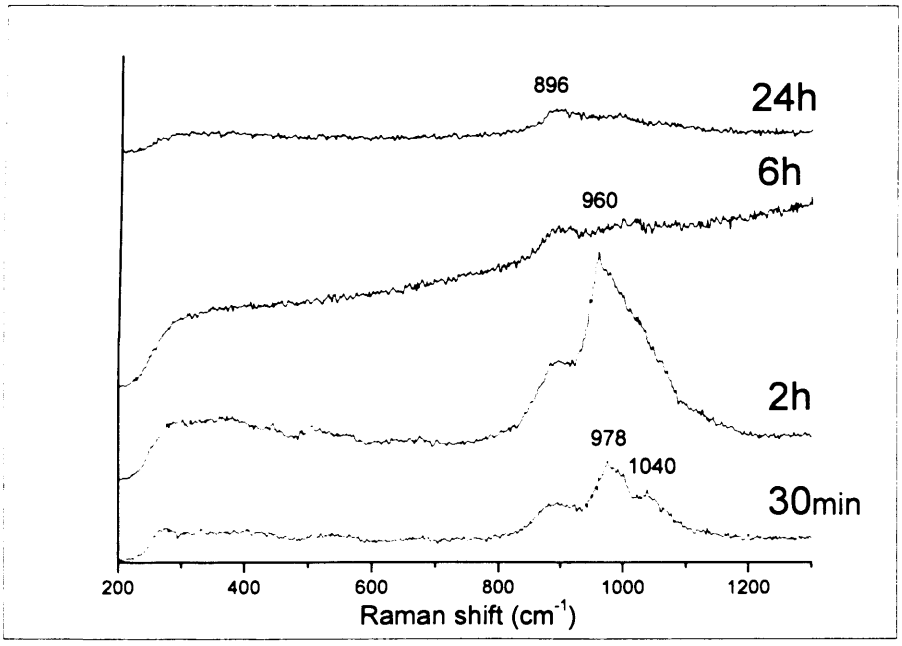

Figure. 5.13- Raman spectrum of the materials prepared over time using hydrazine.

5.3.3.2 Characterisation of the new material prepared using $NaBH_4$

A series of new materials were prepared via a reduction of $VOPO_4.2H_2O$ with sodium borohydride ($NaBH_4$) (as described in section 2.1.4) and at different reaction times (30min, 2, 6 and 24hours). The materials were characterised using X-ray diffraction, laser Raman spectroscopy and BET surface area measurements.

Table 5.10 –Experimental details of materials prepared via reduction of $VOPO_4.2H_2O$ with sodium borohydride ($NaBH_4$) in ethanol solvent.

Entry	Sample name	Reaction time (hours)	T °C
1	VPB_{30min}	0.5	reflux
2	VPB_{2h}	2	reflux
3	VPB_{6h}	6	reflux
4	VPB_{24h}	24	reflux

XRD shows that after 30 minutes of reaction, the $VOPO_4.2H_2O$ was totally transferred to new phases (as shown in Figure 5.14) indicating the power of the reducing agent. As the reaction time increased (2h, 6h and 24h) the materials tended to give two phases ($Na_{0.45}VOPO_4$ $1.58H_2O$, $VOHPO_4.0.5H_2O$) as assigned in table 5.12. The sample obtained after 24 hours appears to be very crystalline, $Na_{0.45}VOPO_4$ $1.58H_2O$, phase characterised by the sharpness and intensity of the reflections produced compared with the other phase that present ($VOHPO_4.0.5H_2O$) reflections.

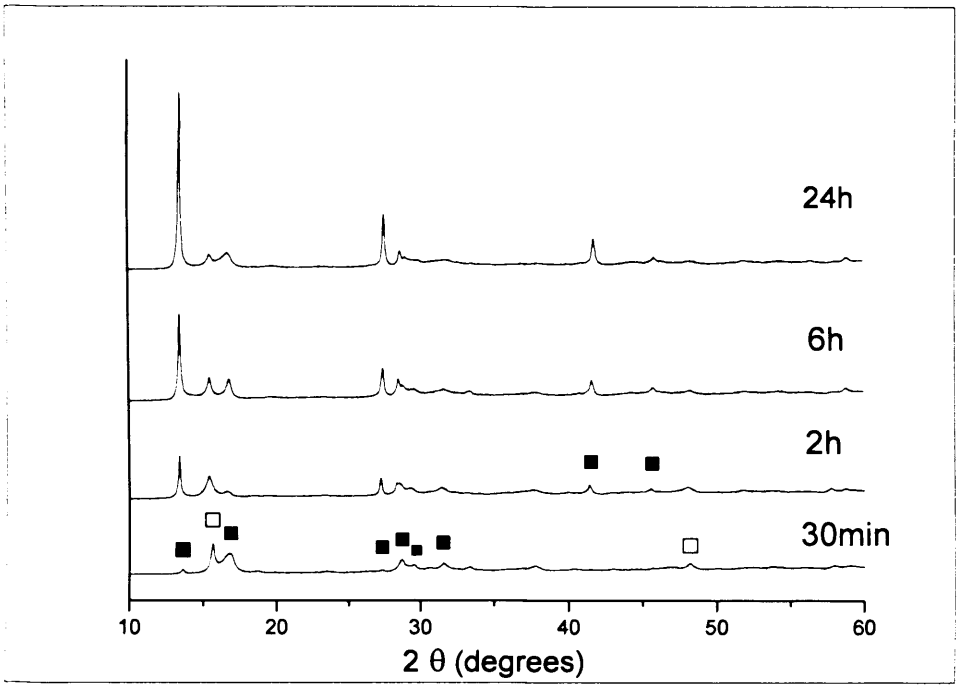

Figure. 5.14-Powder diffraction pattern of the materials prepared over time using $NaBH_4$. Key: ■ $Na_{0.45}VOPO_4$ $1.58H_2O$, □ $VOHPO_4.0.5H_2O$

Table 5.12- XRD possible assignations of the new materials prepared via reduction of $VOPO_4.2H_2O$ with sodium borohydride ($NaBH_4$) at different times.

VPB_{30min}			**VPB_{2h}**		
No.	**d_{obs}**	**Possible assignation**	**No.**	**d_{obs}**	**Possible assignation**
1	6.56	$Na_{0.45}VOPO_4 \cdot 1.58H_2O$	1	6.59	$Na_{0.45}VOPO_4 \cdot 1.58H_2O$
2	5.66	$VOHPO_4.0.5H_2O$	2	5.73	$VOHPO_4.0.5H_2O$
3	5.27	$Na_{0.45}VOPO_4 \cdot 1.58H_2O$	3	5.30	$Na_{0.45}VOPO_4 \cdot 1.58H_2O$
4	3.26	$Na_{0.45}VOPO_4 \cdot 1.58H_2O$	4	3.27	$Na_{0.45}VOPO_4 \cdot 1.58H_2O$
5	3.10	$Na_{0.45}VOPO_4 \cdot 1.58H_2O$	5	3.14	$Na_{0.45}VOPO_4 \cdot 1.58H_2O$
6	2.18	$Na_{0.45}VOPO_4 \cdot 1.58H_2O$	6	2.18	$Na_{0.45}VOPO_4 \cdot 1.58H_2O$
VPB_{6h}			**VPB_{24h}**		
No.	**d_{obs}**	**Possible assignation**	**No.**	**d_{obs}**	**Possible assignation**
1	6.53	$Na_{0.45}VOPO_4 \cdot 1.58H_2O$	1	6.53	$Na_{0.45}VOPO_4 \cdot 1.58H_2O$
2	5.65	$VOHPO_4.0.5H_2O$	2	5.65	$VOHPO_4.0.5H_2O$
3	5.28	$Na_{0.45}VOPO_4 \cdot 1.58H_2O$	3	5.28	$Na_{0.45}VOPO_4 \cdot 1.58H_2O$
4	3.24	$Na_{0.45}VOPO_4 \cdot 1.58H_2O$	4	3.24	$Na_{0.45}VOPO_4 \cdot 1.58H_2O$
5	3.10	$Na_{0.45}VOPO_4 \cdot 1.58H_2O$	5	3.10	$Na_{0.45}VOPO_4 \cdot 1.58H_2O$
6	2.2	$Na_{0.45}VOPO_4 \cdot 1.58H_2O$	6	2.2	$Na_{0.45}VOPO_4 \cdot 1.58H_2O$

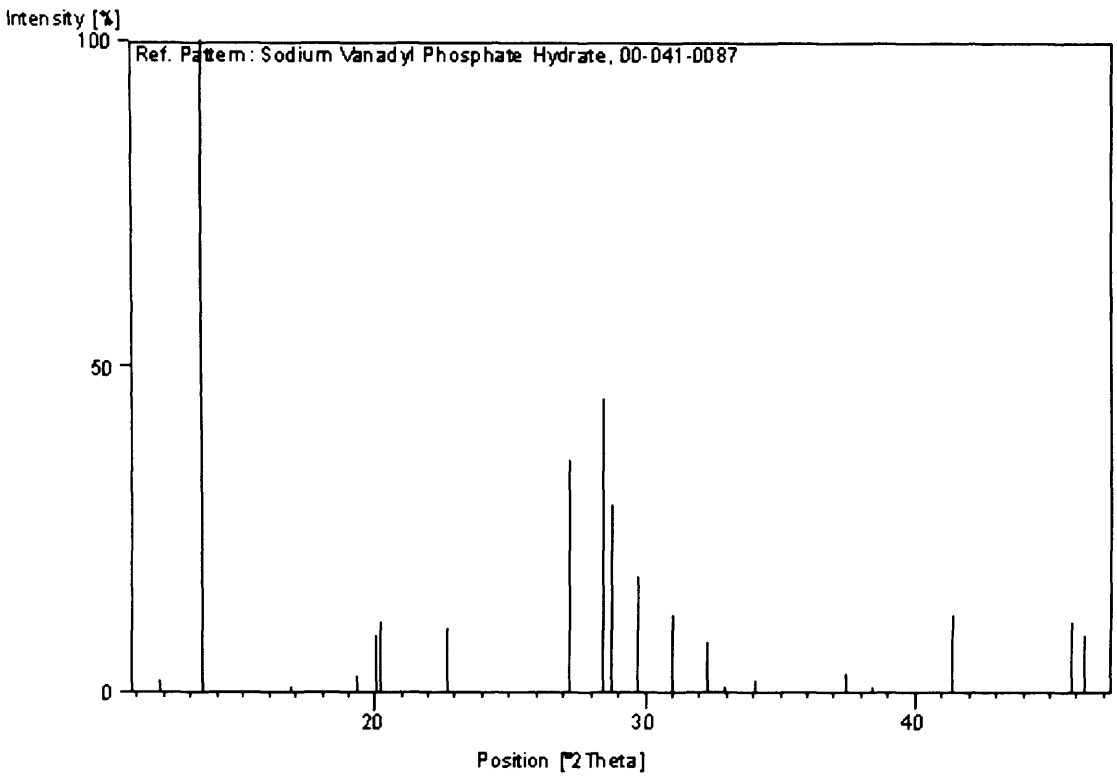

Figure.5.14- Atypical Powder diffraction pattern of $Na_{0.45}VOPO_4.1.58H_2O$ as reported in literature [17].

The Raman spectra of the samples prepared for different reaction times are presented in Figure 5.15. The sample prepared for 30 minutes shows a strong band at 942 cm^{-1} and then this band decreases with the appearance of other bands at 867 and 1010 cm^{-1} with increasing reaction times to 24 hours. There is a small band present for all the samples at 987 cm^{-1}, which can be assigned to $VOHPO_4.0.5H_2O$ phase. It is well known from the literature, that the Raman bands between 850cm^{-1} 1200 cm^{-1} are related to the stretching modes of V-O and P-O bonds [15]. Therefore, it is possible that these bands (at 867 and 1010 cm^{-1}) can be assigned to the new phase $Na_{0.45}VOPO_4 \cdot 1.58H_2O$.

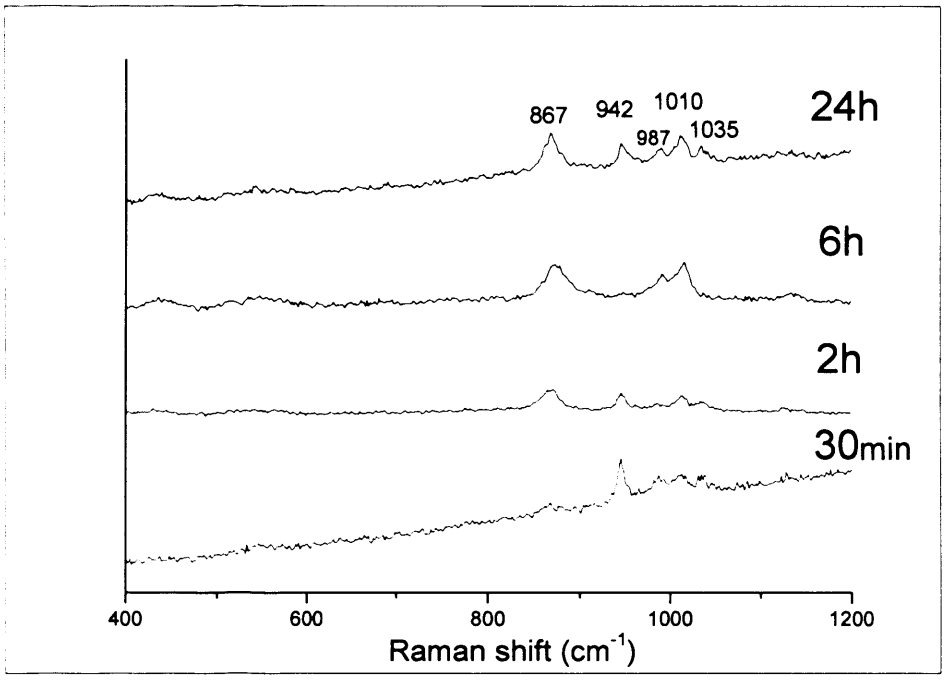

Figure. 5.15- Laser Raman spectrum of the materials prepared over time using $NaBH_4$.

5.3.3.3 Characterisation of activated samples

5.3.3.3.1 Characterisation of activated sample prepared using N_2H_4

The powder XRD patterns of the new material prepared using hydrazine after activation for n-butane oxidation for 24hours is shown in Figure 5.16. The sample shows characteristic pattern with all reflections assigned to β-$VOPO_4$ phase with [201] (d-spacing = 3.42Å) as the main feature. A summary of the XRD reflections are shown in Table 5.13.

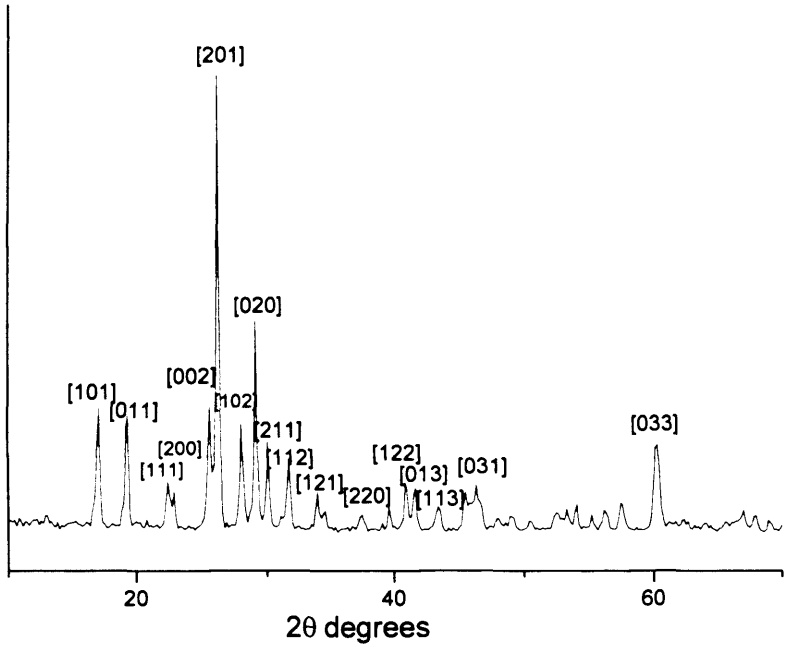

Figure. 5.16-.Powder diffraction patterns of activated catalysts prepared using hydrazine for 24h, VPH_{24hc}.

Table 5.13 - XRD reflections of the new material (VPH_{24c}) after activation, following reference of β-$VOPO_4$ reflections [9, 15].

VPH_{24c}			β-$VOPO_4$	
refl.	**d_{obs}**	**I/I_0**	**d_{obs}**	**plane**
1	5.24	38	5.19	101
2	4.63	35	4.62	011
3	3.97	25	3.96	111
4	3.91	24	3.89	200
5	3.51	31	3.47	002
6	3.42	100	3.38	201
7	3.19	29	3.17	102
8	3.08	67	3.07	020
9	2.98	27	2.97	211
10	2.83	26	2.82	112
11	2.65	18	2.64	121
12	2.42	14	2.41	220
13	2.22	14	2.21	122
14	2.18	16	2.17	013
15	2.09	9	2.09	113
16	2.01	10	1.99	203
17	1.97	9	1.96	031

The Raman spectra of the sample (VPH_{24c}) after the activation show a good correlation with the XRD results (Figure 5.17). All the bands observed are typical spectra of β-$VOPO_4$ phase as presented in Table 5.14. This indicates that the material prepared using hydrazine as reducing agent, which gave an unknown phase, led to formation of β-$VOPO_4$ phase after activation with an n-butane, air mixture.

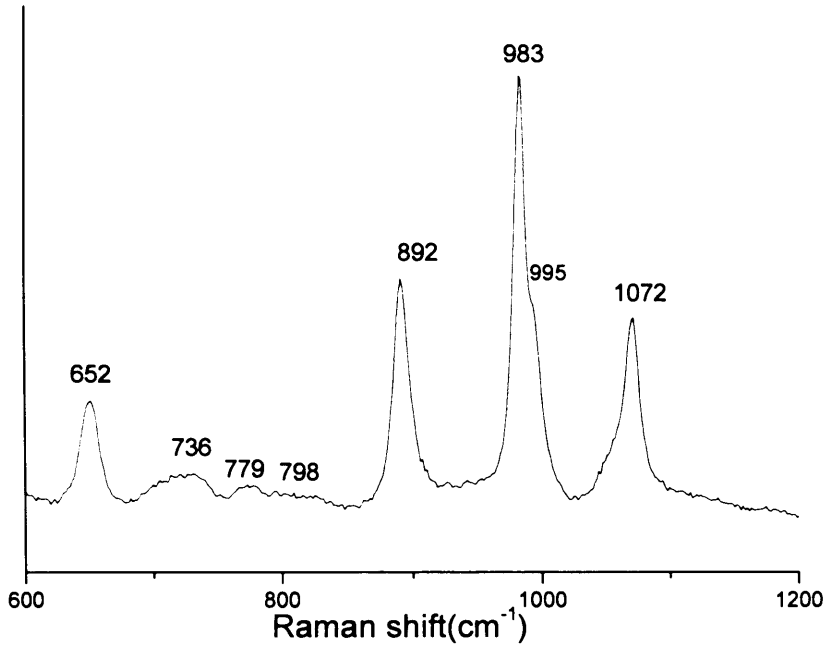

Figure. 5.17- Laser Raman spectrum of activated catalyst prepared using hydrazine for 24h, VPH_{24hc}.

Table 5.14- The Raman peaks of the new material (VPH_{24c}) after activation, following reference β-$VOPO_4$ [15]

Sample VPH_{24hc} after activation		**β-$VOPO_4$**	
Peaks (cm^{-1})	**I/I_0**	**Peaks (cm^{-1})**	**I/I_0**
1072	strong	1075	strong
995	shoulder	997 sh	shoulder
983	very strong	986	very strong
892	strong	892	strong
798	very weak	804	very weak
779	very weak	782	very weak
736	very weak	741	very weak
652	medium	656	medium

5.3.3.3.2 Characterisation of activated sample prepared using $NaBH_4$

The powder XRD patterns of the new material prepared using $NaBH_4$, after activation for n-butane oxidation is shown in Figure 5.18. The patterns show the main reflections with 2θ=26.62° (d-spacing = 3.34Å) and 2θ=27.40° (d-spacing = 3.25Å) as main features which cannot be assigned to the reported VPO phases. However, there are some other reflections present that can be assigned to some VPO phases expected after the activation (as shown in Table 5.15). This suggests that the $Na_{0.45}VOPO_4 \cdot 1.58H_2O$ transformed to a new phase after activation.

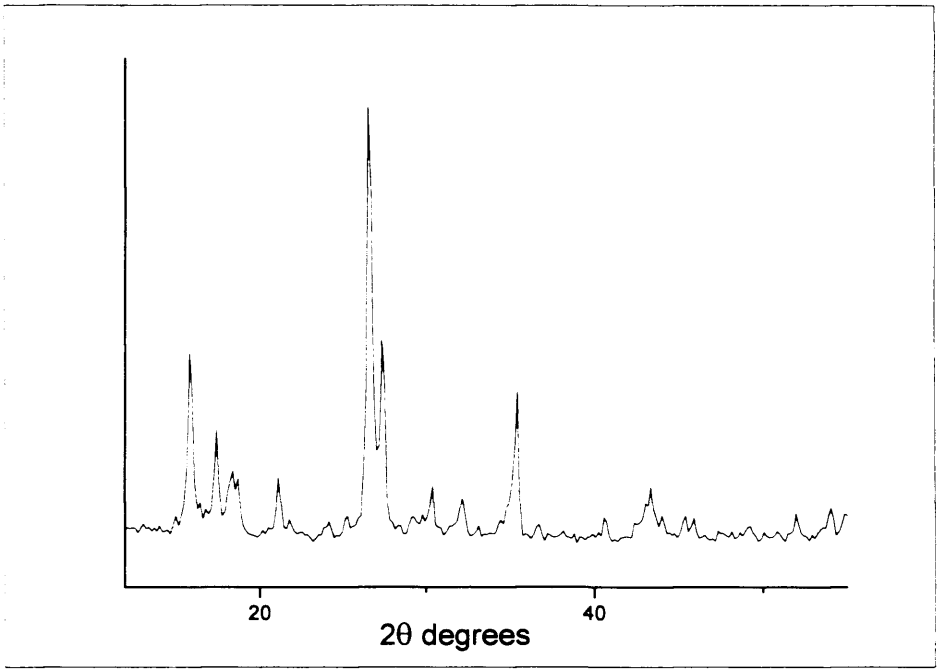

Figure. 5.18- Powder diffraction patterns of activated catalysts prepared using NaBH4 for 24h. (VPB_{24hc}).

Table 5.15- XRD reflections of sample VPB_{24hc} after activation.

Sample VPB_{24hc}			
No	**Pos. [°2Th.]**	**d-spacing [Å]**	**Possible assignation**
1	15.88	5.57	$(VO)_2P_2O_7$
2	17.44	5.08	
3	21.18	4.19	γ-$VOPO_4$
4	24.12	3.68	
5	**26.62**	**3.34**	
6	**27.40**	**3.25**	
7	30.38	2.94	
8	32.1	2.78	
9	35.42	2.53	
10	43.10	2.10	$(VO)_2P_2O_7$

The Raman spectra of the sample (VPB_{24c}) after the activation show the main band at 865 cm^{-1} with relatively small bands at 1022, 1001 and 663 cm^{-1} (Figure 5.19). These bands did not match any recognized VPO phase, indicating that the transformation of

the mixed phases (Na0.45VOPO4·1.58H_2O and $VOHPO_4$.0.5H_2O) to a new phase after activation.

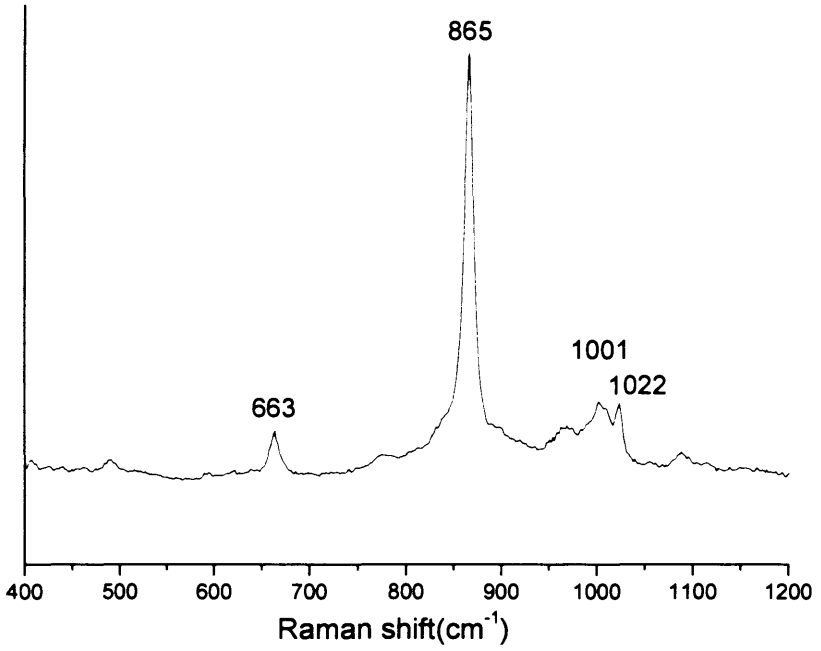

Figure. 5.19- Laser Raman spectrum of patterns of activated catalysts prepared using NaBH4 for 24h.(VPB_{24hc}).

5.4 Discussion

5.4.1 New materials prepared using hydrogen in high-pressure autoclave

The catalyst precursors $VOHPO_4.0.5H_2O$ were successfully prepared via a novel route using hydrogen as reducing agent. This material appears to be poorly crystalline $VOHPO_4.0.5H_2O$ by the poor intensity of the reflections produced (Figure5.1). However, other reflections are present after the activation for butane oxidation, indicating that the starting material $VOPO_4.2H_2O$ was not fully reduced under the reaction conditions. This is also confirmed by the Raman spectra obtained after the reaction.

The incomplete reduction of $VOPO_4.2H_2O$ could be attributed to low hydrogen solubility in water. It is known that hydrogen is not very soluble in water; only 1.9 mg (0.95mmole) dissolves in a litre of water at 0°C at one atmosphere [1] which represent less than half of the amount (0.5mmole) needed to complete this reaction. However, increasing the pressure of the hydrogen gas will increase its solubility in the water, which can induce the reduction to take place.

Activating the new materials that were prepared using hydrogen for n-butane oxidation shows a mixture of $(VO)_2P_2O_7$ (IV) and some $VOPO_4$ (V) phases, which also suggests the incomplete reduction through the reaction. Furthermore, the testing data of this material shows a lower selectivity for maleic anhydride (5.3%) with (44%) conversion of n-butane compared to standard material prepared using VPD route which typically give 61% selectivity for maleic anhydride with (44%) conversion of n-butane. This could be attributed to the presence of some $VOPO_4$ (V) phases. It has been reported that

α_1-$VOPO_4$ is not selective for n-butane oxidation [5]. As a result, the active site of $(VO)_2P_2O_7$ can be obstructed by the presence of the unselective sites.

5.4.2 Materials prepared using hydrogen via direct route to $(VO)_2P_2O_7$

Another preparative route was also investigated in order to reduce the $VOPO_4.2H_2O$ (V) directly to the active phase $(VO)_2P_2O_7$ (IV) by using hydrogen. It was found that the temperatures have a great influence on the reaction. At 250°C and 350°C, the XRD patterns have one unknown reflection (2θ=21.24°), which makes it difficult for the bulk structure to be proposed even though some suggestions can be made. However, there are some other reflections present that can be assigned to α_1-$VOPO_4$. In addition, the Raman spectra of the samples are very similar (Figure 5.11) and show a strong correlation with the published spectrum for α_1-$VOPO_4$ [10]. There is a conflict between XRD and Raman results, and the phases detected in the bulk structures do not match with the phases detected at the surface. Powder XRD does not detect phases if their content is less than 5%. Additionally, it is likely that some processes could take place on the surface of the material (e.g. dehydration) and therefore, as Raman spectroscopy is a surface sensitive technique, so the changes occurring in the material would be more readily detected than using XRD which is a bulk technique. Moreover, it could be suggested that the materials are partially dehydrated to give α_1-$VOPO_4$ phase or the surface of the materials are dehydrated and the bulk structure is in hydrated form which gave in expected XRD peaks at (2θ=21.24°),

In contrast, reducing the $VOPO_4.2H_2O$ at 450°C with hydrogen flow through a water vapour and without it led to the active phase $(VO)_2P_2O_7$ indicating the influence of the temperature on the reduction as shown in Figure 5.8 a, and b respectively. However, the

materials reduced through a water vapour seem to be delayed and taking a longer time to be totally transformed compared with the results obtained without it. Furthermore, the water effect could prevent the dehydration step of $VOPO_4.2H_2O$ to α_I-$VOPO_4$ phase which therefore, delay the reduction taking place.

Bordes *et al.* [18] proposed the transformation of most VPO phases to $(VO)_2P_2O_7$ as shown in Figure 5.20, which can demonstrate the reduction mechanism of $VOPO_4.2H_2O$ to the active phase $(VO)_2P_2O_7$ through dehydration process.

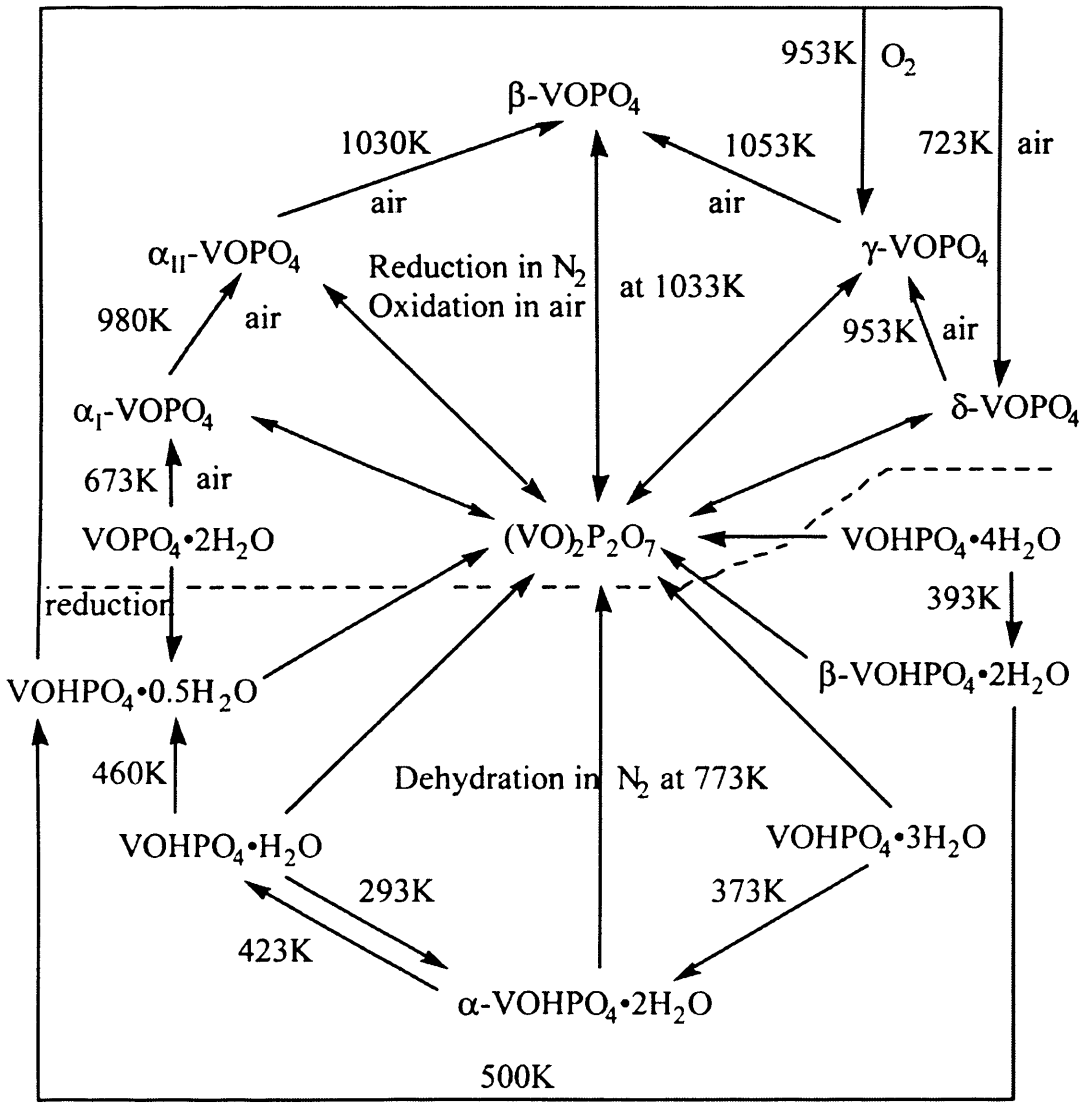

Figure 5.20- The possible phase transformations in the VPO system [18].

5.4.3 Materials prepared using new reducing agent (N_2H_4 and $NaBH_4$)

In the last section of this chapter, the use of new reducing agents hydrazine (N_2H_4) and sodium borohydride ($NaBH_4$) were explored. It was found that the reaction of $VOPO_4.2H_2O$ with hydrazine gave a new phase after 24 hours, which is believed to be V(V) after determining the oxidation state of the sample indicates that no reduction occurs. This phase has transformed to β-$VOPO_4$ after activation for n-butane at 400°C oxidation, which was confirmed by the unique characteristic XRD pattern and Raman spectra of β-$VOPO_4$.

According to the literature [19] β-$VOPO_4$ was prepared by the decomposition of $NH_4(VO_2)_2PO_4$ in dry air. However, this requires a high temperature (600°C) for 10 h before the β-$VOPO_4$ was obtained.

It could be proposed that the hydrazine may intercalate in the reaction with the $VOPO_4.2H_2O$ structure, or with $VOPO_4.H_2O$ through the reaction

The reaction of $VOPO_4.2H_2O$ with sodium borohydride was found to give $Na_{0.45}VOPO_4$ $1.58H_2O$ as the main phase with the present of VOHPO4.0.5H2O as minor phase. This suggests that the $VOPO_4.2H_2O$ was reduced to (IV) under the reaction condition. However, the presence of sodium cations could favour the reaction to give $Na_{0.45}VOPO_4$ $1.58H_2O$ instead of the catalyst precursor VOHPO4.0.5H2O.

This phase was converted to an unknown phase after activation for n-butane as shown by the XRD pattern and Raman. However, there are some reflections that can be assigned to $(VO)_2P_2O_7$ and other $VOPO_4$ phases.

5.5 Conclusions

Vanadium phosphate catalysts have successfully been prepared in aqueous media using hydrogen. The catalysts precursors obtained were poorly crystalline VOHPO4.0.5H2O and a minor amount of an impurity detected by a reflection in the XRD pattern. Activating these materials for n-butane oxidation show low selectivity of MA (5%), which could be attributed to the presence of V(V) phases after activation.

The direct route using hydrogen as reducing agent shows a promising path way for preparing the active phase $(VO)_2P_2O_7$ directly from the $VOPO_4.2H_2O$ at high temperature (over 450°C). In contrast, mixture of partially dehydrated $VOPO_4$ phases were detected at 250°C and 350°C, indicating the dehydration of $VOPO_4.2H_2O$ under the reaction conditions.

It was found that the reaction of $VOPO_4.2H_2O$ with hydrazine gave a new phase after 24 hours, which is believed to be V(V) after determining the oxidation state of the sample indicates that no reduction occurs. This phase has transformed to β-$VOPO_4$ after activation for n-butane at 400°C oxidation, which was confirmed by the unique characteristic XRD pattern and Raman spectra of β-$VOPO_4$. This could facilitate a new preparative route for β-$VOPO_4$ at lower temperature compared with the conventional method reported in the literature [19].

The use of sodium borohydride as a reducing agent led to the formation of new vanadium phosphate phase $Na_{0.45}VOPO_4$ $1.58H_2O$ with VOHPO4.0.5H2O as minor phase detected which can be attributed to the present of Na^+ cation.

5.6 References

[1] G. Centi, F. Trifiro` , J.R. Ebner, V.M. Franchetti, Chem. Rev. 88 (1998) 55.

[2] M. T. Sananes, I. J. Ellison, S. Sajip, A. Burrows, C. J. Kiely, J. C. Volta and G. J. Hutchings, J. Chem. Soc., Faraday Trans., 1996, 92, 1, 137.

[3] G.J. Hutchings, J. Mater. Chem. 14 (2004) 3385.

[4] G. J. Hutchings, A. Desmartin-Chamel, O. Oliver, J. C. Volta, Nature 348 (1994) 41.

[5] C.J. Kiely, A. Burrows, G.J. Hutchings, K.E. Bere, J.C. Volta, A. Tuel and M. Abon, Faraday Discuss., (1996), 105, 103

[6] G.J. Hutchings and R. Higgins, *J. Catal.*, (1996), **162**, 153

[7] Ramon A. Mount and Harold Raffelson, assigned to Monsanto Company U.S.A patent 4,337,174 (1982)

[8] J. K. Bartley, J. A. Lopez-Sanchez, G. J. Hutchings, Catal. Today, 81, 197 (2003)

[9] E. Bordes, Catal. Today 1 (1987) 499.

[10] V. V Guliants,. J. B. Benziger, S. Sundaresan, I. E. Wachs, J. M. Jehng, J.E. Roberts, Catal. Today, 28(1996)275-295.

[11] Y. LI, L. LI, H. LIAO and H. WANG, J. Mater. Chem. 9 (1999) 2675.

[12] A. Hajos in: Houben-Weyl-Müller, Methoden der organischen Chemie. Band IV/1d, Thieme, Stuttgart 1981, p. 1.

[13] J . GAO, F. GUAN, Y. ZHAO, W. YANG and Y. MA, Mater. Chem. Phys. 71 (2001) 215.

[14] E. R. H. Walker, Chem. Soc. Rev. 5 (1976) 23.

[15] F. Ben Abdelouahab, R. Olier, N. Guilhaume, F. Lefebvre and

J. C. Volta, J. Catal., 1992, 134, 151.

[16] http://www.engineeringtoolbox.com/gases-solubility-water-d_1148.html

[17] N. Casan, P. Amoros, R. Ibanez, E. Martinez-Tamayo, A. Belton-Porter, D. Beltran-Porter, J. Inclusion Phenomena, 6, 193, (1988).

[18] E. Bordes, Catal. Today 1987, 1, 499.

[19] F. Ben Abdelouahab, J.C. Volta, R. Olier, J. Catal. 148 (1994) 334.

CHAPTER 6

Conclusion and future work

6.1 Conclusion

It has been reported that the catalytic activity of the vanadium phosphate catalysts depends on the preparation methods of the catalyst precursors $VOHPO_4.0.5H_2O$ [1]. The catalyst that is generally considered to be the main active phase for the selective oxidation of n-butane to maleic anhydride, is usually derived from the activation of $VOHPO_4.0.5H_2O$, which gives a catalyst comprising of $(VO)_2P_2O_7$ as the main phase. The *in situ* transformation of the precursors $VOHPO_4.0.5H_2O$ to the active catalyst $(VO)_2P_2O_7$ is often topotactic, which means that the morphology and the surface area of the catalyst is controlled by the morphology and the surface area of the precursor. Consequently, careful preparation of the catalyst precursor $VOHPO_4.0.5H_2O$ is the key important factor for obtaining an effective catalyst.

In this thesis, new preparative routes have been explored and characterised for the synthesis of vanadium phosphate precursors. These precursors have been tested for the selective oxidation of n-butane to maleic anhydride. In addition, new reducing agents have been used to reduce vanadium phosphate dihydrate $VOPO_4.2H_2O$ for the purpose of preparing the catalyst precursors $VOHPO_4.0.5H_2O$ with different morphology. In chapter 3, long chain alkane (octane) has been used as co-solvent and also for the treatment of $VOPO_4.2H_2O$ prior to the reduction step with alcohol (1-butanol). These materials have been characterised and tested for n-butane selective oxidation. Three different morphologies of $VOHPO_4.0.5H_2O$ precursor have been successfully prepared via three different routes with the use of octane solvent. From these results, we can say that octane solvent can play an important role in $VOHPO_4{\cdot}0.5H_2O$ preparation. The

reaction of $VOPO_4.2H_2O$ with octane solvent shows the possibility of the intercalation of the octane solvent between the layers of $VOPO_4.2H_2O$. This can lead to the formation of $VOHPO_4.0.5H_2O$ precursors with a new morphology after the reduction step using 1-butanol. In addition, adding the solvent together with the reducing agent leads to the formation of $VOHPO_4.0.5H_2O$ with a different ratio of [001]/ [220] intensity and new morphology. Testing these samples shows that the samples with a rosette morphology exhibit the highest conversion and selectivity compared with the new materials prepared. Interestingly, The XRD patterns of the four activated catalysts are very similar and the main reflections can all be assigned to poorly crystalline $(VO)_2P_2O_7$. The only remarkable difference is the ratios of the [200] and [024] intensity which the high ratio for the catalyst prepared via C route and decreases in the order C > D > B $\geq$ A. This can be attributed to the nature of the original precursors and their morphologies. Moreover, there is no other phases were detected in the final catalyst of all materials prepared using the three routes described.

In chapter 4, the use of small amounts of vanadium phosphate materials as seeds during the reaction of $VOPO_4.2H_2O$ with alcohols has been studied using different alcohols (1-octanol, 2-methy-1-propanol, 2-butanol and 3-octanol). These particular solvents were selected based on the differences of the morphology of the resulting V-P-O material during a standard VPD preparation. The use of the seeds during the reaction of $VOPO_4.2H_2O$ with alcohols has been shown to be effective not only in altering the morphology of the product, but also in inducing certain phase transformations. The use of a seed in these cases shows that the rate of material formation can be increased. For example, the rate of $VOHPO_4{\cdot}0.5H_2O$ formation is high (*i.e.* 90% yield in 10 min) for the seeded reaction based on the theoretical yield of the $VOHPO_4{\cdot}0.5H_2O$ compared to

standard reaction without seed using 1-octanol (~10%). Moreover, the addition of small amount of $VOHPO_4 \cdot 0.5H_2O$ (0.05 g) as a seed to the reaction mixture can overcome a barrier to $VOHPO_4 \cdot 0.5H_2O$ formation that prevents the $VOHPO_4 \cdot 0.5H_2O$ material crystallising and aggregating at reflux temperatures (185°C). This has proved beneficial in the formation of catalyst precursors for the partial oxidation of butane to MA.

The use of the $VOHPO_4 \cdot 0.5H_2O$ seeds (platelet and rosette) with the reaction of $VOPO_4 \cdot 2H_2O$ with iso-butanol and 2-butanol alcohols showed also a significant effect on the morphology of the recovered $VOHPO_4 \cdot 0.5H_2O$ precursors.

The reaction of the dihydrate ($VOPO_4 \cdot 2H_2O$) using 3-octanol at the reflux temperature leads typically to the formation of $VO(H_2PO_4)_2$ phase as reported in most studies [2]. This phase $VO(H_2PO_4)_2$ has a negligible activity and selectivity for the partial oxidation of butane to MA [2]. However, this study demonstrates that seeding the reaction of $VOPO_4.2H_2O$ using 3-octanol with $VOHPO_4.0.5H_2O$ seeds (rosette or platelet) can control the reaction and form $VOHPO_4.0.5H_2O$ with a distinctive morphology. Additionally, Studying the reaction time online shows that $VO(H_2PO_4)_2$ could be transformed to $VOHPO_4.0.5H_2O$, which has been attempted previously without success. This is the first report of such a transformation occurring in the liquid phase. Finally, testing these samples under reaction conditions shows that they demonstrate high selectivity toward MA and good conversion compared to $VO(H_2PO_4)_2$.

In chapter 5, new materials have been prepared using hydrogen and two strong reducing agents (hydrazine and sodium borohydride). When hydrogen was used as a reducing agent in aqueous media, the catalyst precursors obtained were poorly crystalline $VOHPO_4.0.5H_2O$ and a minor amount of an impurity detected by a reflection in the

XRD pattern. Activating these materials for n-butane oxidation show low selectivity of MA (5%), which could be attributed to the presence of V(V) phases after activation. The presence of VOPO4 phases after activation indicate that the materials was not fully reduced which can attributed to low solubility of hydrogen in water.

The hydrogen also has been used via. a direct route, in order to prepare the active catalyst $(VO)_2P_2O_7$ from $VOPO_4.2H_2O$ at different temperatures. This route shows a promising path way for preparing the active phase $(VO)_2P_2O_7$ directly from the $VOPO_4.2H_2O$ at high temperature (over 450°C). However, mixtures of $VOPO_4$ phases were detected at 250°C and 350°C, indicating the dehydration of $VOPO_4.2H_2O$ under these temperatures compared to 450°C.

It was found that the reaction of $VOPO_4.2H_2O$ with hydrazine gave a new phase after 24 hours, which is believed to be V(V) after determining the oxidation state of the sample indicates that no reduction occurs. This phase has transformed to β-$VOPO_4$ after activation for n-butane at 400°C oxidation, which was confirmed by the unique characteristic XRD pattern and Raman spectra of β-$VOPO_4$. This could facilitate a new preparative route for β-$VOPO_4$ at lower temperature compared with the conventional method reported in the literature [3].

The use of sodium borohydride as a reducing agent led to the formation of new vanadium phosphate phase $Na_{0.45}VOPO_4.1.58H_2O$ with VOHPO4.0.5H2O as minor phase detected which can be attributed to the present of Na^+ cation.

6.2 Future work

In view of all the work presented in this thesis which would be improved with better characterisation of the vanadium phosphate materials and determining the new phases that found in the investigations. The characterisation techniques available during this study can facilitate the vanadium phosphate materials bulk to be determined, although the powder x-ray diffraction was shown to be reasonably insensitive particularly to minor phases present in the material. In addition, the Raman spectroscopy can only provide limited information on these phases.

Some new unknown phases were obtained in this study which suggests additional characterisation techniques to be used in order to identify the new phases and get a clear picture of their morphologies.^{31}P NMR and XPS techniques should be used to assist with the identification of these phases and can distinguished between V^{3+}, V^{4+} and V^{5+} phases and also provide an information on the nature of the oxidation state of the catalyst surface.

The vanadium phosphate dihydrate $VOPO_4.2H_2O$ showed a high capability of intercalation with different compounds. Therefore, it can be suggested to investigate the intercalation of new solvents with $VOPO_4.2H_2O$ which will be useful to observe a change in the morphology of the catalyst precursors $VOHPO_4.0.5H_2O$.

Moreover, as it was shown that the use of $VOHPO_4.0.5H_2O$ seeds (rosette or platelet) during the reaction of $VOPO_4.2H_2O$ with different alcohols can alter the morphology of the catalyst precursor $VOHPO_4.0.5H_2O$ and also can favour the transformations of certain phases during the reaction. These observations can open a great opportunity for

future study to investigate the effect of direct agents during the synthesis of the catalyst precursors $VOHPO_4.0.5H_2O$

6.3 References

[1] G.J. Hutchings, J. Mater. Chem 14 (2004) 3385.

[2] J. K. Bartley, C. Rhodes, C. J. Kiely, A. F. Carley, G. J. Hutchings, *Phys. Chem. Chem. Phys.* 2000, *21,* 4999-5006.

[3] F. Ben Abdelouahab, J.C. Volta, R. Olier, J. Catal. 148 (1994) 334.

Appendix 4.1 Characterisation of new materials prepared by reacting of $VOPO_4.2H_2O$ with 1-octanol and different amount of rosette seed (0.01, 0.05 and 0.1g)

Table 6.1- Experimental details of the materials prepared using different amounts of rosette seed (0.01, 0.05 and 0.1g)

Entry	V-P-O seed	Seed amount	T °C	Weight (g)
1	$VOHPO_4{\cdot}0.5H_2O$ (rosette)	0.01	185	1.8
2	$VOHPO_4{\cdot}0.5H_2O$ (rosette)	0.05	185	1.7
3	$VOHPO_4{\cdot}0.5H_2O$ (rosette)	0.1	185	1.62

Condition: 2g $VOPO_4.2H_2O$ +100ml 1-octanol

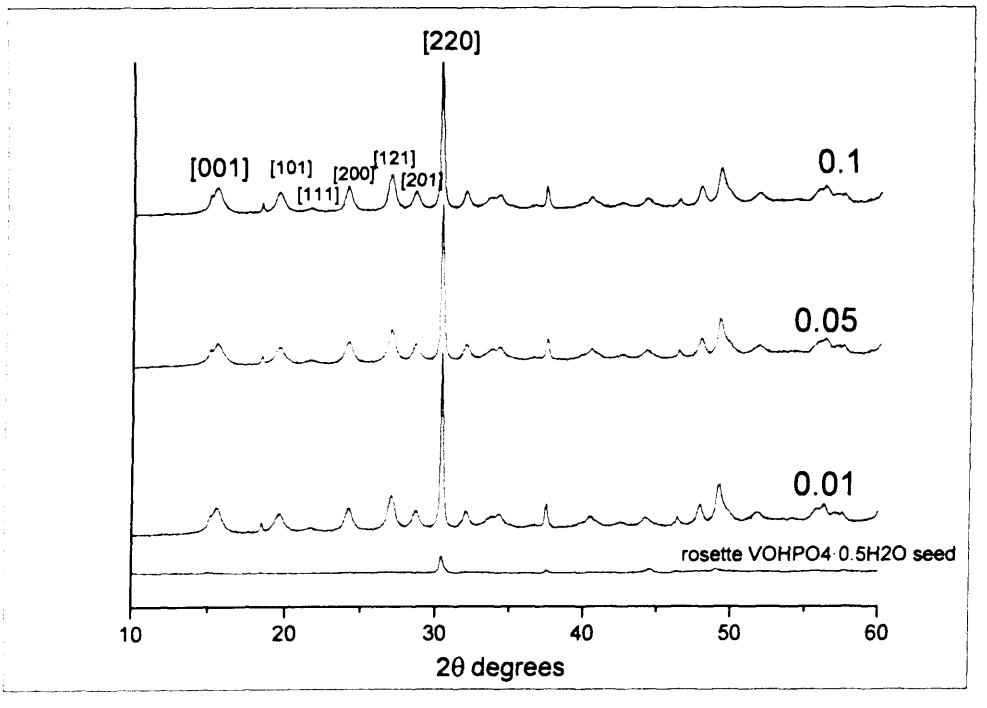

Figure 6.1-Powder diffraction pattern of Samples prepared by reacting of $VOPO_4.2H_2O$ with 1-octanol and different amount of rosette seed (0.01, 0.05 and 0.1g)

Appendix 4.2 Characterisation of new materials prepared by reacting of $VOPO_4.2H_2O$ with 1-octanol and different amount of $VO(H_2PO_4)_2$ seed (0.01, 0.05 and 0.1g)

Table 6.2- Experimental details of the materials prepared using different amounts of $VO(H_2PO_4)_2$ seed (0.01, 0.05 and 0.1g)

Entry	V-P-O seed	Seed amount	T °C	Weight (g)
1	$VO(H_2PO_4)_2$ seed	0.01	185	1.8
2	$VO(H_2PO_4)_2$ seed	0.05	185	0.9
3	$VO(H_2PO_4)_2$ seed	0.1	185	0.4

Condition: 2g $VOPO_4.2H_2O$ +100ml 1-octanol

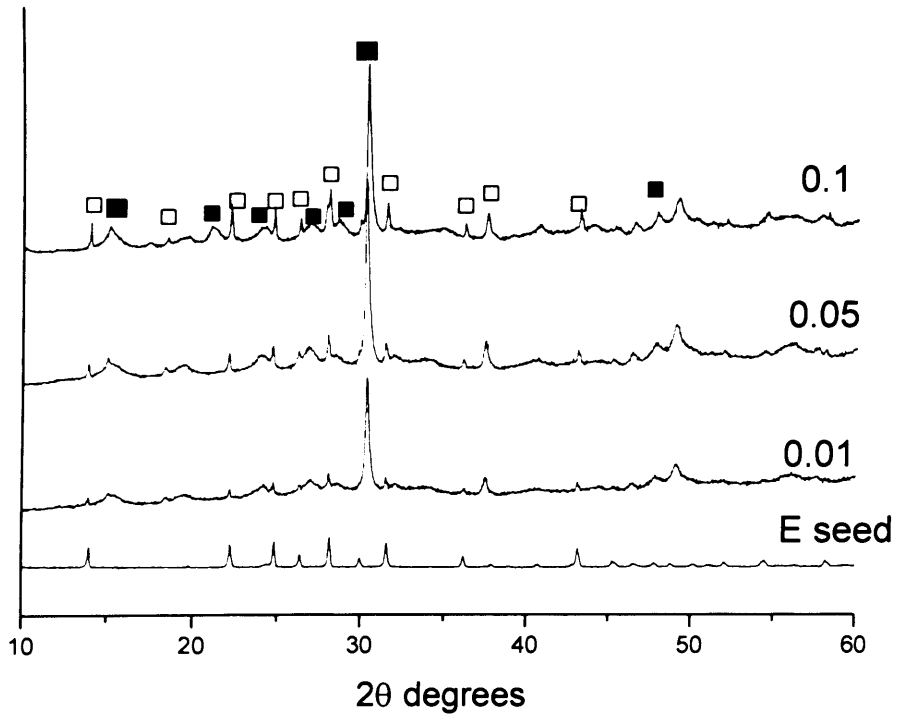

Figure 6.2- The XRD patterns of new materials prepared by reacting of $VOPO_4.2H_2O$ with 1-octanol and different amount of $VO(H_2PO_4)_2$ seed (0.01, 0.05 and 0.1g)). Keys: ■; $VOHPO_4{\cdot}0.5H_2O$ and □; $VO(H_2PO_4)_2$

Appendix 4.3 Characterisation of new materials prepared by reacting of $VOPO_4.2H_2O$ with 1-octanol and prepared using different materials as seed (0.05g)

Appendix 4.3- Experimental details of the materials prepared reacting of $VOPO_4.2H_2O$ with 1-octanol and prepared using different materials as seed (0.05g)

Entry	Seed	Seed amount	T °C	Yield (g)
1	SiO_2	0.05	185	0.09
2	Carbon	0.05	185	0.12
3	SiC	0.05	185	0.09
4	BN	0.05	185	0.14
5	V_2O_5	0.05	185	0.07
6	TiO_2	0.05	185	0.1
7	Al_2O_3	0.05	185	0.07

Condition: 2g $VOPO_4.2H_2O$ +100ml 1-octanol

Appendix 4.4 Characterisation of new materials prepared by reacting of $VOPO_4.2H_2O$ with 3-octanol and different amount of rosette $VOHPO_4 \cdot 0.5H_2O$ seed (0.01, 0.05 and 0.1g)

Table 6.3- Experimental details of the materials prepared using different amounts of rosette $VOHPO_4 \cdot 0.5H_2O$ seed (0.01, 0.05 and 0.1g)

Entry	V-P-O seed	Seed amount	T (°C)	Weight (g)
1	Rosette $VOHPO_4 \cdot 0.5H_2O$	0.01	Reflux	1.57
2	Rosette $VOHPO_4 \cdot 0.5H_2O$	0.05	Reflux	1.4
3	Rosette $VOHPO_4 \cdot 0.5H_2O$	0.1	Reflux	1.6

Condition: 2g $VOPO_4.2H_2O$ +100ml 3-octanol

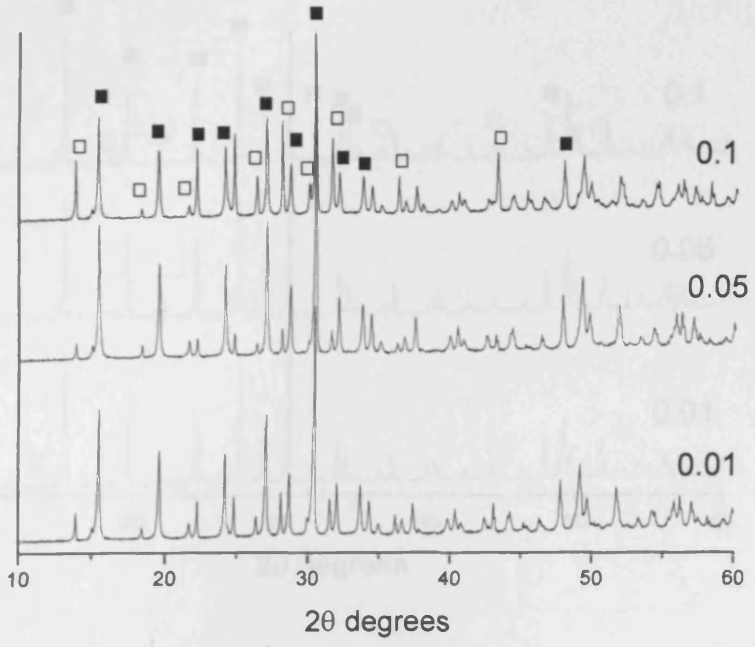

Figure 6.4- The XRD patterns of new materials prepared by reacting of $VOPO_4.2H_2O$ with 3-octanol and different amount of rosette $VOHPO_4 \cdot 0.5H_2O$ (0.01, 0.05 and 0.1g)). Keys: ■; $VOHPO_4 \cdot 0.5H_2O$ and □; $VO(H_2PO_4)_2$

Appendix 4.5 Characterisation of new materials prepared by reacting of $VOPO_4.2H_2O$ with 3-octanol and different amount of rosette $VOHPO_4{\cdot}0.5H_2O$ seed (0.01, 0.05 and 0.1g)

Table 6.4- Experimental details of the materials prepared using different amounts of platelet $VOHPO_4{\cdot}0.5H_2O$ seed (0.01, 0.05 and 0.1g)

Entry	V-P-O seed	Seed amount	T (°C)	Weight (g)
1	Platelet $VOHPO_4{\cdot}0.5H_2O$	0.01	Reflux	1.63
2	Platelet $VOHPO_4{\cdot}0.5H_2O$	0.05	Reflux	1.58
3	Platelet $VOHPO_4{\cdot}0.5H_2O$	0.1	Reflux	1.67

Condition: 2g $VOPO_4.2H_2O$ +100ml 3-octanol

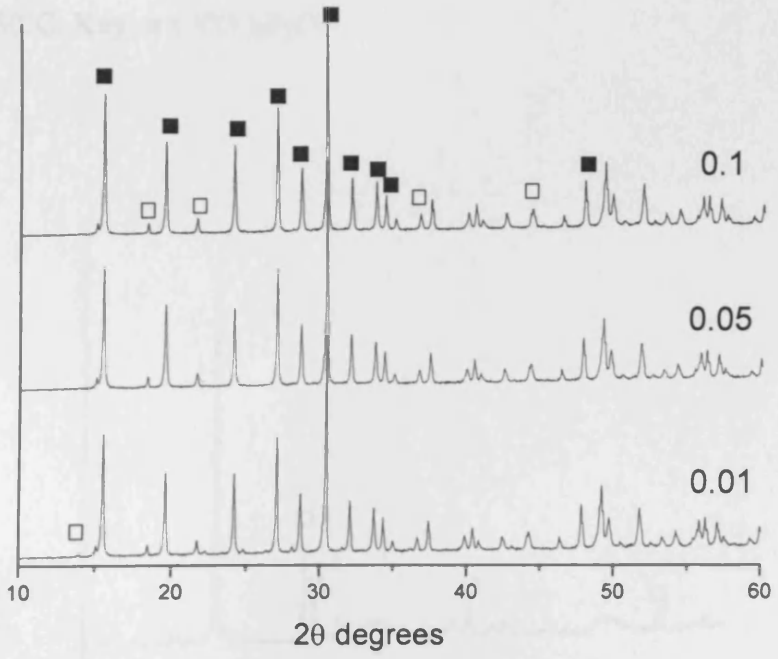

Figure 6.5- The XRD patterns of new materials prepared by reacting of $VOPO_4.2H_2O$ with 3-octanol and different amount of platelet $VOHPO_4{\cdot}0.5H_2O$ (0.01, 0.05 and 0.1g)). Keys: ■; $VOHPO_4{\cdot}0.5H_2O$ and □; $VO(H_2PO_4)_2$

(6) Appendix 5.1- The XRD patterns of activated samples prepared using direct route at 450˚C and 250 ˚C respectively.

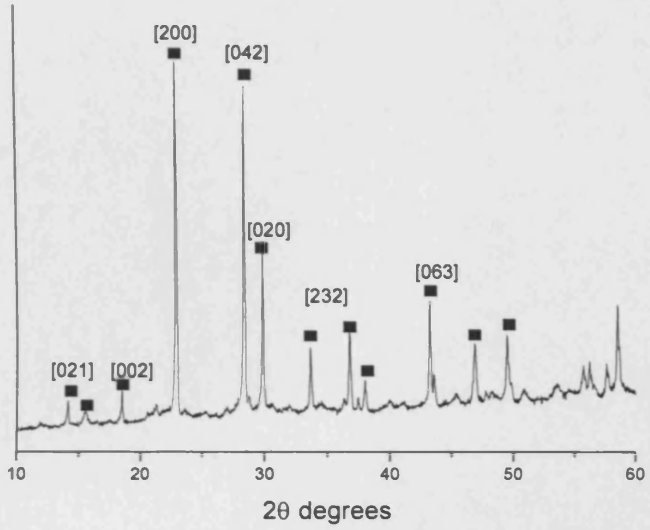

Figure. 6.6- XRD patterns for the activated catalysts prepared using direct route (using hydrogen) at 450˚C. Key: ■ (VO)$_2$P$_2$O$_7$

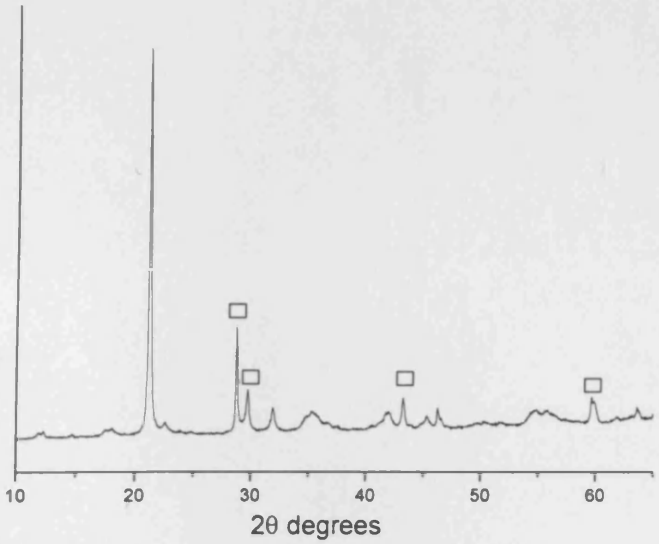

Figure. 6.7- XRD patterns for the activated catalysts prepared using direct route (using hydrogen) at 250˚C. Key: □ α_1-VOPO$_4$.